

THERMODYNAMICALLY CONTROLLED SYNTHESIS OF  
COVALENT NANOCAPSULES

by

XUEJUN LIU

A dissertation submitted to the  
Graduate School-New Brunswick  
Rutgers, The State University of New Jersey

In partial fulfillment of the requirements

For the degree of

Doctor of Philosophy

Graduate Program in Chemistry and Chemical Biology

Written under the direction of

Professor Ralf Warmuth

And approved by

\_\_\_\_\_  
\_\_\_\_\_  
\_\_\_\_\_  
\_\_\_\_\_

New Brunswick, New Jersey

October, 2008

## ABSTRACT OF THE DISSERTATION

### Thermodynamically Controlled Synthesis of Covalent Nanocapsules

By XUEJUN LIU

Dissertation Director:

Professor Ralf Warmuth

Chapter 1 gives a general overview about molecular container compounds.

In Chapter 2, a new method for the room temperature stabilization of fluorophenoxycarbene is described. In this approach, photolysis of incarcerated fluorophenoxydiazirine generated fluorophenoxycarbene in the inner phase of a hemicarcerand, which protected the carbene from dimerization. As a result of its high stability,  $^1\text{H}$ ,  $^{13}\text{C}$  and  $^{19}\text{F}$  NMR spectroscopic properties of this carbene were obtained at room temperature. The reaction of the incarcerated carbene with bulk phase water and its inner phase conformation were explored.

The synthesis of covalent nanocapsules is challenging and current multi-step syntheses give nanocapsules only in relatively low overall yield. In Chapter 3 and 4, a dynamic covalent chemistry approach has been developed to prepare nanocapsules in high yield in a single step from multiple small building blocks. Nanometersized molecular capsules of this type have potential for applications in drug, pesticide and RNA delivery and as nanoreactors. In Chapter 3, three different nanocapsules, whose structures resemble a distorted tetrahedron, octahedron, or square antiprism, are described. These capsules are

prepared by condensation reactions between 4, 6, and 8 tetraformyl cavitands **40** and 8, 12, and 16 ethylenediamines **43**, respectively. They have cavity volumes of 450-3000 Å<sup>3</sup>. In Chapter 4, synthesis of a series of distorted tetrahedral nanocapsules through reaction of **40** with rigid linear diamines **48a-c** is described. These capsules form 1:1 and 1:2 complexes with tetraalkylammonium salts of appropriate size, in which the tetraalkylammonium guests are encapsulated in the cavity of the nanocapsule.

In Chapter 5, dynamic combinatorial libraries (DCL) of polyimino nanocapsules are constructed by reacting **40** with a combination of 2 or 3 different diamine linkers **41**, **44d**, **48a**, and **48b**.

In Chapter 6, the syntheses of water-soluble nanocapsules are described. They are prepared by attaching hydrophilic functional groups and charged groups to the nanocapsules. Binding studies in water revealed that these nanocapsules encapsulate negatively charged organic compounds. The water soluble nanocapsules possess large portals and a roomy inner cavity and potentially may serve as devices for drug delivery and controlled release applications.

## ACKNOWLEDGEMENTS

I would like to gratefully and sincerely thank my advisor, Dr. Ralf Warmuth, for his guidance, encouragement, support, and most importantly, his friendship during my graduate studies at Rutgers University. His unlimited zeal for chemistry and science has been one of the major driving forces through my graduate career. I am also very grateful for having an exceptional doctoral committee and wish to thank Dr. Piotr Piotrowiak, Dr. Laurence Romsted, Dr. Daniel Seidel and Dr. Edward Castner for their input, accessibility and valuable discussions.

I am also indebted to the members of the Warmuth Group with whom I have interacted during the past five years. Particularly, I would like to acknowledge Dr. Ashim J. Thakur, Dr. Yong Liu, James Bennett, Di Xu for discussions and lectures on related topics that helped me improve my knowledge in the area. I extend my thanks to the Department of Chemistry. In particular, I would like to thank Dr. Seho Kim for assistance with my NMR work. Special thanks also go out to the graduate program director Dr. Matha Cotter and coordinator Ms. Melissa Grunweg.

Most importantly, none of these would have been possible without the love and support from my family. I would like to express my heart-felt gratitude to my wife Meng. I thank my parents, Xinhua and Zhuying, for their faith in me and allowing me to be as ambitious as I wanted.

Finally, I appreciate the financial support from Rutgers University and NSF that funded parts of the research discussed in this dissertation.

## DEDICATION

To my wife Meng Xu.

To my parents Xinhua Liu and Zhuying Li.

## Table of Contents

Abstract of the Dissertation.....	ii
Acknowledgements.....	iv
Dedication.....	v
List of Figures .....	xii
List of Schemes.....	xviii
List of Tables.....	xxi
Chapter 1 General introduction.....	1
References .....	6
Chapter 2 Room-temperature stabilization of fluorophenoxycarbene inside a hemicarcerand .....	8
2.1 Introduction .....	8
2.2 Results and discussion.....	11
2.2.1 Synthesis of fluorophenoxydiazirine hemicarceplex.....	11
2.2.2 Photolysis of fluorophenoxydiazirine hemicarceplex .....	14
2.2.3 Spectroscopic studies of fluorophenoxycarbene and its inner phase reactivity	16
2.3.4 Conformational analysis of fluorophenoxycarbene inside the inner phase of the hemicarcerand.....	21
2.3 Conclusions .....	28
2.4 Experimental section .....	28

2.4.1 General procedure.....	28
2.4.2 Synthesis of hemicarceplex <b>7⊙4</b> .....	28
2.4.3 Synthesis of hemicarceplex <b>7⊙3</b> .....	29
2.4.4 Synthesis of hemicarceplexes <b>7⊙15</b> and <b>7⊙16</b> .....	30
2.5 References .....	31
Chapter 3 Thermodynamically controlled multi-component synthesis of nanocontainer molecules and solvent effect studies.....	34
3.1 Introduction .....	34
3.2 Results and discussion.....	44
3.2.1 Synthesis of tetraformyl cavitand <b>40</b> .....	44
3.2.2 Condensation reaction between tetraformyl cavitand and diamine linkers.....	45
3.2.3 One-pot multicomponent synthesis of covalent molecular nanocapsules .....	48
3.2.4 Characterization of covalent molecular nanocapsule .....	55
3.2.5 Diffusion rate of nanocapsules .....	64
3.2.6 Diamino linker effect on the condensation reaction.....	71
3.2.8 Concentration Effects .....	73
3.2.9 Mechanistic and energetic aspects of molecular nanocapsule formation in solution .....	74
3.2.10 Template effect.....	77
3.3 Conclusions .....	78

3.4 Experimental section .....	79
3.4.1 General procedure.....	79
3.4.2 Gel Permeation Chromatography .....	79
3.4.3 Diffusion rate measurement of hexamer <b>47a</b> <sup>[18a]</sup> .....	80
3.4.4 Synthesis of tetraformyl cavitand <b>40</b> .....	83
3.4.5 Synthesis of octaiminohemicarcerand <b>45a</b> ( <i>Procedure A</i> ) .....	84
3.4.6 Synthesis of octaiminohemicarcerand <b>45b</b> .....	85
3.4.7 Synthesis of octaiminohemicarcerand <b>45c</b> .....	85
3.4.8 Synthesis of octaiminohemicarcerand <b>45d</b> .....	86
3.4.9 Synthesis of octaiminohemicarcerand <b>45e</b> .....	86
3.4.10 Synthesis and characterization of hexameric capsule <b>46a</b> and <b>47a</b> .....	87
3.4.11 Synthesis and characterization of tetrameric capsule <b>46b</b> and <b>47b</b> .....	88
3.4.12 Synthesis and characterization of octameric capsule <b>46c</b> and <b>47c</b> .....	90
3.5 References .....	91
Chapter 4 Multi-component synthesis of tetracavitand nanocapsules .....	93
4.1 Introduction .....	93
4.2 Results and discussion.....	93
4.2.1 Condensation of tetraformyl cavitand with diamines.....	93
4.2.2 Characterization of the nanocapsules <b>49a-c</b> .....	96
4.2.3 Diffusion rate of nanocapsules .....	100



4.2.4 Encapsulation of tetraalkylammonium bromides inside nanocapsules .....	101
4.2.5 Hydrocarbon adsorption inside nanocapsules .....	111
4.3 Conclusions .....	113
4.4 Experimental section .....	114
4.4.1 General procedure.....	114
4.4.2 DOSY experiments.....	115
4.4.3 Synthesis of hexadecaiminonanocapsule <b>49a</b> ( <i>Procedure A</i> ).....	115
4.4.4 Synthesis of hexadecaiminonanocapsule <b>49b</b> .....	116
4.4.5 Synthesis of hexadecaiminonanocapsule <b>49c</b> .....	117
4.4.6 Reduction of <b>49c</b> .....	118
4.5 References .....	120
Chapter 5 Dynamic combinatorial libraries of polyimino nanocapsules.....	121
5.1 Introduction .....	121
5.2 Results and discussion.....	122
5.2.1 System selection .....	122
5.2.2 DCL from <i>meta</i> -phenylenediamine ( <b>A</b> ) and <i>meta</i> -xylylenediamine ( <b>B</b> ).....	122
5.2.3 DCL from <i>meta</i> -xylylenediamine ( <b>B</b> ) and benzidine( <b>C</b> ) .....	126
5.2.4 DCL from <i>meta</i> -phenylenediamine ( <b>A</b> ) and benzidine ( <b>C</b> ).....	137
5.2.5 DCL from <i>meta</i> -phenylenediamine ( <b>A</b> ), <i>meta</i> -xylylenediamine ( <b>B</b> ) and benzidine ( <b>C</b> ) .....	139

5.2.6 DCL from <i>meta</i> -phenylenediamine ( <b>A</b> ) and <i>para</i> -phenylenediamine ( <b>D</b> ).....	140
5.3 Conclusions .....	142
5.4 Experimental section .....	142
5.4.1 General procedure.....	142
5.4.2 Preparation of DCLs.....	143
5.4.3 Molecular mechanics calculation and molecular dynamics simulation. ....	144
5.5 References .....	145
Chapter 6 Synthesis of water-soluble nanocapsules .....	146
6.1 Introduction .....	146
6.2 Results and discussion.....	153
6.2.1 Attachment of carboxylic acid group to the linker of the octahedral nanocapsule with pentyl feet .....	153
6.2.2 Synthesis of a water soluble octahedral nanocapsule with butanol feet.....	155
6.2.3 Complexation studies .....	159
6.2.4 Synthesis of a water-soluble rhombicuboctahedral nanocapsule .....	171
6.3 Future application of the water-soluble nanocapsules in drug-delivery system ...	177
6.4 Conclusions .....	178
6.5 Experimental section .....	178
6.5.1 General procedure.....	178
6.5.2 NMR complexation studies .....	179

6.5.3 DOSY experiments.....	180
6.5.4 Synthesis of <b>65</b> .....	180
6.5.5 Synthesis of <b>66</b> .....	181
6.5.6 Synthesis of <b>68</b> .....	182
6.5.7 Synthesis of MOM-protected tetrabromocavitand <b>73</b> .....	182
6.5.8 Synthesis of MOM-protected tetraformyl cavitand <b>74</b> .....	183
6.5.9 Synthesis of butanol-footed hexameric nanocapsule <b>76</b> .....	184
6.5.10 Synthesis of MOM-protected rhombicuboctahedral nanocapsule <b>79</b> .....	185
6.5.11 Reduction of MOM-protected rhombicuboctahedral nanocapsule <b>79</b> to form <b>81</b> .....	186
6.5.12 Acylation of MOM-protected rhombicuboctahedral nanocapsule <b>81</b> to form <b>82</b> .....	187
6.5.13 MOM-deprotection and saponification of rhombicuboctahedral nanocapsule to form <b>83</b> .....	188
6.6 References .....	189
Appendix. Compound number and stucture .....	192
Curriculum Vita .....	215

## List of Figures

Figure 1.1 Molecular container complex and energy profile for hemicarceplex decomplexation.....	2
Figure 2.1 Incarcerated cyclobutadiene and <i>o</i> -benzyne.....	10
Figure 2.2 Partial $^1\text{H}$ NMR spectra (400 MHz, $\text{CD}_2\text{Cl}_2$ , 25 °C) of hemicarceplex <b>7</b> ⊙ <b>4</b> : a) before and b) after photolysis ( $\lambda > 320$ nm, 77 K, 2 h); c) same solution as b) after complete decomposition. Signals assigned to protons of incarcerated <b>4</b> (▼), <b>3</b> (●), <b>15</b> (↓), and <b>16</b> (◆) are marked. $\text{H}_a$ , $\text{H}_o$ , $\text{H}_m$ , and $\text{H}_i$ are protons of host <b>7</b> . ....	16
Figure 2.3 Concentration change of <b>7</b> ⊙ <b>3</b> vs. time ( $\text{CD}_2\text{Cl}_2$ , 25 °C) in the presence (■) and absence (○) of pyridine- $d_5$ . The amount of <b>7</b> ⊙ <b>3</b> was estimated from the integral of proton H1 of the guest <b>3</b> .....	19
Figure 2.4 $^{19}\text{F}$ NMR spectrum (282.232 MHz, $\text{CD}_2\text{Cl}_2$ , 25 °C) of partially decomposed <b>7</b> ⊙ <b>3</b> , referenced to $\text{CFCl}_3$ . Signals assigned to $^{19}\text{F}$ of incarcerated <b>3</b> (●), <b>16</b> (◆) and two further photoproducts of <b>7</b> ⊙ <b>4</b> (∇, ✕) are marked. ....	20
Figure 2.5 $^1\text{H}$ - $^{19}\text{F}$ NOE difference spectrum (399.971 MHz, $\text{CD}_2\text{Cl}_2$ , 28 °C) of <b>7</b> ⊙ <b>3</b> .....	24
Figure 2.6 $^{19}\text{F}$ Chemical shift correction. All structures fully optimized at PBE1PBE/ 6-311++G(2d,p).....	25
Figure 2.7 $^{13}\text{C}$ Chemical shift correction. All structures fully optimized at PBE1PBE/ 6-311++G(2d,p).....	26
Figure 3.1 Structure of Sherburn's pentamer. ....	41
Figure 3.2 Gel permeation chromatograms of the crude products formed after 2 days in the TFA-catalyzed reaction of <b>40</b> with two equivalents of <b>43</b> in THF (a), $\text{CHCl}_3$ (b), $\text{CH}_2\text{Cl}_2$ (c), $\text{CH}_2\text{ClCH}_2\text{Cl}$ (d) and $\text{CCl}_2\text{HCCl}_2\text{H}$ (e). (f) Products formed in $\text{CH}_2\text{Cl}_2$ spiked	

with <b>46a</b> . Retention time (in minutes) and estimated molecular weight (in parenthesis) are reported for main peaks. ....	49
Figure 3.3 Reversed-phase HPLC chromatograms of the crude reaction mixture after imine reduction and boramine hydrolysis for a) <b>47a</b> and b) <b>47c</b> . ....	53
Figure 3.4 $^1\text{H}$ NMR spectra of (a) crude products formed in the reaction of <b>40</b> with two equivalents of <b>43</b> in the presence of 10 mol% TFA in chloroform after 69 hrs ( $\text{CDCl}_3$ ; 400 MHz; 22 °C) and (b) of <b>47a</b> • $24\text{CF}_3\text{CO}_2\text{H}$ ( $\text{CD}_3\text{OD}$ + 0.4 v% TFA- <i>d</i> ; 500 MHz; 7 °C). (c) $^{13}\text{C}$ NMR spectrum of <b>47a</b> • $24\text{CF}_3\text{CO}_2\text{H}$ ( $\text{CD}_3\text{OD}$ + 0.4 v% TFA- <i>d</i> ; 100 MHz; 25 °C)...	56
Figure 3.5 MALDI-TOF mass spectrum of <b>47a</b> . ....	58
Figure 3.6 Cartoon structure of <b>47b</b> and positions A, B, C, and D. ....	58
Figure 3.7 Partial $^1\text{H}$ NMR spectra (400 MHz; 22 °C) of (a) crude products formed in the reaction of <b>40</b> with two equivalents of <b>43</b> in the presence of 10 mol% TFA in THF after 2 days (in $\text{CDCl}_3$ ; signals assigned to <b>46b</b> are marked) and (b) of <b>47b</b> • $16\text{CF}_3\text{COOH}$ in $\text{CD}_3\text{OD}$ + 0.4 v% TFA- <i>d</i> . (c) Partial $^{13}\text{C}$ NMR spectra (100 MHz, 22 °C, $\text{CD}_3\text{OD}$ + 0.4 v% TFA- <i>d</i> ) of <b>47b</b> • $16\text{CF}_3\text{COOH}$ . Tick marks are separated by 0.1 ppm. ....	60
Figure 3.8 MALDI-TOF mass spectrum of <b>47b</b> . ....	61
Figure 3.9 Partial $^1\text{H}$ NMR spectra (400 MHz; 22 °C) of (a) crude products formed in the reaction of <b>40</b> with two equivalents of <b>43</b> in the presence of 10 mol% TFA in $\text{CH}_2\text{Cl}_2$ after 67 hrs (in $\text{CDCl}_3$ ; signals assigned to <b>46c</b> are marked) and (b) of <b>47c</b> • $32\text{CF}_3\text{COOH}$ in $\text{CD}_3\text{OD}$ + 0.4 v% TFA- <i>d</i> . (c) Partial $^{13}\text{C}$ NMR spectra (100 MHz, 22 °C, $\text{CD}_3\text{OD}$ + 0.4 v% TFA- <i>d</i> ) of <b>47c</b> • $32\text{CF}_3\text{COOH}$ . Tick marks are separated by 0.1 ppm. ....	63
Figure 3.10 MALDI-TOF mass spectrum of <b>47c</b> . ....	64
Figure 3.11 Views along the $C_3$ (a, c) and $C_4$ axis (b, d) of energy-minimized structures of	

<b>47a</b> •24H <sup>+</sup> (a, b: space-filling model; Amber* force field, <sup>[19a]</sup> GB/SA water solvation model <sup>[19b]</sup> ) and <b>46a</b> (c, d: stick model; H and pentyl groups omitted; Amber force field*, <sup>[19a]</sup> vacuum). .....	67
Figure 3.12 Views along the two C <sub>2</sub> axes of energy-minimized structures of <b>47b</b> •16H <sup>+</sup> (Amber* force field, <sup>[19a]</sup> GB/SA water-solvation model <sup>[19b]</sup> ). Atom coloring: C gray; H white; O red; N blue.....	68
Figure 3.13 Top and side views of energy-minimized structures of <b>47c</b> •32H <sup>+</sup> (Amber* force field, <sup>[19a]</sup> GB/SA water-solvation model <sup>[19b]</sup> ). Atom coloring: C gray; H white; O red; N blue.....	69
Figure 3.14 Linker effect on the condensation of <b>40</b> with <b>44a-j</b> and <b>43</b> . .....	72
Figure 3.15 Percentage of <b>46a</b> and <b>46b</b> vs. time for the condensation of <b>40</b> and 2 equivalents <b>43</b> in CHCl <sub>3</sub> with different initial concentration [ <b>40</b> ]. .....	74
Figure 3.16 Partial <sup>1</sup> H NMR spectra (a, c, e and f, 400 MHz; b and d, 300 MHz; 22 °C; CDCl <sub>3</sub> ) during the formation of <b>46a</b> after 1.7 (a), 24 (b) and 69 hrs (c), and <b>46c</b> after 0.7 (d), 9 (e) and 31 hrs (f). The imine signals H <sub>imine</sub> for <b>46a</b> (◆), <b>46b</b> (▼) and <b>46c</b> (●) are marked.....	75
Figure 4.1 GPC-traces of products in the TFA catalyzed condensation of 4 eq. <b>40</b> with 8 eq. <b>48a</b> (A), <b>48b</b> (B), <b>48c</b> (C) and <b>48d</b> (D). Retention time (in min) and estimated molecular weight (in parenthesis, in Da) are given for each peak. Column temperature: (A) and (B) 25 °C, (C) and (D) 60 °C. ....	95
Figure 4.2 <sup>1</sup> H-NMR spectrum (500 MHz; C <sub>6</sub> D <sub>5</sub> CD <sub>3</sub> ; 25 °C) of <b>49a</b> . Multiplets assigned to protons H <sub>imine</sub> , H <sub>a</sub> , H <sub>o</sub> , H <sub>m</sub> , and H <sub>i</sub> are marked. ....	97
Figure 4.3 Energy-minimized space-filling models of nanocapsules <b>49a-c</b> (MM3, <sup>[5]</sup> gas-	

phase). Pentyl groups are omitted. Atom coloring: C grey; O red; N blue; H white. ....	101
Figure 4.4 Partial $^1\text{H}$ NMR spectra (500 MHz, $\text{THF-}d_8$ ; 278 K) of <b>49a</b> in the presence of 20 eq. $(n\text{-C}_5\text{H}_{11})_4\text{NBr}$ (A), $(n\text{-C}_6\text{H}_{13})_4\text{NBr}$ (B), or $(n\text{-C}_7\text{H}_{15})_4\text{NBr}$ (C). Signals assigned to protons of encapsulated guests of 1:1 and 2:1 complexes are marked with filled circles and asterisks, respectively. ....	103
Figure 4.5 Binding isotherm for the encapsulation of $(n\text{-C}_5\text{H}_{11})_4\text{NBr}$ inside <b>49a</b> in $\text{THF-}d_8$ at $-5\text{ }^\circ\text{C}$ showing saturation of binding sites $S$ ( $0 \leq S \leq 1$ ; $\blacktriangle$ ), mole fraction of <b>49a</b> $\odot(n\text{-C}_5\text{H}_{11})_4\text{NBr}$ ( $\square$ ) and mole fraction of <b>49a</b> $\odot(2(n\text{-C}_5\text{H}_{11})_4\text{NBr})$ ( $\circ$ ) as function of the guest concentration. ....	108
Figure 4.6 Energy-minimized space-filling model of <b>49a</b> $\odot(n\text{-C}_6\text{H}_{13})_4\text{N}^+$ (A); <b>49a</b> $\odot(n\text{-C}_7\text{H}_{15})_4\text{N}^+$ (B) and <b>49a</b> $\odot(n\text{-C}_8\text{H}_{17})_4\text{N}^+$ (C) (MM3, <sup>[5]</sup> gas-phase). Coloring: <b>49a</b> aquamarine; guest orange. ....	110
Figure 4.7 Adsorption isotherms of <b>49a</b> with benzene. ....	112
Figure 4.8 TPD profile of <b>49a</b> pre-adsorbed with benzene at $25\text{ }^\circ\text{C}$ . ....	113
Figure 5.1 MALDI-TOF mass spectrum of DCL from <b>A</b> and <b>B</b> . ....	124
Figure 5.2 Partial $^1\text{H}$ NMR spectra (500 MHz, $\text{CDCl}_3$ , $25\text{ }^\circ\text{C}$ ) of a) <b>A</b> <sub>4</sub> , c) <b>B</b> <sub>4</sub> , e) <b>C</b> <sub>8</sub> , and DCLs from <b>40</b> and linker b) <b>A</b> + <b>B</b> ; d) <b>B</b> + <b>C</b> ; f) <b>A</b> + <b>C</b> ; g) <b>A</b> + <b>B</b> + <b>C</b> . ....	125
Figure 5.3 MALDI-TOF mass spectrum of DCL from <b>B</b> and <b>C</b> . ....	127
Figure 5.4 Energy-minimized structures of tetramer <b>C</b> <sub>8</sub> , <b>B</b> <sub>4<b>C</b><sub>4</sub>-1 and <b>C</b><sub>4<b>B</b><sub>4</sub>-2. ....</sub></sub>	130
Figure 5.5 MALDI-TOF mass spectrum of DCL from <b>A</b> and <b>C</b> . ....	138
Figure 5.6 MALDI-TOF mass spectrum of DCL from <b>A</b> and <b>D</b> . ....	141
Figure 5.7 Partial $^1\text{H}$ NMR spectra (500 MHz, toluene- $d_8$ , $25\text{ }^\circ\text{C}$ ) of a) <b>A</b> <sub>4</sub> , c) <b>D</b> <sub>8</sub> , and b) the DCL from tetraformyl cavitand <b>40</b> and linker <b>A</b> and <b>D</b> . ....	141

Figure 6.1 Water-soluble macrocyclic host: $\beta$ -cyclodextrin. ....	146
Figure 6.2 Water-soluble cavitands bearing quaternary ammonium moieties in the upper rim or phosphoric acid in the feet. ....	147
Figure 6.3 Rebek's water-soluble tetracarboxyl deep cavitand <b>54</b> . ....	148
Figure 6.4 Diederich's water-soluble PEG-footed deep cavitand <b>55</b> . ....	149
Figure 6.5 Gibb's water-soluble deep cavitand <b>56</b> bearing eight carboxylic acid groups and its 2:1 capsular complex. ....	149
Figure 6.6 Molecular capsule <b>59</b> from two calix[4]arene moieties <b>57</b> and <b>58</b> through ionic interactions. ....	150
Figure 6.7 The first water-soluble hemicarcerand <b>60</b> and its tris-bridged analogue <b>61</b> . ....	151
Figure 6.8 Water-soluble hemicarcerand-like chiral host <b>62</b> . ....	152
Figure 6.9 $^1\text{H}$ NMR spectrum (0.2 wt% DCl/D <sub>2</sub> O, 25 °C, 500 MHz) of <b>76</b> ·24HCl. ....	159
Figure 6.10 Neutral and negatively charged organic guest molecules. ....	159
Figure 6.11 Binding isotherm for the encapsulation of Boc-Asp-OH in <b>76</b> ·24HCl in D <sub>2</sub> O at 25 °C (pD 4.7, [ <b>76</b> ] = 0.21 mM) showing binding site saturation $S$ ( $0 \leq S \leq 1$ ) as a function of the guest concentration [Guest]: experimental data (◆) and best fit (■). ....	163
Figure 6.12 Binding isotherm for the encapsulation of <i>p</i> -TsOH inside the octahedral hexamer <b>76</b> ·24HCl in D <sub>2</sub> O at 25 °C (pD 1.0, [ <b>76</b> ] = 0.22 mM) showing binding site saturation $S$ ( $0 \leq S \leq 1$ ) as a function of the guest concentration: experimental data (◆) and best fit (■). ....	166
Figure 6.13 $^1\text{H}$ NMR spectra (500 MHz, D <sub>2</sub> O, 25 °C) of a) 4-MUP and <b>76</b> ·24HCl in the presence of 4-MUP b) 0.9 equiv., c) 2.8 equiv., and d) 4.6 equiv., pD 4.3, [ <b>76</b> ] = 0.21 mM. ....	168



Figure 6.14 Proposed partial structure of the complex formed between 4-MUP and <b>76</b> ·24HCl.....	169
Figure 6.15 Nucleotides and the chemical shifts with or without the presence of the host <b>76</b> (pD = 4.3, [ <b>76</b> ] = 0.2 mM). ....	171
Figure 6.16 MALDI-TOF mass spectrum of the acylation product <b>82</b> . ....	175
Figure 6.17 <sup>1</sup> H NMR spectrum (500 MHz, DMSO- <i>d</i> <sub>6</sub> , 25 °C) of nanocapsule <b>83</b> .....	177

## List of Schemes

Scheme 1.1 Reversible covalent bonds: a) imine formation and exchange; b) hydrazone formation and exchange; c) ester formation and exchange; d) disulfide exchange; and e) olefin metathesis. ....	5
Scheme 2.1 Reactions of carbenes, a) C-H insertion, b) C=C addition, c) dimerization. ..	9
Scheme 2.2 Spin states of carbenes and Arduengo carbene, R = admantyl <sup>[3]</sup> . ....	9
Scheme 2.3 Generation of fluorophenoxycarbene and its subsequent reactions. ....	11
Scheme 2.4 Synthesis of diol hermicarcerand <b>8</b> and diazirine hemicarceplex <b>7</b> ⊙ <b>4</b> . ....	13
Scheme 2.5 Photolysis of <b>4</b> and reactions of <b>3</b> in the inner phase of <b>7</b> . ....	18
Scheme 2.6 Resonance stabilization of <b>3</b> . ....	20
Scheme 2.7 Potential energy surface for the <i>cis-trans</i> equilibration of <b>3</b> . ....	22
Scheme 3.1 Self-assembly of a cuboctahedral nanocage from 12 <i>bis</i> -platinum clips <b>21</b> and 8 triangular tripyridyl units <b>22</b> . ....	35
Scheme 3.2 Construction of a M <sub>6</sub> L <sub>4</sub> self-assembled octahedral nanocage. ....	36
Scheme 3.3 Formation of Pt-coordinated tri-cavitand assemblies. ....	37
Scheme 3.4 Formation of dithiocarbamate cavitand based coordination molecular loops and tetrahedral nanocages. ....	38
Scheme 3.5 Rebek's hydrogen bonded cylindrical dimeric capsule. ....	39
Scheme 3.6 Self-assembly of a hydrogen bonded hexameric nanocapsule. ....	40
Scheme 3.7 Multistep synthesis of a covalent hexameric nanocapsule by Sherman and coworkers. ....	41
Scheme 3.8 Reversible Schiff base chemistry: a) imine formation/dissociation; b) transimination, and c) imine metathesis. ....	43

Scheme 3.9 Thermodynamically controlled synthesis of an octaiminohemicarcerand. ....	43
Scheme 3.10 Synthesis of tetraformyl cavitand <b>40</b> .....	44
Scheme 3.11 The condensation reactions between cavitand <b>40</b> and diamines <b>44a-g</b> .....	46
Scheme 3.12 12-, 18-, and 24-component syntheses of tetrahedral, octahedral and square anti-prismatic nanocapsules <b>46a</b> , <b>46b</b> and <b>46c</b> and their reduction. ....	49
Scheme 3.13 Proposed intramolecular catalysis of acetal spanner cleavage.....	51
Scheme 4.1 The condensation reactions between cavitand <b>40</b> and diamine <b>48a-d</b> . ....	94
Scheme 5.1 The product distribution of DCL from <b>A</b> and <b>B</b> .....	124
Scheme 5.2 The product distribution of DCL from <b>B</b> and <b>C</b> .....	128
Scheme 5.3 Calculation of the strain energy in the imine-cavitand part of tetramer <b>C<sub>8</sub></b> . 134	
Scheme 5.4 Calculation of the strain energy in the complete linkers of tetramer <b>C<sub>8</sub></b> . ....	135
Scheme 5.5 Calculation of the strain energy in the imines of tetramer <b>C<sub>8</sub></b> . ....	136
Scheme 5.6 Calculation of the acetal-linker interaction energy in tetramer <b>C<sub>8</sub></b> .....	137
Scheme 5.7 The product distribution of DCL from <b>A</b> and <b>C</b> .....	139
Scheme 6.1 Attachment of twenty-four carboxylic acid groups to the linker of the octahedral nanocapsule with pentyl feet. ....	153
Scheme 6.2 Attachment of forty-eight carboxylic acid groups to the linker of the pentyl-footed octahedral nanocapsule <b>47a</b> . ....	154
Scheme 6.3 Synthesis of MOM protected butanol-footed tetraformyl cavitand <b>74</b> . ....	157
Scheme 6.4 Condensation of tetraformyl cavitand <b>74</b> and ethylenediamine <b>43</b> followed by reduction leading to water-soluble octahedral nanocapsule <b>76·24HCl</b> .....	158
Scheme 6.5 Condensation of tetraformyl cavitand <b>74</b> and 1,3,5-tris( <i>p</i> -aminophenyl)benzene <b>78</b> leading to rhombicuboctahedral nanocapsule <b>79</b> .....	172

Scheme 6.6 Reduction of the polyimino rhombicuboctahedral nanocapsule <b>79</b> and post functionalization. ....	173
Scheme 6.7 Proposed mechanism of intramolecular benzoxazine formation. ....	175

## List of Tables

Table 2.1 $^1\text{H}$ , $^{19}\text{F}$ , and $^{13}\text{C}$ NMR chemical shifts of <b>3</b> , referenced to TMS or $\text{CFCl}_3$ . .....	22
Table 3.1 Yields <sup>i</sup> , mass ( $m/z$ ) and imine chemical shifts $\delta_{\text{H(imine)}}$ of <b>45a-h</b> in the TFA-catalyzed condensation of <b>40</b> with 2 equivalents <b>44a-j</b> . .....	47
Table 3.2 Yields <sup>a</sup> (in %) of <b>46a</b> , <b>46b</b> and <b>46c</b> in the TFA-catalyzed condensation of <b>40</b> with 2 equivalents <b>43</b> in different solvents. ....	54
Table 3.3 Chemical shifts, integrations and multiplets of <b>46a-c</b> and <b>47a-c</b> in their $^1\text{H}$ NMR spectra <sup>v</sup> . .....	57
Table 3.4 Sum formulas and MALDI-TOF mass of <b>47a-c</b> . ....	58
Table 3.5 Diffusion constants $D$ in $\text{CD}_3\text{OD} + 0.4 \text{ v\% TFA-}d$ at $25^\circ\text{C}$ , solvodynamic diameters $d$ and cavity volume of <b>47a-c</b> . ....	65
Table 3.6 Calculation of $(K_{\text{interEM}})_{\text{min}}$ and the number of intermolecular/intramolecular steps for the assembly of <b>46a-d</b> . ....	70
Table 4.1 Yields of <b>49a-d</b> in the TFA-catalyzed condensation of <b>40</b> with 2 equivalents <b>48a-d</b> . ....	95
Table 4.2 Chemical shifts, integrations and multiplets of <b>49a-c</b> in $^1\text{H}$ NMR spectra <sup>iv</sup> . ....	98
Table 4.3 Sum formulas and MALDI-TOF mass of <b>49a-c</b> . ....	99
Table 4.4 Diffusion constants $D$ in $\text{CDCl}_3$ at $25^\circ\text{C}$ and solvodynamic radii $r^{\text{a}}$ of <b>49a-c</b> . ....	101
Table 4.5 Complexation induced shift (CIS) of guest protons for complexes <b>49a</b> ⊙ $\text{R}_4\text{N}^+\text{Br}^-$ and <b>49a</b> ⊙ $2(\text{pentyl}_4\text{N}^+\text{Br}^-)$ in $\text{THF-}d_8$ at $-5^\circ\text{C}$ and guest's van der Waals volume <sup>[8]</sup> . ....	104
Table 4.6 Thermodynamic properties ( $\Delta G_{298}$ , $\Delta H_{298}$ and $T\Delta S_{298}$ at 298 K in kcal/mol) of	

complexes <b>49a</b> ⊙R <sub>4</sub> NBr. ....	105
Table 4.7 MALDI-TOF MS data for complexes formed in THF- <i>d</i> <sub>8</sub> . ....	106
Table 5.1 Strain energy and acetal-linker stabilization energy in three tetramers <b>C</b> <sub>8</sub> , <b>B</b> <sub>4<b>C</b><sub>4</sub>-1, and <b>C</b><sub>4<b>B</b><sub>4</sub>-2 (kcal/mol).....</sub></sub>	133
Table 6.1 Yields of polyimino- hexamer in the TFA-catalyzed condensation of ethylenediamine <b>43</b> and cavitands with different feet groups. ....	155
Table 6.2 Chemical shifts and diffusion rates ( <i>D</i> , x 10 <sup>-6</sup> cm <sup>2</sup> /s) for the free guests and free <b>76</b> ·24HCl in D <sub>2</sub> O at 25 °C. ....	161
Table 6.3 Upfield shifts of the <i>tert</i> -butyl protons and the guest diffusion rates ( <i>D</i> , x 10 <sup>-6</sup> cm <sup>2</sup> /s) for the encapsulation of Boc-Asp-OH in <b>76</b> ·24HCl in D <sub>2</sub> O at 25 °C (pD 4.7, [ <b>76</b> ] = 0.21 mM).....	161
Table 6.4 <i>Q</i> and <i>K</i> <sub>n</sub> (M <sup>-1</sup> ) for the binding of <b>76</b> ·24HCl with Boc-Asp-OH (pD 4.7) and <i>p</i> -TsOH (pD 1.0) in D <sub>2</sub> O at 25 °C. ....	164
Table 6.5 Upfield shifts of the methyl protons and the guest diffusion rates ( <i>D</i> , x 10 <sup>-6</sup> cm <sup>2</sup> /s) for the encapsulation of <i>p</i> -TsOH in <b>76</b> ·24HCl in D <sub>2</sub> O at 25 °C (pD 1.0, [ <b>76</b> ] = 0.22 mM).....	165
Table 6.6 Buffer effect on the upfield shifts of the methyl protons for the encapsulation of <i>p</i> -TsOH in <b>76</b> ·24HCl in D <sub>2</sub> O at 25 °C ([ <i>p</i> -TsOH] = 0.13 mM, [ <b>76</b> ] = 0.22 mM).....	165
Table 6.7 Upfield shifts of the methyl protons for the encapsulation of 4-MUP (monosodium salt) in <b>76</b> ·24HCl in D <sub>2</sub> O at 25 °C (pD 4.2, [ <b>76</b> ] = 0.24 mM).....	167
Table 6.8 Line width (LW) of the guest methyl protons in the encapsulation of Boc-Asp-OH (pD 4.7), <i>p</i> -TsOH (pD 1.0) and 4-MUP (pD 4.2, sodium salt) in <b>76</b> ·24HCl in D <sub>2</sub> O at 25 °C ([ <b>76</b> ] = 0.22 mM). ....	170

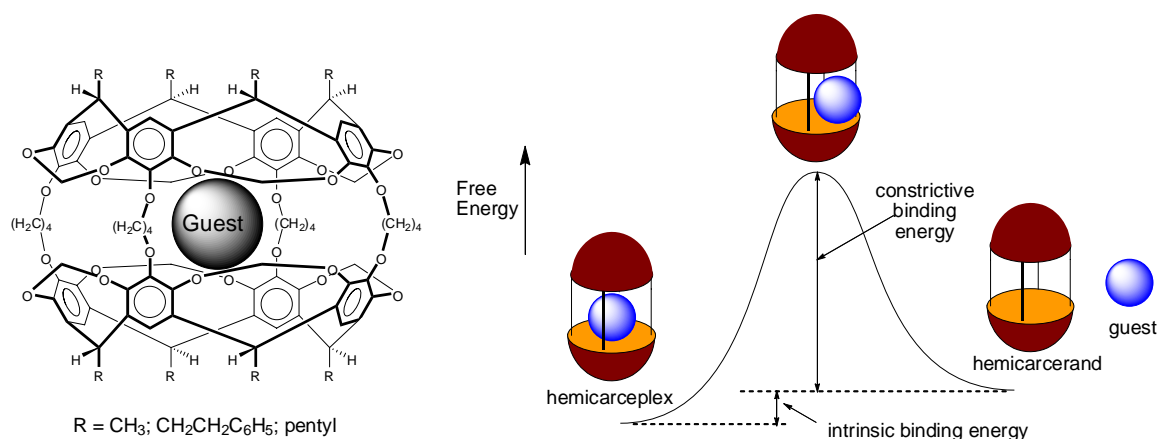


## Chapter 1 General introduction

Molecular recognition lies at the heart of most biological phenomena. One example is the specific, non-covalent interaction between receptor molecules and substrates.<sup>[1]</sup> Non-covalent interactions are also important in numerous other biological processes, such as enzyme catalysis, molecular transport and gene expression. In order to understand the complex binding events underlying these biological processes, organic chemists have designed artificial molecular systems to mimic the binding behavior and function of their biological counterparts.<sup>[2]</sup> For example, host molecules and assemblies have been constructed and used to study the weak intermolecular forces that are associated with the binding of organic guest molecules. These studies have posed further interesting questions related to the chemical reactivity of the guest molecule after its binding inside the space-restricted environment of the host's binding site.<sup>[3]</sup> In the past thirty years, numerous novel host compounds have been synthesized and their structures have been elucidated.<sup>[4]</sup>

Molecular container compounds are a new type of host molecules that were developed by Donald J. Cram.<sup>[5]</sup> They are spherical, hollow molecules with inner cavities, which can typically accommodate one guest molecule (Figure 1.1). The molecular container shown in Figure 1.1 has a cavity volume of  $\sim 200 \text{ \AA}^3$  and allows for the encapsulation of one organic guest molecule, such as benzene or even naphthalene. These host-guest complexes are usually stable at room temperature for months. Intrinsic binding energy as well as constrictive binding energy contribute to these unusually high complex stabilities (Figure 1.1). Steric effects, increased host conformational energy (gating) and changes in





**Figure 1.1** Molecular container complex and energy profile for hemicarceplex decomplexation.

the solvation energy as the guest passes through a size-restricted opening in the host shell contribute to the magnitude of constrictive binding energy.<sup>[6]</sup> Due to their unique properties, molecular container compounds are of great interest as nanoreactors,<sup>[7a-b]</sup> for drug delivery,<sup>[7c]</sup> separation technology,<sup>[7d]</sup> and photoinduced electron transfer.<sup>[7e]</sup>

Cavitands are the building blocks for closed-shell molecular containers. They are bowl-shaped molecules with rigid concave surfaces.<sup>[4a]</sup> They are synthesized by covalently bridging the upper rim of resorcinarenes. In cavitands, complementary organic guest molecules can bind inside the cavity and decomplexation occurs with little or no steric hindrance.<sup>[8]</sup> Carcerands are synthesized by covalently connecting two hemispherical cavitands together using short spacer groups.<sup>[9]</sup> Solvent molecules or other small solutes template the reaction and the shell closure. The encapsulated guests in these carceplexes cannot leave the cavity without the breaking covalent bonds in the host shell.

Hemicarcerands, alternatively, have larger portals compared to carcerands and allow for the encapsulation of one guest molecule.<sup>[10]</sup> These hemicarceplexes are stable at ambient temperature and can be purified and characterized by routine analytical techniques. However, the guest molecule can be released at elevated temperature. Hemicarcerands have become a new powerful tool for physical organic chemists to stabilize short-lived reactive intermediates and to investigate their properties, under ordinary working conditions.<sup>[11]</sup> Hemicarcerands have also been used to encapsulate small drug molecules, such as amantadine.<sup>[12]</sup>

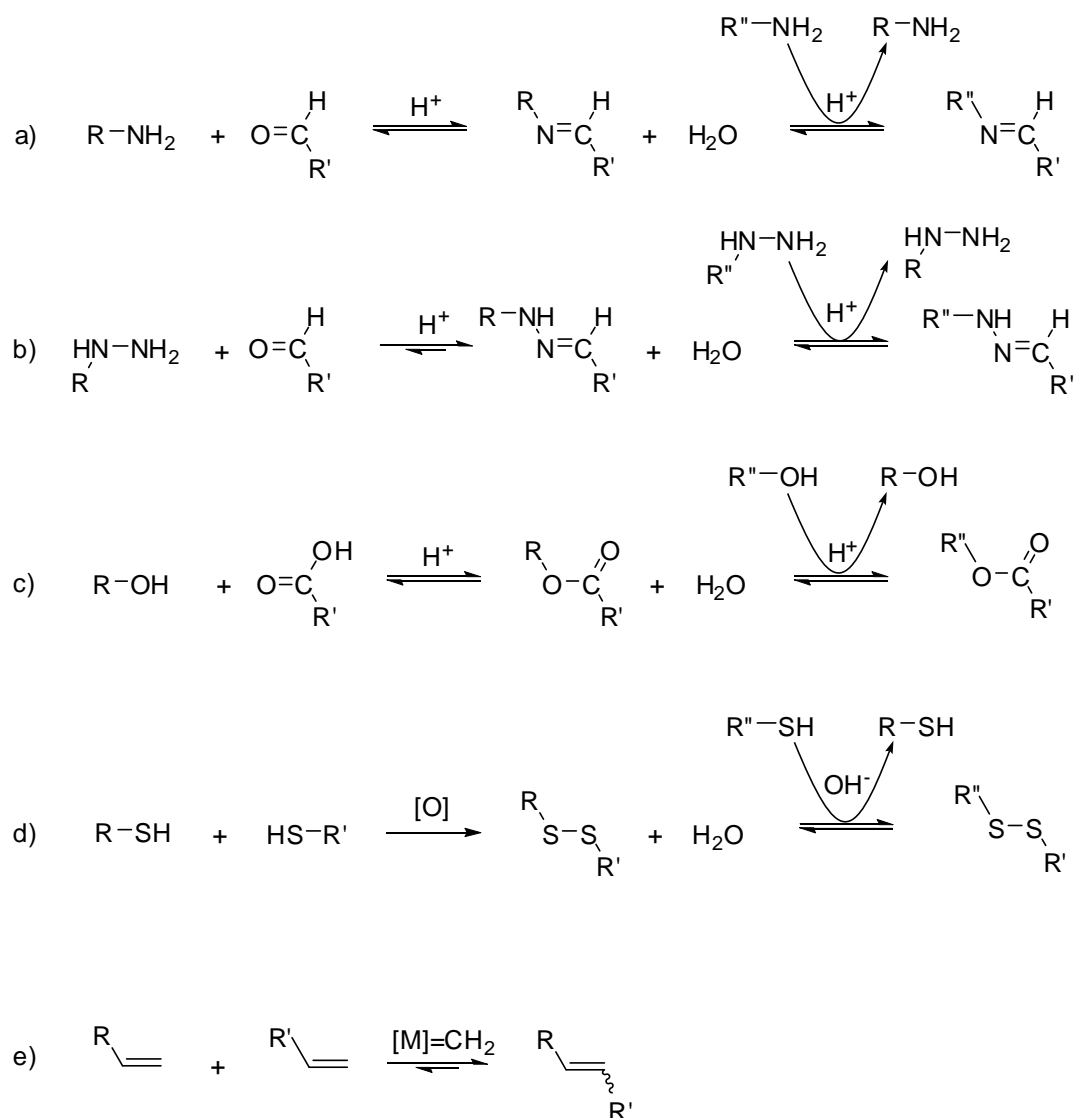
In Chapter 2, I will show that, by applying the concept of reactive intermediate stabilization by incarceration, the otherwise fleeting fluorophenoxycarbene becomes stable at room temperature inside a hemicarcerand. As a result of its high stability, the spectroscopic properties, the inner phase geometry and the reactivities of this singlet carbene could be investigated all under ordinary working conditions.

Some applications for container molecules require much larger cavity volumes. For example, in order to encapsulate small drug molecules or pesticides, most of which have molecular weights of 300 – 400 Da, a cavity volume of  $\sim 1 \text{ nm}^3$  is needed. The delivery of biomacromolecules, such as peptides, proteins or oligonucleotides requires an even larger cavity volume. Nanometer-sized molecular capsules have been successfully assembled in high yield through noncovalent interactions, such as hydrogen bonding, ion pairing, metal coordination and hydrophobic effect.<sup>[4c-e]</sup> Compared to these noncovalent capsules, covalent capsules have considerably higher stability and are easier to functionalize.

However, covalent synthesis of molecular nanocapsules remains challenging. Several multi-step syntheses of covalent nanocapsules composed of three, five or six cavitands have been reported by the groups of J. C. Sherman and M. Sherburn, but gave the nanocapsules only in relatively low overall yield.<sup>[13]</sup>

Dynamic covalent chemistry provides an opportunity to prepare nanocapsules with high yield in a single step from multiple small building blocks. Dynamic covalent chemistry involves reversible chemical reactions that are under thermodynamic control.<sup>[14]</sup> The most important feature of this chemistry is that it introduces “proof-reading” and “error correction” mechanisms into the synthesis. Due to their reversibility, covalent bonds form and reopen until the correct, most stable bonds are present. Therefore, the designed product, here a nanocapsule, will eventually form as long as it is the thermodynamically most stable product. Imines, hydrazones, esters, disulfides and olefins, with an appropriate catalyst, are among the most frequently used reversible bonds (Scheme 1.1).<sup>[15]</sup> The reversibility of the imine bond formation has been used by Stoddart and Cram to study dynamic hemicarcerands and hemicarceplexes.<sup>[16]</sup>

In Chapter 3 and 4, I will show that a series of nanocontainer molecules can be synthesized in high yield and simplicity through reversible imine bond formation. Structurally different cages with different assembly numbers can be prepared from one set of building blocks by varying the solvent, which plays a key role in tuning the relative population of these nanocontainer species. Encapsulation studies with tetraalkylammonium salts have revealed interesting molecular recognition properties of



**Scheme 1.1** Reversible covalent bonds: a) imine formation and exchange; b) hydrazone formation and exchange; c) ester formation and exchange; d) disulfide exchange; and e) olefin metathesis.

these nanocontainer molecules. Dynamic combinatorial libraries of polyimino nanocapsules, discussed in Chapter 5, can be constructed in the presence of multiple diamino building blocks. In Chapter 6, I will discuss the synthesis of water-soluble nanocontainer molecules. Binding studies in water have revealed that these containers

encapsulate negatively charged organic compounds.

## References

1. E. V. Anslyn, D. A. Dougherty, *Modern Physical Organic Chemistry*, University Science Books, USA, **2006**, p. 207-222.
2. F. Diederich, *Angew. Chem. Int. Ed.* **2007**, *46*, 68.
3. D. Fiedler, D. H. Leung, R. G. Bergman, K. N. Raymond, *Acc. Chem. Res.* **2005**, *38*, 349.
4. a) D. J. Cram, *Science*, **1983**, *219*, 1177; b) D. J. Cram, *Nature*, **1992**, *356*, 29; c) L. R. MacGillivray, J. L. Atwood, *Nature*, **1997**, *389*, 469; d) B. Olenyuk, J. A. Whiteford, A. Fechtenkotter, P. J. Stang, *Nature* **1999**, *398*, 796; e) M. Yoshizawa, M. Tamura, M. Fujita, *Science* **2006**, *312*, 251.
5. D. J. Cram, J. M. Cram, *Container Molecules and their Guests*, Royal Society of Chemistry, Cambridge, UK, **1994**.
6. A) K. N. Houk, K. Nakamura, C. Sheu, A. E. Keating, *Science*, **1996**, *273*, 627; b) J. Yoon, D. J. Cram, *Chem. Commun.* **1997**, 1505.
7. A) R. Warmuth, *J. Incl. Phenom.* **2000**, *37*, 1; b) A. Lutzen, *Angew. Chem. Int. Ed.* **2005**, *44*, 1000; c) C. L. D. Gibb, B. C. Gibb, *J. Am. Chem. Soc.*, **2004**, *126*, 11408; d) S. T. Mough, J. C. Goeltz, K. T. Holman, *Angew. Chem. Int. Ed.* **2004**, *43*, 5631; e) C. Pagba, G. Zordan, E. Galoppini, E. L. Piatnitski, S. Hore, K. Deshayes, P. Piotrowiak, *J. Am. Chem. Soc.*, **2004**, *126*, 9888.
8. D. J. Cram, S. Karbach, H.-E. Kim, C. B. Knobler, E. F. Maverick, J. L. Ericson, R. C. Helgeson, *J. Am. Chem. Soc.*, **1988**, *110*, 2229.
9. J. A. Bryant, M. T. Blanda, M. Vincenti, D. J. Cram, *J. Am. Chem. Soc.* **1991**, *113*, 2167.
10. R. Warmuth, J. Yoon, *Acc. Chem. Res.* **2001**, *34*, 95.
11. a) D. J. Cram, M. E. Tanner, R. Thomas, *Angew. Chem. Int. Ed. Engl.* **1991**, *30*, 1024; b) R. Warmuth, *Angew. Chem. Int. Ed. Engl.* **1997**, *36*, 1347.
12. M. L. C. Quan, D. J. Cram, *J. Am. Chem. Soc.* **1991**, *113*, 2754.
13. a) D. A. Makeiff, J. C. Sherman, *Chem. Eur. J.* **2003**, *9*, 3253; b) E. S Barrett, J. L. Irwin, A. J. Edwards, M. S. Sherburn, *J. Am. Chem. Soc.* **2004**, *126*, 16747; c) D. A. Makeiff, J. C. Sherman, *J. Am. Chem. Soc.* **2005**, *127*, 12363.
14. S. J. Rowan, S. J. Cantrill, G. R. L. Cousins, J. K. M. Sanders, J. F. Stoddart, *Angew. Chem. Int. Ed.* **2002**, *41*, 898.

15. P. T. Corbett, J. Leclaire, L. Vial, K. R. West, J-L Wietor, J. K. M. Sanders, S. Otto, *Chem. Rev.* **2006**, *106*, 3652.
16. S. Ro, S. J. Rowan, A. R. Pease, D. J. Cram, J. F. Stoddart, *Org. Lett.* **2000**, *2*, 2411.

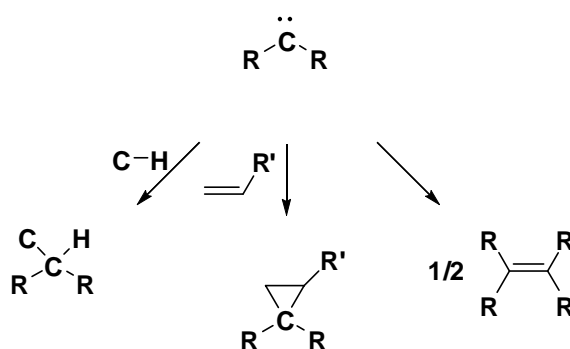
## Chapter 2 Room-temperature stabilization of fluorophenoxycarbene inside a hemicarcerand

(This work was done in collaboration with Prof. R. A. Moss and Prof. R. R. Sauers.)

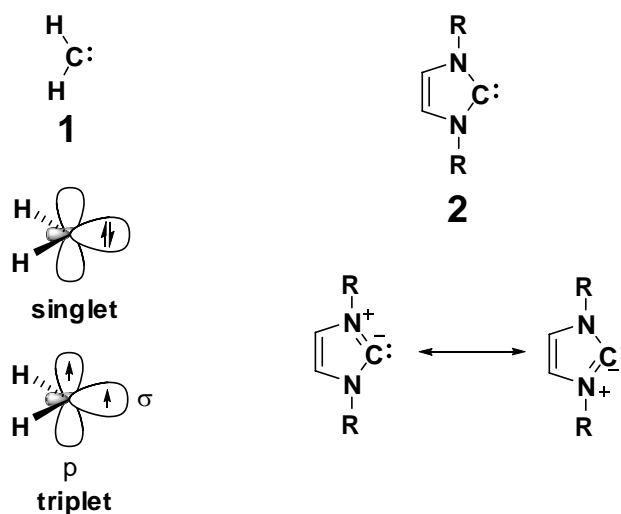
### 2.1 Introduction

Carbenes are important reactive intermediates in many organic transformations (Scheme 2.1).<sup>[1]</sup> Methylene (:CH<sub>2</sub>) **1**, which is the simplest carbene, is an electron deficient fleeting species. Carbenes can have two spin states (Scheme 2.2). In triplet carbenes, two unpaired electrons individually occupy the  $\sigma$  and p orbitals. In singlet carbenes, both electrons pair in the  $\sigma$  orbital. The triplet is the ground state of methylene with a singlet-triplet energy splitting of  $\Delta E_{ST} \sim 9$  kcal/mol.<sup>[2a]</sup> The stability and reactivity of carbenes can be modulated via substituents.<sup>[2]</sup> Heterocyclic carbenes have singlet ground states and are stabilized by electron donating substituents. For example, the Arduengo carbene **2** is stable at room temperature (Scheme 2.2).<sup>[3]</sup> Spectroscopic investigation of more reactive carbenes have been accomplished by matrix isolation.<sup>[4]</sup> Hemicarcerands have also been widely used to stabilize reactive intermediates in their inner phase.<sup>[5]</sup> They stabilize reactive intermediates by surrounding the reactive guest, which will neither be able to dimerize, nor to react with reactants in the bulk that are too large to pass through holes in the host shell. Using this approach, the spectroscopic properties and reactivities of cyclobutadiene,<sup>[6a]</sup> benzyne<sup>[6b]</sup> and other highly reactive species have been investigated in some cases even at room temperature for the first time (Figure 2.1). A further extension of this approach would be the stabilization of an otherwise fleeting carbene by incarceration.

In an earlier investigation by R. Warmuth and M. A. Marvel, phenylcarbene was generated inside a hemicarcerand and almost quantitatively inserted into inward pointing C-H bonds of the surrounding hemicarcerand even at 77 K.<sup>[7a]</sup> In an extension of this work, C. Kemmis and R. Warmuth estimated a life time of  $t_{1/2} \sim 4$  min at 77 K for incarcerated phenylcarbene, which is too short for its NMR spectroscopic observation at elevated temperature.<sup>[7b]</sup>

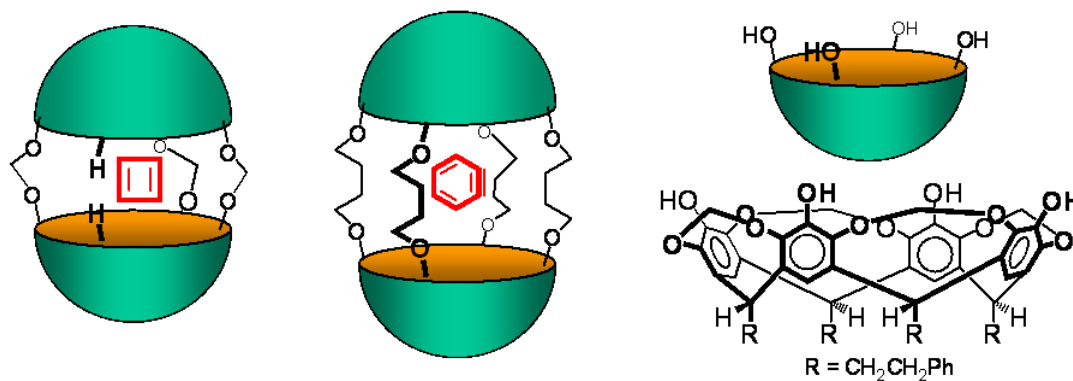


**Scheme 2.1** Reactions of carbenes, a) C-H insertion, b) C=C addition, c) dimerization.



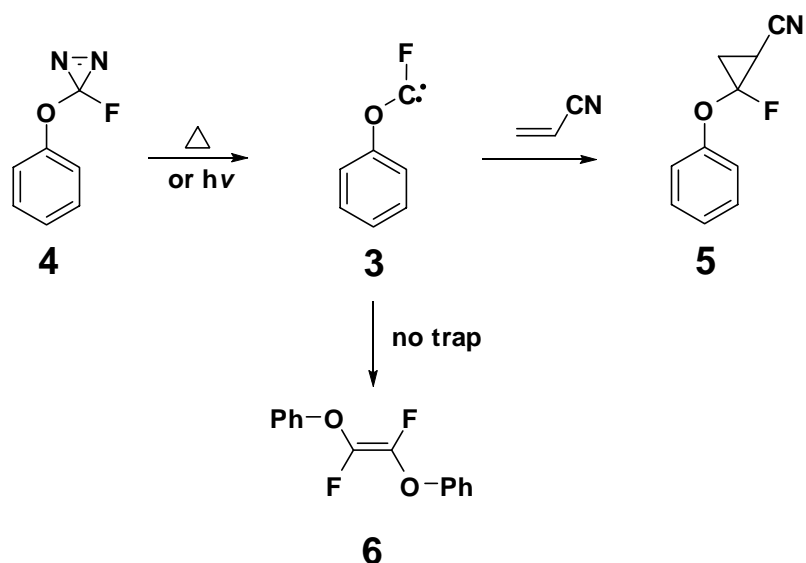
**Scheme 2.2** Spin states of carbenes and Arduengo carbene, R = adamantyl<sup>[3]</sup>.





**Figure 2.1** Incarcerated cyclobutadiene and *o*-benzyne.

For my study, I choose fluorophenoxycarbene **3**, which can be generated via thermolysis (50 °C) or photolysis of 3-fluoro-3-phenoxydiazirine **4** (Scheme 2.3).<sup>[8]</sup> Fluorophenoxycarbene **3** is a singlet carbene. It is intrinsically stabilized by the electron donating substituents, to such an extent, that it doesn't insert into C-H bonds. However, if generated in the presence of electron-poor or rich alkenes, it affords the corresponding cyclopropanes. In the absence of an alkene trap, it dimerizes in the sub-millisecond time scale. CPK models show that fluorophenoxycarbene **3** and its diazirine precursor **4** have an appropriate size and shape to fit into hemicarcerand **7** with four  $-\text{O}(\text{CH}_2)_4\text{O}-$  linkers. Furthermore, fluorophenoxycarbene carries an NMR sensitive fluorine "label", which allows its detection without interference of the host and also provides insight into the electronic properties of this carbene. All these considerations made fluorophenoxycarbene the ideal target for my investigation.



**Scheme 2.3** Generation of fluorophenoxycarbene and its subsequent reactions.

In this chapter, the room temperature stabilization of the otherwise fleeting fluorophenoxycarbene inside a hemicarcerand will be described. As a result of its high stability, the spectroscopic properties of this singlet carbene, its inner phase geometry and reactivities could be investigated all under ordinary conditions.

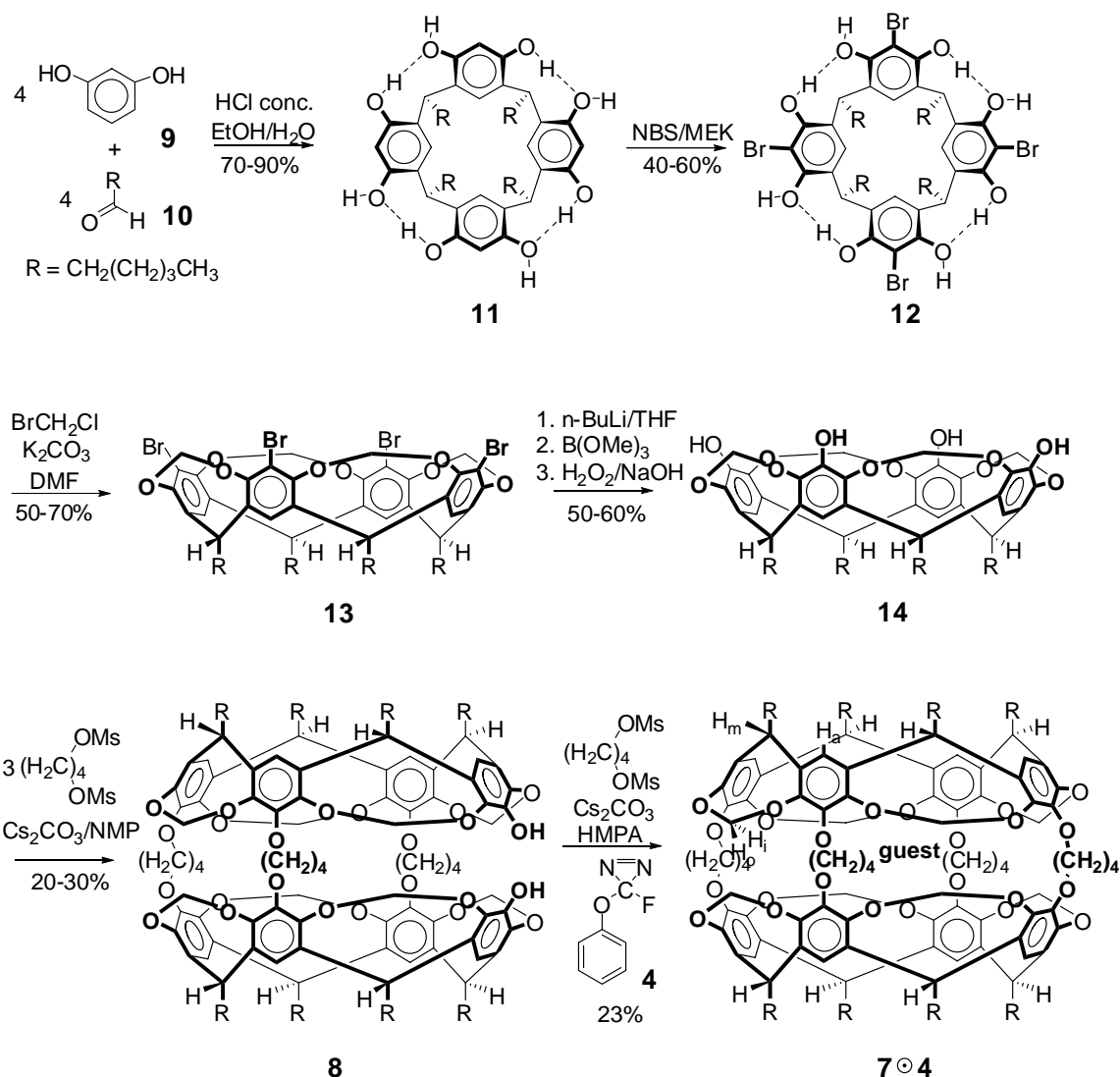
## 2.2 Results and discussion

### 2.2.1 Synthesis of fluorophenoxydiazirine hemicarceplex

The synthesis of the fluorophenoxydiazirine hemicarceplex **7**⊙**4** is outlined in Scheme 2.4. Hemicarcerand diol **8** was synthesized starting from resorcinol **9** and hexanal **10**.<sup>[9,10]</sup> The condensation reaction of resorcinol and hexanal gave resorcin[4]arene **11** in high yield. Subsequent bromination with NBS yields tetrabromooctol **12**. Adjacent resorcinol units in the tetrabromooctol were bridged by methylene groups to form tetrabromocavitand **13**. Bromine-lithium exchange followed by trapping the intermediate

tetralithiocavitand with trimethyl borate and subsequent peroxidation gave the tetrol cavitand **14**. The diol hemicarcerand **8** was prepared from the tetrol cavitand by linking two cavitands together by three tetramethylene bridges.

The known fluorophenoxycarbene precursor 3-fluoro-3-phenoxydiazirine (**4**)<sup>[8]</sup> was developed by the group of Prof. R. Moss and was provided by Dr. G. Chu of Prof. R. Moss group and was incarcerated. Diol **8** was stirred with Cs<sub>2</sub>CO<sub>3</sub>, MsO(CH<sub>2</sub>)<sub>4</sub>OMs (Ms = MeSO<sub>2</sub>) and excess 3-fluoro-3-phenoxydiazirine (**4**) in HMPA (hexamethyl phosphoramide) for six days under nitrogen in the dark at room temperature. The synthesis of the hemicarceplex is a templated reaction. By choosing HMPA as solvent, only **4** can serve as template and is incarcerated by shell closure. The crude product was purified by column chromatography and repurified by HPLC. The diazirine hemicarceplex **7**⊙**4** was obtained in 23% yield based on diol **8**.



**Scheme 2.4** Synthesis of diol hermicarcerand **8** and diazirine hemicarceplex **7⊙4**.

Spectroscopic studies support the presence of one guest **4** inside the inner phase of **7**. The <sup>1</sup>H NMR spectrum of **7⊙4** (Figure 2.2 a) clearly shows a set of upfield shifted signals for the phenyl protons of **4** at  $\delta$  = 6.33, 5.09 and 3.02 ppm ( $\Delta\delta$  = 0.89, 2.27 and 4.16 ppm), which is due to the shielding environment encountered by **4** after encapsulation. Upfield shifts  $\Delta\delta$  of this magnitude would not be expected, if the guest is bound to the outside of hemicarcerand **7** and are consistent with **4** being in the inner phase. Furthermore, sets of

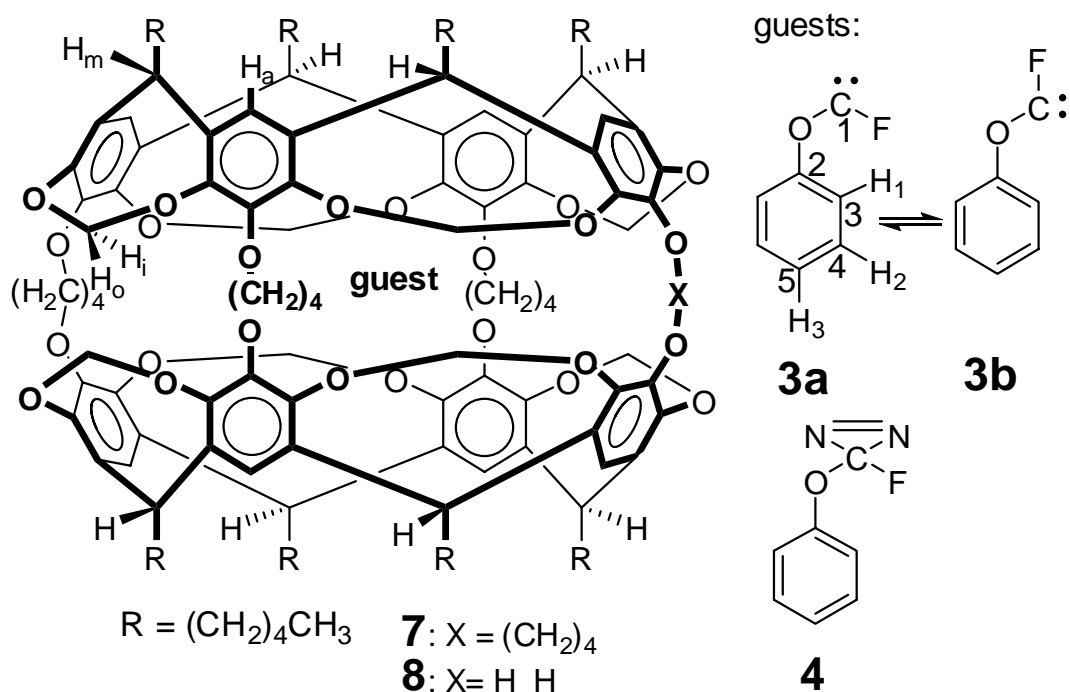
two multiplets, each integrating for four protons, are observed for the aryl protons  $H_a$ , the spanner protons  $H_i$ ,  $H_o$  and the methine protons  $H_m$ . This and the upfield shift of the guest suggest that the guest is aligned along the  $C_4$  axis of the host and that the guest tumbles slowly around the equatorial axes on the NMR time scale. In the  $^{19}\text{F}$  NMR spectrum, the fluorine atom of the guest in **7**⊙**4** resonates at  $\delta_F = -117.3$  ppm, which is slightly upfield shifted compared to free **4** ( $\delta_F = -116$  ppm).<sup>[8]</sup> The  $^{13}\text{C}$  NMR spectrum of **7**⊙**4** is also consistent with its structure. C1 of encapsulated **4** (see Chart 2.1) resonates at  $\delta_C = 86.9$  ppm ( $^1J_{CF} = 270$  Hz) and that of free **4** at  $\delta_C = 86.7$  ppm ( $^1J_{CF} = 271$  Hz).<sup>[8]</sup> The low resolution FAB-MS of **7**⊙**4** gives three major peaks at  $m/z = 2129$  (30%) for the molecular ion  $[\text{M}]^{++}$ , at  $m/z = 2102$  (15%) for  $[\text{M}-\text{N}_2+1]^\oplus$  and at  $m/z = 1977$  (100%) for the empty host  $[\text{M}-\text{4}]^{++}$ . The latter ion results from hemicarceplex dissociation after ionization and is usually observed for hemicarceplexes.

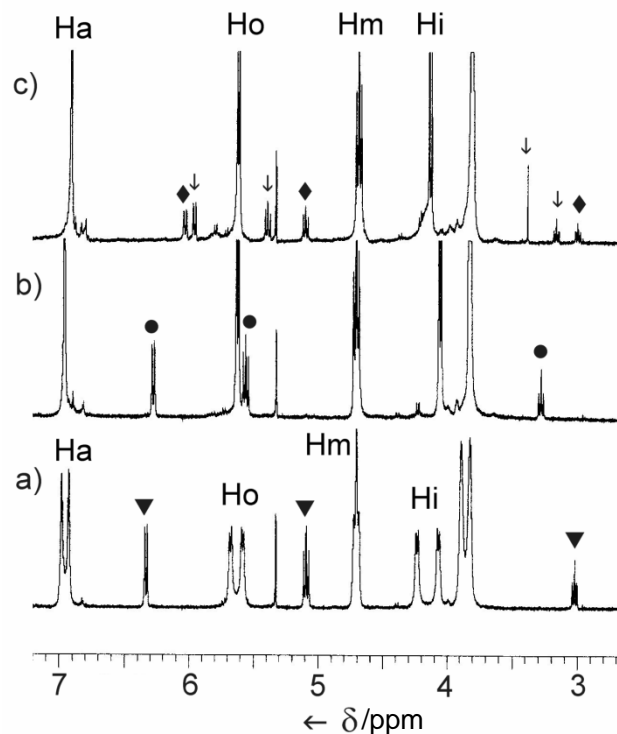
## 2.2.2 Photolysis of fluorophenoxydiazirine hemicarceplex

Hemicarceplex **7**⊙**4** was photolyzed in  $\text{CD}_2\text{Cl}_2$  at 77 K ( $\lambda > 320$  nm) in order to generate the expected carbene. The solution of **7**⊙**4** was placed in an NMR tube and was degassed by four freeze-pump-thaw cycles to remove oxygen. Then, the tube was sealed off under vacuum. The sample was cooled in a partially silvered dewar flask filled with liquid nitrogen (77 K). The sample tube was placed in the light beam such that the bottom part of the frozen solution was in the focal point of the light beam (4-5 mm diameter). Then, the frozen sample was irradiated with the output of an Oriel Hg Power-Max lamp operating at 200 W. A 10 cm water-filter and a 320 nm cutoff filter (WG 320) were placed between the lamp and the sample. First, the front of the sample was irradiated for

10 minutes, followed by 10 minutes of irradiation after the sample tube had been turned by 180°. After each 2x10 minute irradiation period, the sample was moved downwards in 5 mm steps until all of the frozen solution had been irradiated (typically 6-7 vertical steps).

Chart 2.1





**Figure 2.2** Partial  $^1\text{H}$  NMR spectra (400 MHz,  $\text{CD}_2\text{Cl}_2$ , 25  $^\circ\text{C}$ ) of hemicarceplex **7**⊙**4**: a) before and b) after photolysis ( $\lambda > 320$  nm, 77 K, 2 h); c) same solution as b) after complete decomposition. Signals assigned to protons of incarcerated **4** (▼), **3** (●), **15** (↓), and **16** (◆) are marked.  $\text{H}_a$ ,  $\text{H}_o$ ,  $\text{H}_m$ , and  $\text{H}_i$  are protons of host **7**.

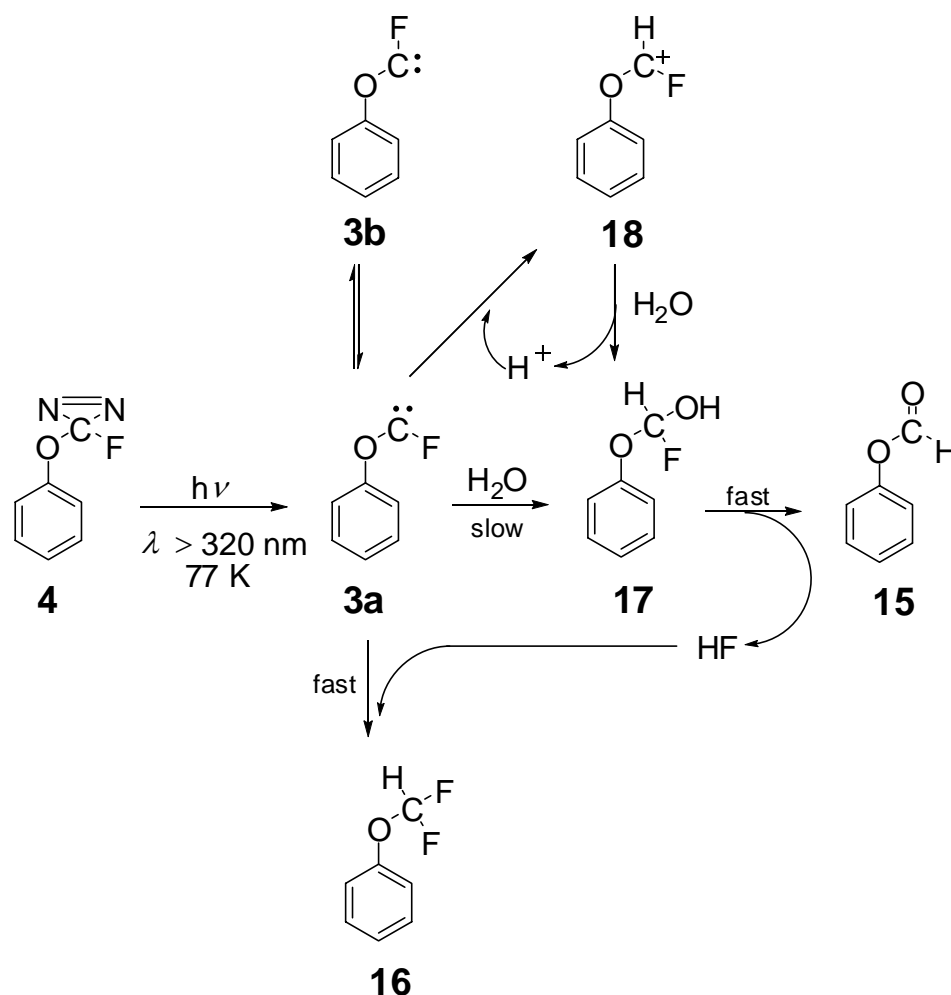
### 2.2.3 Spectroscopic studies of fluorophenoxycarbene and its inner phase reactivity

A new hemicarceplex was formed after photolysis in 93% yield (Figure 2.2 b). The newly generated species is assigned to fluorophenoxycarbene hemicarceplex **7**⊙**3**. The yield was determined from the integral of the guest **3** proton H1 ( $\delta = 6.28$  ppm), using the signal assigned to the host's methyl groups ( $\delta = 0.94$  ppm) as an internal standard. The exclusive presence of fluorophenoxycarbene **3** inside **7** is based on the following observations.

First, the UV absorption of the host **7** decreases sharply above 275 nm. Therefore the  $^1\text{H}$  NMR spectra recorded before and after photolysis (Figure 2.2 a, b) must be due to the photolysis of the encapsulated carbene precursor **4**. Before photolysis, the rotations of **4** around the equatorial axes of **7** are frozen (Figure 2.2 a).<sup>[10]</sup> Therefore there are sets of two signals (integration 4 H : 4 H) for each of host's most characteristic protons ( $\text{H}_a$ ,  $\text{H}_o$ , and  $\text{H}_i$ ). This means that the northern hemisphere of **7** is not equivalent to the southern hemisphere. After photolysis, the guest molecule **3** becomes smaller and it tumbles faster around the equatorial axes, which results in the simplification of the host signals (Figure 2.2 b).

Second, the newly generated hemicarceplex **7**⊙**3** slowly decomposed to form two new, stable hemicarceplexes in approximately equal amount: the phenyl formate hemicarceplex **7**⊙**15** and the phenyl(difluoromethyl) ether hemicarceplex **7**⊙**16** (Figure 2.2 c and Scheme 2.5). Both are the expected water trapping products of **7**⊙**3**. The water comes from residual water dissolved in  $\text{CD}_2\text{Cl}_2$ . These two hemicarceplexes were separated by semi-preparative HPLC and were further characterized. The identity of the first hemicarceplex **7**⊙**15** is supported through independent synthesis. It shows identical NMR spectroscopic properties as authentic **7**⊙**15** prepared by heating phenyl formate into empty hemicarcerand **7**. Hemicarceplex **7**⊙**15** was further characterized by FAB-MS, which shows two major peaks at  $m/z = 2100 [\text{M}+1]^+$  and  $1978 [\text{M}-15+1]^+$ . The second hemicarceplex **7**⊙**16** was identified by comparison of the NMR spectroscopic properties of the encapsulated **16** with those of free **16**. Almost identical chemical shifts and coupling constants were observed in  $^{19}\text{F}$  NMR spectroscopic studies for both molecules.

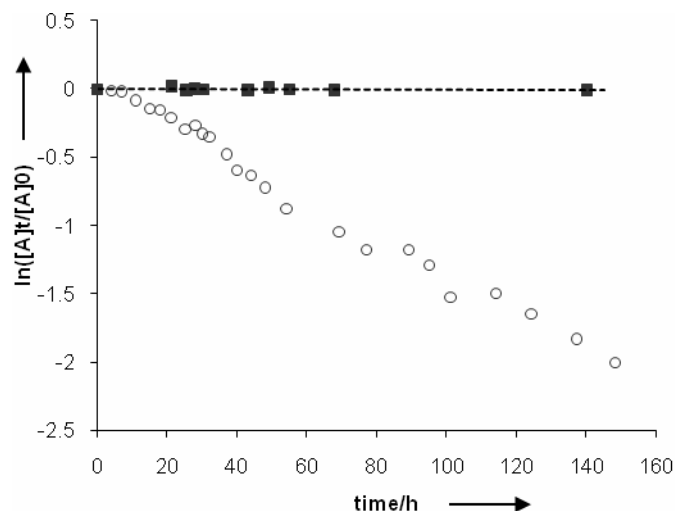




**Scheme 2.5** Photolysis of **4** and reactions of **3** in the inner phase of **7**.

In the  $^{19}\text{F}$  NMR spectrum, the  $^{19}\text{F}$  of the guest inside hemicarceplex **7**⊙**16** resonates at  $\delta_{\text{F}} = -82.9 \text{ ppm}$  ( $^2J_{\text{HF}} = 73.3 \text{ Hz}$ ) (Figure 2.4) while that of free **16** resonates at  $\delta_{\text{F}} = -81.39 \text{ ppm}$  ( $^2J_{\text{HF}} = 74 \text{ Hz}$ ).<sup>[11]</sup> In addition, almost identical H-F coupling constants were measured for the free and encapsulated **16**. FAB-MS also gives consistent results for this compound. There are two major peaks at  $m/z = 2122 [\text{M}+1]^{\oplus}$  and  $1978 [\text{M}-\mathbf{16}+1]^{\oplus}$ .

Decomposition of **7**⊙**3** is due to the reaction of **3** with water to form **7**⊙**15** and HF. The

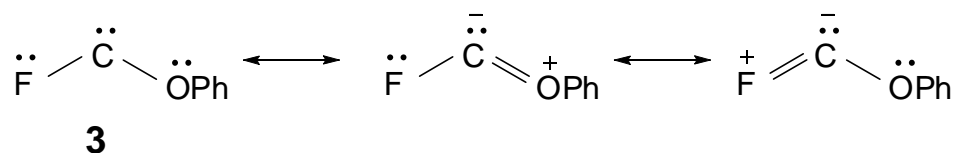


**Figure 2.3** Concentration change of **7⊕3** vs. time ( $\text{CD}_2\text{Cl}_2$ , 25 °C) in the presence (■) and absence (○) of pyridine- $d_5$ . The amount of **7⊕3** was estimated from the integral of proton H1 of the guest **3**.

latter reacts with another **7⊕3** to form **7⊕16**. Further investigations showed that the inner phase decomposition of fluorophenoxycarbene **3** is catalyzed by acid. The proposed catalytic cycle is shown in Scheme 2.5 (**3a** → **18** → **17** → **15**). The catalytic amount of acid probably comes from traces of DCl in  $\text{CD}_2\text{Cl}_2$ . However, if the acid was neutralized by addition of pyridine- $d_5$  before photolysis, the encapsulated carbene **3** survived for six days without decomposition (Figure 2.3). In the hydrophobic inner phase of **7**, water itself is not acidic enough to catalyze the reaction, presumably because of the high energetic cost of charge separation to form **18OH**<sup>+</sup>.

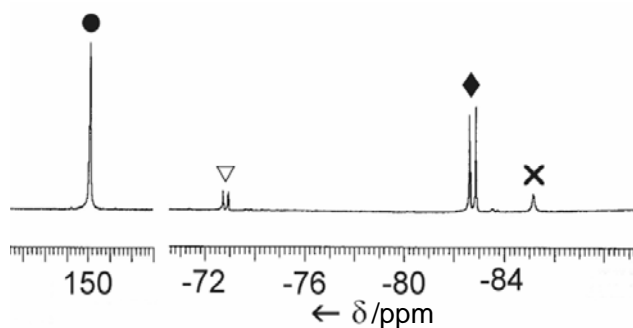
Several factors contribute to the high stability of this incarcerated carbene **3**.

1. Delocalization of fluorine and oxygen lone pair electrons into the carbene empty p orbital significantly stabilizes this reactive carbene (Scheme 2.6).<sup>[8]</sup>



**Scheme 2.6** Resonance stabilization of **3**.

Moss and coworkers defined **3** as an ambiphilic carbene based on experimental results and calculations. In cyclopropanations, ambiphilic carbenes can behave as either electrophile or nucleophile, depending on the specific alkene substituents.<sup>[12]</sup> The delocalization effect also retards the reaction of **3** with the electron-rich host **7**, including the reaction with the aromatic rings or the acetal groups of **7**. Carbene C-H insertion has been observed for more reactive carbene hemicarceplex systems.<sup>[13]</sup> The delocalization effect can be seen in the <sup>19</sup>F NMR spectroscopic studies of **7**⊙**3**. The <sup>19</sup>F NMR spectrum of **7**⊙**3** reveals that the fluorine center of **3** is fairly electron-positive, which was



**Figure 2.4** <sup>19</sup>F NMR spectrum (282.232 MHz, CD<sub>2</sub>Cl<sub>2</sub>, 25 °C) of partially decomposed **7**⊙**3**, referenced to CFC<sub>l</sub><sub>3</sub>. Signals assigned to <sup>19</sup>F of incarcerated **3** (●), **16** (◆) and two further photoproducts of **7**⊙**4** (▽, ×) are marked.

concluded from the high  $^{19}\text{F}$  chemical shift  $\delta_{\text{F}} = 149.8$  ppm (Figure 2.4).<sup>[14]</sup> Also the unusually large fluorine-carbenic carbon coupling constant of the incarcerated guest **3** ( $\delta_{\text{C}} = 285.7$  ppm,  $^1J_{\text{CF}} = 569$  Hz) supports this conclusion (Table 2.1).<sup>[14]</sup> Unusually large  $^1J_{\text{CF}}$  in F-substituted carbocations have been interpreted by Olah and coworkers with similar electron donation from the fluorine to the carbenium carbon.<sup>[14]</sup>

2. The surrounding host **7** prevents carbene **3** from dimerizing.<sup>[1]</sup> During the formation of hemicarceplex **7**⊙**4**, only one molecule of **4** can be encapsulated in each host **7** due to the limited space. On the other hand, the photochemically generated carbene **3** is too large to exit **7** at ambient temperature. Therefore, the possibility of carbene dimerization is excluded.

3. The hydrophobicity of the inner phase and its inability to “solvate” charged guests, strongly decrease the basicity of **3**, thus preventing its reaction with water in the bulk.

#### **2.3.4 Conformational analysis of fluorophenoxycarbene inside the inner phase of the hemicarcerand**

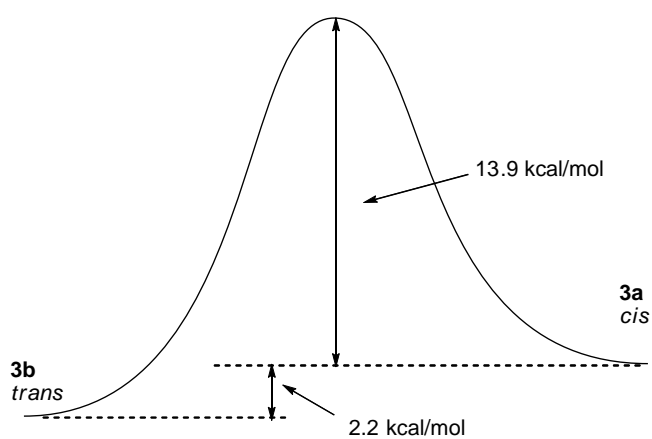
Gas phase DFT calculations (B3LYP/6-31G\*) carried out by Professor R. Sauers showed that the *trans*- conformation of **3** (**3b**) is more stable than the *cis*- conformation **3a** by  $\Delta H^{\circ} = 2.2$  kcal/mol (Scheme 2.7). Interestingly, a detailed NMR conformational analysis of incarcerated carbene **3** supports the opposite conformational preference inside hemicarcerand **7**.

**Table 2.1**  $^1\text{H}$ ,  $^{19}\text{F}$ , and  $^{13}\text{C}$  NMR chemical shifts of **3** (see Chart 2.1 for labeled structure), referenced to TMS or  $\text{CFCl}_3$ .

<i>Nuclei</i>	$\delta_{\text{expt}}$	$\delta_{\text{calc}}^{[a]}$		$\delta_{\text{corr}}$	
		<i>cis</i>	<i>trans</i>	<i>cis</i>	<i>trans</i>
H1	6.28	7.13	7.7		
H2	5.56	7.57	7.62		
H3	3.28	7.47	7.56		
F	149.8	179.1	159.4	159.1	141.1
C1	285.7	297.1	309.0	290.3	301.8
C2	148.0	158.3	159.6	156.0	157.3
C3	117.4	125.8	122.6	124.6	121.5
C4	129.9	133.1	134.1	131.6	132.6
C5	124.7	131.4	131.6	130.0	130.2

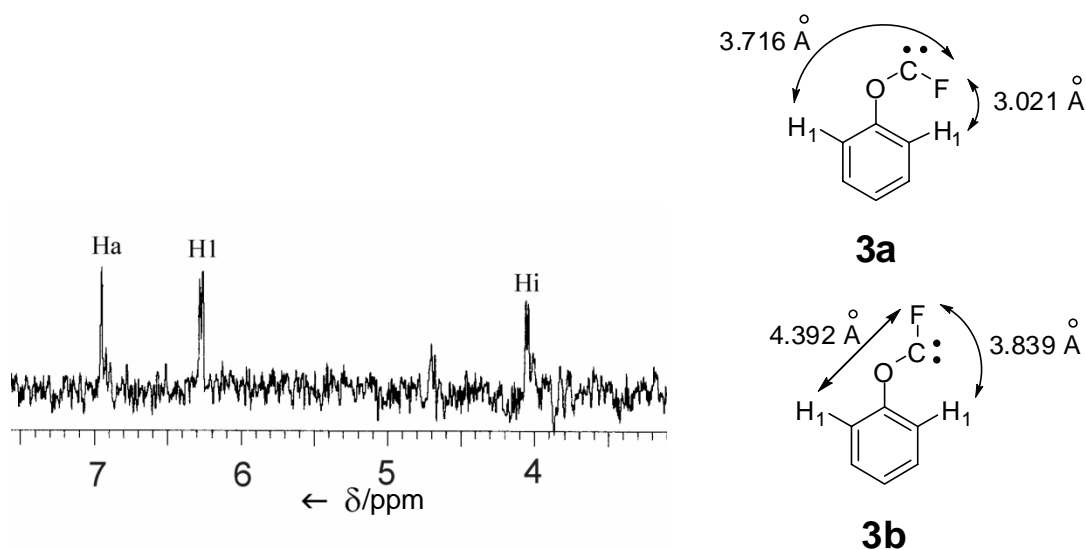
[a] GIAO chemical shift tensors (PBE1PBE/6-311G++(2d,p) relative to TMS ( $^1\text{H}$ ,  $^{13}\text{C}$ ) or  $\text{CFCl}_3$

( $^{19}\text{F}$ ). \*Calculations were carried out by Prof. R. Sauers.\*



**Scheme 2.7** Potential energy surface for the *cis-trans* equilibration of **3**.

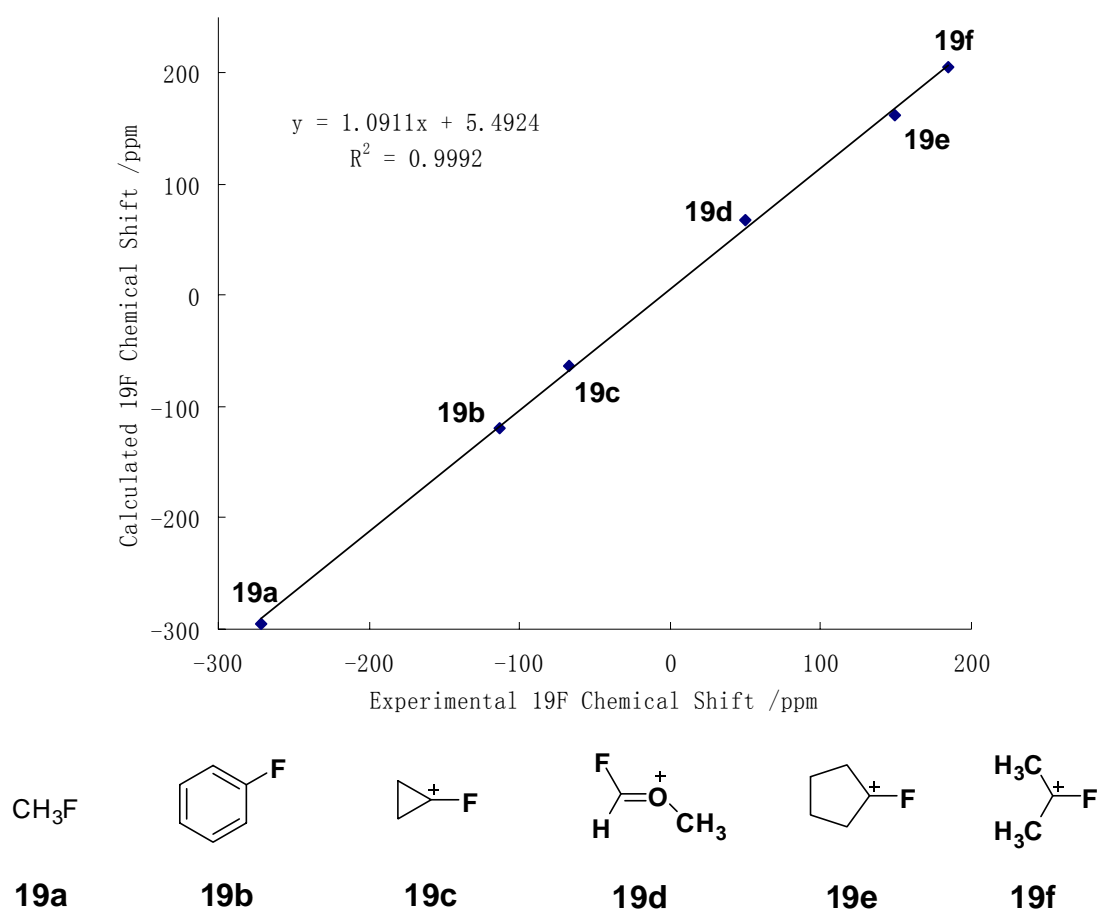
Heteronuclear hydrogen-fluorine NOE experiments of **7**⊙**3** showed that **3a** rather than **3b** is the predominant conformation in the inner phase of **7**. Typically an NOE is observed between two nuclei, if their internuclear distance  $r$  is within 4-5 Å. In this case, the intensity of the NOE is proportional to  $1/r^6$ .<sup>[15]</sup> For free **3**, the distances between H<sub>1</sub> and F are calculated to be 3.021 and 3.716 Å in **3a** while they are 3.839 and 4.392 Å in **3b** (Figure 2.5). A strong NOE interaction was observed between H<sub>1</sub> and fluorine atom for the hemicarceplex **7**⊙**3** (Figure 2.5). This strong H<sub>1</sub>-F NOE interaction most likely comes from **3a** instead of **3b**. Furthermore, strong intermolecular NOE interaction between H<sub>i</sub> of **7** and <sup>19</sup>F in **7**⊙**3** is also observed (Figure 2.5), which further supports the presence of **3a**, since such an NOE is not expected for **3b**. The preferred *cis*-conformation of **3** inside **7** agrees with conformational analyses of *n*-alkanes inside other molecular capsules, which show that coiled conformations are preferred to extended ones in the inner phase, if space is limited.<sup>[16]</sup> The observation of an equal intense NOE between H<sub>a</sub> of **7** and <sup>19</sup>F of **3** can also be explained with the *cis*-conformation, but may also indicate that a small population of **3b** can't be excluded (Figure 2.5). However, based on low temperature NMR studies (vide infra), less than ~5% of **3** are in the *trans*-conformation, if at all.



**Figure 2.5**  $^1\text{H}$ - $^{19}\text{F}$  NOE difference spectrum (399.971 MHz,  $\text{CD}_2\text{Cl}_2$ , 28 °C) of **7**⊙**3**.

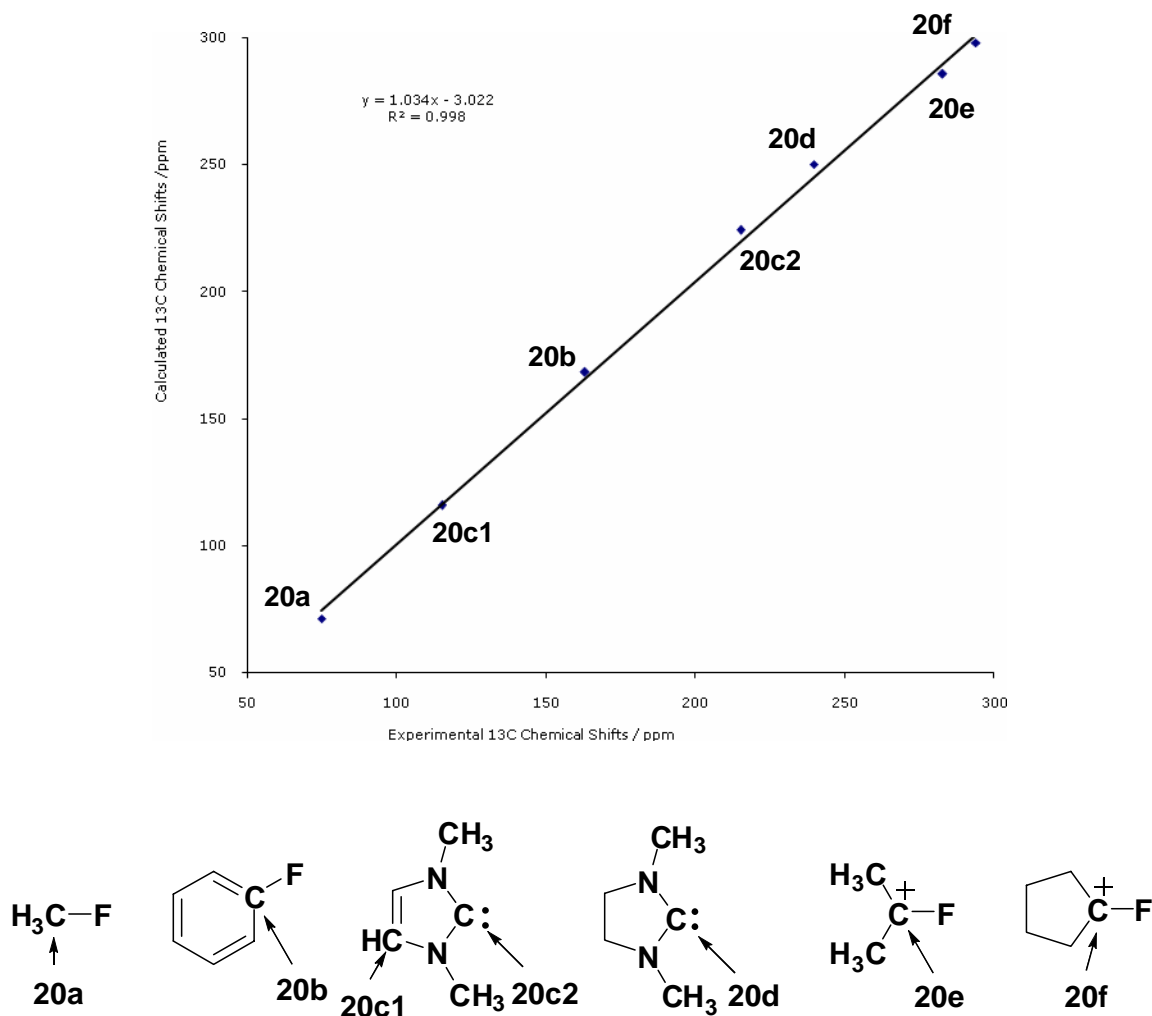
Comparison of the experimental  $\delta_{\text{F}}$  and  $\delta_{\text{C}}$  values of **3** with those predicted by chemical-shift calculations also supports that **3a** is the major isomer inside the inner phase of **7** (Table 2.1). DFT chemical shift calculations typically overestimate  $^{19}\text{F}$  and  $^{13}\text{C}$  shifts, which makes a precise prediction difficult. However, in a recent study, Olah and coworkers showed that the experimental  $\delta_{\text{F}}$  and  $\delta_{\text{C}}$  values of several F-substituted carbocations correlate linearly with those obtained from gauge-independent atomic orbital (GIAO) chemical-shift calculations.<sup>[17]</sup> Prof. R. Sauers showed that similar correlations are also observed when the experimental  $\delta_{\text{F}}$  and  $\delta_{\text{C}}$  values of  $\text{C}_6\text{H}_5\text{F}$ ,  $\text{CH}_3\text{F}$ , 1,3-dimethylimidazolidin-2-ylid-ene,<sup>[19a]</sup> 1,3-dimethylimidazol-2-ylidene,<sup>[19a,b]</sup> 1-fluoro-1-cyclopentyl cation,<sup>[14]</sup> 1-fluoro-1-cyclopropyl cation<sup>[17]</sup> and 2-fluoro-2-cyclopropyl cation<sup>[17]</sup> are compared with those calculated at the PBE1PBE/6-311++G(2d,p) level<sup>[18]</sup> (Figure 2.6 and 2.7). Using these correlations, the computed  $\delta_{\text{F}}$  and  $\delta_{\text{C}}$  values of free **3a** and **3b** in Table 2.1 were corrected:  $\delta_{\text{F}}^{\text{corr}}$  (**3a**) = 159.1,  $\delta_{\text{F}}^{\text{corr}}$  (**3b**) = 141.1,  $\delta_{\text{C}}^{\text{corr}}$  (**3a**) =

290.3,  $\delta_{\text{C1}}^{\text{corr}}$  (**3b**) = 301.8 ppm. Furthermore, if one takes into consideration that  $^{19}\text{F}$  and  $^{13}\text{C}$  chemical shifts of encapsulated guest are upfield shifted by  $\Delta\delta_{\text{F}} \sim 1\text{-}2$  and  $\Delta\delta_{\text{C}} \sim 1\text{-}2$  ppm, the computed, corrected  $\delta_{\text{F}}$  and  $\delta_{\text{C}}$  values for incarcerated *cis*- **3a** are in better agreement with the experimental values (Table 2.1,  $\delta_{\text{F}} = 149.8$ ,  $\delta_{\text{C}} = 285.7$  ppm). This suggests that **3a** is the major isomer inside **7**.



**Figure 2.6**  $^{19}\text{F}$  Chemical shift correction. All structures fully optimized at PBE1PBE/ 6-311++G(2d,p).





**Figure 2.7**  $^{13}\text{C}$  Chemical shift correction. All structures fully optimized at PBE1PBE/6-311++G(2d,p).

In the  $^{19}\text{F}$  NMR spectrum of **7**⊙**3**, only one  $^{19}\text{F}$  signal is observed for **3** (S/N = 427, linewidth  $W_{1/2} = 18$  Hz) (Figure 2.4). Furthermore, at low temperature ( $-70$  °C) no additional  $^{19}\text{F}$  signal for the possible minor isomer was observed and the only detectable  $^{19}\text{F}$  signal for encapsulated **3** resonates at approximately the same chemical shift as measured at room temperature ( $\delta_{\text{F}} = 150.0$  ppm at  $-70$  °C;  $\delta_{\text{F}} = 149.8$  ppm at  $25$  °C). This suggests that either the isomerization between **3a** and **3b** inside **7** is fast at room

temperature and -70 °C, so that an averaged signal is observed, or that one conformation is predominantly present inside **7** (higher than 95%). In the latter case, one can estimate from the measured S/N  $\sim 427$  and the observation of only one  $^{19}\text{F}$  signal that the ratio **3a/3b** must be greater than 200. We exclude an exchange rate between **3a** and **3b** that is fast on the  $^{19}\text{F}$  NMR time scale based on the following simulations. From the calculated  $^{19}\text{F}$  chemical shift values for free **3a** and **3b** ( $\delta_{\text{F}}^{\text{corr}}$  (**3a**) = 159.1,  $\delta_{\text{F}}^{\text{corr}}$  (**3b**) = 141.1 ppm) and the signal line width ( $W_{1/2}$  = 18 Hz), the isomerization rate was estimated by dynamic NMR simulations for different populations of carbene conformations (95:5  $\geq$  **3a:3b**  $\geq$  5:95).<sup>[20]</sup> The isomerization rate constant must be  $k \geq 1 \times 10^7 \text{ s}^{-1}$  in order to generate a signal with S/N and lineshape similar to those observed experimentally (Figure 2.4). From this rate the isomerization activation enthalpy  $\Delta H_{\text{simulation}}^{\ddagger} = 7.92 \text{ kcal/mol}$  for **3a**  $\rightarrow$  **3b** was calculated by assuming that  $\Delta S^{\ddagger} = 0$  ( $A = 6.2 \times 10^{12} \text{ s}^{-1}$ ,  $T = 298 \text{ K}$ ).<sup>[21]</sup> This activation enthalpy, which sets the upper limit below which fast exchange is observed differs substantially from the activation energy predicted by DFT calculations (B3LYP/6-31G\*):  $\Delta H_{\text{calcd}}^{\ddagger} = 13.9 \text{ kcal/mol}$  for **3a**  $\rightarrow$  **3b** and  $\Delta H_{\text{calcd}}^{\ddagger} = 16.1 \text{ kcal/mol}$  for **3b**  $\rightarrow$  **3a** (Scheme 2.7). If indeed exchange would be fast, the large activation energy difference between DFT calculation and dynamic NMR simulation must be due to a considerable host stabilization effect on the transition state for **3a**  $\rightleftharpoons$  **3b**, which is impossible. Therefore, exchange must be slow on the  $^{19}\text{F}$  NMR time scale at room temperature and the lower limit for the conformational ratio is 200:1. The  $^{19}\text{F}$  signal observed for **7**⊙**3** must be due to one major conformation. Combined with the hydrogen-fluorine NOE experiments, the *cis*- conformation **3a** must be at least 3 kcal/mol more stable than **3b** inside **7**. Thus, we can conclude that encapsulation destabilizes **3b** by  $\Delta H > 5 \text{ kcal/mol}$

relative to **3a**.

## 2.3 Conclusions

Fluorophenoxycarbene is a transient reactive intermediate. If incarcerated, it persists for days without decomposition. The inner phase reaction of the carbene with water is catalyzed by acid.  $^1\text{H}$ - $^{19}\text{F}$  heteronuclear NOE experiments and  $^{19}\text{F}/^{13}\text{C}$  NMR spectroscopic studies suggest that the *cis-trans* equilibrium is reversed in the hemicarcerand's inner phase, and that encapsulation destabilizes the *trans*- conformation relative to the *cis*- conformation by more than 5 kcal/mol.

## 2.4 Experimental section

### 2.4.1 General procedure

All reactions were conducted under an argon atmosphere. Reagents and chromatography solvents were used as purchased from Aldrich without further treatment. NMR spectra were recorded on Varian 300 or 400 MHz FT-NMR spectrometers.

### 2.4.2 Synthesis of hemicarceplex **7**⊙**4**

3-Fluoro-3-phenoxydiazirine **4** (90 mg) was added to a suspension of **8** (200 mg, 0.105 mmol), 1,4-butanediol dimesylate (78 mg, 0.32 mmol), and  $\text{Cs}_2\text{CO}_3$  (1.37 g) in dry HMPA (5 mL). The suspension was stirred for six days under nitrogen in the dark at room temperature. The reaction was quenched by the addition of brine/ $\text{H}_2\text{O}$  (40 mL). The precipitate was filtered off, washed with water (3x10 mL) and methanol (2 mL), and

dried at high vacuum. The crude product was dissolved in the minimum amount of  $\text{CH}_2\text{Cl}_2$  and purified by column chromatography (silica gel,  $\text{EtOAc}/\text{CH}_2\text{Cl}_2$ ) and repurified by HPLC to give **7**⊖**4** (51 mg, 23 % yield) as a white powder.

$^1\text{H}$  NMR (399.969 MHz,  $\text{CD}_2\text{Cl}_2$ , 25 °C):  $\delta$  = 6.98 (s, 4 H; aryl-*H*),  $\delta$  = 6.93 (s, 4 H; aryl-*H*), 6.33 (d,  $^3J(\text{H}, \text{H})$  = 7.6 Hz, 2 H; **4**), 5.67 (d,  $^2J(\text{H}, \text{H})$  = 6.8 Hz, 4 H;  $\text{OCH}_{\text{outer}}\text{HO}$ ), 5.58 (d,  $^2J(\text{H}, \text{H})$  = 6.0 Hz, 4 H;  $\text{OCH}_{\text{outer}}\text{HO}$ ), 5.09 (t,  $^3J(\text{H}, \text{H})$  = 7.6 Hz, 2H; **4**), 4.70 (t,  $^3J(\text{H}, \text{H})$  = 7.2 Hz, 8 H;  $\text{CH}_{\text{methine}}$ ), 4.23 (d,  $^2J(\text{H}, \text{H})$  = 6.4 Hz, 4 H;  $\text{OCH}_{\text{inner}}\text{HO}$ ), 4.07 (d,  $^2J(\text{H}, \text{H})$  = 6.8 Hz, 4 H;  $\text{OCH}_{\text{inner}}\text{HO}$ ), 3.89 (br s, 8 H;  $\text{OCH}_2\text{CH}_2$ ), 3.82 (br s, 8 H;  $\text{OCH}_2\text{CH}_2$ ), 3.02 (t,  $^3J(\text{H}, \text{H})$  = 7.6 Hz, 1 H; **4**), 2.27-2.25 (m, 16 H;  $\text{OCH}_2\text{CH}_2$ ), 1.82 (br s, 16 H), 1.45-1.33 (m, 48 H), 0.93 (t, 24 H);  $^{19}\text{F}$  NMR (282.227 MHz,  $\text{CD}_2\text{Cl}_2$ , 25 °C):  $\delta$  = -117.3 (s);  $^{13}\text{C}$  NMR (75.428 MHz,  $\text{CD}_2\text{Cl}_2$ , 25 °C):  $\delta$  = 151.2 (**4**), 148.4, 148.2, 144.4, 139.4, 138.8, 129.5 (**4**), 124.2 (**4**), 117.5 (**4**), 115.2, 114.3, 98.7, 98.3, 86.9 (d,  $^1J(\text{C}, \text{F})$  = 270 Hz, **4**), 72.5, 72.3, 37.5, 32.4, 30.3, 28.0, 23.1, 14.3; FAB-MS (NBA matrix):  $m/z$ : 2129 (30)  $[\text{M}]^{++}$ , 1977 (100)  $[\text{M}-\text{4}]^{++}$ ; C, H, N analysis calcd (%) for  $\text{C}_{127}\text{H}_{157}\text{N}_2\text{O}_{25}\text{F}$ : C 71.59, H 7.43, N 1.31, found: C 71.50, H 7.17, N 1.02.

### 2.4.3 Synthesis of hemicarceplex **7**⊖**3**

A solution of **7**⊖**4** (3-20 mg) and pyridine- $d_5$  (0 or 30  $\mu\text{L}$ ) in  $\text{CD}_2\text{Cl}_2$  (450  $\mu\text{L}$ ) was placed in a pyrex NMR tube and was degassed by four freeze-pump-thaw cycles under vacuum. The NMR tube was sealed off under vacuum. The sample was cooled in a partially silvered dewar flask filled with liquid nitrogen. The sample tube was placed in the light beam such that the bottom part of the frozen solution was in the focal point (4-5 mm diameter). It was irradiated with the output of an Oriel Hg Power-Max lamp

operating at 200 W. A 10 cm water-filter and a 320 nm cutoff filter (WG 320) were placed between the lamp and the sample. Firstly, the front of the sample was irradiated for 10 minutes, followed by 10 minutes of irradiation after the sample tube had been turned by 180°. After each 2x10 minute irradiation period, the sample was moved downwards in 5 mm steps until all of the frozen solution had been irradiated (typically 6-7 vertical steps). The photolysis yield of **7**⊙**3** was determined by the integral of the guest proton H1 ( $\delta = 6.28$ ), using the signal assigned to the host's methyl groups ( $\delta = 0.94$ ) as an internal standard.

<sup>1</sup>H NMR (399.969 MHz, CD<sub>2</sub>Cl<sub>2</sub>, 25 °C):  $\delta = 6.96$  (s, 8 H; aryl-*H*), 6.28 (d, <sup>3</sup>*J*(H, H) = 7.6 Hz, 2 H; **3**), 5.62 (d, <sup>2</sup>*J*(H, H) = 6.8 Hz, 8 H; OCH<sub>outer</sub>HO), 5.56 (t, <sup>3</sup>*J*(H, H) = 7.6 Hz, 2 H; **3**), 4.70 (t, <sup>3</sup>*J*(H, H) = 7.2 Hz, 8 H; CH<sub>methine</sub>), 4.06 (d, <sup>2</sup>*J*(H, H) = 7.2 Hz, 8 H; OCH<sub>inner</sub>HO), 3.83 (br s, 8 H; OCH<sub>2</sub>CH<sub>2</sub>), 3.82 (br s, 8 H; OCH<sub>2</sub>CH<sub>2</sub>), 3.28 (t, (d, <sup>3</sup>*J*(H, H) = 7.6 Hz, 1 H; **3**), 2.26-2.23 (m, 16 H; OCH<sub>2</sub>CH<sub>2</sub>), 1.84 (br s, 16 H), 1.46-1.34 (m, 48 H), 0.94 (t, 24 H); <sup>19</sup>F NMR (282.227 MHz, CD<sub>2</sub>Cl<sub>2</sub>, 25 °C):  $\delta = 149.8$  (s); <sup>13</sup>C NMR (75.428 MHz, CD<sub>2</sub>Cl<sub>2</sub>, 25 °C):  $\delta = 285.7$  (d, <sup>1</sup>*J*(C, F) = 569 Hz, **3**), 148.7, 148.0 (**3**), 144.5, 144.3, 139.2, 138.9, 129.9 (**3**), 124.7 (**3**), 117.4 (**3**), 115.2, 114.4, 114.2, 98.6, 72.6, 72.0, 37.3, 32.3, 30.2, 30.0, 27.9, 27.8, 23.0, 14.1.

#### 2.4.4 Synthesis of hemicarceplexes **7**⊙**15** and **7**⊙**16**

Hemicarceplexes **7**⊙**15** and **7**⊙**16** were isolated by semi-preparative HPLC from a photolyzed solution of **7**⊙**4** after complete hydrolysis of **7**⊙**3**.

Data for **7**⊙**15**: <sup>1</sup>H NMR (299.940 MHz, CDCl<sub>3</sub>, 25 °C):  $\delta = 6.88$  (s, 8 H; aryl-*H*), 5.95 (d, <sup>3</sup>*J*(H, H) = 8.1 Hz, 2 H; **15**), 5.61 (d, <sup>2</sup>*J*(H, H) = 6.9 Hz, 8 H; OCH<sub>outer</sub>HO), 5.35 (t,

$^3J(\text{H}, \text{H}) = 7.5 \text{ Hz}$ , 2 H; **15**), 4.71 (t,  $^3J(\text{H}, \text{H}) = 8.1 \text{ Hz}$ , 8 H;  $\text{CH}_{\text{methine}}$ ), 4.15 (d,  $^2J(\text{H}, \text{H}) = 7.2 \text{ Hz}$ , 8 H;  $\text{OCH}_{\text{inner}}\text{HO}$ ), 3.84 (br s, 16 H;  $\text{OCH}_2\text{CH}_2$ ), 3.36 (s, 1 H; **15**), 3.12 (t,  $^3J(\text{H}, \text{H}) = 7.5 \text{ Hz}$ , 1 H; **15**), 2.22-2.17 (m, 16 H;  $\text{OCH}_2\text{CH}_2$ ), 1.86 (br s, 16 H), 1.41-1.33 (m, 48 H), 0.93 (t, 24 H); FAB-MS (NBA matrix):  $m/z$ : 2100 (55)  $[M+1]^+$ , 1978 (100)  $[M-15+1]^+$ . Data for **7**⊙**16**:  $^1\text{H}$  NMR (399.968 MHz,  $\text{CDCl}_3$ , 25 °C):  $\delta$  = 6.87 (s, 8 H; aryl- $\text{H}$ ), 6.02 (d,  $^3J(\text{H}, \text{H}) = 8.8 \text{ Hz}$ , 2 H; **16**), 5.61 (d,  $^2J(\text{H}, \text{H}) = 8.0 \text{ Hz}$ , 8 H;  $\text{OCH}_{\text{outer}}\text{HO}$ ), 5.07 (t,  $^3J(\text{H}, \text{H}) = 7.6 \text{ Hz}$ , 2 H; **16**), 4.71 (t,  $^3J(\text{H}, \text{H}) = 8.4 \text{ Hz}$ , 8 H;  $\text{CH}_{\text{methine}}$ ), 4.22 (m, 8 H;  $\text{OCH}_{\text{inner}}\text{HO}$ ), 3.85 (br s, 16 H;  $\text{OCH}_2\text{CH}_2$ ), 2.96 (t,  $^3J(\text{H}, \text{H}) = 7.6 \text{ Hz}$ , 1 H; **16**), 2.22-2.20 (m, 16 H;  $\text{OCH}_2\text{CH}_2$ ), 1.86 (br s, 16 H), 1.44-1.33 (m, 48 H), 0.92 (t, 24 H);  $^{19}\text{F}$  NMR (282.227 MHz,  $\text{CD}_2\text{Cl}_2$ , 25 °C):  $\delta_{\text{F}}$  = -82.9 (d,  $^2J_{\text{HF}} = 73.3 \text{ Hz}$ ); FAB-MS (NBA matrix):  $m/z$ : 2122 (30)  $[M+1]^+$ , 1978 (100)  $[M-16+1]^+$ .

## 2.5 References

1. M. Jones, Jr., R. A. Moss in *Reactive Intermediate Chemistry*, (Ed.: R. A. Moss, M. S. Platz, M. Jones, Jr.), John Wiley & Sons, Inc., **2004**, chapter 7, p. 273-328.
2. a) M. B. Smith, J. March, *March's Advanced Organic Chemistry*, 5th edition, Reactions, Mechanism and Structure, John Wiley & Sons, Inc. **2001**, p. 247-252; b) R. A. Moss, in *Carbene Chemistry: From Fleeting Intermediates to Powerful Reagents* (Ed.: G. Bertrand), FontisMediaMarcel Dekker, Lausanne, **2002**, p.57; c) R. A. Moss, *Acc. Chem. Res.* **1980**, *13*, 58.
3. P. Chen in *Advances in Carbene Chemistry* (Ed.: U. H. Brinker), JAI Press Inc., Stamford, **1998**, volume 2, p. 45-75.
4. W. Sander, *Angew. Chem. Int. Ed. Engl.* **1994**, *33*, 1455.
5. a) R. Warmuth, *Eur. J. Org. Chem.* **2001**, 423; b) W. Kirmse, *Angew. Chem. Int. Ed.* **2005**, *44*, 2476.
6. a) D. J. Cram, M. E. Tanner, R. Thomas, *Angew. Chem. Int. Ed. Engl.* **1991**, *30*, 1024; b) R. Warmuth, *Angew. Chem. Int. Ed. Engl.* **1997**, *36*, 1347.
7. a) R. Warmuth and M. A. Marvel, *Angew. Chem. Int. Ed.* **2000**, *39*, 1117; b) C. Kemmis, R. Warmuth, *J. Supramol. Chem.* **2001**, *1*, 253.

8. R. A. Moss, G. Kmiecik-Lawrynowicz, K. Krogh-Jespersen, *J. Org. Chem.* **1986**, *51*, 2168.
9. a) L. M. Tunstad, J. A. Tucker, E. Dalcanele, J. Weiser, J. A. Bryant, J. C. Sherman, R. C. Helgeson, C. B. Knobler, D. J. Cram, *J. Org. Chem.* **1989**, *54*, 1305; b) S. K. Kurdistani, R. C. Helgeson, D. J. Cram, *J. Am. Chem. Soc.* **1995**, *117*, 1659; b) R. Warmuth, M. A. Marvel, *Angew. Chem. Int. Ed.* **2000**, *39*, 1117.
10. J. A. Bryant, M. T. Blanda, M. Vincenti, D. J. Cram, *J. Am. Chem. Soc.* **1991**, *113*, 2167.
11. S. V. Pasenok, Y. L. Yagupolskii, W. Tyrre, D. Naumann, *Z. Anorg. Allg. Chem.* **1999**, *625*, 831.
12. F. A. Carey, R. J. Sundberg, *Advanced Organic Chemistry*, 4th edition, Part B: Reaction and Synthesis, Kluwer Academic/Plenum Publishers, **2000**, 614-651.
13. R. Warmuth, M. A. Marvel, *Chem. Eur. J.* **2001**, *7*, 1209.
14. G. A. Olah, G. Liang, Y. K. Mo, *J. Org. Chem.* **1974**, *39*, 2394.
15. W. R. Croasmun and R. M. K. Carlson, *Two-Dimensional NMR Spectroscopy: Applications for Chemists and Biochemists*, 2nd Edition, John Wiley and Sons, Inc. USA, **1994**, 327-336.
16. A. Scarso, L. Trembleau, J. Rebek, Jr., *Angew. Chem. Int. Ed.* **2003**, *42*, 5499.
17. G. K. S. Prakash, G. Rasul, A. Burrichter, K. K. Laali, G. A. Olah, *J. Org. Chem.* **1996**, *61*, 9253.
18. Gaussian 03 (Revision B.02), M. J. Frisch, G. W. Trucks, H. B. Schlegel, G. E. Scuseria, M. A. Robb, J. R. Cheeseman, J. A. Montgomery, Jr., T. Vreven, K. N. Kudin, J. C. Burant, J. M. Millam, S. S. Iyengar, J. Tomasi, V. Barone, B. Mennucci, M. Cossi, G. Scalmani, N. Rega, G. A. Petersson, H. Nakatsuji, M. Hada, M. Ehara, K. Toyota, R. Fukuda, J. Hasegawa, M. Ishida, T. Nakajima, Y. Honda, O. Kitao, H. Nakai, M. Klene, X. Li, J. E. Knox, H. P. Hratchian, J. B. Cross, C. Adamo, J. Jaramillo, R. Gomperts, R. E. Stratmann, O. Yazyev, A. J. Austin, R. Cammi, C. Pomelli, J. W. Ochterski, P. Y. Ayala, K. Morokuma, G. A. Voth, P. Salvador, J. J. Dannenberg, V. G. Zakrzewski, S. Dapprich, A. D. Daniels, M. C. Strain, O. Farkas, D. K. Malick, A. D. Rabuck, K. Raghavachari, J. B. Foresman, J. V. Ortiz, Q. Cui, A. G. Baboul, S. Clifford, J. Cioslowski, B. B. Stefanov, G. Liu, A. Liashenko, P. Piskorz, I. Komaromi, R. L. Martin, D. J. Fox, T. Keith, M. A. Al-Laham, C. Y. Peng, A. Nanayakkara, M. Challacombe, P. M. W. Gill, B. Johnson, W. Chen, M. W. Wong, C. Gonzalez, J. A. Pople, Gaussian, Inc., Pittsburgh, PA, **2003**.
19. a) D. Bourissou, O. Guerret, F. P. Gabbaï, G. Bertrand, *Chem. Rev.* 2000, **100**, 39; b) A. J. Arduengo, III, H. V. R. Dias, R. L. Harlow, M. Kline, *J. Am. Chem. Soc.* **1992**, *114*, 5530.

20. a) J. B. Lambert, H. F. Shurvell, D. A. Lightner, R. G. Cooks, *Organic Structural Spectroscopy*, Prentice-Hall, Inc. **1998**, p. 96-98; b) H. J. Reich, *WINDNMR: NMR Spectrum Calculations*, V7.1, **2005**.
21. F. A. Carey, R. J. Sundberg, *Advanced Organic Chemistry*, 4th edition, Part A: Structure and Mechanism, Kluwer Academic/Plenum Publishers, **2000**, p. 187-250.

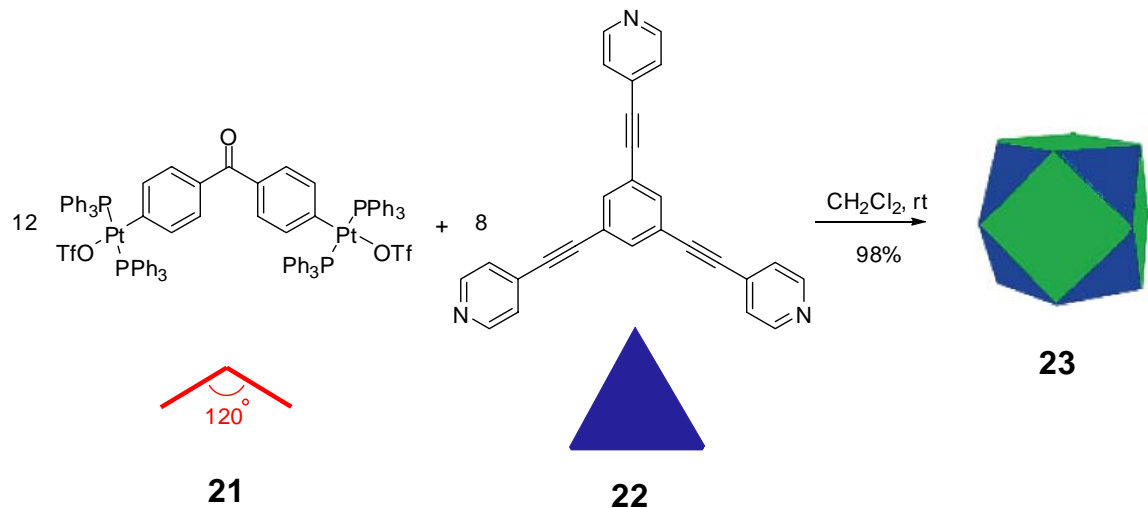


## Chapter 3 Thermodynamically controlled multi-component synthesis of nanocontainer molecules and solvent effect studies

### 3.1 Introduction

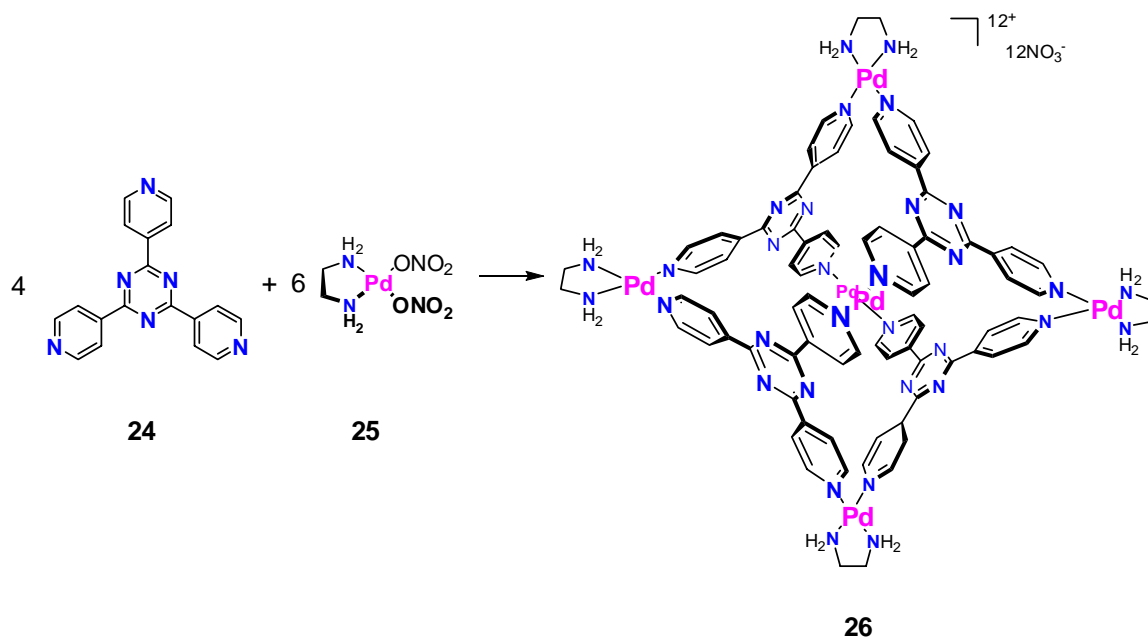
Molecular container compounds have opened an exciting and challenging field of organic chemistry.<sup>[1]</sup> Single molecules have been encapsulated inside carcerands and hemicarcerands.<sup>[1a, 2]</sup> Recently, a large number of nanometer-sized cage assemblies have also been reported.<sup>[3]</sup> Due to their much larger cavities compared to hemicarcerands, they have demonstrated special applications in catalysis, reaction control and separation technology. Both non-covalent and covalent approaches have been utilized to construct these nanocage compounds.

Directional bonding methodology has been used by Peter J. Stang and coworkers to build up highly symmetric metal-coordination cages based on complementary building blocks with predefined geometries.<sup>[4a]</sup> In the edge-directed self-assembly, usually linear ditopic subunits are used to predefine the edges of the desired polyhedral cages, and are connected by corner pieces. On the other hand, in the face-directed self-assembly, tritopic or tetratopic subunits are used to predefine the faces of the desired polyhedral cages. They are clipped together through face-to-face subunits. For example, a cuboctahedral nanocage **23** with a hydrodynamic diameter of 5.0 nm has been formed with 98% yield from 12 *bis*-platinum clips **21** and 8 triangular tripyridyl units **22** (Scheme 3.1).<sup>[4b]</sup> Other highly symmetrical polyhedra, such as a dodecahedron, a truncated tetrahedron and a trigonal prism have also been assembled with high yields (~90%) using the directional bonding methodology.



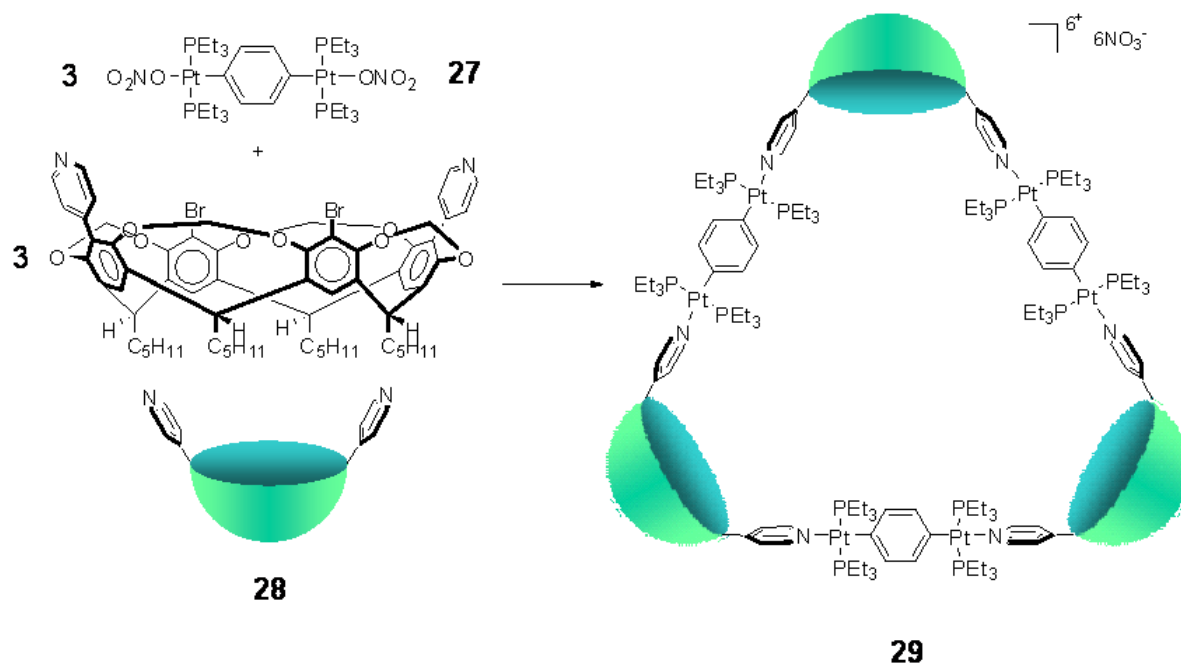
**Scheme 3.1** Self-assembly of a cuboctahedral nanocage from 12 *bis*-platinum clips **21** and 8 triangular tripyridyl units **22**.

Molecular paneling is a similar strategy used by Fujita et al. to construct large coordination capsules from a Pd(II)-cornered square complex **25** (Scheme 3.2).<sup>[5]</sup> Three-dimensional (3D) assemblies have been successfully constructed, where (en)Pd<sup>2+</sup> (en = ethylenediamine) is used to panel planar multidentate organic ligands together. The coordination cages have good solubility in water due to the charged Pd centers. Therefore the hydrophobic inner cavities have demonstrated high affinity with organic substrates in aqueous solution. The encapsulated guests have shown non-classical reaction behavior. For example, in a Diels-Alder addition between anthracene and maleimide guests, reactions preferentially happened at a terminal anthracene ring rather than the center one.<sup>[5d]</sup>

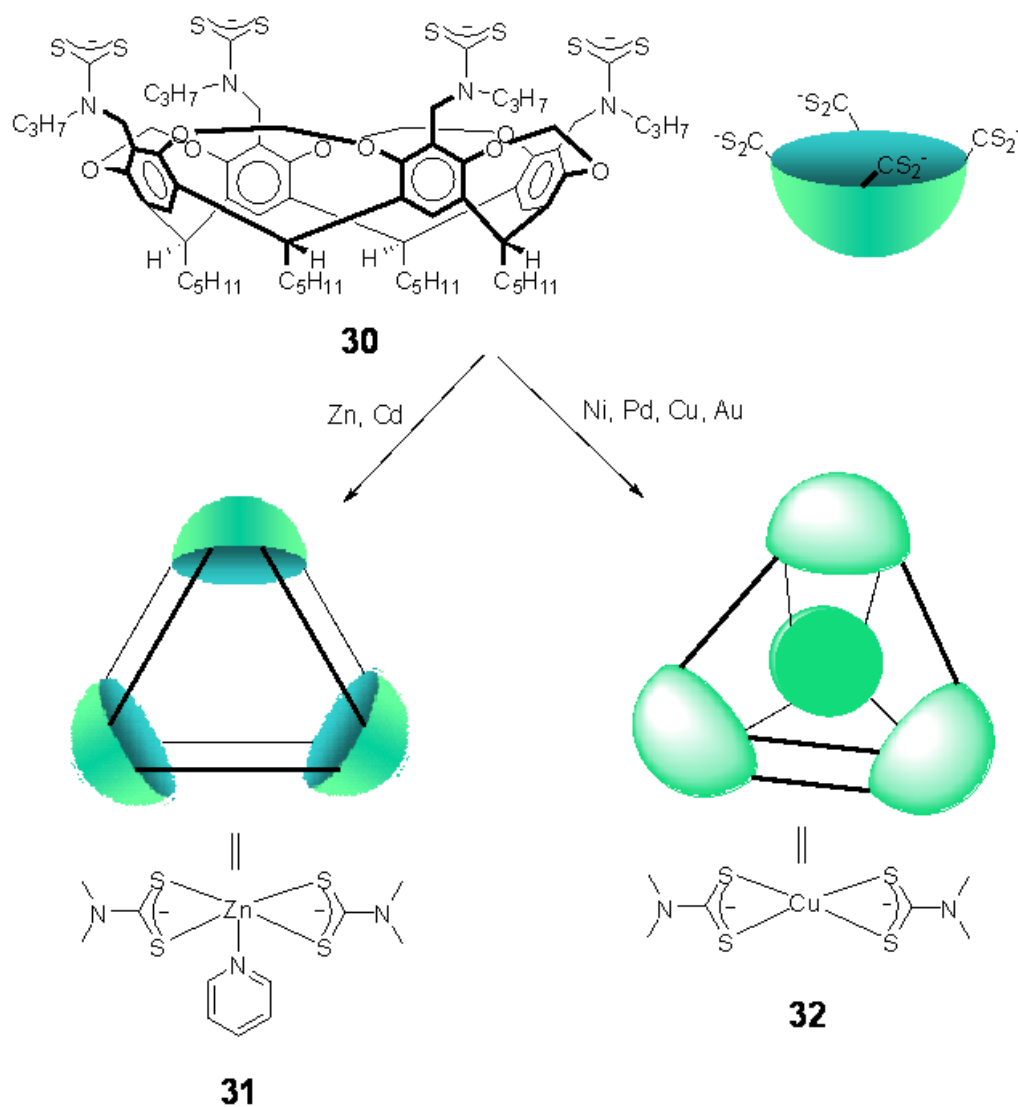


**Scheme 3.2** Construction of a  $M_6L_4$  self-assembled octahedral nanocage.

Metal-ligation has also been used to assemble cavitand-based components into nanoscale molecular hosts. Several tri-cavitand assemblies have been reported by Sherburn, Stang and coworkers (Scheme 3.3).<sup>[6a]</sup> Three bispyridyl cavitands **28**, which have the preorganized  $60^\circ$  angle between the opposing aromatic units, were brought together by three Pt-complexes **27** and gave excellent yields (85-95%) of cyclic trimeric species **29**. Molecular loops **31** were also prepared by Beer and coworkers using dithiocarbamate functionalized cavitands **30** assembled with square-based pyramidal metals (Zn, Cd) (Scheme 3.4).<sup>[6b,c]</sup> Moreover, assembling with square planar metals (Au, Cu, Ni, Pd) gave tetrahedral nanocages **32** (Scheme 3.4). Strong binding of fullerenes ( $C_{60}$  and  $C_{70}$ ) inside these nanocages is due to favorable electronic interactions between the electron-deficient guests and the electron-rich dithiocarbamate moieties of the hosts.<sup>[6c]</sup>



**Scheme 3.3** Formation of Pt-coordinated tri-cavitand assemblies.



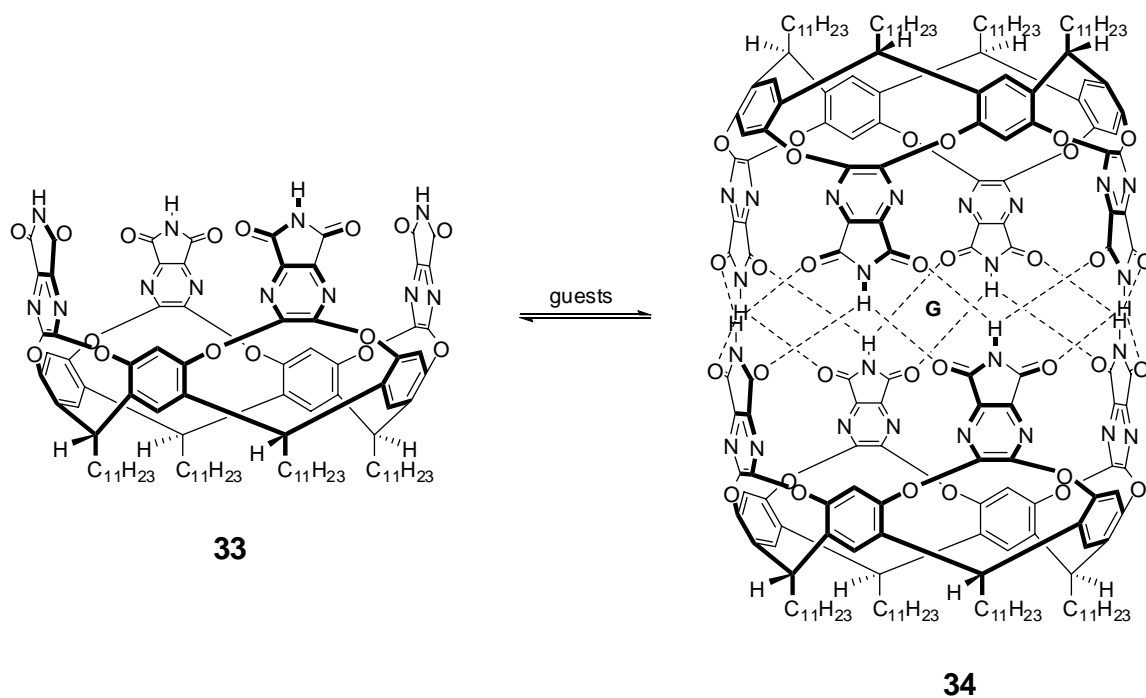
**Scheme 3.4** Formation of dithiocarbamate cavitand based coordination molecular loops and tetrahedral nanocages.

Self-assembly via hydrogen bonding is an alternative pathway to make large cages.<sup>[7]</sup>

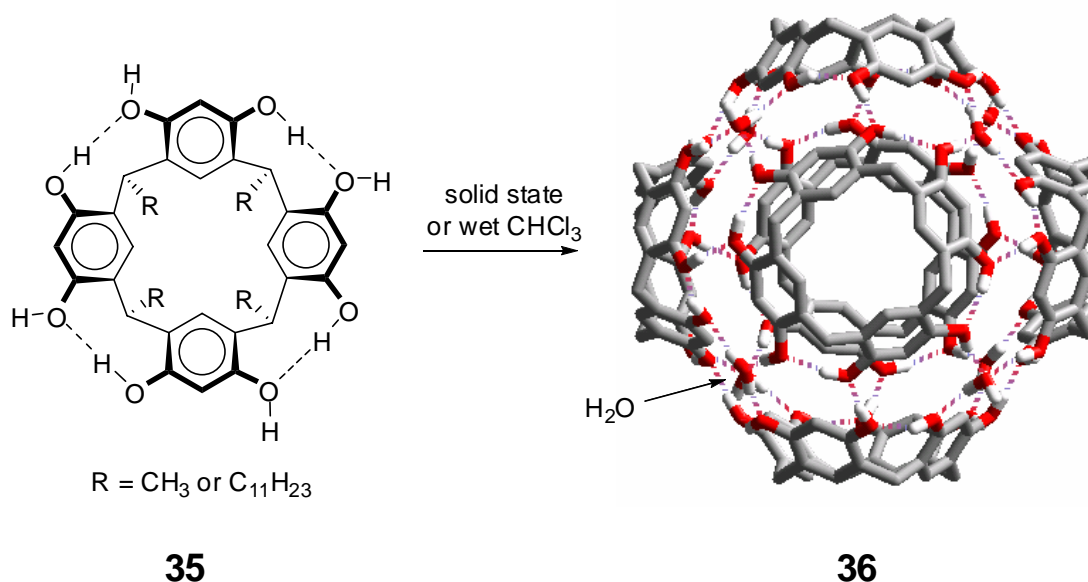
Rebek and co-workers have used an extended cavitand **33** to form a hydrogen bonding cylindrical capsule **34** in organic solvents that has a cavity of 420 Å<sup>3</sup> (Scheme 3.5).<sup>[7a]</sup>

The capsule **34** forms only if the inner cavity is properly filled. More than one guest

molecule are encapsulated in most cases. Therefore, this capsule provides a unique space to investigate intermolecular phenomena when two or more molecules are simultaneously encapsulated, which are difficult to observe in the bulk phase. Jerry Atwood's group at University of Missouri-Columbia has reported a hexamer **36** that is formed through hydrogen bonding between six *C*-methyl-resorcin[4]arene molecules **35** and eight water molecules in the solid state and in solution (Scheme 3.6).<sup>[7b]</sup> It has a cavity volume of  $\sim 1375 \text{ \AA}^3$ . The hydrogen bonded hexamer capsule can also be assembled in wet organic solvents. The encapsulation of solvent molecules as well as tetraalkylammonium salts inside this hexamer has been studied in detail.<sup>[7c,d]</sup> However, hydrogen bonded capsules are labile especially in competing hydrogen bonding solvents, such as water, DMSO, and DMF,<sup>[3,8]</sup> and the inclusion complexes don't survive chromatographic purification.

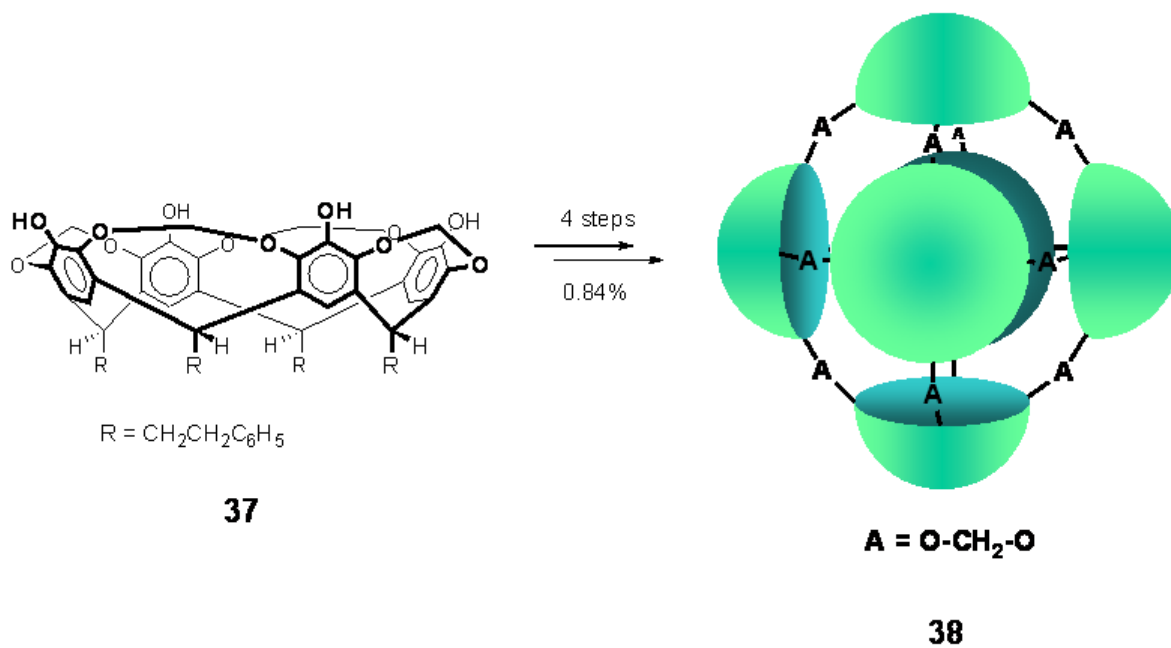


**Scheme 3.5** Rebek's hydrogen bonded cylindrical dimeric capsule.

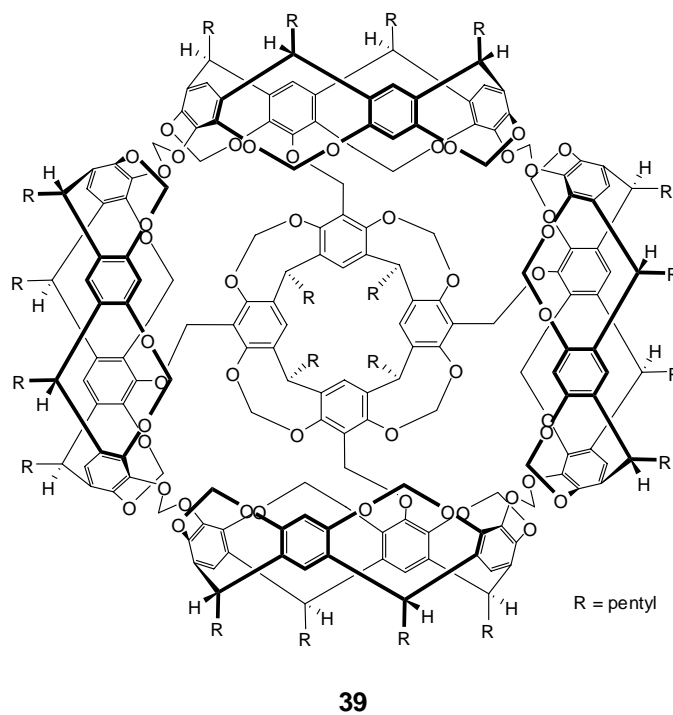


**Scheme 3.6** Self-assembly of a hydrogen bonded hexameric nanocapsule.

Kinetically controlled covalent bond formation has been used in the stepwise synthesis of large container molecules composed of more than two cavitands.<sup>[9]</sup> Compared to hydrogen bonded systems, these nanocages display considerably greater stability. However, their syntheses are laborious and overall yields low. Sherman et al. connected three cavitands to a trimeric capsule, which was capped on both sides with aromatic rings.<sup>[9a]</sup> They also reported a multi-step synthesis route towards hexameric container molecule **38**, which is composed of six cavitands (Scheme 3.7).<sup>[9b]</sup> Seven DMSO molecules were encapsulated during the final step. Only 0.8% yield was achieved for the four step synthesis starting from the known tetrol cavitand **14**. Another covalently bonded five-cavitand assembly **39**, known as ‘super bowl’, was prepared by Sherburn and co-workers in 19% yield and features a cavity volume of 1050 Å<sup>3</sup> (Figure 3.1).<sup>[9c]</sup> It is structurally related to Sherman’s hexamer **38**, but lacks one cavitand, which creates a large portal, through which guest transport in or out of the cavity is possible.



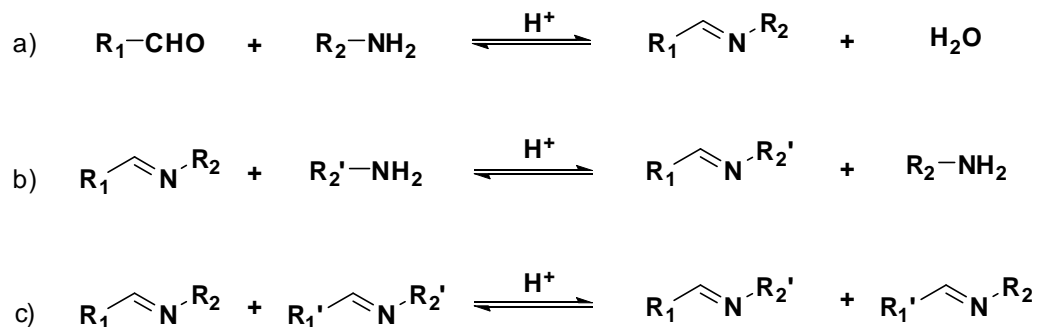
**Scheme 3.7** Multistep synthesis of a covalent hexameric nanocapsule by Sherman and coworkers.



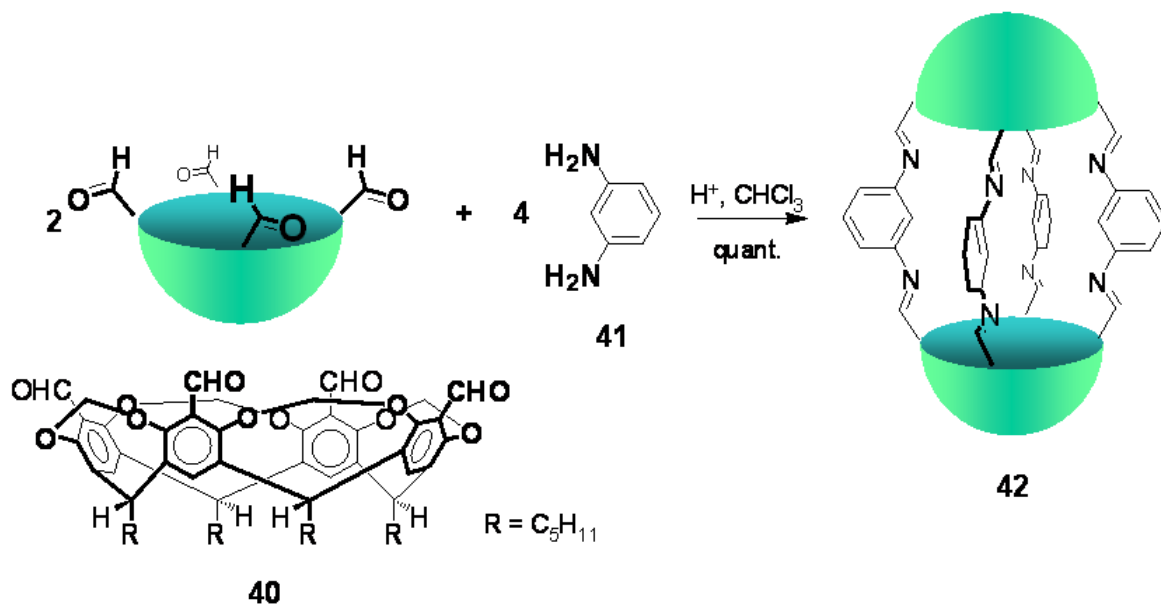
**Figure 3.1** Structure of Sherburn's 'super bowl'.



Recently, dynamic covalent chemistry has been applied for the synthesis of molecular capsules. Dynamic covalent chemistry is widely used to synthesize complex molecular architectures.<sup>[10]</sup> This approach makes use of the reversible nature of certain covalent bond formations, including disulfides, esters, hydrozones, imines and oximes. Especially, the reversible Schiff base chemistry has been of great importance in the synthesis of macrocycles, catenanes, rotaxanes, molecular grids and other three dimensional assemblies.<sup>[11]</sup> For example, a spectacular dynamic covalent synthesis of a molecular Borromean ring using metal templated imine formation has been reported by Stoddart and co-workers.<sup>[11c]</sup> Due to the reversibility of imine bonds, the product distribution is controlled by their thermodynamic stabilities. Kinetic products are converted to thermodynamic products through the following three possible pathways: imine formation/dissociation, transimination and imine metathesis (Scheme 3.8).<sup>[10]</sup> Stoddart, Cram and co-workers have also studied the formation of a dynamic octaiminohemicarcerand and possible guest exchange mechanisms.<sup>[12]</sup> Octaiminohemicarcerand **42** was formed by condensation between two tetraformyl cavitands **40** and four *meta*-phenylenediamines **41** in CHCl<sub>3</sub> (Scheme 3.9). The dynamic nature of octaiminohemicarcerand **42** was confirmed by a bridging unit exchange with another substituted *meta*-phenylenediamine, which gave a statistical distribution of six different octaiminohemicarcerands.



**Scheme 3.8** Reversible Schiff base chemistry: a) imine formation/dissociation; b) transimination, and c) imine metathesis.



**Scheme 3.9** Thermodynamically controlled synthesis of an octaiminohemicarcerand.

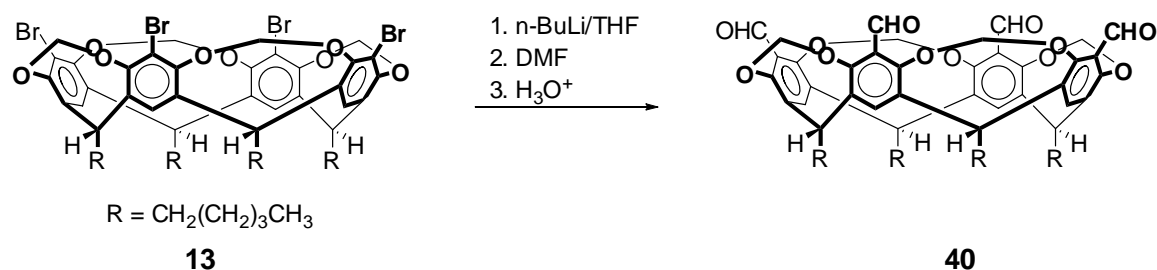
The study by Cram and Stoddart inspired this part of my Ph.D. thesis work. My major goal was to further explore reversible Schiff base chemistry for the synthesis of molecular container compounds. In this chapter, a series of one-pot multicomponent synthesis of nanometer-sized container molecules will be discussed. These nanocontainers are prepared from tetraformyl cavitand **40** and ethylenediamine **43**, utilizing reversible imine

bond chemistry to link reactants together. It was also discovered that structurally different containers that vary in their assembly numbers can be formed from one set of building blocks and that the solvent plays a key role in tuning the relative population of these nanocontainers.

## 3.2 Results and discussion

### 3.2.1 Synthesis of tetraformyl cavitand **40**

Tetraformyl cavitand (**40**) was synthesized according to a reported procedure but with some modifications (Scheme 3.10).<sup>[12,13]</sup> Tetrabromocavitand **13**, the starting material for **40**, was synthesized according to a known procedure.<sup>[14]</sup> Tetrabromocavitand **13** was then metalated with *n*-butyl lithium in THF. The aryl lithium was trapped with DMF as electrophile to produce **40**.<sup>[15]</sup> After workup with aqueous ammonium chloride, crude **40** was chromatographed on silica gel with CH<sub>2</sub>Cl<sub>2</sub>/EtOAc. Since high purity of **40** was essential for the dynamic covalent nanocapsule synthesis, trace amounts of impurities were removed by normal phase HPLC using THF/CH<sub>2</sub>Cl<sub>2</sub> as the mobile phase, if necessary.



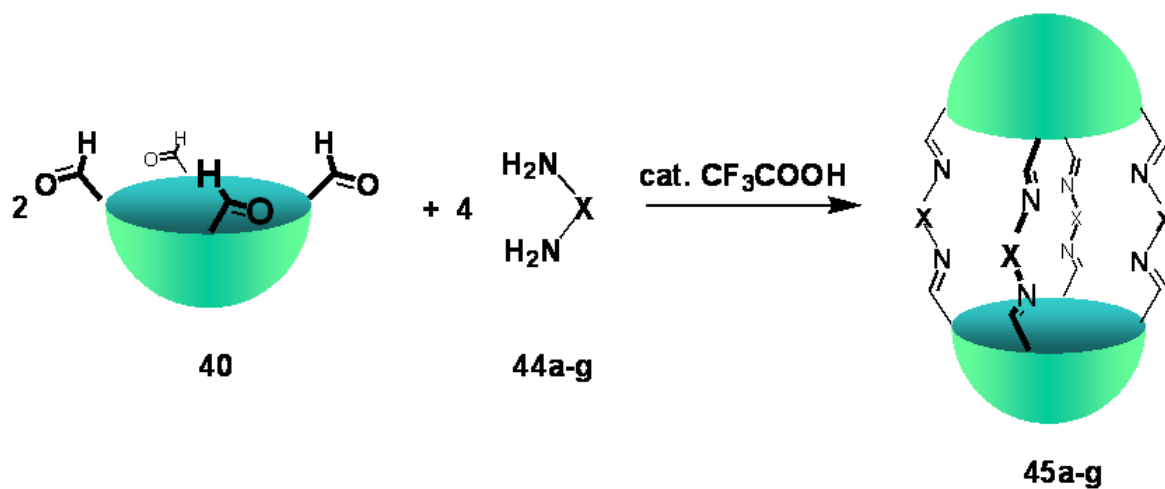
**Scheme 3.10** Synthesis of tetraformyl cavitand **40**.

### 3.2.2 Condensation reaction between tetraformyl cavitand and diamine linkers

Condensation reactions between **40** and ten commercially available diamines **44a-j** were carried out using similar conditions as described in Cram and Stoddart's study (Scheme 3.11 and Table 3.1). The reactions were started by direct mixing **40** and **44x** (ratio 1:2) in chloroform in the presence of catalytic amounts of trifluoroacetic acid (TFA) at room temperature.  $^1\text{H}$  NMR, GPC and MS were used to monitor the reaction progress.


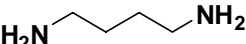
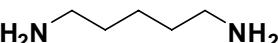
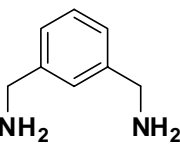
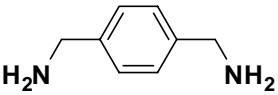
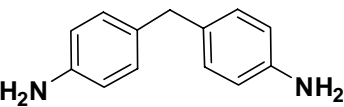
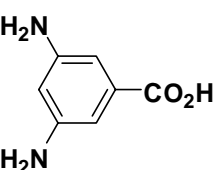

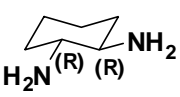
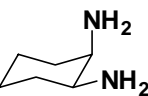
The nature of the diamine reactant had a significant effect on the outcome of these condensation reactions (Table 3.1). When tetraformyl cavitand **40** reacted with 1,3-diaminopropane (**44a**), 1,4-diaminobutane (**44b**) or 1,5-diaminopentane (**44c**), hemicarcerands **45a-c** formed quantitatively. For example, octaiminohemicarcerand **45a** shows only one set of signals for the imine protons  $\text{H}_{\text{imine}}$  ( $\delta_{\text{H}} = 8.38$  ppm), the aryl protons  $\text{H}_{\text{a}}$  ( $\delta_{\text{H}} = 7.11$  ppm), the outward pointing protons  $\text{H}_{\text{outer}}$  ( $\delta_{\text{H}} = 5.65$  ppm), the methine protons  $\text{H}_{\text{methine}}$  ( $\delta_{\text{H}} = 4.86$  ppm) and the inward pointing protons  $\text{H}_{\text{inner}}$  ( $\delta_{\text{H}} = 4.45$  ppm). GPC of **45a** gave only one peak at  $t_{\text{r}} = 7.29$  min corresponding to a molecular weight around 2,000 Da. The FAB-MS of **45a** shows one major peak at  $m/z = 2010.7$  (100%,  $[\text{M}+\text{H}]^+$ ). The condensation reactions of **40** with the benzylic *meta*-xylylene diamine (**44d**) and *para*-xylylene diamine (**44e**) gave octaiminohemicarcerands **45d-e**, too. Aromatic diamines gave somewhat different results. The condensation with 4,4'-methylenedianiline (**44f**) and 3,5-diaminobenzoic acid (**44g**), which is structurally similar to *meta*-phenylenediamine **41** used earlier by Cram and Stoddart,<sup>[12]</sup> gave octaiminohemicarcerands **45f-g** as the major products. However, under identical conditions, the reaction with *para*-phenylenediamine (**44h**) gave a tetrameric

nanoacapsule with molecular weight around 4,000 Da (based on GPC). This reaction will be further discussed in Chapter 4. The condensation with cyclohexyl diamines (**44i** and **44j**) gave polymeric products. For example, the condensation with optically pure (*R,R*)-1,2-diaminocyclohexane (**44i**) gave products with molecular weight higher than 25,000 Da, which is the upper molecular weight cut-off of our GPC system.



**Scheme 3.11** The condensation reactions between cavitand **40** and diamines **44a-g**.

**Table 3.1** Yields<sup>i</sup>, mass ( $m/z$ ) and imine chemical shifts  $\delta_{\text{H(imine)}}$  of **45a-h** in the TFA-catalyzed condensation of **40** with two equivalents of **44a-j**.

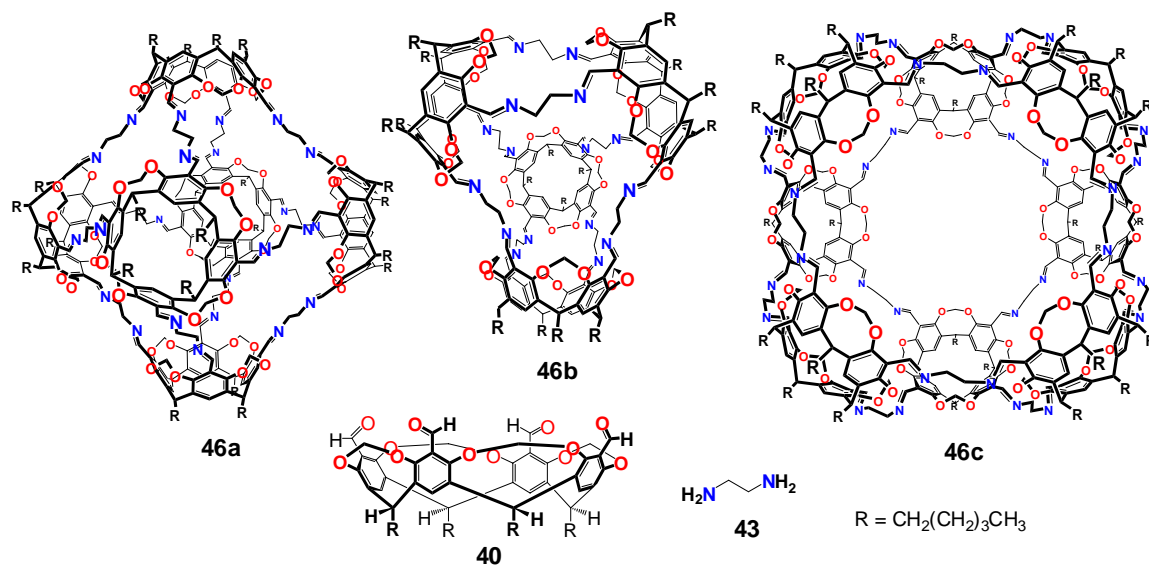
compd.	$\text{H}_2\text{N}-\text{X}-\text{NH}_2$	<b>45x</b>			
		yield	mass $\text{M}+\text{H}^+$		$\delta_{\text{H(imine)}}$
		%	calc'd.	found	(ppm)
<b>44a</b>		>95	2010.1	2010.7	8.38
<b>44b</b>		>95	2066.2	2066.8	8.37
<b>44c</b>		>95	2123.27	2123.32	8.35
<b>44d</b>		>95	2259.21	2259.27	8.44
<b>44e</b>		>95	2259.21	2258.90	8.33
<b>44f</b>		79	2508.14	2505.83 <sup>iii</sup>	8.56
<b>44g<sup>ii</sup></b>		61	1159.5 <sup>iv</sup>	1159.4 <sup>iv</sup>	8.54
<b>44h</b>		53	4294.16	4296.89 <sup>iii</sup>	8.58/8.43
<b>44i</b>					
<b>44j</b>					

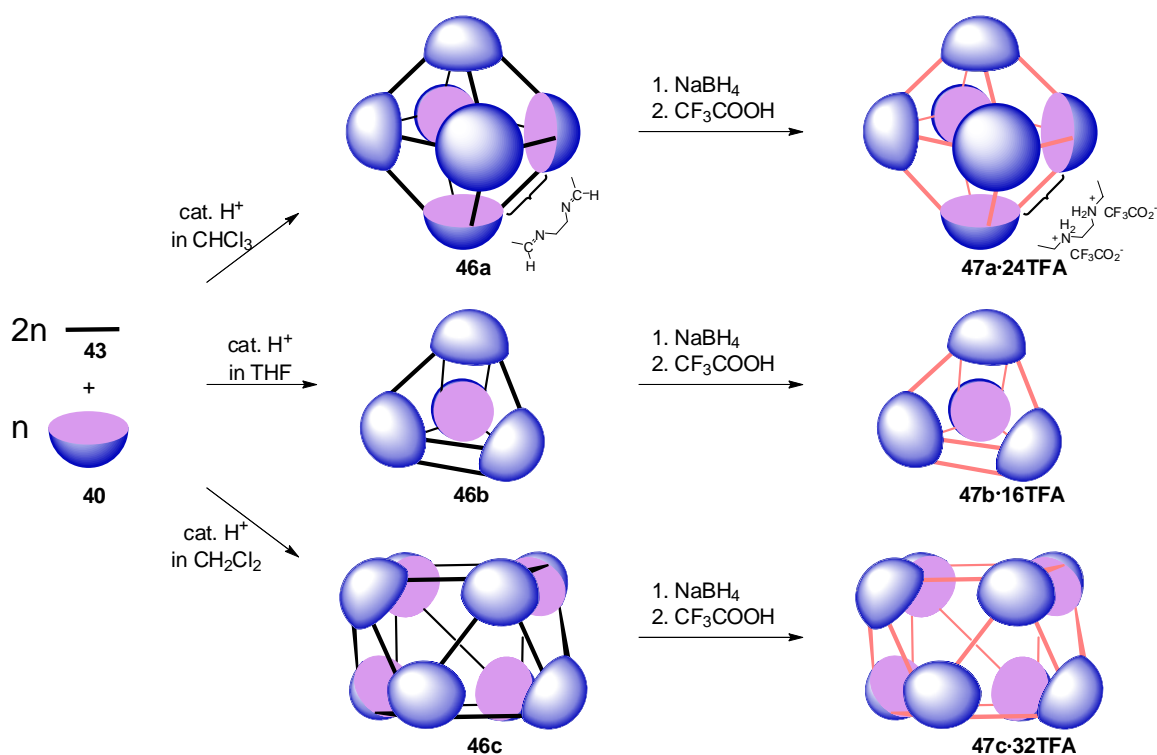
<sup>i</sup> Reaction in  $\text{CHCl}_3$  unless otherwise noted. <sup>ii</sup> Reaction in DMSO. <sup>iii</sup> not calibrated. <sup>iv</sup>  $[\text{M}-2\text{H}]^{2-}$ .

### 3.2.3 One-pot multicomponent synthesis of covalent molecular nanocapsules

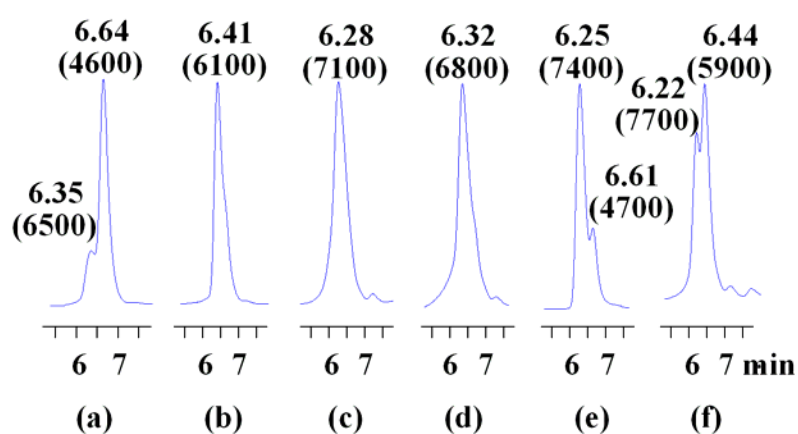
When **40** reacted with ethylenediamine **43** in a ratio of 1:2 in the presence of catalytic amounts of TFA in chloroform, the hexameric nanocapsule **46a** formed in ~80% yield based on  $^1\text{H}$  NMR spectroscopy and GPC (corresponding to molecular weight ~6,000 Da) (Chart 3.1 and Figure 3.2 b). This nanocapsule **46a** formed from the condensation between six cavitands **40** and twelve ethylenediamines **43** (Scheme 3.12). To isolate and purify this nanocapsule, the imine bonds in **46a** were reduced with  $\text{NaBH}_4$ , which “fixed” the nanocapsule structure. After HPLC purification, the trifluoroacetate salt **47a**·24TFA was isolated in 63% yield based on cavitand **40** (Scheme 3.12).

Chart 3.1





**Scheme 3.12** 12-, 18-, and 24-component syntheses of tetrahedral, octahedral and square anti-prismatic nanocapsules **46a**, **46b** and **46c** and their reduction.



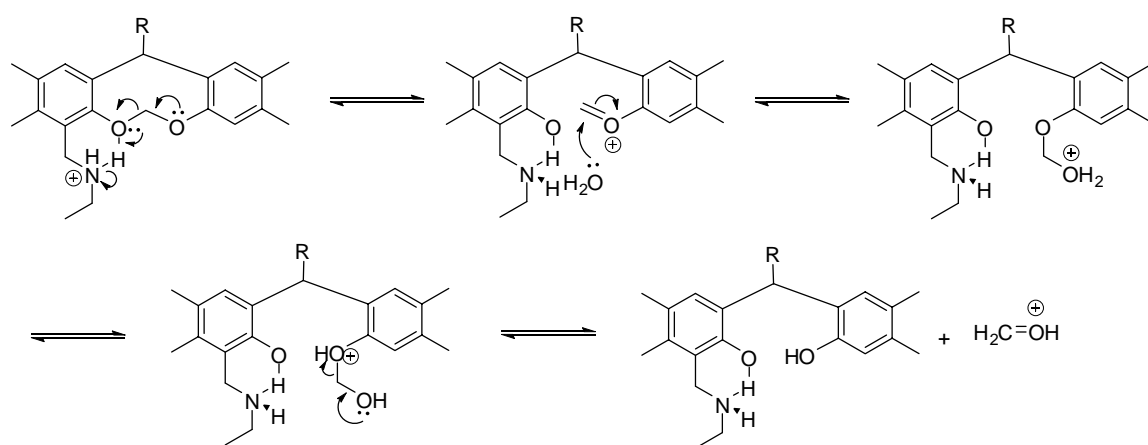
**Figure 3.2** Gel permeation chromatograms of the crude products formed after two days in the TFA-catalyzed reaction of **40** with two equivalents of **43** in THF (a),  $\text{CHCl}_3$  (b),  $\text{CH}_2\text{Cl}_2$  (c),  $\text{CH}_2\text{ClCH}_2\text{Cl}$  (d) and  $\text{CCl}_2\text{HCCl}_2\text{H}$  (e). (f) Products formed in  $\text{CH}_2\text{Cl}_2$  spiked with **46a**. Retention time (in minutes) and estimated molecular weight (in parenthesis) are reported for main peaks.



Interestingly, the shape and size of the molecular nanocapsules formed in the condensation between tetraformyl cavitand **40** and ethylenediamine **43** can be controlled by solvents. The condensation between **40** and **43**, which gives ~80% hexamer **46a** in chloroform, was carried out in THF under otherwise identical conditions, and was followed by GPC. It was found that in THF tetrameric species, including **46b**, formed, which are composed of four cavitands and eight linkers (Chart 3.1 and Scheme 3.12). After two days the system reached an equilibrium and the tetrameric species (molecular weight ~4,600 Da) accounted for ~90% of all products (Figure 3.2 a). The left shoulder (MW 6,500 Da) in the GPC of the products was assigned to species with molecular weight similar to that of hexamer **46a**. The reaction mixture was subjected to reduction with NaBH<sub>4</sub>, followed by hydrolysis with aqueous HCl solution. The crude products were further purified by reversed-phase HPLC. The major species **47b** in the HPLC chromatogram, which accounted for ~35% of all products, was isolated in 31% yield based on cavitand **40** (Scheme 3.12). This yield is consistent with the yield of the major product in the <sup>1</sup>H spectrum of the condensation mixture.

Even though chloroform and dichloromethane have very similar solvent properties, the condensation products in both solvents varied considerably. When the condensation between **40** and **43** was carried out in dichloromethane, the octameric nanocapsule **46c** formed as the major product in 65% yield (Chart 3.1 and Scheme 3.12). In the GPC chromatogram of the condensation products in dichloromethane, the major species (>75%) eluted ( $t_r = 6.28$  min) before hexamer **46a** ( $t_r = 6.41$  min) (Figure 3.2). Based on the retention time ( $t_r = 6.28$  min), the molecular weight of the earlier eluting species was

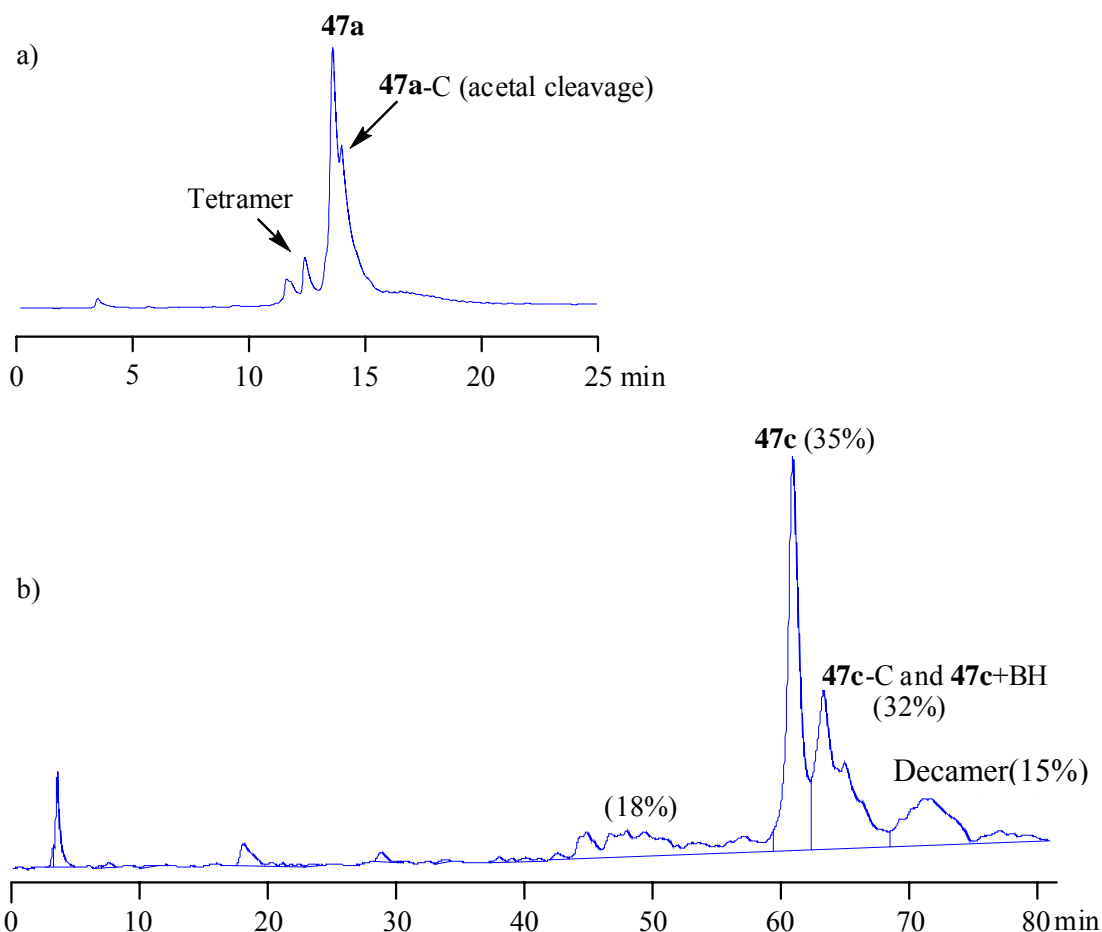
estimated to be ~7,000 Da, which suggests eight cavitand subunits (MW = 928). Imine bonds in the condensation products were reduced using the same procedure described for **46a** and **46b**. The polyamino product mixture was again purified by reversed-phase HPLC and the major product **47c** was isolated in 25% yield based on cavitand **40** (Scheme 3.12). The lower yield after reduction is proposed to be due to partial decomposition of the octameric nanocapsule **47c** during the acidic work-up (Scheme 3.13).



**Scheme 3.13** Proposed intramolecular catalysis of acetal spanner cleavage.

Acetal cleavage during the acidic work-up step explains the substantial lower yields of the isolated **47a** (63%) and **47c** (25%), as compared to that of **46a** (80%) and **46c** (65%). In both cases, the reduction of the imine bonds with NaBH<sub>4</sub> was fast (< 3 hrs) and quantitative based on <sup>1</sup>H NMR analysis and led to boramines R<sub>2</sub>N-BH<sub>2</sub>. The acidic work-up (9:1 methanol/concentrated HCl) was relatively slow (3.5 to 4.5 days). The slow hydrolysis of boramine is possibly due to the difficulty in reaching the boron center by

water/methanol molecules, since the boron center could rotate into the cavity. Hydrolysis under basic conditions was even slower because nonprotonated secondary amino groups are poor leaving groups. There are 24 and 32 acetal groups in **47a** and **47c**, respectively. As a result, one out of four of **47a** (25%), and one out of three of **47c** (33%, 12% higher) would become byproducts, if one out of 96 (~1%) acetal groups is cleaved. Furthermore less hydrolysis time was needed for **47a** compared to **47c** (3.5 days vs. 4.5 days), which resulted in less acetal group cleavage for **47a**. The difficulty in separating the byproducts from **47a** and **47c** also accounts for some of the product loss. During the reversed-phase HPLC purification, the byproducts eluted slightly later than **47a** and **47c** (Figure 3.3). In contrast to **47a** and **47c**, the extent of acetal cleavage for **47b** was substantially lower.



**Figure 3.3** Reversed-phase HPLC chromatograms of the crude reaction mixture after imine reduction and boramine hydrolysis for a) **47a** and b) **47c**.

As shown in Table 3.2, the condensation products vary considerably in different solvents. In chloroform, hexamer **46a** is obtained in 80% yield accompanied by 4-5% tetramer **46b**. In THF, the major product is tetramer **46b** (35%) with ~5% hexamer **46a** and octamer **46c** present. In dichloromethane, 65% octamer **46c** is obtained with <5% hexamer **46a** present. The product distribution also changes in other solvents. In 1,2-dichloroethane ( $\text{CH}_2\text{ClCH}_2\text{Cl}$ ) and 1,1,2,2-tetrachloroethane ( $\text{CHCl}_2\text{CHCl}_2$ ), the major product is

octamer **46c** and yields are about 26% and 33% based on  $^1\text{H}$  NMR integration. In  $\text{CHCl}_2\text{CHCl}_2$ , 17% hexamer **46a** is also observed. The results clearly demonstrate the dynamic nature of these molecular nanocapsules. Thermodynamic stabilities determine the product distribution. The condensation between **40** and **43** in toluene was not performed due to the limited solubility of **40** in toluene.

**Table 3.2** Yields<sup>a</sup> (in %) of **46a**, **46b** and **46c** in the TFA-catalyzed condensation of **40** with 2 equivalents **43** in different solvents.

Entry	Solvent	<b>46a</b>	<b>46b</b>	<b>46c</b>
1	$\text{CHCl}_3$	80	4-5	0
2	THF	5 <sup>b</sup>	35 <sup>b</sup> (31) <sup>c</sup>	5 <sup>b</sup>
3	$\text{CH}_2\text{Cl}_2$	< 5	0	65
4	$\text{CH}_2\text{ClCH}_2\text{Cl}$	0	0	26
5	$\text{CHCl}_2\text{CHCl}_2$	17	0	33

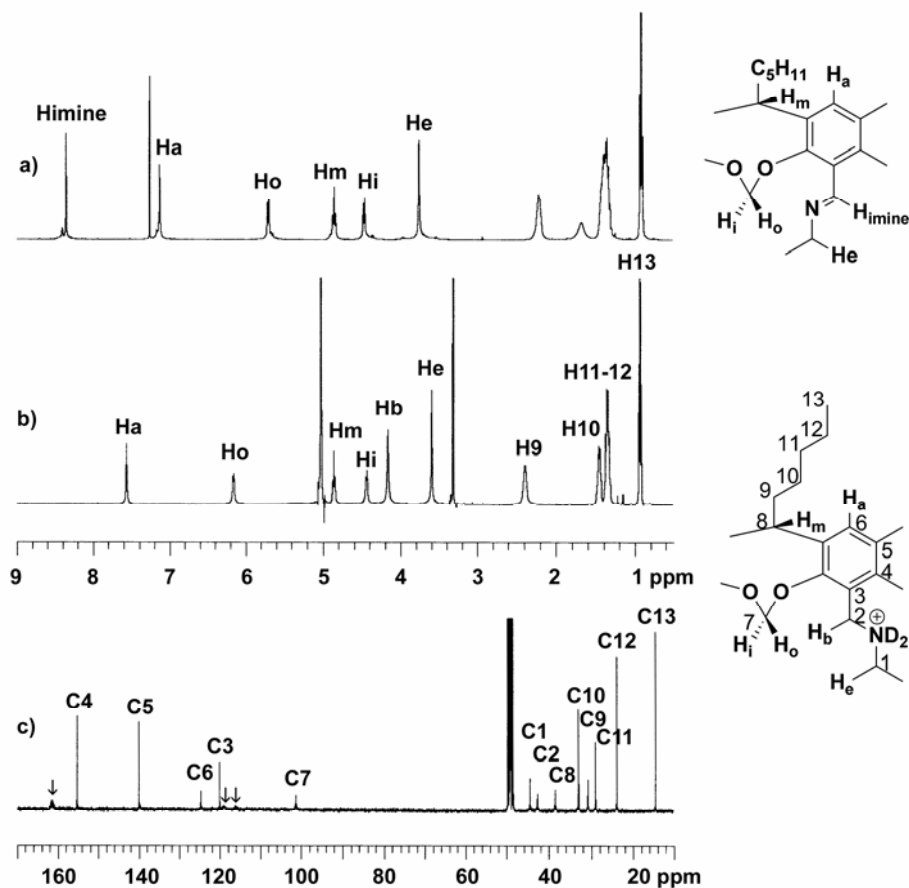
<sup>a</sup> Determined by integration of selected product signals in the  $^1\text{H}$  NMR spectrum of the crude products unless otherwise noted. <sup>b</sup> Determined by HPLC of the  $\text{NaBH}_4$ -reduced reaction mixture. <sup>c</sup> Isolated yield of **47b**•16 $\text{CF}_3\text{COOH}$ .

These solvent effects are due to the different solvation of the nanocapsules by the solvents. Compared to other molecular capsules, nanocapsules **46a-c** have much larger portals, which allows for easy solvent molecule passage in and out of the cavities.

Therefore, it is unlikely that space occupancy is the only reason that is responsible for the considerably different outcomes in different solvents. Instead, the interactions of the solvent, that is in the inner cavity or inside an opening in the host shell, with the linkers will be affected by the geometry of the nanocapsules, thus shift their relative stabilities.

### 3.2.4 Characterization of covalent molecular nanocapsules

The structure of the molecular nanocapsules **46a** and **47a** was determined by NMR spectroscopy and mass spectrometry.  $^1\text{H}$  NMR spectra of **46a** and **47a** show simplified signals, which are only consistent with a highly symmetric structure (Figure 3.4). For example, **47a** shows only one set of signals for the aryl protons  $\text{H}_a$  ( $\delta_{\text{H}} = 7.55$  ppm), the outward pointing protons  $\text{H}_o$  ( $\delta_{\text{H}} = 6.16$  ppm), the methine protons  $\text{H}_m$  ( $\delta_{\text{H}} = 4.85$  ppm), the inward pointing protons  $\text{H}_i$  ( $\delta_{\text{H}} = 4.43$  ppm), the benzylic protons  $\text{H}_b$  ( $\delta_{\text{H}} = 4.16$  ppm) and the ethylene protons  $\text{H}_e$  ( $\delta_{\text{H}} = 3.59$  ppm) (Figure 3.4 b and Table 3.3).  $^{13}\text{C}$  NMR spectra of **46a** and **47a** are also consistent with the proposed octahedral structure (Figure 3.4 c). MALDI-TOF MS of **47a** displays the major signal at  $m/z = 5912.26$  Da, which is assigned to  $\text{M}+\text{H}^+$  (Figure 3.5 and Table 3.4). Taking into account the GPC and MALDI-TOF MS results, only a molecule with an octahedral symmetry can give the signal patterns observed by  $^1\text{H}$  and  $^{13}\text{C}$  NMR spectroscopy.<sup>[17]</sup>



**Figure 3.4**  $^1\text{H}$  NMR spectra of (a) crude products formed in the reaction of **40** with two equivalents of **43** in the presence of 10 mol% TFA in chloroform after 69 hrs ( $\text{CDCl}_3$ ; 400 MHz; 22 °C) and (b) of **47a**·24CF<sub>3</sub>CO<sub>2</sub>H ( $\text{CD}_3\text{OD}$  + 0.4 v% TFA-*d*; 500 MHz; 7 °C). (c)  $^{13}\text{C}$  NMR spectrum of **47a**·24CF<sub>3</sub>CO<sub>2</sub>H ( $\text{CD}_3\text{OD}$  + 0.4 v% TFA-*d*; 100 MHz; 25 °C); signals marked with (↓) are for CF<sub>3</sub>CO<sub>2</sub><sup>-</sup>.

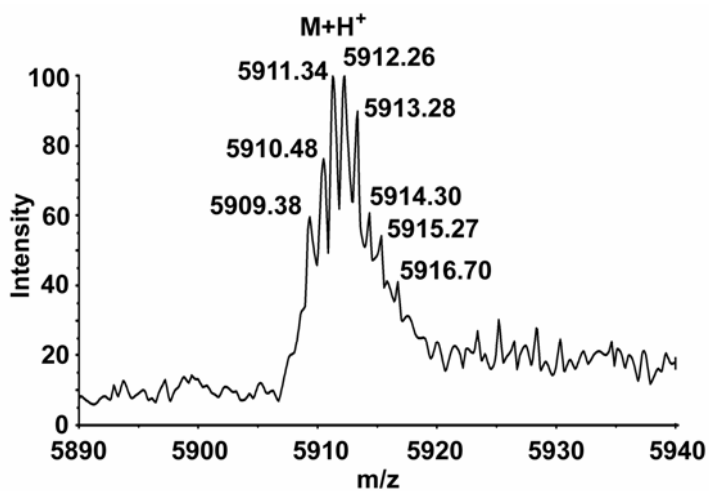
**Table 3.3** Chemical shifts, integrations and multiplicities of proton resonances of **46a-c** and **47a-c** in their  $^1\text{H}$  NMR spectra <sup>v</sup>.

compd.		H <sub>imine</sub>	H <sub>a</sub>	H <sub>o</sub>	H <sub>m</sub>	H <sub>i</sub>	H <sub>b</sub>	H <sub>e</sub>
<b>46a</b> <sup>i</sup>	$\delta_{\text{H}}$ (ppm)	8.34	7.12	5.70	4.83	4.46		3.75
	integration	24	24	24	24	24		48
	multiplet	<i>s</i>	<i>s</i>	<i>d</i>	<i>t</i>	<i>d</i>		<i>sb</i>
<b>47a</b> <sup>ii</sup>	$\delta_{\text{H}}$ (ppm)		7.55	6.16	4.85	4.43	4.16	3.59
	integration		24	24	24	24	24	48
	multiplet		<i>s</i>	<i>s</i>	<i>d</i>	<i>t</i>	<i>sb</i>	<i>sb</i>
<b>46b</b> <sup>i</sup>	$\delta_{\text{H}}$ (ppm)	8.41	7.17/7.14					
	integration							
	multiplet	<i>s</i>	<i>s/s</i>					
<b>47b</b> <sup>iii</sup>	$\delta_{\text{H}}$ (ppm)		7.55	6.45/6.14/6.08	4.86	4.58/4.40/4.39	4.26/4.21, 4.13/4.02	3.60
	integration		16	4/8/4	16	4/8/4	8/8, 8/8	32
	multiplet		<i>sb</i>	<i>d/d/d</i>	<i>m</i>	<i>d/d/d</i>	<i>d/d, d/d</i>	<i>m</i>
<b>46c</b> <sup>i</sup>	$\delta_{\text{H}}$ (ppm)	8.45/8.13	~7.13/7.08	5.82/5.58		4.44/4.36/4.30		
	integration	16/16	16/16	8/24		16/8/8		
	multiplet	<i>s/s</i>	<i>s/s</i>	<i>d/d</i>		<i>d/d/d</i>		
<b>47c</b> <sup>iv</sup>	$\delta_{\text{H}}$ (ppm)		7.55/7.54	6.17	4.86	4.46	4.16	3.61/3.57
	integration		32	32	32	32	64	32/32
	multiplet		<i>sb</i>	<i>m</i>	<i>m</i>	<i>m</i>	<i>m</i>	<i>s/s</i>

<sup>i</sup> CDCl<sub>3</sub>, 22 °C, 400 MHz; <sup>ii</sup> CD<sub>3</sub>OD + 0.4 v% TFA-*d*, 7 °C, 300 MHz; <sup>iii</sup> CD<sub>3</sub>OD + 0.4 v% TFA-*d*, 12.7 °C, 400 MHz; <sup>iv</sup> CD<sub>3</sub>OD + 0.4

v% TFA-*d*, 25 °C, 400 MHz; <sup>v</sup> for assignment see structure in Figure 3.4.

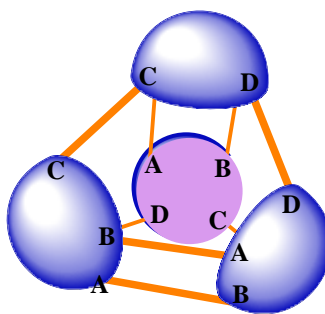




**Figure 3.5** MALDI-TOF mass spectrum of **47a**.

**Table 3.4** Sum formulas and MALDI-TOF mass of **47a-c**.

compd.	molecular formula	$m/z$ , $M+H^+$	
		calc'd.	found
<b>47a</b>	$C_{360}H_{480}N_{24}O_{48}$	5912.61	5912.26
<b>47b</b>	$C_{240}H_{320}N_{16}O_{32}$	3941.40	3941.85
<b>47c</b>	$C_{480}H_{640}N_{32}O_{64}$	7882.81	7883.35

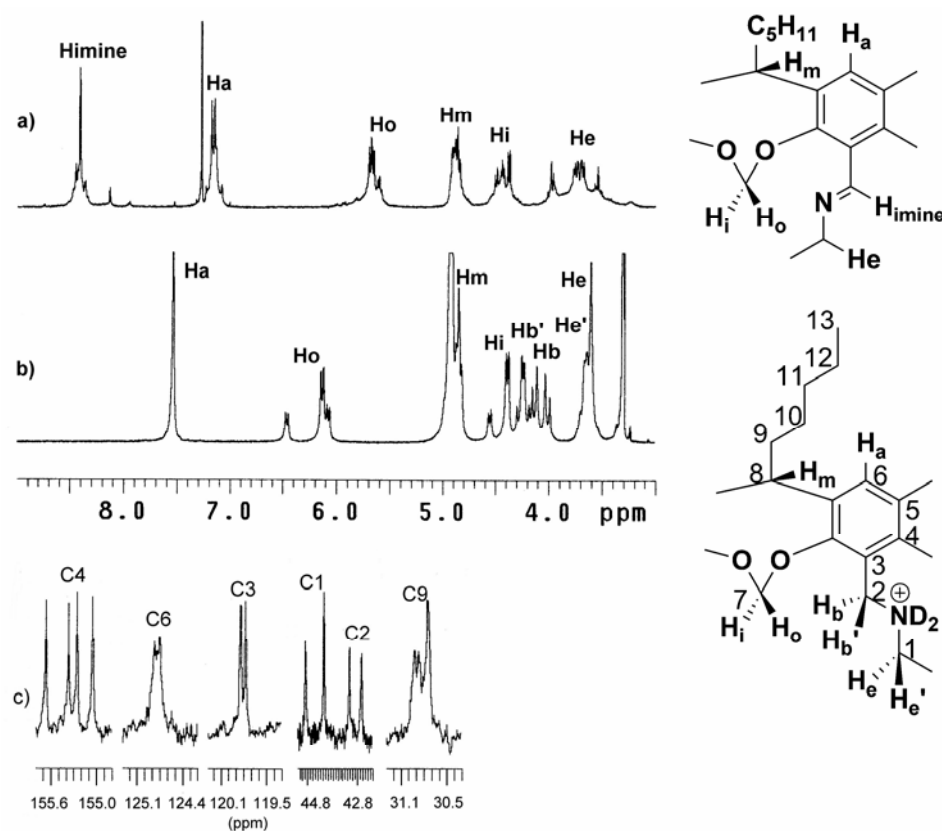


**Figure 3.6** Cartoon structure of **47b** and positions A, B, C, and D.

$^1\text{H}$  and  $^{13}\text{C}$  NMR spectroscopy and molecular modeling studies suggest that the tetrameric products **46b** and **47b** can be described as distorted tetrahedra (Scheme 3.12).<sup>[47b,c]</sup> In the distorted tetrahedron **46b** (or **47b**), each cavitand doubly connects with another cavitand at the *A* and *B* positions and singly links to the remaining two cavitands at the *C* and *D* positions (Figure 3.6). This results in two chemically different linkers. Furthermore, all cavitands are equivalent, but have only one mirror plane, that dissects the cavitand between the *A*-*B* and *C*-*D* positions. Hence, in the  $^1\text{H}$  NMR spectrum, two sets of signals with equal intensity are expected for the aryl protons ( $\text{H}_a$ ), each of the two diastereotopic benzyl protons ( $\text{H}_b$ ,  $\text{H}_b'$ ), and each of the two diastereotopic ethylene protons ( $\text{H}_e$ ,  $\text{H}_e'$ ). On the other hand, three sets of signals in a 4:8:4 ratio are expected for the inward and outward pointing acetal protons ( $\text{H}_i$ ,  $\text{H}_o$ ), the methine protons ( $\text{H}_m$ ) and all other protons in the feet ( $\text{H}_{9-13}$ ). In the  $^{13}\text{C}$  NMR spectrum, one expects two carbon signals with equal intensity for carbons  $\text{C}_{1-3}$ ,  $\text{C}_6$ , three signals in a 1:2:1 ratio for each of carbon  $\text{C}_{7-13}$ , and four signals in a 1:1:1:1 ratio for each carbon  $\text{C}_4$  and  $\text{C}_5$ .

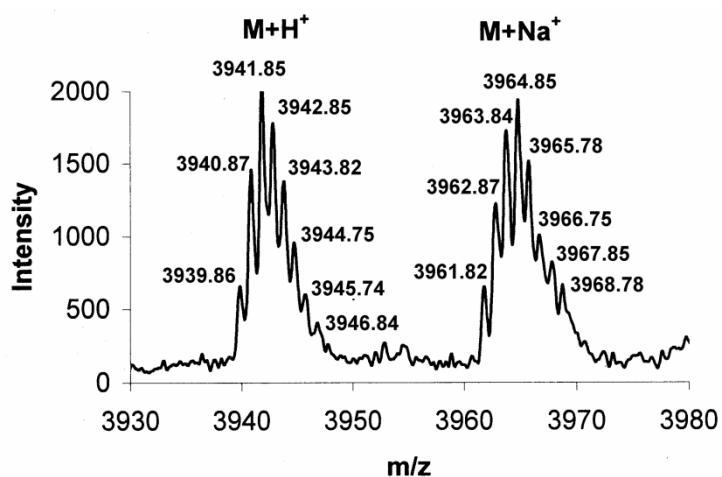
Signals in the  $^1\text{H}$  and  $^{13}\text{C}$  NMR spectra of **47b** were assigned by a combination of  $^1\text{H}$ - $^1\text{H}$  COSY,  $^1\text{H}$ - $^1\text{H}$  TOCSY and  $^1\text{H}$ - $^{13}\text{C}$  HMQC 2D spectroscopy as well as by comparison with the chemical shifts of hexamer **47a** and octaiminohemicarcerands **45a-e**. Due to strong line broadening and in part low signal dispersion, not all of these specific signal patterns are observed. However, in the  $^1\text{H}$  NMR spectrum of **47b**, three clearly separated doublets are observed at 6.54, 6.14 and 6.08 ppm (integration ratio 4:8:4), which are assigned to  $\text{H}_o$  (Figure 3.7 b and Table 3.3). Each couples to one of three doublets at 4.58, 4.40 and 4.39 ppm (ratio 4:4:8), which are assigned to  $\text{H}_i$ . The protons for  $\text{H}_b/\text{H}_b'$  are

also well separated into two AB systems, as expected. These two AB systems have chemical shifts at 4.26, 4.21, 4.13 and 4.02 ppm with an integration ratio of 8:8:8:8. In the  $^{13}\text{C}$  NMR spectrum of **47b**, the expected signal patterns are observed for  $\text{C}_{1-3}$ ,  $\text{C}_4$ ,  $\text{C}_6$ , and  $\text{C}_9$  (Figure 3.7 c). Clearly observed are two signals with approximately equal intensity for each of  $\text{C}_{1-3}$  and  $\text{C}_6$ , four signals for  $\text{C}_4$  with intensity 1:1:1:1, and three signals for  $\text{C}_9$  with intensity 1:1:2.



**Figure 3.7** Partial  $^1\text{H}$  NMR spectra (400 MHz; 22 °C) of (a) crude products formed in the reaction of **40** with two equivalents of **43** in the presence of 10 mol% TFA in THF after two days (in  $\text{CDCl}_3$ ; signals assigned to **46b** are marked) and (b) of **47b**·16CF<sub>3</sub>COOH in  $\text{CD}_3\text{OD}$  + 0.4 v% TFA-*d*. (c) Partial  $^{13}\text{C}$  NMR spectra (100 MHz, 22 °C,  $\text{CD}_3\text{OD}$  + 0.4 v% TFA-*d*) of **47b**·16CF<sub>3</sub>COOH.

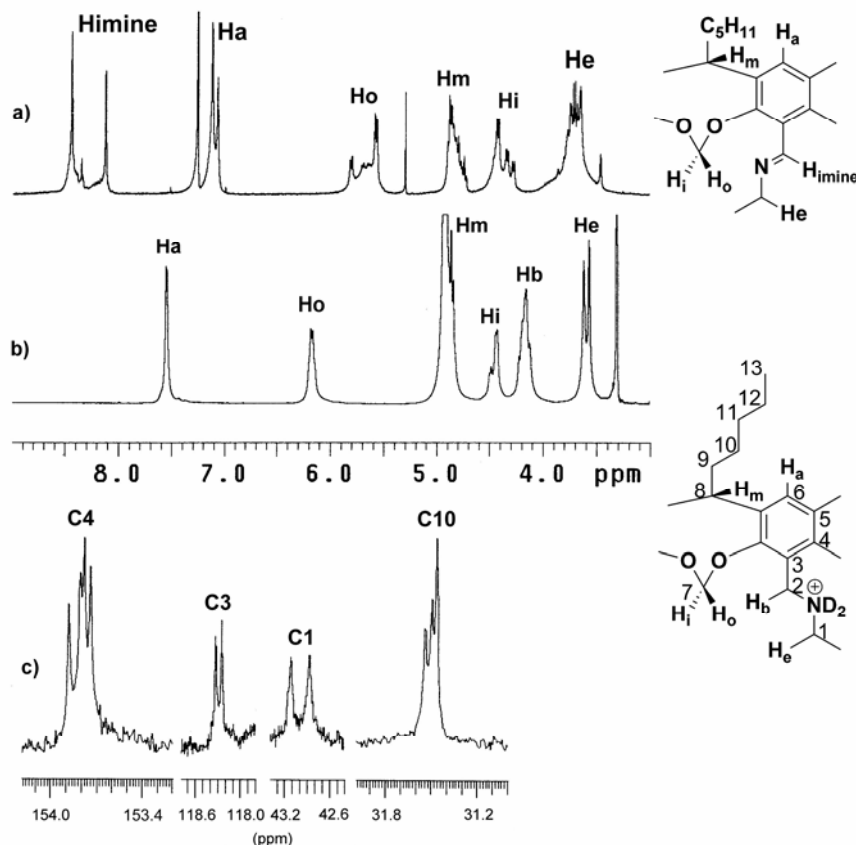
The MALDI-TOF mass spectrum of crude **47b** shows strong signals for protonated **47b** and **47b** + Na<sup>+</sup>. After isolation, the MALDI-TOF mass spectrum of **47b** shows two signals at  $m/z = 3941.85$  (M+H<sup>+</sup>) and  $3963.84$  (M+Na<sup>+</sup>) (Figure 3.8 and Table 3.4), which supports that the tetrameric polyimino product **46b** is composed of four cavitands and eight linkers, connected together by 16 imine bonds.



**Figure 3.8** MALDI-TOF mass spectrum of **47b**.

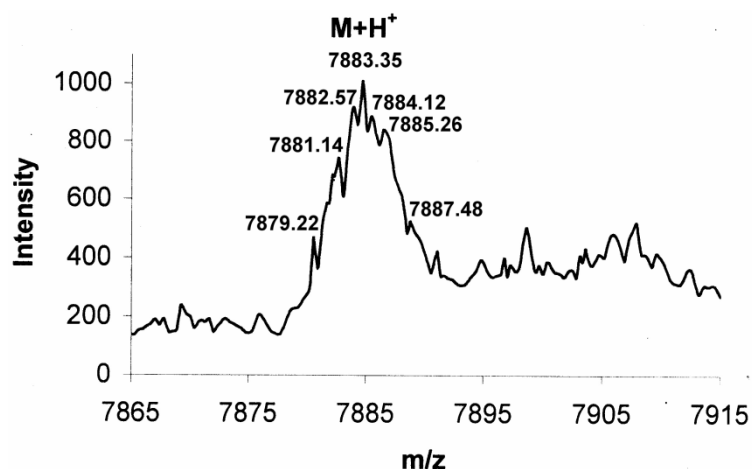
Based on their NMR features (vide infra), the octameric nanocapsules **46c** and **47c** have  $D_{4d}$  symmetry and can be described as a square antiprism (Scheme 3.12).<sup>[17]</sup> The square antiprism has two parallel squares that are twisted by 45°. Each vertex connects to the neighboring four vertices and forms up and down triangles. In **46c**, the eight cavitands occupy the vertex positions and the diamine linkers lie upon the edges. Based on its  $D_{4d}$  symmetry, the expected splitting patterns in the <sup>1</sup>H NMR and <sup>13</sup>C NMR of **46c** and **47c** are identical to those described for the tetramer **46b** and **47b**.

Indeed,  $^1\text{H}$ ,  $^{13}\text{C}$  NMR spectroscopy and molecular modeling studies support the structure assignment. In the  $^1\text{H}$  NMR spectra, greater signal dispersion is observed for the condensation product **46c** before reduction (Figure 3.9 a and Table 3.3). The two singlets at 8.45 and 8.13 ppm (ratio 16:16) are assigned to the 32 imine protons of **46c** ( $\text{H}_{\text{imine}}$ ). The singlet at 7.08 ppm is assigned to 16 aryl protons  $\text{H}_{\text{a}}$  and the remaining 16 aryl protons are part of the broad singlet at 7.13 ppm. Two doublets at 5.82 and 5.58 ppm (ratio 8:24) are assigned to the 32 outward pointing acetal protons  $\text{H}_{\text{o}}$ , which couple to the 32 inward pointing acetal protons  $\text{H}_{\text{i}}$  at 4.44, 4.36 and 4.30 ppm (ratio 16:8:8). In the  $^{13}\text{C}$  NMR spectrum of **47c** (Figure 3.9 c), the expected signal patterns are observed for  $\text{C}_1$ ,  $\text{C}_3$ ,  $\text{C}_4$  and  $\text{C}_{10}$ : two signals for each of  $\text{C}_1$  and  $\text{C}_3$  with equal intensity, four signals for  $\text{C}_4$  with equal intensity, and three signals for  $\text{C}_{10}$  in a ratio 1:1:2.



**Figure 3.9** Partial  $^1\text{H}$  NMR spectra (400 MHz; 22  $^\circ\text{C}$ ) of (a) crude products formed in the reaction of **40** with two equivalents of **43** in the presence of 10 mol% TFA in  $\text{CH}_2\text{Cl}_2$  after 67 hrs (in  $\text{CDCl}_3$ ; signals assigned to **46c** are marked) and (b) of **47c**· $32\text{CF}_3\text{COOH}$  in  $\text{CD}_3\text{OD} + 0.4 \text{ v}\%$  TFA-*d*. (c) Partial  $^{13}\text{C}$  NMR spectra (100 MHz, 22  $^\circ\text{C}$ ,  $\text{CD}_3\text{OD} + 0.4 \text{ v}\%$  TFA-*d*) of **47c**· $32\text{CF}_3\text{COOH}$ .

The MALDI-TOF mass spectrum of **47c** shows a strong signal at  $m/z = 7883.35$  (Figure 3.10 and Table 3.4), which is the expected  $m/z$  ratio for the protonated octameric nanocapsule **47c**.



**Figure 3.10** MALDI-TOF mass spectrum of **47c**.

There is no evidence for the presence of structurally more complex species. Catenated tetrameric, hexameric or octameric species, that could have the same molecular weight as **47a-c**, will have lower symmetry and therefore more complicated NMR splitting patterns.

### 3.2.5 Diffusion rate of nanocapsules

The solvodynamic diameters of the nanocapsules **47a-c** were determined from diffusion NMR studies. Diffusion studies using the bipolar pulse pair longitudinal eddy-current-delay (BPP-LED) pulse sequence in CD<sub>3</sub>OD with 0.4 v% CF<sub>3</sub>CO<sub>2</sub>D yielded a diffusion rate constant  $D = (2.28 \pm 0.09) \times 10^{-6} \text{ cm}^2/\text{s}$  for **47a**, which was used to calculate the solvodynamic diameter  $d = 3.2 \text{ nm}$  from the Stokes-Einstein equation by assuming that **47a** is a sphere (Table 3.5).<sup>[18a]</sup> The diffusion rates of **47b** and **47c** are  $(2.42 \pm 0.07) \times 10^{-6} \text{ cm}^2/\text{s}$ , and  $(1.84 \pm 0.06) \times 10^{-6} \text{ cm}^2/\text{s}$ , respectively (Table 3.5). **47b** can also be viewed as a sphere, whereas **47c** resembles an oblate ellipsoid. However, the aspect ratio  $\rho = a(\text{width})/b(\text{height}) = 35/25 = 1.4$ , which is taken from the energy-minimized structure of

**47c**•32H<sup>+</sup>, is so small that the Stokes-Einstein equation is still applicable for the solvodynamic diameter calculation.<sup>[26]</sup>

$$\text{Stokes-Einstein equation: } D = \frac{kT}{3\pi d\eta} \quad (3.1)$$

$D$ , diffusion rate constant;  $k$ , Boltzmann constant;  $T$ , temperature;  $d$ , particle diameter;  $\eta$ , solvent viscosity.

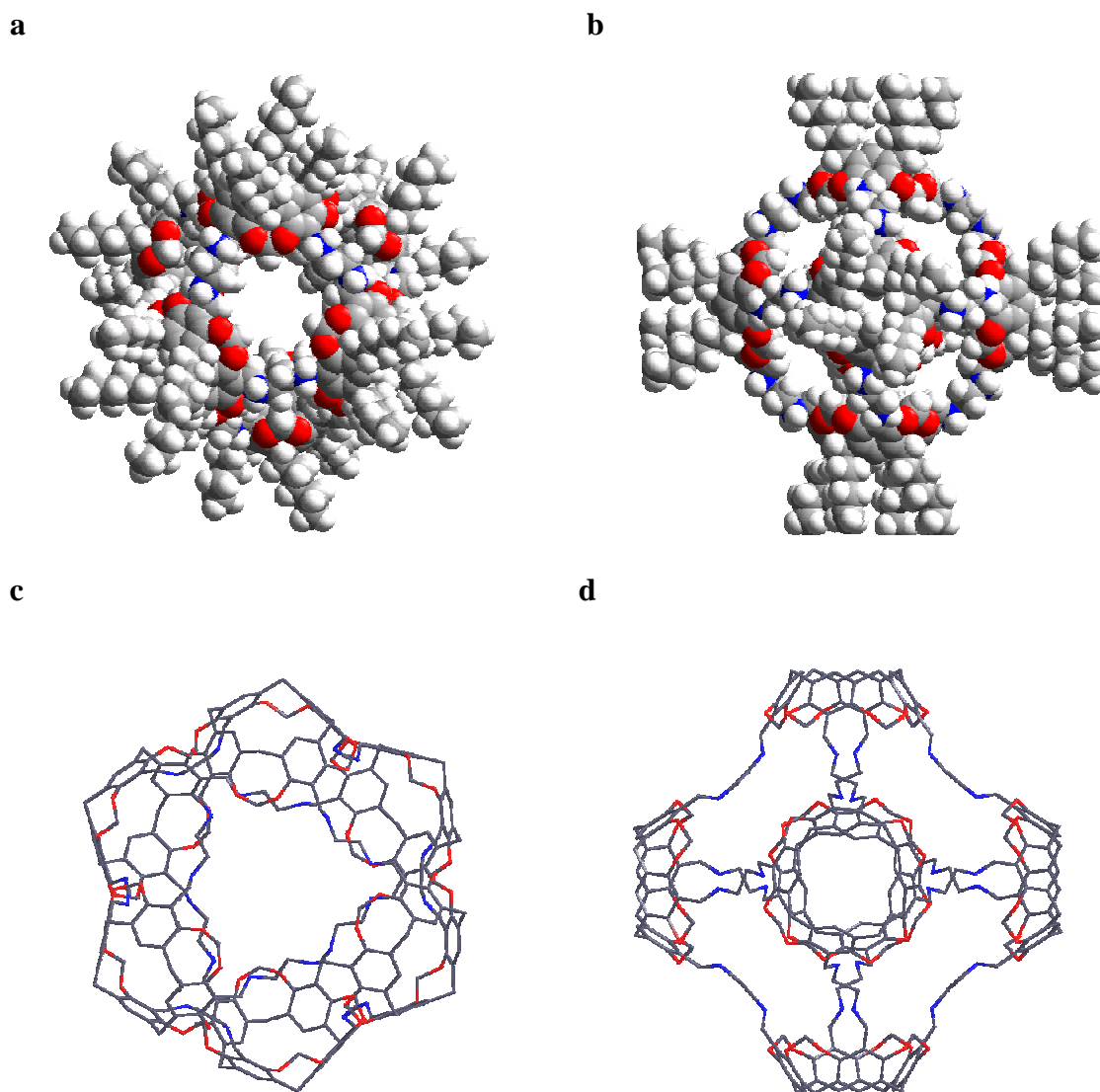
**Table 3.5** Diffusion constants  $D$  in CD<sub>3</sub>OD + 0.4 v% TFA- $d$  at 25 °C, solvodynamic diameters  $d$  and cavity volumes of **47a-c**.

compd.	$D$ (x10 <sup>-6</sup> cm <sup>2</sup> /s)	$d$ (Å)	cavity volume (Å <sup>3</sup> )
<b>47a</b>	2.28 ± 0.09	32	1700
<b>47b</b>	2.42 ± 0.07	30	450
<b>47c</b>	1.84 ± 0.06	40	3000

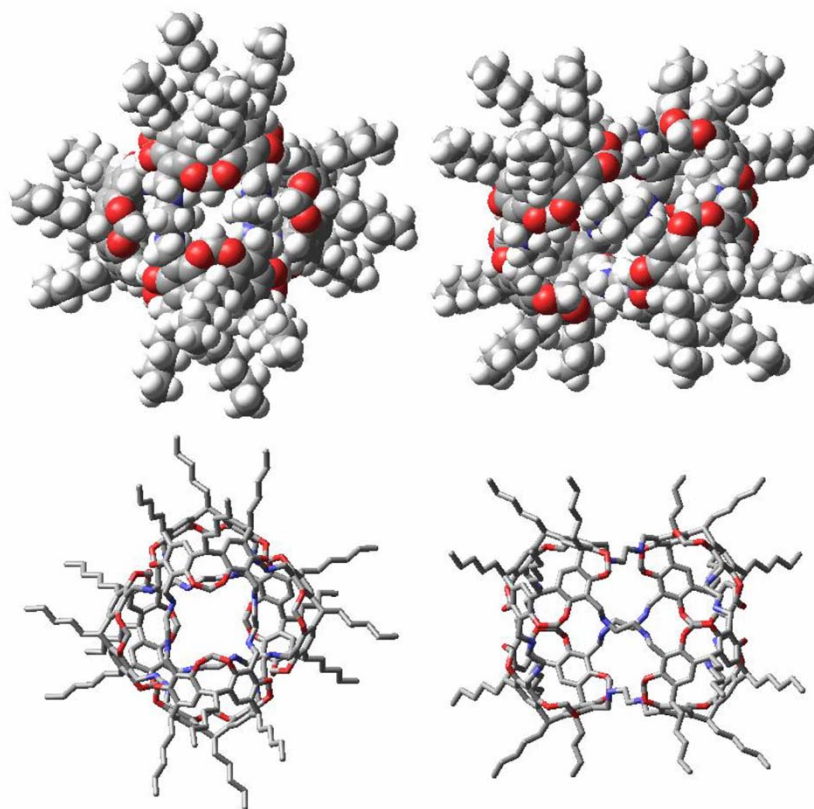
Molecular mechanics modeling studies (Amber\* force field) showed an approximate 1700 Å<sup>3</sup> inner cavity of **47a** (Figure 3.11 and Table 3.5), which is large enough to encapsulate multiple-guest molecules or a single biomolecule.<sup>[19]</sup> The tetramer **47b** has a cavity volume of approximate 450 Å<sup>3</sup> (Table 3.5).<sup>[19]</sup> This was calculated by connecting the centers of each cavitand and calculating the volume of the tetrahedron formed. Four of the six portals are nearly spherical with a diameter of 7-8 Å. Views along the two  $C_2$  axes of energy-minimized structure of **47b** are shown (Figure 3.12). On the other hand, the octamer **47c** has a cavity volume of approximate 3000 Å<sup>3</sup> (Table 3.5).<sup>[19]</sup> This was



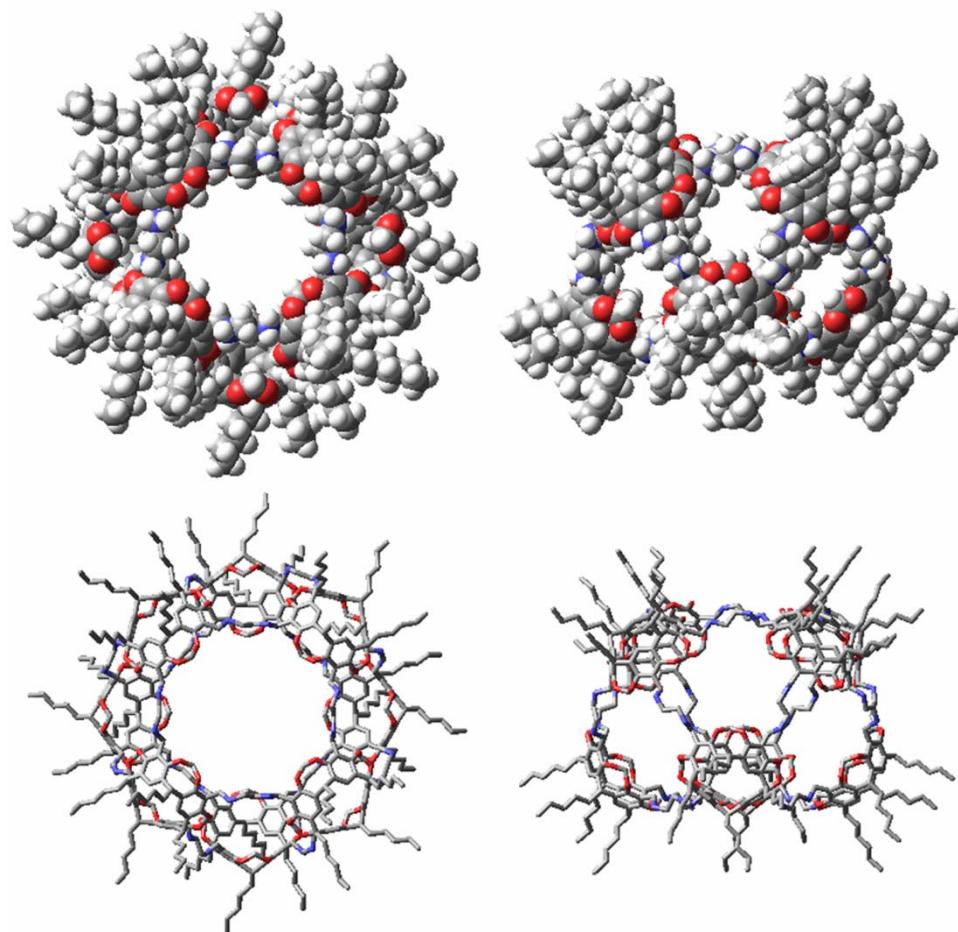
estimated by connecting the centers of each cavitand and calculating the volume of the formed square antiprism. To our knowledge, the octameric nanocapsule **47c** is one of the largest capsules based on resorcin[4]arene building blocks. Its triangular portal has a diameter of 8 Å, and the quadrangular portal has a diameter of 12 Å. Top and side views of the energy-minimized structure of **47c** are shown in Figure 3.13.



**Figure 3.11** Views along the  $C_3$  (a, c) and  $C_4$  axis (b, d) of energy-minimized structures of **47a**•24H<sup>+</sup> (a, b: space-filling model; Amber\* force field,<sup>[19a]</sup> GB/SA water solvation model<sup>[19b]</sup>) and **46a** (c, d: stick model; H and pentyl groups omitted; Amber\* force field;<sup>[19a]</sup> vacuum).



**Figure 3.12** Views along the two  $C_2$  axes of energy-minimized structures of **47b**•16H<sup>+</sup> (Amber\* force field,<sup>[19a]</sup> GB/SA water-solvation model<sup>[19b]</sup>). Atom coloring: C gray; H white; O red; N blue.



**Figure 3.13** Top and side views of energy-minimized structures of **47c**•32H<sup>+</sup> (Amber\* force field,<sup>[19a]</sup> GB/SA water-solvation model<sup>[19b]</sup>). Atom coloring: C gray; H white; O red; N blue.

Ercolani has developed a model to treat thermodynamically controlled competition reactions between self-assembly and nonlinear random polymerization. This model requires two input parameters: the intermolecular equilibrium constant of monofunctional reactants,  $K_{\text{inter}}$ , and the average effective molarity of the self-assembly, EM.<sup>[25]</sup> The product  $K_{\text{inter}}\text{EM}$  must be higher than a certain limit in order for efficient self-assembly to take place.  $K_{\text{inter}}\text{EM}$  can be calculated from the number of components in the assembly,  $N$ ,

the number of bonds joining those components together,  $B$ , and the number of functional sites in the building blocks in a binary system,  $l$  and  $m$  (Equation 3.5). For the condensation reaction under investigation, tetraformyl cavitand **40** has four reaction sites and ethylenediamine **43** has two reaction sites (Table 3.6).  $K_{\text{interEM}}$  for each assembly was calculated and is listed together with the numbers of intermolecular steps vs. that of intramolecular steps in Table 3.6. If  $K_{\text{inter}}$  is considered as constant for all cases, it can be seen that the assembling of the three nanocapsules **46a-c** have similar effective molarity requirements ( $K_{\text{interEM}} \geq 6.82, 5.95$  and  $5.59$ ), whereas the formation of the hypothetical octaminohemisarcosine **46d** needs a much higher effective molarity ( $K_{\text{interEM}} \geq 10.29$ ).

**Table 3.6** Calculation of  $(K_{\text{interEM}})_{\text{min}}$  and the number of intermolecular/intramolecular steps for the assembly of **46a-d**.

compd.	$l$	$m$	$N$	$B$	$\chi_{S\text{max}}$	$\chi_c$	$b$	$K_{\text{interEM}} \geq$	# inter/intra
<b>46a</b>	4	2	18	24	0.89	0.58	1.73	5.95	17/7
<b>46b</b>	4	2	12	16	0.85	0.58	1.73	6.82	11/5
<b>46c</b>	4	2	24	32	0.92	0.58	1.73	5.59	23/9
<b>46d</b>	4	2	6	8	0.71	0.58	1.73	10.29	5/3

$$\chi_{S\text{max}} = \frac{N-1}{N+1} \quad (3.2), \text{ reacted functional groups in the polymer when the assembly } S \text{ has}$$

the highest concentration;

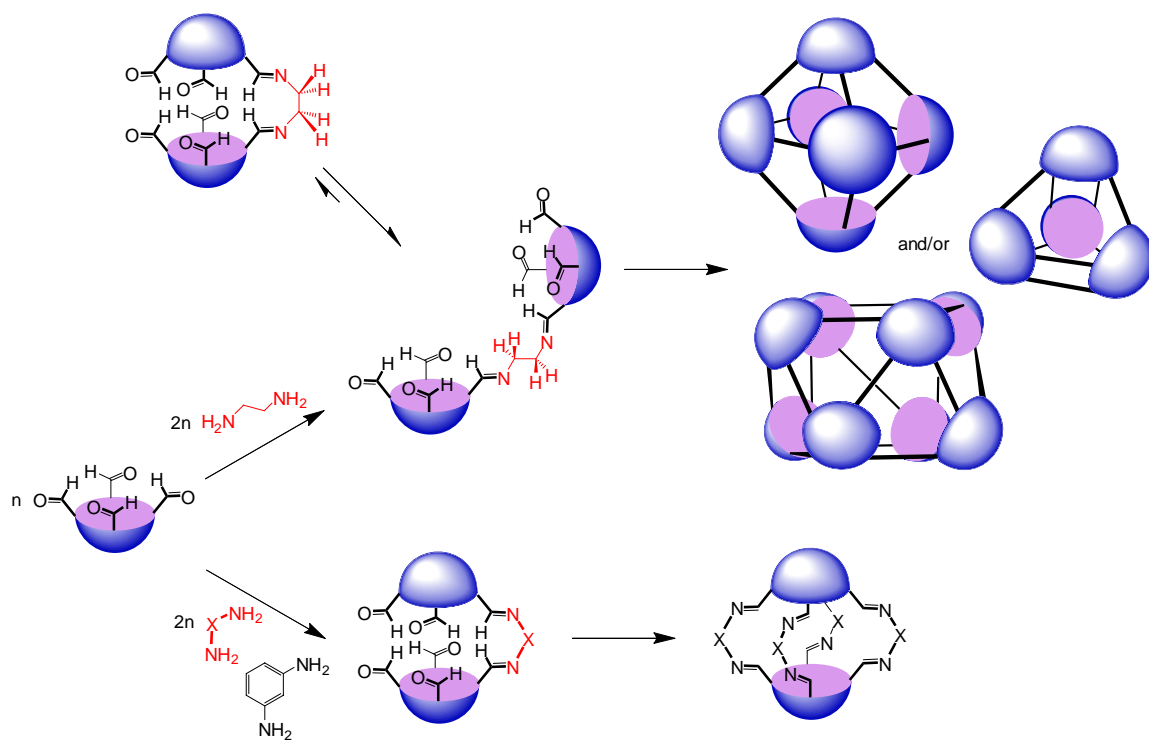
$$\chi_c = \frac{1}{\sqrt{(l-1)(m-1)}} \quad (3.3), \text{ critical gel-point;}$$

$$b = 1/\chi_c \quad (3.4);$$

$$K_{\text{inter}} EM \geq \left[ \frac{100}{B} \frac{b^{N+1}}{(b-1)^2} \right]^{1/(B-N+1)} \quad \text{when } \chi_{\text{Smax}} > \chi_{\text{c}}, \quad (3.5).$$

### 3.2.6 Diamino linker effect on the condensation reaction

The observed linker effects on the formation of octaiminohemicarcerands **45a-g** (Table 3.1) might arise from the relative conformation of the linkers required to achieve the orientation of the two cavitands in an octaimine hemicarcerand and the high entropic penalty of forming larger capsules or polymeric products. It can be summarized as follows: flexible diamines, such as **44a-c**, **44d** and **44e**, which can adopt many low energy conformations, or rigid diamines, such as **44f** and **44g**, in which the angle between the two C-N bonds is  $\sim 120^\circ$ , yield octaimine hemicarcerands. Linear rigid diamines, such as **44h**, yield tetrameric capsules (Chapter 4). Ethylenediamine **43** is flexible, but doesn't yield the hypothetical hemicarcerand **46d**. Molecular mechanics calculations show that the ethylenediamine units adopt an *anti*-conformation in the hexameric capsule **46a**, but a *gauche*-conformation in **46d**, which outweighs the higher entropic penalty to form the larger capsules (Figure 3.14). Therefore **46a** is less strained than **46d** and is thermodynamically more favorable. Surprisingly, **44i** and **44j** don't yield an octaimine hemicarcerand, even though the two C-N bonds in **44i** and **44j** are in a *gauche* conformation. We speculate that the latter octaimine hemicarcerands are disfavored by unfavorable rim-to-linker interactions.



**Figure 3.14** Linker effect on the condensation of **40** with **44a-j** and **43**.

### 3.2.7 Effects of acid catalyst and excess of ethylenediamine

Solvent has a considerable effect on the outcome of the condensation reaction (Table 3.2). Another critical component is the catalyst. Typically, the condensation reactions reached the final equilibria after approximate two days in the presence of 2.5 mol% TFA per formyl group. Extended reaction times (greater than four days) caused a slow decrease in the yields. This slow decomposition was acid dependent. If unfiltered chloroform (or dichloromethane) was used for the formation of **46a** (or **46c**), the reaction solution became yellow within one day as the consequence of the larger amounts of HCl in the solvent. Lewis acids have also been used to catalyze transimination reactions.<sup>[23]</sup>  $\text{MgSO}_4$  catalyzed the octaiminohemicarcerand formation with much slower rate compared to TFA (6 days vs. 1 h).<sup>[10,13b]</sup> Lehn and coworkers showed that transimination reactions catalyzed

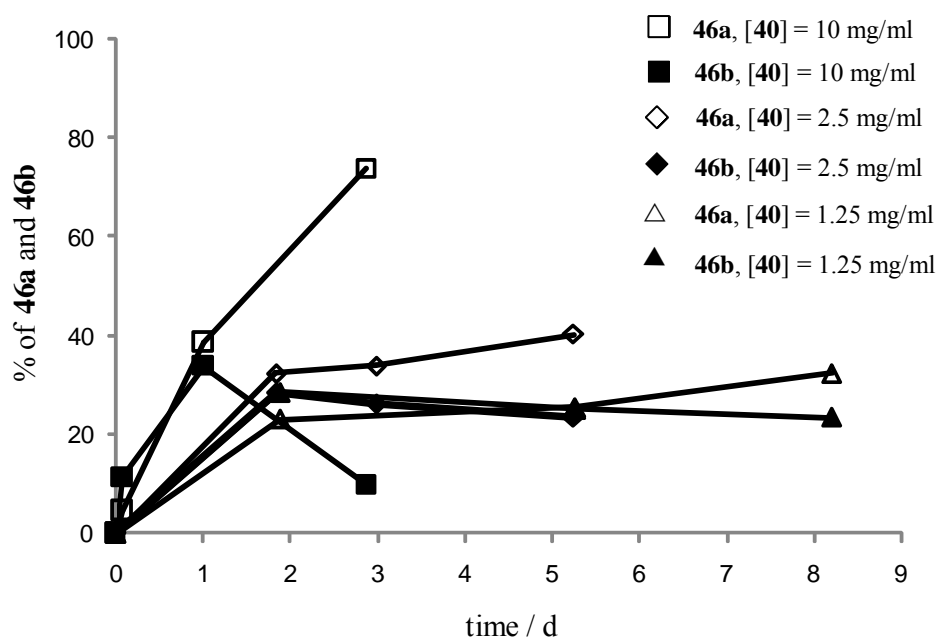
by  $\text{Sc}(\text{OTf})_3$  show similar reaction rates as those catalyzed by TFA.<sup>[23a]</sup> However, it turned out that the nanocapsule formation catalyzed by  $\text{Sc}(\text{OTf})_3$  was considerably slower than with TFA in our case. For example, if the formation of **46c** was catalyzed by  $\text{Sc}(\text{OTf})_3$ , ~18% unreacted formyl groups were observed after 17 hrs and all signals were broadened in the  $^1\text{H}$  NMR spectrum. On the other hand, it was found that a slight excess of ethylenediamine **43** (~2.5 mol%) greatly accelerated the condensation reactions through a transimination mechanism.

### 3.2.8 Concentration Effects

In a dynamic assembly system, the building block concentration can influence the oligomer-to-polymer ratio as well as the distribution of the oligomers. Jacobsen-Stockmayer theory predicts the existence of a critical monomer concentration below which only oligomers are present.<sup>[27]</sup> For reactions carried out below the critical monomer concentration, the oligomer distribution is controlled by the building block concentration and the stability of individual oligomers. If applied to the condensation reaction between **40** and **43**, this theory predicts that the ratio **46a/46b** should decrease, as the concentration is lowered. When the condensation between **40** and **43** in chloroform was carried out at lower concentration of **40** ( $[\text{40}] = 2.5$  and  $1.25$  mg/ml) as compared to the condensation that gave ~80% **46a** and a **46a/46b** ratio of 80/5 at  $[\text{40}] = 10$  mg/ml, the reaction became slower (Figure 3.15). Even though it was not certain that the reaction carried out at  $[\text{40}] = 1.25$  mg/ml was fully equilibrated after eight days, the ratio of **46a/46b** only changed from 0.8 to 1.4 within the final six days. This indicates that the **46a/46b** ratio, even after extended reaction time, will likely be much smaller compared to



that obtained at normal concentration ( $[40] = 10 \text{ mg/ml}$ ) at equilibrium, supporting the theoretical considerations.

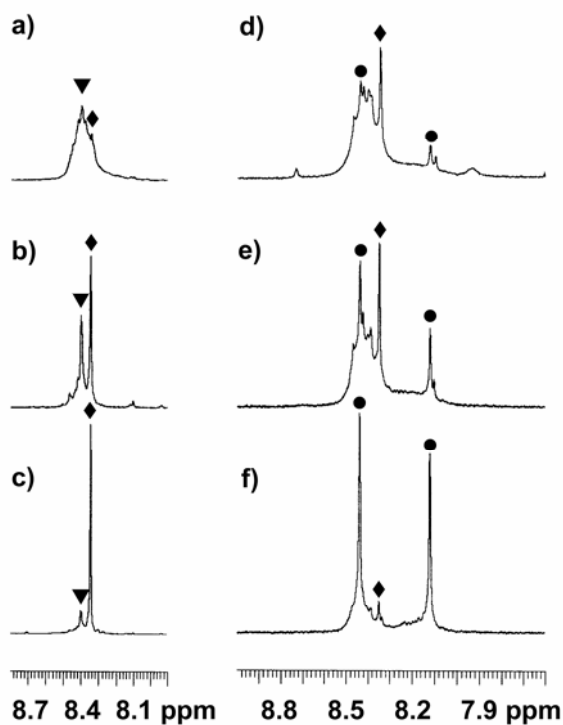


**Figure 3.15** Percentage of **46a** and **46b** vs. time for the condensation of **40** and two equivalents **43** in  $\text{CHCl}_3$  with different initial concentration  $[40]$ .

### 3.2.9 Mechanistic and energetic aspects of molecular nanocapsule formation in solution

Close analysis of the  $^1\text{H}$  NMR spectra during the capsule formation shines light on some mechanistic aspects of the nanocapsule **46a-c** formation (Figure 3.15 and 3.16). In Table 3.3, the chemical shifts for the characteristic imine protons ( $\text{H}_{\text{imine}}$ ) are 8.34, 8.41 and (8.45, 8.13) ppm for **46a**, **46b** and **46c**, respectively. During the hexamer **46a** formation (Figure 3.16 a-c), the initially formed imine signal at  $\delta = 8.41$  ppm decreased (from

~33% at 24 h to 9% at equilibrium), while a neighboring signal at  $\delta = 8.34$  ppm increased correspondingly (from 39% to 74%). This indicates the evolution of **46a** from **46b**, which was also observed in the GPC chromatograms. Similar phenomena were observed during the octamer **46c** formation (Figure 3.16 d-f). After a short reaction time (0.7 h), the characteristic imine signal for **46a** predominated (~18%) with ~7% **46c** present. As the reaction progressed, the imine signals for **46c** grew gradually and that for **46a** decreased. After an additional 1.5 days, the reaction reached equilibrium and contained



**Figure 3.16** Partial  $^1\text{H}$  NMR spectra (a, c, e and f, 400 MHz; b and d, 300 MHz; 22  $^\circ\text{C}$ ;  $\text{CDCl}_3$ ) during the formation of **46a** after 1.7 (a), 24 (b) and 69 hrs (c), and **46c** after 0.7 (d), 9 (e) and 31 hrs (f). The imine signals  $\text{H}_{\text{imine}}$  for **46a** ( $\blacklozenge$ ), **46b** ( $\blacktriangledown$ ) and **46c** ( $\bullet$ ) are marked.

5% **46a** and 65% **46c**. This shows that smaller capsules are formed as kinetic products, which require less imine bond formation compared to larger capsules, and subsequently grow into a larger, thermodynamically more stable capsule.

The lack of linear oligomers or 2D sheets can be rationalized by an unfavorable enthalpy effect, since these possible products have unreacted formyl and amino groups at their ends or periphery. A model reaction has been carried out to determine the thermodynamics of imine formation. The equilibrium constant of the reaction between tetraformyl cavitand **40** and *n*-butylamine was analyzed by <sup>1</sup>H NMR spectroscopy and its temperature dependence was measured. The reaction was carried out in water saturated CDCl<sub>3</sub> in the presence of 7.1 mg **40**, four equivalents of *n*-butylamine and 0.04 equivalents TFA. A single point equilibrium constant was calculated from the integration of the unreacted formyl protons (*CHO*, δ = 10.4-10.2 ppm), all imine protons (*CHN*, δ = 8.6-8.0 ppm), water (*H<sub>2</sub>O*, δ = 1.8 ppm) and the α-methylene protons of unreacted *n*-butylamine (*CH<sub>2</sub>NH<sub>2</sub>*, δ = 2.7 ppm). The reaction temperature varied from 298 K to 318 K. The equilibrium constant was calculated as

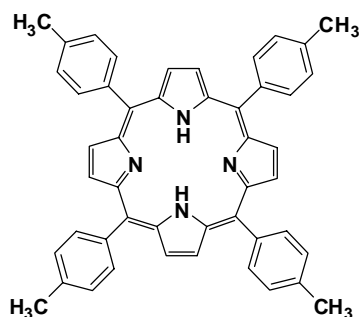
$$K = [\text{CHN}] \times [\text{H}_2\text{O}] / ([\text{CHO}] \times [\text{CH}_2\text{NH}_2]), \quad (3.6)$$

A van't Hoff plot gave Δ*H* = -6.5 kcal/mol and Δ*S* = -8.5 cal/mol/K. The equilibrium constant at 298 K is *K*<sub>298K</sub> = 770 ± 50, which corresponds to Δ*G* = -3.9 kcal/mol. Therefore, each unreacted formyl or amino group will disfavor linear oligomers or 2D sheets by Δ*G* > 3.9 kcal/mol compared to fully reacted nanocapsules with the same

number of building blocks. This is consistent with observations by others. Polymeric products were seldom observed in the synthesis of Schiff base macrocycles.<sup>[24]</sup>

### 3.2.10 Template effect

Template effects have been observed during hemicarcerand formation when only one guest molecule served as the template.<sup>[20,21]</sup> For large capsules, the cavities usually are big enough to accommodate more than one guest molecule, and these molecules can serve as a template jointly during capsule formation. Resorcinarene encapsulates several chloroform molecules during formation of the hydrogen bonded hexameric capsule **36** in wet chloroform.<sup>[22]</sup> When Sherman et al. prepared the hexameric capsule **38** through a multi-step synthesis, they found that seven DMSO solvent molecules were encapsulated permanently.<sup>[9b]</sup> The carceplex formation was shown to be controlled by a multi-guest molecule template effect. DMSO was a much better template than DMA or DMF. The formation of **46a** was investigated in the presence of 5,10,15,20-tetra-*p*-tolyl-21*H*,23*H*-porphine (vide infra), which according to molecular modeling studies would fit into the cavity such that the four methyl groups are located in four equatorial cavitands of **46a**. <sup>1</sup>H NMR showed that the condensation was not affected by this porphyrin and no guest encapsulation was observed either. Also (*n*-butyl)<sub>4</sub>NBr was not able to serve as a template during the formation of **46a**.



5,10,15,20-tetra-*p*-tolyl-21*H*,23*H*-porphine

### 3.3 Conclusions

Covalent molecular nanocapsules have been synthesized in one-pot procedures through the condensation of tetraformyl cavitand with ethylenediamine. This thermodynamically driven reaction is straightforward and very efficient, which paves a new way to make covalent large capsules. Studies have shown that solvent plays a vital role in controlling the geometry of the nanocapsules, from a distorted tetrahedron in THF, an octahedron in chloroform to a square antiprism in  $\text{CH}_2\text{Cl}_2$ . These nanocapsules have inner cavities large enough to encapsulate multiple guest molecules. The applications in host-guest chemistry are being explored in the Warmuth lab.

The requirements to obtain a high yield of a covalent nanocapsule include: a) the bond formations must be reversible and the targeted compound should be the thermodynamically most stable species among all possible products; b) the stoichiometry of the building blocks must be correct; and c) the geometries of the starting components are important and if chosen adequately allow the assembly of a predicted nanocapsule species.

### 3.4 Experimental section

#### 3.4.1 General procedure

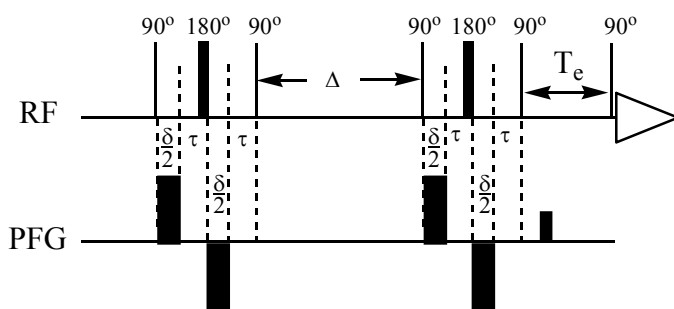
All reactions were conducted under argon. Reagents and chromatography solvents were purchased from Aldrich and used without further purification. NMR spectra were recorded on Varian 300, 400 or 500 MHz FT-NMR spectrometers.  $^1\text{H}$  NMR spectra recorded in  $\text{CDCl}_3$  or  $\text{CD}_3\text{OD}$  were referenced to residual  $\text{CHCl}_3$  and  $\text{CHD}_2\text{OD}$  at 7.26 ppm and 3.30 ppm, respectively.  $^{13}\text{C}$  NMR spectra recorded in  $\text{CDCl}_3$  or  $\text{CD}_3\text{OD}$  were referenced to  $\text{CDCl}_3$  and  $\text{CD}_3\text{OD}$  at 77.0 ppm and 49.0 ppm, respectively. Mass spectra were recorded on an Applied Biosystems Voyager DE-Pro mass spectrometer in reflector mode (MALDI-TOF). 2',4',6'-Trihydroxylacetophenone (THAP) was used as the matrix. For the compounds reported here, positive molecular ions were usually detected as proton or sodium adducts.

#### 3.4.2 Gel permeation chromatography

Gel permeation chromatography was performed on a Varian Rainin Dual Pump HPLC system equipped with dual wavelength UV/Vis detector, Eppendorf CH-30 column heater and Jordi GPC column (cross linked DVB;  $10^3$  Å pore size; MW cutoff ~ 25,000; 7.8 mm  $\times$  30 cm) with  $\text{CH}_2\text{Cl}_2$ /1%  $\text{NEt}_3$  as mobile phase at 60 °C and a flow of 1 ml/min. Approximate molecular weights of analytes were determined from a semi logarithmic calibration plot ( $\ln(\text{MW})$  against retention time) using benzene (MW 78); cavitand **40** (MW 928) and a NMP hemicarceplex (MW 2348)<sup>[28]</sup> as molecular weight standards.

### 3.4.3 Diffusion rate measurement of hexamer **47a**<sup>[18a]</sup>

Diffusion measurements were carried out with hexamer **47a** (5 mg) in 0.6 ml CD<sub>3</sub>OD containing 0.4 % (v/v) CF<sub>3</sub>COOH. Spectra were recorded on a Varian UNITY 400 NMR spectrometer operating at a <sup>1</sup>H frequency of 400 MHz with a <sup>1</sup>H/<sup>19</sup>F/<sup>31</sup>P/<sup>13</sup>C 5mm PFG autoswitchable probe, which has actively shielded z-axis gradients of up to 60 G cm<sup>-1</sup> strength, using the bipolar pulse pair longitudinal eddy-current-delay (BPP-LED) pulse scheme:<sup>[18b-d]</sup>



The diffusion rate was calculated from the decay of the signal intensity with increasing field gradient strength:

$$I = I_0 \exp[-D\gamma^2 G^2 \delta^2 (\Delta + 2/3 \delta + 3/4 \tau)]$$

$$\ln(I) = -D\gamma^2 G^2 \delta^2 (\Delta + 2/3 \delta + 3/4 \tau) + \ln(I_0)$$

$$= -\text{const.} \times D \times G^2 + \ln(I_0)$$

$$\text{with const.} = \gamma^2 \delta^2 (\Delta + 2/3 \delta + 3/4 \tau)$$

$G = gcal \times gzlvl6$ , gradient strength (gauss/cm)

$gzlvl6 = \text{arrayed}$

$\gamma$ , proton gyromagnetic ratio

$D$ , diffusion rate ( $\text{cm}^2/\text{s}$ )

$\delta$ , gradient duration

$\Delta$ , time delay

$\tau$ , time delay

The field gradients were calibrated with the residual  $^1\text{H}$  signal in a  $\text{D}_2\text{O}$  sample containing 1%  $\text{H}_2\text{O}$ . The literature value of  $D(\text{HDO}) = (1.902 \pm 0.002) \times 10^{-5} \text{ cm}^2\text{s}^{-1}$  was used for the self-diffusion rate of HDO at  $25^\circ\text{C}$ .<sup>[18e]</sup>

#### Diffusion measurement parameters

	$\gamma[\text{s}^{-1}\text{gauss}^{-1}]$	$\delta[\text{s}]$	$\Delta[\text{s}]$	$\tau[\text{s}]$	const.
HDO	26752.22	0.003	0.15	0.0002	980.018
Hexamer	26752.22	0.003	0.20	0.0002	1302.075

$g_{\text{cal}} = 0.0016481$  on 400 MHz  $^1\text{H}$  NMR.

#### Experimental data

##### HDO

$g_{\text{zlvl6}}$	$G = g_{\text{cal}} \times g_{\text{zlvl6}}$	$G^2$	I	$\ln(I)$
1000	1.6481	2.716234	100	4.60517
1500	2.47215	6.111526	91.8619	4.520286
2000	3.2962	10.86493	82.8133	4.416589
3000	4.9443	24.4461	60.9835	4.110603
4000	6.5924	43.45974	41.108	3.716203



5000	8.2405	67.90584	25.3693	3.23354
6000	9.8886	97.78441	14.6457	2.684147
7000	11.5367	133.0954	8.24523	2.109635
8000	13.1848	173.839	5.02518	1.614461

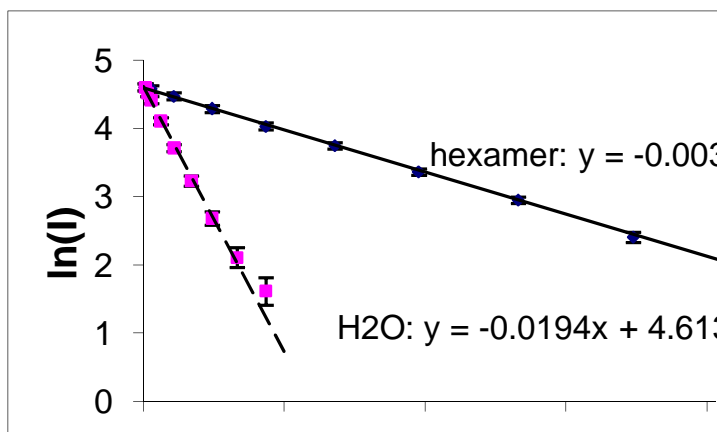
### Hexamer 47a

gzlvl6	$G = g_{\text{cal}} \times \text{gzlvl6}$	$G^2$	I	$\ln(I)$
1000	1.6481	2.716234	100	4.60517
2000	3.2962	10.86493	97.6088	4.580968
4000	6.5924	43.45974	87.7544	4.474542
6000	9.8886	97.78441	72.9098	4.289223
8000	13.1848	173.839	56.4263	4.032935
10000	16.481	271.6234	42.4835	3.749116
12000	19.7772	391.1376	28.8682	3.362741
14000	23.0734	532.3818	19.1312	2.951321
16000	26.3696	695.3558	11.0824	2.405358
18000	29.6658	880.0597	7.38488	1.999435

Plot  $\ln(I)$  vs.  $G^2$ , slope = -const.  $\times D$ , intercept =  $\ln(I_0)$

$$D(\text{hexamer}) = [\text{slope}(\text{hexamer})/\text{slope}(\text{HDO})] \times D(\text{HDO}) \times [\text{const.}(\text{HDO})/\text{const.}(\text{hexamer})]$$

	slope	$\Delta(\text{slope})$	$D [\text{cm}^2 \text{s}^{-1}]$	$\Delta(D) [\text{cm}^2 \text{s}^{-1}]$
HDO	-0.00194	0.000638	$1.902 \times 10^{-5}$	$0.002 \times 10^{-5}$
Hexamer	-0.00310	7.249E-5	$2.282 \times 10^{-6}$	$9.218 \times 10^{-8}$



#### Determination of Solvodynamic radius $r$ :

Application of the Stokes-Einstein equation

$$D = \frac{kT}{6\pi\eta r}$$

with  $k = 1.38066 \times 10^{-23} \text{ J K}^{-1}$

$T = 298 \text{ K}$

$\eta = (0.602 \pm 0.002) \text{ mPa s}^{-1}$  (Viscosity of  $\text{CD}_3\text{OD}$  at  $25^\circ\text{C}$ ) <sup>[18f]</sup>

gave

$r = 1.59 \pm 0.06 \text{ nm}$

#### 3.4.4 Synthesis of tetraformyl cavitand **40**

Tetraformyl cavitand **40** was synthesized according to the reported procedure with some modifications.<sup>[12,13]</sup> Tetrabromocavitand **13** (5.0 g, 4.42 mmol) was dried overnight in a 500 ml 3-necked round bottom flask at high vacuum at  $110^\circ\text{C}$ . Then, it was dissolved in

250 ml dry THF. The solution was cooled to -78 °C and 2.5 M n-butyl lithium/hexanes solution (14.1 ml, 35.4 mmol) was added into the reaction flask. The reaction mixture was stirred at -78 °C for 20 min. Then, it was warmed up to 0 °C and stirred for 30 min at 0 °C. The reaction mixture was again cooled to -78 °C and dry *N,N*-dimethylformamide (DMF) (dried over freshly activated 4 Å molecular sieves for 24 h, while protected under argon) (13.7 ml, 177 mmol) was added into the reaction flask. After stirring at -78 °C for 10 min, it was warmed up to room temperature and stirred for additional 1 h at room temperature. The reaction was quenched with 100 ml 5% NH<sub>4</sub>Cl aq, extracted with 200 ml EtOAc. The aq. layer was back-extracted twice with 100 ml EtOAc. The organic layers were combined and washed with 100 ml saturated NaHCO<sub>3</sub> aq., 100 ml brine, dried over MgSO<sub>4</sub> and concentrated down. The crude product was purified by flash column chromatography on silica gel with 95:5 (vol/vol) CH<sub>2</sub>Cl<sub>2</sub>/EtOAc (*R<sub>f</sub>* = 0.15), which gave tetrafromyl cavitand **40** as a white powder (1.66 g, 40% yield). If necessary, the product was further purified by normal phase HPLC using 2.3 vol % THF/CH<sub>2</sub>Cl<sub>2</sub> as the mobile phase.

### 3.4.5 Synthesis of octaiminohemicarcerand **45a** (*Procedure A*)

Cavitand **40** (37.2 mg, 0.0401 mmol) was added to a solution of 1,3-diaminopropane **44a** (6.3 mg, 0.085 mmol) and trifluoroacetic acid (0.20 μL) in CDCl<sub>3</sub> (3 mL). The solution was stirred for 57.5 hrs under argon at room temperature. The solvent was removed and the residue was dried overnight at high vacuum at room temperature. The product was a yellow powder (> 95% yield). <sup>1</sup>H NMR (300 MHz, CDCl<sub>3</sub>, 25 °C): δ = 8.38 (s, 8H; CH=N), 7.11 (s, 8 H; aryl-*H*), 5.65 (d, <sup>2</sup>*J*(H, H) = 7.6 Hz, 8 H; OCH<sub>outer</sub>HO), 4.86 (t, <sup>3</sup>*J*(H,

H) = 8.0 Hz, 8 H;  $CH_{\text{methine}}$ ), 4.45 (d,  $^2J(\text{H}, \text{H}) = 7.6$  Hz, 8 H;  $OCH_{\text{innerHO}}$ ), 3.56 (t,  $^3J(\text{H}, \text{H}) = 7.6$  Hz, 16 H;  $NCH_2$ ), 2.25-2.20 (m, 16 H), 1.68 (m, 8 H;  $NCH_2CH_2$ ), 1.43-1.32 (m, 48 H), 0.91 (t, 24 H).  $^{13}\text{C}$  NMR (75 MHz,  $\text{CDCl}_3$ , 25 °C):  $\delta$  = 155.4, 153.5, 138.6, 124.2, 121.3, 100.7, 62.4, 36.8, 34.0, 32.3, 30.3, 27.9, 23.1, 14.5. FT-IR ( $\text{CHCl}_3$ ):  $\nu$  2925.8 (s), 2855.8 (s), 1641.5 (s), 1602.6 (m), 1587.3 (m), 979.9 (s). FAB-MS (NBA matrix):  $m/z$ : 2010.7 (100%,  $[\text{M}+\text{H}]^+$ , 2010.1 (calcd)).

### 3.4.6 Synthesis of octaiminohemicarcerand **45b**

Application of *procedure A* with 1,4-diaminobutane **44b** instead of **44a** (69 hrs reaction time) gave **45b** as a yellow powder (> 95% yield).  $^1\text{H}$  NMR (300 MHz,  $\text{CDCl}_3$ , 25 °C):  $\delta$  = 8.37 (s, 8H;  $CH=N$ ), 7.10 (s, 8 H; aryl- $H$ ), 5.59 (d,  $^2J(\text{H}, \text{H}) = 7.5$  Hz, 8 H;  $OCH_{\text{outerHO}}$ ), 4.87 (t,  $^3J(\text{H}, \text{H}) = 8.1$  Hz, 8 H;  $CH_{\text{methine}}$ ), 4.49 (d,  $^2J(\text{H}, \text{H}) = 7.5$  Hz, 8 H;  $OCH_{\text{innerHO}}$ ), 3.51 (br s, 16 H;  $NCH_2$ ), 2.23-2.17 (m, 16 H), 1.59 (m, 16 H;  $NCH_2CH_2$ ), 1.41-1.32 (m, 48 H), 0.92 (t, 24 H).  $^{13}\text{C}$  NMR (75 MHz,  $\text{CDCl}_3$ , 25 °C):  $\delta$  = 156.2, 153.6, 138.7, 124.5, 121.5, 100.4, 62.6, 36.7, 32.2, 30.0, 25.5, 27.8, 23.0, 14.4. FT-IR ( $\text{CHCl}_3$ ):  $\nu$  2921.5 (s), 2859.2 (s), 1637 (s), 1605.9 (m), 1578.6 (m), 1150.4 (m), 1088.2 (s), 1014.2 (s), 979.2 (s). FAB-MS (NBA matrix):  $m/z$ : 2066.8 (100%,  $[\text{M}+\text{H}]^+$ , 2066.2 (calcd)).

### 3.4.7 Synthesis of octaiminohemicarcerand **45c**

Application of *procedure A* with 1,5-diaminopentane **44c** instead of **44a** (21.5 hrs reaction time) gave octaimine **45c** as a yellow powder (> 95% yield).  $^1\text{H}$  NMR (300 MHz,  $\text{CDCl}_3$ , 25 °C):  $\delta$  = 8.35 (s, 8H;  $CH=N$ ), 7.12 (s, 8 H; aryl- $H$ ), 5.59 (d,  $^2J(\text{H}, \text{H}) = 7.5$  Hz, 8 H;  $OCH_{\text{outerHO}}$ ), 4.86 (t,  $^3J(\text{H}, \text{H}) = 7.8$  Hz, 8 H;  $CH_{\text{methine}}$ ), 4.42 (d,  $^2J(\text{H}, \text{H}) = 7.2$  Hz,

8 H;  $\text{OCH}_{\text{inner}}\text{HO}$ ), 3.50 (m, 16 H;  $\text{NCH}_2$ ), 2.23-2.17 (m, 16 H), 1.6-1.4 (m, 24 H;  $\text{NCH}_2\text{CH}_2\text{CH}_2$ ), 1.4-1.2 (m, 48 H), 0.91 (t, 24 H).  $^{13}\text{C}$  NMR (75 MHz,  $\text{CDCl}_3$ , 25 °C):  $\delta$  = 157.2, 153.6, 139.6, 138.7, 129.4, 126.1, 125.4, 124.0, 121.7, 100.8, 66.2, 36.8, 32.3, 30.2, 27.9, 23.1, 14.5. MS (MALDI-TOF)  $m/z$ : 2123.32 ( $\text{M}+\text{H}^{\oplus}$ , 100%); Calcd for  $\text{C}_{132}\text{H}_{169}\text{N}_8\text{O}_{16}+\text{H}^{\oplus}$ : 2123.27.

### 3.4.8 Synthesis of octaiminohemicarcerand **45d**

Application of *procedure A* with *meta*-xylylene diamine **44d** instead of **44a** (24.5 hrs reaction time) gave octaimine **45d** as a yellow powder (> 95% yield).  $^1\text{H}$  NMR (300 MHz,  $\text{CDCl}_3$ , 25 °C):  $\delta$  = 8.44 (s, 8H;  $\text{CH}=\text{N}$ ), 7.17 (s, 8 H; aryl-*H*), 7.11 (s, 4 H;  $-\text{C}_6\text{H}_4-$ ), 6.96 (d,  $^3J(\text{H}, \text{H}) = 7.8$  Hz, 8 H;  $-\text{C}_6\text{H}_4-$ ), 6.80 (t,  $^3J(\text{H}, \text{H}) = 7.2$  Hz, 4 H;  $-\text{C}_6\text{H}_4-$ ), 5.48 (d,  $^2J(\text{H}, \text{H}) = 7.2$  Hz, 8 H;  $\text{OCH}_{\text{outer}}\text{HO}$ ), 4.88 (t,  $^3J(\text{H}, \text{H}) = 8.1$  Hz, 8 H;  $\text{CH}_{\text{methine}}$ ), 4.72 (s, 16 H;  $\text{NCH}_2$ ), 4.48 (d,  $^2J(\text{H}, \text{H}) = 7.5$  Hz, 8 H;  $\text{OCH}_{\text{inner}}\text{HO}$ ), 2.25 (m, 16 H), 1.5-1.2 (m, 48 H), 0.93 (t,  $^3J(\text{H}, \text{H}) = 6.9$  Hz, 24 H).  $^{13}\text{C}$  NMR (75 MHz,  $\text{CDCl}_3$ , 25 °C):  $\delta$  = 157.2, 153.6, 139.6, 138.7, 129.4, 126.1, 125.4, 124.0, 121.7, 100.8, 66.2, 36.8, 32.3, 30.2, 27.9, 23.1, 14.5. MS (MALDI-TOF)  $m/z$ : 2259.27 ( $\text{M}+\text{H}^{\oplus}$ , 100%); Calcd for  $\text{C}_{144}\text{H}_{160}\text{N}_8\text{O}_{16}+\text{H}^{\oplus}$ : 2259.21.

### 3.4.9 Synthesis of octaiminohemicarcerand **45e**

Application of *procedure A* with *para*-xylylene diamine **44e** instead of **44a** (24.5 hrs reaction time) gave octaimine **45e** as a yellow powder (> 95% yield).  $^1\text{H}$  NMR (300 MHz,  $\text{CDCl}_3$ , 25 °C):  $\delta$  = 8.33 (s, 8H;  $\text{CH}=\text{N}$ ), 7.18 (s, 16 H;  $-\text{C}_6\text{H}_4-$ ), 7.10 (s, 8 H; aryl-*H*), 5.32 (d,  $^2J(\text{H}, \text{H}) = 7.2$  Hz, 8 H;  $\text{OCH}_{\text{outer}}\text{HO}$ ), 4.82 (t,  $^3J(\text{H}, \text{H}) = 7.8$  Hz, 8 H;  $\text{CH}_{\text{methine}}$ ),

4.60 (br s, 16 H;  $\text{NCH}_2$ ), 4.16 (d,  $^2J(\text{H}, \text{H}) = 7.5$  Hz, 8 H;  $\text{OCH}_{\text{inner}}\text{HO}$ ), 2.20 (br s, 16 H), 1.5-1.2 (m, 48 H), 0.91 (t,  $^3J(\text{H}, \text{H}) = 6.9$  Hz, 24 H).  $^{13}\text{C}$  NMR (75 MHz,  $\text{CDCl}_3$ , 25 °C):  $\delta$ =157.2, 153.4, 138.6, 138.3, 128.2, 124.0, 121.6, 99.8, 66.2, 36.6, 32.2, 30.1, 27.8, 23.0, 14.5. MS (MALDI-TOF)  $m/z$ : 2258.90 ( $\text{M}+\text{H}^+$ , 100%); Calcd for  $\text{C}_{144}\text{H}_{160}\text{N}_8\text{O}_{16}+\text{H}^+$ : 2259.21.

### 3.4.10 Synthesis and characterization of hexameric capsule **46a** and **47a**

A solution of **40** (85.8mg, 92.3  $\mu\text{mol}$ ), ethylene-1,2-diamine **43** (11.1 mg, 184.6  $\mu\text{mol}$ ) and  $\text{CF}_3\text{CO}_2\text{H}$  (TFA) (0.45  $\mu\text{L}$ , 1  $\mu\text{mol}$ ) in  $\text{CHCl}_3$  was stirred at room temperature under argon for 70 hrs. A small sample was removed from the reaction mixture and the solvent evaporated at high vacuum to yield a yellow solid that contained 82% of **46a** ( $^1\text{H}$  NMR integration).  $^1\text{H}$  NMR ( $\text{CDCl}_3$ ; 22 °C; 400 MHz)  $\delta_{\text{H}}$  8.34 (s, 24H,  $\text{CHN}$ ); 7.12 (s, 24H,  $\text{H}_{\text{aryl}}$ ); 5.70 (d,  $J = 7.5$  Hz, 24H,  $\text{OCH}_{\text{out}}\text{HO}$ ); 4.83 (t,  $J = 8$  Hz, 24H,  $\text{CH}(\text{CH}_2)_4\text{CH}_3$ ); 4.46 (d,  $J = 7.5$  Hz, 24H,  $\text{OCH}_{\text{in}}\text{HO}$ ); 3.75 (sb, 48H,  $\text{NCH}_2$ ); 2.25-2.15 (m, 48H,  $\text{CHCH}_2(\text{CH}_2)_3\text{CH}_3$ ); 1.5-1.3 (m, 144H,  $\text{CHCH}_2(\text{CH}_2)_3\text{CH}_3$ ); 0.91 (t,  $J = 7.1$  Hz, 72H;  $\text{CHCH}_2(\text{CH}_2)_3\text{CH}_3$ ).  $^{13}\text{C}$  NMR ( $\text{CDCl}_3$ ; 22 °C; 100 MHz)  $\delta_{\text{C}}$  157.7, 153.6, 138.8, 124.5, 121.7, 100.5, 63.2, 36.7, 32.3, 30.1, 27.9, 23.0, 14.4. FT-IR ( $\text{CHCl}_3$ )  $\nu$  2956.8 (s), 2929.6 (s), 2872.1 (sh), 2855.6 (s) 1641.5 (s), 1602.6 (m), 1587 (m), 1361.3 (m), 1112.3 (w), 1088.9 (m), 980 (s). ESI-MS ( $\text{CH}_2\text{Cl}_2$ ;  $\text{CH}_3\text{CN}$  (1:5):  $m/z$  1954.9 (100 %,  $[\text{M}+3\text{H}]^{3+}$ , calcd 1955.1); 1466.9 (13 %,  $[\text{M}+4\text{H}]^{4+}$ , calcd 1466.8); 1173.7 (3 %,  $[\text{M}+5\text{H}]^{5+}$ , calcd 1173.7). Nanocontainer **46a** was used for the next step without further purification.  $\text{NaBH}_4$  (150 mg; 4 mmol) and  $\text{CH}_3\text{OH}$  (0.5 mL) were added to a vigorously stirred solution of crude **46a**. After 30 minutes, excess  $\text{NaBH}_4$  was destroyed by the addition of water (1 mL). The

solvent was removed at reduced pressure and the residue dissolved in CH<sub>3</sub>OH/conc. HCl (10:1). After 3.5 days at room temperature, the solvent was removed and the crude product was purified by reversed phase HPLC (Vydac RP-18; 10  $\mu$ m; 300 Å; 21 x 250 mm; CH<sub>3</sub>OH/H<sub>2</sub>O/TFA (gradient 85/15/0.1 to 98/2/0.1; 15 min, isocratic 98/2/0.1; 10 min); 15 mL/min; 280 nm;  $t_{\text{retention}}(\mathbf{47a}) = 13.4$  min), which gave **47a**·24CF<sub>3</sub>COOH as a white solid (84 mg; 63 % yield based on **40**). <sup>1</sup>H NMR (CD<sub>3</sub>OD; 0.4% CF<sub>3</sub>COOD; 7 °C; 300 MHz)  $\delta_{\text{H}}$ ; 7.55 (s, 24H, H<sub>aryl</sub>); 6.16 (d,  $J = 6.9$  Hz, 24H, OCH<sub>out</sub>HO); 4.85 (t,  $J = 7.6$  Hz, 24H, CH(CH<sub>2</sub>)<sub>4</sub>CH<sub>3</sub>); 4.43 (d,  $J = 6.9$  Hz, 24H, OCH<sub>in</sub>HO); 4.16 (sb, 48H, NCH<sub>2</sub>Ar); 3.59 (sb, 48H, N(CH<sub>2</sub>)<sub>2</sub>N); 2.38 (sb, 48H, CHCH<sub>2</sub>(CH<sub>2</sub>)<sub>3</sub>CH<sub>3</sub>); 1.6-1.2 (m, 144H, CHCH<sub>2</sub>(CH<sub>2</sub>)<sub>3</sub>CH<sub>3</sub>); 0.92 (t,  $J = 7.1$  Hz, 72H; CHCH<sub>2</sub>(CH<sub>2</sub>)<sub>3</sub>CH<sub>3</sub>). <sup>13</sup>C NMR (CDCl<sub>3</sub>; 22 °C; 75 MHz)  $\delta_{\text{C}}$  160.5 (q;  $J = 37.8$  Hz), 155.1, 139.9, 124.6, 119.9, 101.2, 44.4, 42.7, 38.5, 33.1, 30.9, 29.1, 24.0, 14.6. ESI-MS (CH<sub>3</sub>OH/H<sub>2</sub>O/TFA (98/2/0.1):  $m/z$  1478.9 ([M+4H]<sup>4+</sup>, calcd 1478.9); 1507.3 ([M+4H+TFA]<sup>4+</sup>, calcd 1507.4); 1535.5 ([M+4H+2TFA]<sup>4+</sup>, calcd 1535.9); 1564.1 ([M+4H+3TFA]<sup>4+</sup>, calcd 1564.4); 1592.5 ([M+4H+4TFA]<sup>4+</sup>, calcd 1592.9); 1620.7 ([M+4H+5TFA]<sup>4+</sup>, calcd 1621.4); 1649.1 ([M+4H+6TFA]<sup>4+</sup>, calcd 1649.9); 1677.4 ([M+4H+7TFA]<sup>4+</sup>, calcd 1678.4); 1706.0 ([M+4H+8TFA]<sup>4+</sup>, calcd 1706.9). Elemental analysis for **47a**·24CF<sub>3</sub>CO<sub>2</sub>H·9H<sub>2</sub>O (C<sub>408</sub>H<sub>522</sub>F<sub>72</sub>N<sub>24</sub>O<sub>105</sub>), found C 55.63%, H 6.17, N 3.84, calcd C 55.62, H 5.97, N 3.82.

### 3.4.11 Synthesis and characterization of tetrameric capsule **46b** and **47b**

A solution of cavitand **40** (255.9 mg, 275  $\mu$ mol), ethylenediamine **43** (34.0 mg, 566  $\mu$ mol) and CF<sub>3</sub>CO<sub>2</sub>H (TFA) (2.17  $\mu$ L, 29  $\mu$ mol) in THF (30.0 mL) was stirred at room temperature for 70 hrs. Then NaBH<sub>4</sub> (2.0g, 52.9 mmol) and MeOH (3.0 mL) were added

into the solution while stirred vigorously. After stirring at room temperature overnight, the solvent was removed at reduced pressure. The solid was stirred with water (50.0 mL) for 20 min to destroy excess NaBH<sub>4</sub> followed by filtration. The precipitate was dissolved in CH<sub>3</sub>OH/conc. HCl (10:1) (165.0 mL). After 4 days at room temperature, the solvent was removed and the crude product was purified by reversed phase HPLC (Vydac RP-18; 10  $\mu$ ; 300 Å; 21  $\times$  250 mm; CH<sub>3</sub>OH/H<sub>2</sub>O/TFA (gradient 85/15/0.1 to 90/10/0.1; 31 min); 10 mL/min; 280 nm;  $t_{\text{retention}}(\mathbf{47b}) = 23.9$  min), which gave **47b**•[CF<sub>3</sub>COOH]<sub>16</sub> as a white solid (122.4 mg; 31 % yield based on **40**). <sup>1</sup>H NMR (CD<sub>3</sub>OD; 0.4% CF<sub>3</sub>COOD; 12.7 °C; 400 MHz):  $\delta_{\text{H}}$ , 7.55 (br s, 16H, H<sub>aryl</sub>); 6.45 (d,  $J = 7.2$  Hz, 4H, OCH<sub>out</sub>HO); 6.14 (d,  $J = 7.2$  Hz, 8H, OCH<sub>out</sub>HO); 6.08 (d,  $J = 7.2$  Hz, 4H, OCH<sub>out</sub>HO); 4.86 (m, 16H, CH(CH<sub>2</sub>)<sub>4</sub>CH<sub>3</sub>); 4.58 (d,  $J = 7.2$  Hz, 4H, OCH<sub>in</sub>HO); 4.40 (d,  $J = 7.2$  Hz, 8H, OCH<sub>in</sub>HO); 4.39 (d,  $J = 7.2$  Hz, 4H, OCH<sub>in</sub>HO); 4.26 (d,  $J = 13.3$  Hz, 8H, NCH<sub>2</sub>Ar); 4.21 (d,  $J = 13.3$  Hz, 8H, NCH<sub>2</sub>Ar); 4.13 (d,  $J = 12.7$  Hz, 8H, NCH<sub>2</sub>Ar); 4.02 (d,  $J = 12.7$  Hz, 8H, NCH<sub>2</sub>Ar); 3.60 (m, 32H, N(CH<sub>2</sub>)<sub>2</sub>N); 2.39 (br s, 32H, CHCH<sub>2</sub>(CH<sub>2</sub>)<sub>3</sub>CH<sub>3</sub>); 1.6-1.3 (m, 96H, CHCH<sub>2</sub>(CH<sub>2</sub>)<sub>3</sub>CH<sub>3</sub>); 0.93 (m, 48H; CHCH<sub>2</sub>(CH<sub>2</sub>)<sub>3</sub>CH<sub>3</sub>). <sup>13</sup>C NMR (CD<sub>3</sub>OD; 25 °C; 100.58 MHz):  $\delta_{\text{C}}$ , 161.8 (q,  $^2J(\text{C}, \text{F}) = 35.4$  Hz, CF<sub>3</sub>COO<sup>-</sup>), 155.52 (C4), 155.23 (C4), 155.11 (C4), 154.91 (C4), 139.87 (C5), 139.82 (C5), 139.68 (C5), 124.73 (C6), 124.67 (C6), 119.69 (C3), 119.63 (C3), 116.43 (q,  $^1J(\text{C}, \text{F}) = 297$  Hz, CF<sub>3</sub>COO<sup>-</sup>), 1.01.39 (C7), 101.04 (C7), 100.96 (C7), 44.75 (C1), 44.01 (C1), 42.98 (C2), 42.50 (C2), 38.33 (C8), 38.12 (C8), 32.82 (C10), 32.79 (C10), 30.77 (C9), 30.72 (C9), 30.60 (C9), 28.86 (C11), 28.83 (C11), 23.85 (C12), 14.40 (C13). MS (MALDI-TOF)  $m/z$ : 3941.85 (M+H<sup>+</sup>, 100%); Calcd for C<sub>240</sub>H<sub>320</sub>N<sub>16</sub>O<sub>32</sub>+H<sup>+</sup>: 3941.40. Elemental analysis: calcd. for C<sub>272</sub>H<sub>346</sub>F<sub>48</sub>N<sub>16</sub>O<sub>69</sub> (**47b**•16CF<sub>3</sub>CO<sub>2</sub>H•5H<sub>2</sub>O): C, 55.79; H, 5.96; N, 3.83; found: C, 55.77%; H, 5.87; N, 3.58.



### 3.4.12 Synthesis and characterization of octameric capsule **46c** and **47c**

A solution of cavitand **40** (362.1 mg, 389.5  $\mu$ mol), ethylenediamine **43** (47.4 mg, 788.7  $\mu$ mol) and CF<sub>3</sub>CO<sub>2</sub>H (TFA) (3.0 L, 40.5  $\mu$ mol) in CH<sub>2</sub>Cl<sub>2</sub> (30.0 mL) was stirred at room temperature for 44 hrs. NaBH<sub>4</sub> (6.0g, 158.6 mmol) and MeOH (4.0 mL) were added to the solution with vigorous stirring. The suspension was stirred at room temperature overnight. The solvent was removed at reduced pressure. The residue was suspended in water (100.0 mL) and stirred for 20 min to destroy excess NaBH<sub>4</sub> followed by filtration. The residue was dissolved in CH<sub>3</sub>OH/conc. HCl (10:1) (135.0 mL). After 4.5 days at room temperature, the solvent was removed and the crude product was purified by reversed phase HPLC (Vydac RP-18; 10  $\mu$ , 300 Å; 21  $\times$  250 mm; CH<sub>3</sub>OH/H<sub>2</sub>O/TFA (gradient 85/15/0.1 to 98/2/0.1; 80 min); 10 mL/min; 280 nm;  $t_{\text{retention}}(\mathbf{47c}) = 58.7$  min), which gave **47c**•[CF<sub>3</sub>COOH]<sub>32</sub> as a white solid (137.6 mg; 25 % yield based on **40**). <sup>1</sup>H NMR (CD<sub>3</sub>OD; 0.4% CF<sub>3</sub>COOD; 25 °C; 400 MHz)  $\delta_{\text{H}}$ , 7.55 & 7.54 (32H, H<sub>aryl</sub>); 6.17 (m, 32H, OCH<sub>out</sub>HO); 4.86 (m, 32H, CH(CH<sub>2</sub>)<sub>4</sub>CH<sub>3</sub>); 4.46 (m, 32H, OCH<sub>in</sub>HO); 4.16 (m, 64H, NCH<sub>2</sub>Ar); 3.61 (s, 32H, N(CH<sub>2</sub>)<sub>2</sub>N); 3.57 (s, 32H, N(CH<sub>2</sub>)<sub>2</sub>N); 2.38 (br s, 64H, CHCH<sub>2</sub>(CH<sub>2</sub>)<sub>3</sub>CH<sub>3</sub>); 1.6-1.2 (m, 192H, CHCH<sub>2</sub>(CH<sub>2</sub>)<sub>3</sub>CH<sub>3</sub>); 0.93 (t,  $J = 7.1$  Hz, 96H, CHCH<sub>2</sub>(CH<sub>2</sub>)<sub>3</sub>CH<sub>3</sub>). <sup>13</sup>C NMR (CD<sub>3</sub>OD; 25 °C; 100.58 MHz)  $\delta_{\text{C}}$ , 162.14 (q, <sup>2</sup> $J(\text{C}, \text{F}) = 36$  Hz, CF<sub>3</sub>COO<sup>-</sup>), 155.29 (C4), 155.21 (C4), 155.19 (C4), 155.15 (C4), 139.92 (C5), 139.86 (C5), 139.84 (C5), 124.66 (C6), 119.73 (C3), 119.65 (C3), 117.75 (q, <sup>1</sup> $J(\text{C}, \text{F}) = 295$  Hz, CF<sub>3</sub>COO<sup>-</sup>), 101.14 (C7), 100.97 (C7), 44.51 (C1), 44.26 (C1), 42.55 (C2), 42.51 (C2), 38.35 (C8), 32.93 (C10), 32.89 (C10), 32.86 (C10), 30.74 (C9), 28.91 (C11), 28.85 (C11), 23.83 (C12), 14.41 (C13). MS (MALDI-TOF)  $m/z$ : 7882.62 (M+H<sup>+</sup>, 100%); Calcd for

$\text{C}_{480}\text{H}_{640}\text{N}_{32}\text{O}_{64}+\text{H}^{\oplus}$ : 7882.81. Elemental analysis: calcd. for  $\text{C}_{544}\text{H}_{770}\text{F}_{96}\text{N}_{32}\text{O}_{177}$  (**47c**•32CF<sub>3</sub>CO<sub>2</sub>H•49H<sub>2</sub>O): C, 52.63; H, 6.25; N, 3.61; found: C, 52.65%; H, 6.07; N, 3.60.

### 3.5 References

1. a) D. J. Cram, J. M. Cram, *Container Molecules and their Guests*, Royal Society of Chemistry, Cambridge, UK, **1994**; b) F. Diederich, *Angew. Chem. Int. Ed.* **2007**, *46*, 68.
2. R. Warmuth, J. Yoon, *Acc. Chem. Res.* **2001**, *34*, 95.
3. K. Rissanen, *Angew. Chem. Int. Ed.* **2005**, *44*, 3652.
4. a) S. R. Seidel, P. J. Stang, *Acc. Chem. Res.* **2002**, *35*, 972; b) B. Olenyuk, J. A. Whiteford, A. Fechtenkotter, P. J. Stang, *Nature* **1999**, *398*, 796.
5. a) M. Fujita, K. Umemoto, M. Yoshizawa, N. Fujita, T. Kusukawa, K. Biradha, *Chem. Commun.* **2001**, 509; b) M. Fujita, M. Tominaga, A. Hori, B. Therrien, *Acc. Chem. Res.* **2005**, *38*, 371; c) V. Maurizot, M. Yoshizawa, M. Kawano, M. Fujita, *Dalton Trans.* **2006**, 2750; d) M. Yoshizawa, M. Tamura, M. Fujita, *Science* **2006**, *312*, 251.
6. a) H. Jude, D. J. Sinclair, N. Das, M. S. Sherburn, P. J. Stang, *J. Org. Chem.* **2006**, *71*, 4155; b) O. D. Fox, M. G. B. Dew, P. D. Beer, *Angew. Chem. Int. Ed.* **2000**, *39*, 135; c) O. D. Fox, J. Cookson, E. J. S. Wilkinson, M. G. B. Dew, E. J. Maclean, S. J. Teat, P. D. Beer, *J. Am. Chem. Soc.* **2006**, *128*, 6990.
7. a) J. Rebek, Jr., *Angew. Chem. Int. Ed.* **2005**, *44*, 2068; b) L. R. MacGillivray, J. L. Atwood, *Nature*, **1997**, *389*, 469; c) A. Shivanyuk, J. Rebek, Jr., *Proc. Natl. Acad. Sci. USA* **2001**, *98*, 7662; d) M. Yamanaka, A. Shivanyuk, J. Rebek, Jr., *J. Am. Chem. Soc.* **2004**, *126*, 2939.
8. P. T. Corbett, J. Leclaire, L. Vial, K. R. West, J.-L. Wietor, J. K. M. Sanders, S. Otto, *Chem. Rev.* **2006**, *106*, 3652.
9. a) D. A. Makeiff, J. C. Sherman, *Chem. Eur. J.* **2003**, *9*, 3253; b) D. A. Makeiff, J. C. Sherman, *J. Am. Chem. Soc.* **2005**, *127*, 12363; c) E. S. Barrett, J. L. Irwin, A. J. Edwards, M. S. Sherburn, *J. Am. Chem. Soc.* **2004**, *126*, 16747.
10. S. J. Rowan, S. J. Cantrill, G. R. L. Cousins, J. K. M. Sanders, J. F. Stoddart, *Angew. Chem. Int. Ed.* **2002**, *41*, 898.
11. a) T. T. Tidwell, *Angew. Chem. Int. Ed.* **2008**, *47*, 1016; b) C. D. Meyer, C. S. Joiner, J. F. Stoddart, *Chem. Soc. Rev.* **2007**, *36*, 1705; c) K. S. Chichak, S. J. Cantrill, A. R.

- Pease, S.-H. Chiu, G. W. V. Cave, J. L. Atwood, J. F. Stoddart, *Science*, **2004**, 304, 1308.
12. S. Ro, S. J. Rowan, A. R. Pease, D. J. Cram, J. F. Stoddart, *Org. Lett.* **2000**, 2, 2411.
  13. a) M. L. C. Quan, D. J. Cram, *J. Am. Chem. Soc.* **1991**, 113, 2754; b) S. Mendoza, P. D. Davidov, A. E. Kaifer, *Chem. Eur. J.* **1998**, 4, 864.
  14. a) L. M. Tunstad, J. A. Tucker, E. Dalcanale, J. Weiser, J. A. Bryant, J. C. Sherman, R. C. Helgeson, C. B. Knobler, D. J. Cram, *J. Org. Chem.* **1989**, 54, 1305; b) J. A. Bryant, M. T. Blanda, M. Vincenti, D. J. Cram, *J. Am. Chem. Soc.* **1991**, 113, 2167.
  15. E. S. Barrett, J. L. Irwin, P. Turner, M. S. Sherburn, *J. Org. Chem.* **2001**, 66, 8227.
  16. H. Boerrigter, W. Verboom, D. N. Reinhoudt, *J. Org. Chem.* **1997**, 62, 7148.
  17. L. R. MacGillivray, J. L. Atwood, *Angew. Chem. Int. Ed.* **1999**, 38, 1018.
  18. a) W. S. Price, *Concept. Magn. Reson.* **1997**, 9, 299; b) D. Wu, A. Chen, C. Johnson, Jr. *J. Magn. Reson. Ser. A* **1995**, 115, 260; c) J. J. Chou, J. L. Baber, A. Bax, *J. Biomol. NMR* **2004**, 29, 299; d) Y. Li, S. Kim, B. Brodsky, J. Baum, *J. Am. Chem. Soc.* **2005**, 127, 10490; e) M. Holz, H. Weingartner, *J. Magn. Reson.* **1991**, 92, 115; f) M. Holz, X. Mao, D. Seiferling, *J. Chem. Phys.* **1996**, 104, 669.
  19. a) D. Q. McDonald, W. C. Still, *Tetrahedron Lett.* **1992**, 33, 7743; b) W. C. Still, A. Tempczyk, R. C. Hawley, T. Hendrickson, *J. Am. Chem. Soc.* **1990**, 112, 6127.
  20. J. C. Sherman, *Chem. Commun.* **2003**, 1617.
  21. D. A. Makeiff, D. J. Pope, J. C. Sherman, *J. Am. Chem. Soc.* **2000**, 122, 1337.
  22. L. Avram, Y. Cohen, *J. Am. Chem. Soc.* **2002**, 124, 15148.
  23. a) N. Giuseppone, J.-L. Schmitt, E. Schwartz, J.-M. Lehn, *J. Am. Chem. Soc.* **2005**, 127, 5528; b) N. Giuseppone, J.-L. Schmitt, J.-M. Lehn, *Angew. Chem. Int. Ed.* **2004**, 43, 4902.
  24. N. E. Borisova, M. D. Reshetova, Y. A. Ustynyuk, *Chem. Rev.* **2007**, 107, 46.
  25. G. Ercolani, *J. Phys. Chem. B* **2003**, 107, 5052.
  26. A. Macchioni, G. Ciancaleoni, C. Zuccaccia, D. Zuccaccia, *Chem. Soc. Rev.* **2008**, 37, 479.
  27. H. Jacobsen, W. H. Stockmayer, *J. Chem. Phys.* **1950**, 18, 1600.
  28. R. Warmuth, E. F. Maverick, C. B. Knobler, D. J. Cram, *J. Org. Chem.* **2003**, 68, 2077.

## Chapter 4 Multi-component synthesis of tetracavitand nanocapsules

### 4.1 Introduction

The results of our previous studies demonstrated that polyimino nanocontainer molecules can be synthesized with high efficiency in a one-pot procedure under thermodynamic control.<sup>[1]</sup> Structurally different nanocapsules with different assembly numbers are constructed from one set of building blocks. Solvent plays a vital role in controlling the relative population of these nanocontainer species.

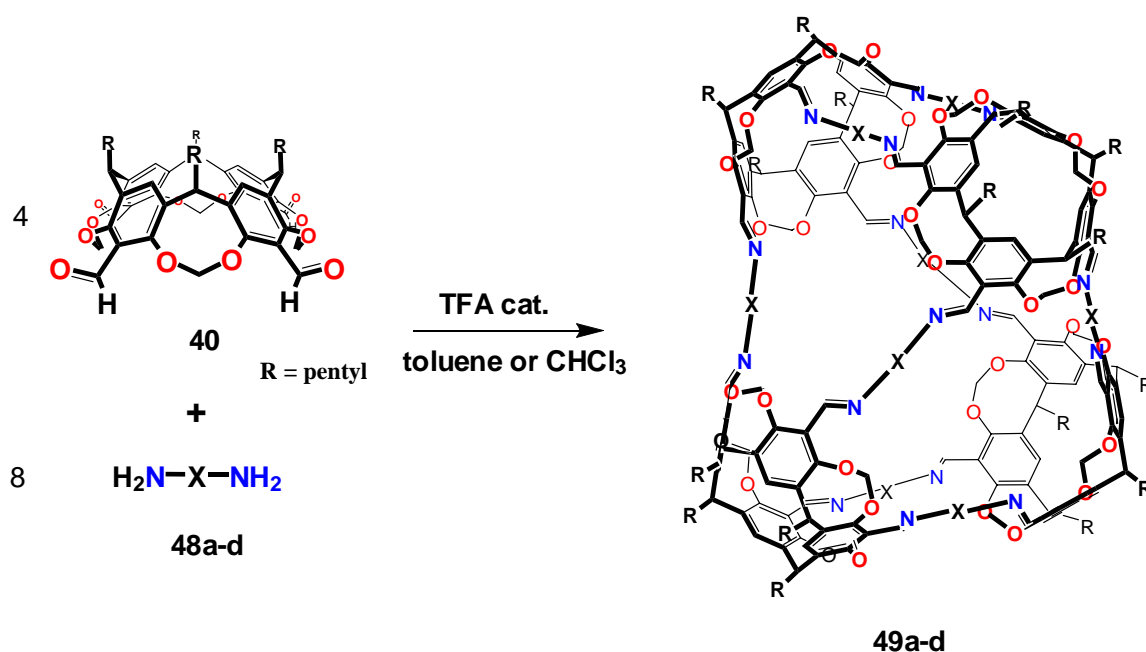
In condensation reactions with tetraformyl cavitand **40** longer alkyl diamines or kinked diamines yielded octaminohemicarcerands quantitatively, whereas ethylenediamine **43** led exclusively to larger capsules due to the preferred *anti*-conformation of the ethylenediamine units. The hypothetical dimeric capsule, in which the ethylenediamine unit would have to adopt a *gauche*-conformation, was not observed. Therefore, rigid, linear diamines should also give large capsules instead of dimeric ones. Here, we will show that linear aromatic diamino linkers result in quantitative formation of tetracavitand nanocapsules,<sup>[1c]</sup> which have the same structure as that obtained with ethylenediamine in THF (**46b**, 35% yield, see Chapter 3, page 49).<sup>[1b]</sup>

### 4.2 Results and discussion

#### 4.2.1 Condensation of tetraformyl cavitand with diamines

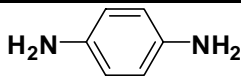
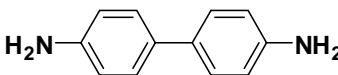
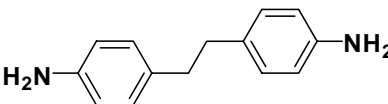
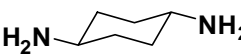
As described in Chapter 3, the condensation between tetraformyl cavitand **40** and *para*-phenylenediamine **48a** (previously numbered as **44h**) in chloroform resulted in the formation of a tetrameric nanocapsule with 60~70% yield within half an hour. It was

observed that the product precipitated out of the reaction system over time. The product had low solubility in other solvents like hexane, dichloromethane, ethyl acetate, dimethylsulfoxide or methanol. However it was quite soluble in toluene. Carrying out the condensation reaction in toluene in the presence of catalytic amounts of trifluoroacetic acid (TFA) increased the product yield to 90% (Scheme 4.1). Addition of activated 4 Å molecular sieves drove the reaction to completion and the tetrameric nanocapsule **49a** was obtained quantitatively (Table 4.1). The GPC profile of the product confirms the presence of a tetracavitand species (Figure 4.1 a).

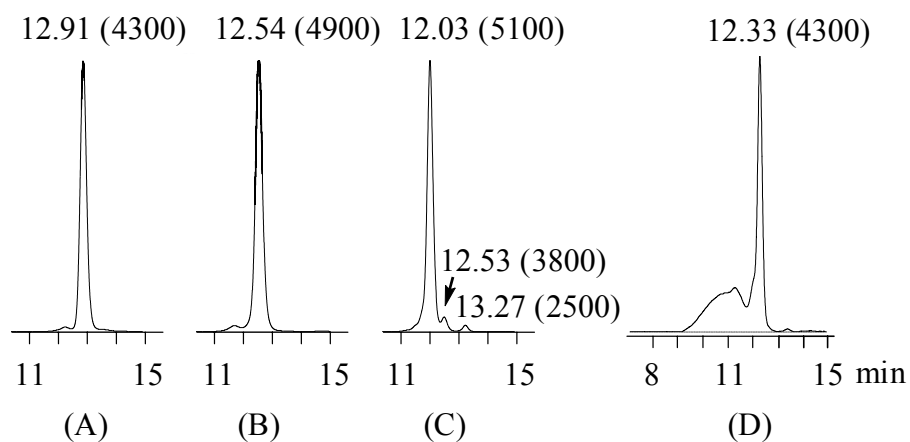


**Scheme 4.1** The condensation reactions between cavitand **40** and diamine **48a-d**.

**Table 4.1** Yields of **49a-d** in the TFA-catalyzed condensation of **40** with 2 equivalents **48a-d**.

compd.	NH <sub>2</sub> -X-NH <sub>2</sub>	<b>49x</b>	
		yield %	<sup>1</sup> H NMR purity %
<b>48a</b> <sup>i</sup>		99	>95
<b>48b</b> <sup>ii</sup>		92	>95
<b>48c</b> <sup>ii</sup>		92	>90
<b>48d</b> <sup>ii</sup>			~50

<sup>i</sup> in toluene; <sup>ii</sup> in chloroform.



**Figure 4.1** GPC-traces of products in the TFA catalyzed condensation of 4 eq. **40** with 8 eq. **48a** (A), **48b** (B), **48c** (C) and **48d** (D). Retention time (in min) and estimated molecular weight (in parenthesis, in Da) are given for each peak. Column temperature: (A) and (B) 25 °C, (C) and (D) 60 °C.

Condensation of cavitand **40** with benzidine **48b**, which has an additional aromatic ring between the amino groups, afforded a similar tetracavitand nanocapsule **49b** in 92% yield (Scheme 4.1, Table 4.1 and Figure 4.1 b). Interestingly, this high yield can only be achieved, if the reaction is carried out in chloroform, since the nanocapsule **49b** underwent quick acetal cleavage in toluene. In toluene, within two days, all intact **49b** was converted into tetrameric species lacking at least one acetal group.

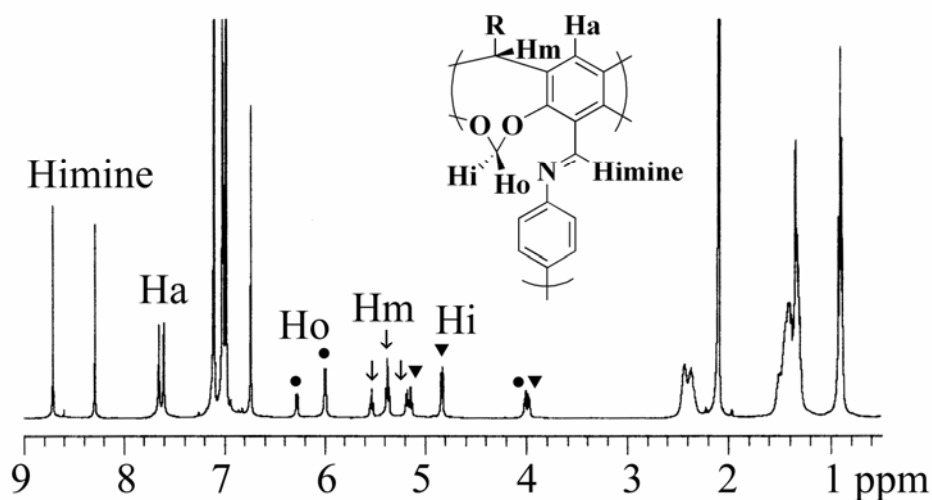
4,4'-Ethylenedianiline **48c**, which has an ethylene spacer between two dianilino- groups, gave a third distorted tetrahedral nanocapsule **49c** in 92% yield in chloroform (Scheme 4.1, Table 4.1 and Figure 4.1 c). The other species present are trimeric and dimeric capsules, which were observed by GPC (Figure 4.1 c) and MALDI-TOF mass spectrometry.

Condensation of cavitand **40** with *trans*-1,4-diaminocyclohexane **48d**, which was carried out under high dilution condition (1/10 of normal concentration), gave a similar tetracavitand nanocapsule **49d** in ~50% yield based on  $^1\text{H}$  NMR integration and GPC chromatography (Figure 4.1 d). Other species are higher molecular weight oligomers. 10% Excess of **48d** didn't help break up these oligomers.

#### 4.2.2 Characterization of nanocapsules **49a-c**

The structure assignment of **49a** is based on  $^1\text{H}$  and  $^{13}\text{C}$  NMR spectroscopy, GPC and MALDI-TOF mass spectrometry. In its  $^1\text{H}$  and  $^{13}\text{C}$  NMR spectra, it shows similar

splitting patterns as the distorted tetrahedral tetramer **46b** (or **47b**) reported in Chapter 3 (Figure 4.2 and Table 4.2). For example, in its  $^1\text{H}$  NMR spectrum, two imine signals  $\text{H}_{\text{imine}}$  at  $\delta_{\text{H}} = 8.71$  and  $8.28$  ppm are observed with equal intensity (integration ratio 8:8). Also, two aryl protons  $\text{H}_{\text{a}}$  are observed at  $\delta_{\text{H}} = 7.65$  and  $7.60$  ppm (ratio 8:8). Three sets of signals with integration 4:8:4 for the outward pointing protons  $\text{H}_{\text{o}}$ , clearly separated from each other, resonate at  $\delta_{\text{H}} = 6.28$ ,  $5.99$  and  $4.01$  ppm. There are also three sets of signals for the methine protons  $\text{H}_{\text{m}}$  at  $\delta_{\text{H}} = 5.53$ ,  $5.37$  and  $5.14$  ppm (ratio 4:8:4) and the inward pointing protons  $\text{H}_{\text{i}}$  at  $\delta_{\text{H}} = 5.17$ ,  $4.83$  and  $3.97$  ppm (ratio 4:8:4). In the MALDI-TOF mass spectrum, the observed major ion with  $m/z = 4294.02$  corresponds to the protonated **49a** (Table 4.3).



**Figure 4.2**  $^1\text{H}$ -NMR spectrum (500 MHz;  $\text{C}_6\text{D}_5\text{CD}_3$ ;  $25^\circ\text{C}$ ) of **49a**. Multiplets assigned to protons  $\text{H}_{\text{imine}}$ ,  $\text{H}_{\text{a}}$ ,  $\text{H}_{\text{o}}$ ,  $\text{H}_{\text{m}}$ , and  $\text{H}_{\text{i}}$  are marked.



**Table 4.2** Chemical shift, integration and multiplicity of proton resonances of **49a-c** in  $^1\text{H}$  NMR spectra <sup>iv</sup>.

compd.		H <sub>imine</sub>	H <sub>a</sub>	H <sub>a-linker</sub>	H <sub>o</sub>	H <sub>m</sub>	H <sub>i</sub>	H <sub>e</sub>
<b>49a</b> <sup>i</sup>	$\delta_{\text{H}}$ (ppm)	8.71/8.28	7.65/7.60	7.01/6.73	6.28/5.99/4.01	5.53/5.37/5.14	5.17/4.83/3.97	
	integration	8/8	8/8	16/16	4/8/4	4/8/4	4/8/4	
	multiplet	<i>s/s</i>	<i>s/s</i>	<i>s/s</i>	<i>d/d/d</i>	<i>t/t/t</i>	<i>d/d/d</i>	
<b>49b</b> <sup>ii</sup>	$\delta_{\text{H}}$ (ppm)	8.66/8.51	7.29/7.28	7.61/7.54/7.19/7.06	5.91/5.87/5.46	5.06-5.00/4.93	4.82/4.75/4.36	
	integration	8/8	8/8	16/16/16/16	4/8/4	12/4	4/8/4	
	multiplet	<i>s/s</i>	<i>s/s</i>	<i>d/d/d/d</i>	<i>d/d/d</i>	<i>m/t</i>	<i>d/d/d</i>	
<b>49c</b> <sup>iii</sup>	$\delta_{\text{H}}$ (ppm)	8.60/8.55	7.27	7.29/7.22/7.05/6.99	5.81/5.71	5.04-4.93	4.78/4.71/4.53	2.90
	integration	8/8	16	16/16/16/16	12/4	16	4/8/4	32
	multiplet	<i>s/s</i>	<i>sb</i>	<i>d/d/d/d</i>	<i>d/d</i>	<i>m</i>	<i>d/d/d</i>	<i>s</i>

<sup>i</sup> toluene-*d*<sub>8</sub>, 25 °C, 500 MHz; <sup>ii</sup> CDCl<sub>3</sub>, 25 °C, 500 MHz; <sup>iii</sup> CDCl<sub>3</sub>, 25 °C, 400 MHz; <sup>iv</sup> for assignment of protons see Figure 4.2.

**Table 4.3** Sum formulas and MALDI-TOF mass of **49a-c**.

compd.	molecular formula	$m/z$ , $M+H^+$	
		calc'd.	found
<b>49a</b>	C <sub>272</sub> H <sub>288</sub> N <sub>16</sub> O <sub>32</sub>	4294.16	4294.02
<b>49b</b>	C <sub>320</sub> H <sub>320</sub> N <sub>16</sub> O <sub>32</sub>	4902.41	4902.62
<b>49c</b>	C <sub>336</sub> H <sub>352</sub> N <sub>16</sub> O <sub>32</sub>	5126.66	5126.15

The structures of **49b** and **49c** are supported in a similar way (Table 4.2 and 4.3). For example, in the MALDI-TOF mass spectra, the major ions at  $m/z = 4902.62$  and  $5126.15$  match protonated **49b** and **49c**, respectively. The hexadecylimino nanocapsule **49c** was further reduced to hexadecylamino nanocapsule **50** by NaBH<sub>3</sub>CN in the presence of Ni(AcO)<sub>2</sub> in THF. The crude product was purified by normal phase HPLC. In the MALDI-TOF mass spectrum of isolated **50**, three predominant peaks at  $m/z = 5159.07$ ,  $5181.03$ ,  $5197.73$ , corresponding to protonated **50**, its sodium and its potassium adduct, respectively, are observed.

The experimental results obtained here suggest that in the condensation reactions with cavitand **40**, tetrameric nanocapsules are the predominant products, if rigid linear diamines are used as the building blocks. Hexameric or octameric capsules, which are formed in their condensation of **40** with 1,2-ethylenediamine **43**, were never observed. On the other hand, octaiminohemicarcerands, that are otherwise quantitatively formed, if 1,3-diaminopropane **44a** or 1,4-diaminobutane **44b** are used as the linker, were not

observed or only as a minor product in the case of 4,4'-ethylenedianiline **48c** (<5% yield). The quantitative formation of tetrameric nanocapsules **49a-c** from rigid linear diamines **48a-c** is due to the preorganized conformation of the cavitand building block **40**. In **40**, the angles between two C<sub>aryl</sub>-C<sub>carbonyl</sub> bonds of opposing and adjacent aromatic units are 61° and 56°, respectively.<sup>[2]</sup> These angles are more appropriate for tetrahedron formation, but they are too small to form a strain-free octahedron or square antiprism, in which these angles are much larger. The high yield of the self-assembly over other nonlinear random polymerization products is due to the polycyclic nature of the assembly (ratio of intramolecular vs. intermolecular steps = 5:11).<sup>[3]</sup>

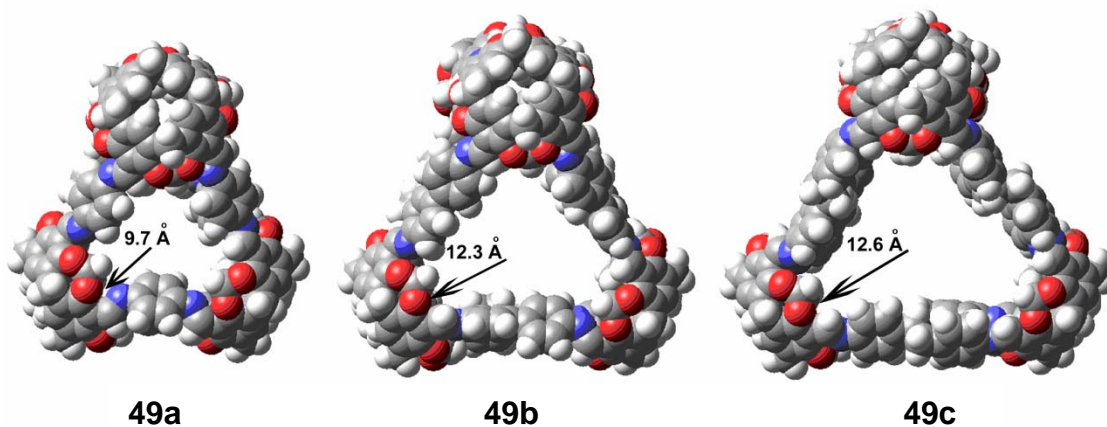
#### 4.2.3 Diffusion rate of nanocapsules

Diffusion ordered spectroscopy (DOSY) was used to measure the diffusion rates of the nanocapsules **49a-c** in chloroform at 298 K (Table 4.4).<sup>[4]</sup> Solvodynamic radii of **49a-c** were calculated according to the Stokes-Einstein equation. The nanocapsules **49a-c** have solvodynamic radii ranging from 12.7 to 14.8 Å in chloroform, which are consistent with the modeled structures from molecular mechanics calculations (Figure 4.3).<sup>[5]</sup> For example, in the energy-minimized structures of **49a** and **49b**, the average distance between the center of the capsule and the center of each cavitand of **49a** is also approximately 2 Å shorter (9.7 Å) when compared with that of **49b** (12.3 Å).

**Table 4.4** Diffusion constants  $D$  in  $\text{CDCl}_3$  at 25 °C and solvodynamic radii  $r^{\text{a)}$  of **49a-c**.

nanocapsule	<b>49a</b>	<b>49b</b>	<b>49c</b>
$D$ in $10^{-10} \text{ m}^2 \text{ s}^{-1}$	$3.19 \pm 0.05$	$2.77 \pm 0.03$	$2.74 \pm 0.02$
$r$ in Å	$12.7 \pm 0.2$	$14.7 \pm 0.2$	$14.8 \pm 0.1$

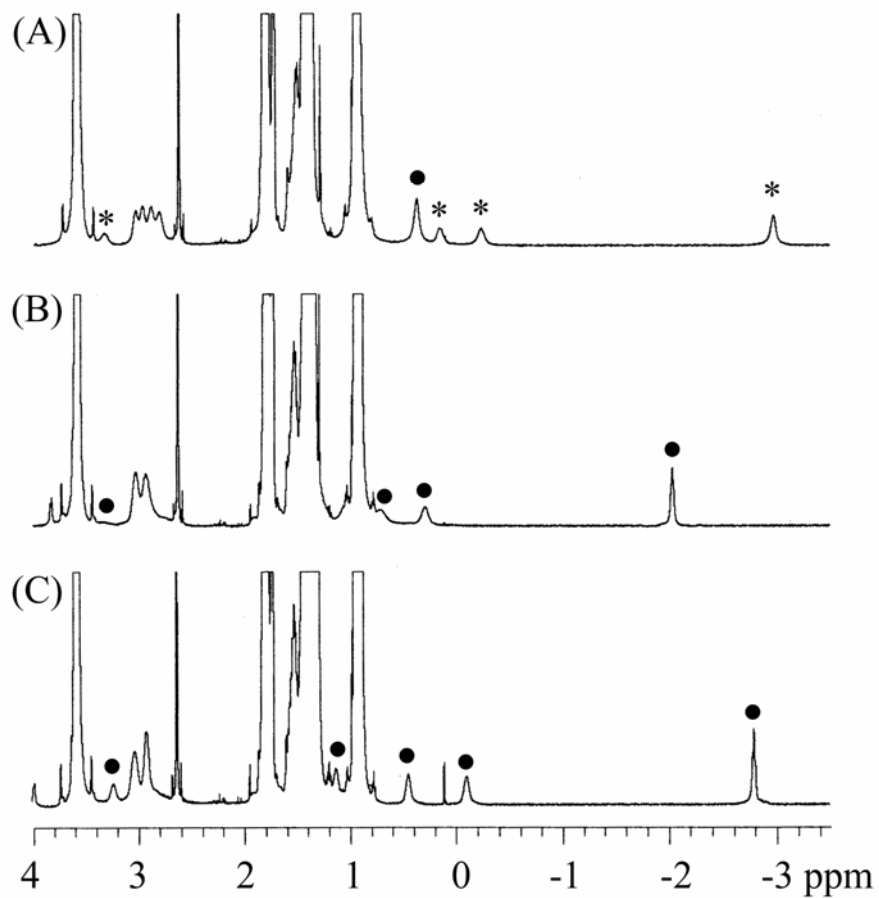
<sup>a)</sup>  $r = kT/6\pi\eta D$  with  $\eta = 0.538 \text{ mPa/s}$ .<sup>[6]</sup>

**Figure 4.3** Energy-minimized space-filling models of nanocapsules **49a-c** (MM3,<sup>[5]</sup> gas-phase). Pentyl groups are omitted. Atom coloring: C grey; O red; N blue; H white.

#### 4.2.4 Encapsulation of tetraalkylammonium bromides inside nanocapsules

Alkyl ammonium compounds are often used as probes to investigate molecular recognition properties of synthetic receptors. Binding of tetraalkylammonium bromides inside nanocapsule **49a** was observed. When 20 eq. of  $(n\text{-C}_5\text{H}_{11})_4\text{NBr}$ ,  $(n\text{-C}_6\text{H}_{13})_4\text{NBr}$ , or  $(n\text{-C}_7\text{H}_{15})_4\text{NBr}$  were mixed with tetramer **49a** in  $\text{THF-}d_8$ , two sets of signals, one for the free and one for the bound guest, were observed in the  $^1\text{H}$  NMR spectrum. The latter

were significantly upfield shifted, which indicates that tetraalkylammonium bromides are encapsulated (Figure 4.4). This is often due to the shielding effect of the aromatic cavitands of **49a**. For each guest, the end methyl groups have the largest complexation induced shift (CIS,  $\Delta\delta = 3.90, 2.94$  and  $3.65$  ppm for encapsulated  $(n\text{-C}_5\text{H}_{11})_4\text{NBr}$ ,  $(n\text{-C}_6\text{H}_{13})_4\text{NBr}$  and  $(n\text{-C}_7\text{H}_{15})_4\text{NBr}$ , respectively) (Table 4.5). This also indicates that the methyl groups protrude fairly deep into the cavitand.<sup>[7]</sup> CIS decreases along the alkyl chain towards the ammonium center (Table 4.5), which suggests that the alkyl chains are fully extended in the cavitand of **49a**. This was confirmed by  $^1\text{H}$ - $^1\text{H}$  COSY experiments, through which the proton-proton connectivity for the encapsulated guest was established. For encapsulated guests with folded alkyl chains, it has been reported that the methyl groups experience much less shielding than some of the other protons in the chain.<sup>[8]</sup> The simultaneous observation of signals for free ( $\delta \sim 3.6$  ppm for the  $\alpha$ -methylene protons) and complexed tetraalkylammonium bromides (Figure 4.4) indicates that the guest in/out exchange rate is slow on the NMR time scale at the experimental temperature. In THF, the counter ion  $\text{Br}^-$  is strongly associated with the ammonium center and should be located inside the cavity.



**Figure 4.4** Partial  $^1\text{H}$  NMR spectra (500 MHz,  $\text{THF-}d_8$ , 278 K) of **49a** in the presence of 20 eq.  $(n\text{-C}_5\text{H}_{11})_4\text{NBr}$  (A),  $(n\text{-C}_6\text{H}_{13})_4\text{NBr}$  (B), or  $(n\text{-C}_7\text{H}_{15})_4\text{NBr}$  (C). Signals assigned to protons of encapsulated guests of 1:1 and 2:1 complexes are marked with filled circles and asterisks, respectively.

**Table 4.5** Complexation induced shift (CIS) of guest protons for complexes **49a**⊙R<sub>4</sub>N<sup>+</sup>Br<sup>−</sup> and **49a**⊙2(pentyl<sub>4</sub>N<sup>+</sup>Br<sup>−</sup>) in THF-*d*<sub>8</sub> at −5 °C and guest's van der Waals volume <sup>[8]</sup>.

Guest	Volume (Å <sup>3</sup> )	PC	Δδ(H <sub>1</sub> )	Δδ(H <sub>2</sub> )	Δδ(H <sub>3</sub> )	Δδ(H <sub>4</sub> )	Δδ(H <sub>5</sub> )	Δδ(H <sub>6</sub> )	Δδ(XH <sub>3</sub> )
( <i>n</i> -C <sub>5</sub> H <sub>11</sub> ) <sub>4</sub> NBr	383	0.31	n.d.	n.d.	n.d.	0.45			0.55
2×( <i>n</i> -C <sub>5</sub> H <sub>11</sub> ) <sub>4</sub> NBr	766	0.61	0.26	n.d.	1.25	1.63			3.9
( <i>n</i> -C <sub>6</sub> H <sub>13</sub> ) <sub>4</sub> NBr	448	0.36	0.26	n.d.	n.d.	0.68	1.1		2.94
( <i>n</i> -C <sub>7</sub> H <sub>15</sub> ) <sub>4</sub> NBr	514	0.41	0.4	0.35	n.d.	0.3	0.84	1.38	3.65

n. d. not determined

Binding constants were obtained by integration of host/guest signals in the <sup>1</sup>H NMR spectra. Based on integration, one guest is encapsulated inside **49a** for (*n*-C<sub>6</sub>H<sub>13</sub>)<sub>4</sub>NBr and (*n*-C<sub>7</sub>H<sub>15</sub>)<sub>4</sub>NBr, which means 1:1 complexes are formed in THF-*d*<sub>8</sub> (Figure 4.4 b and c). Molecular ions for complexes with one guest are also observed in MALDI-TOF MS (Table 4.7). Binding constants are calculated as followed:

$$K = \frac{[HG]}{[H][G]}$$

Both the total host concentration [H]<sub>0</sub> and the total guest concentration [G]<sub>0</sub> are known. The complex concentration ([HG]) was calculated from the integration of methyl protons of the encapsulated (*n*-C<sub>6</sub>H<sub>13</sub>)<sub>4</sub>NBr or (*n*-C<sub>7</sub>H<sub>15</sub>)<sub>4</sub>NBr. The free host concentration [H] is the difference between the total host concentration [H]<sub>0</sub> and the complex concentration [HG], [H] = [H]<sub>0</sub> − [HG]. The free guest concentration [G] is calculated from the

integration of  $\alpha$ -methylene protons of the free guest, or the difference between the total guest concentration  $[G]_0$  and the complex concentration  $[HG]$ ,  $[G] = [G]_0 - [HG]$ . The temperature dependence of the binding constants was measured between 268 and 308 K. Linear van't Hoff plots revealed the thermodynamics of the complexation. For (*n*-C<sub>6</sub>H<sub>13</sub>)<sub>4</sub>NBr and (*n*-C<sub>7</sub>H<sub>15</sub>)<sub>4</sub>NBr, the binding in THF-*d*<sub>8</sub> is weak with binding constants  $K_{298K} = 45 \text{ M}^{-1}$  and  $69 \text{ M}^{-1}$ , respectively (Table 4.6). The binding interactions are exothermic along with entropy loss in THF-*d*<sub>8</sub>.

**Table 4.6** Thermodynamic properties ( $\Delta G_{298}$ ,  $\Delta H_{298}$  and  $T\Delta S_{298}$  at 298 K in kcal/mol) of complexes **49a**⊙R<sub>4</sub>NBr.

Guest	Solvent	$\Delta G_{298}$	$\Delta H_{298}$	$T\Delta S_{298}$	$K_I (\text{M}^{-1})$
( <i>n</i> -C <sub>6</sub> H <sub>13</sub> ) <sub>4</sub> NBr	THF- <i>d</i> <sub>8</sub>	-2.3	-6.6	-4.3	45±5
( <i>n</i> -C <sub>7</sub> H <sub>15</sub> ) <sub>4</sub> NBr	THF- <i>d</i> <sub>8</sub>	-2.5	-6.9	-4.4	69±7
( <i>n</i> -C <sub>7</sub> H <sub>15</sub> ) <sub>4</sub> NBr	toluene- <i>d</i> <sub>8</sub>	-4.6	1.3	5.9	2500±200
( <i>n</i> -C <sub>7</sub> H <sub>15</sub> ) <sub>4</sub> NBr	CDCl <sub>3</sub>	n.c.	n.c.	n.c.	n.c.
( <i>n</i> -C <sub>8</sub> H <sub>17</sub> ) <sub>4</sub> NBr	THF- <i>d</i> <sub>8</sub>	n.c.	n.c.	n.c.	n.c.

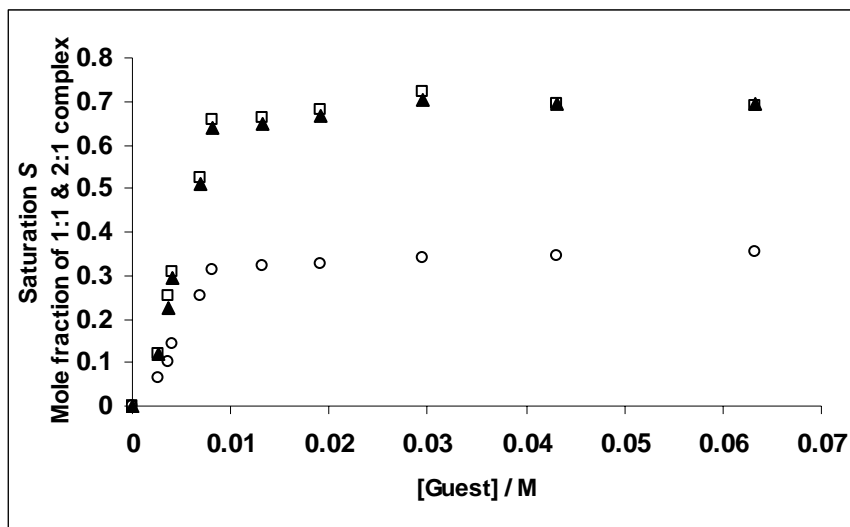
n.c.: no complexation;  $K_I$  at 298 K;  $K_I = [\mathbf{49a} \odot \text{R}_4\text{NBr}] / [\mathbf{49a}] [\text{R}_4\text{NBr}]$



**Table 4.7** MALDI-TOF MS data for complexes formed in THF-*d*<sub>8</sub>.

MALDI-TOF MS	free host (M+H <sup>+</sup> )			1:1 complex (M+R <sub>4</sub> N <sup>+</sup> )			1:2 complex (M+R <sub>4</sub> NBr+R <sub>4</sub> N <sup>+</sup> )		
	calc'd.	found	Δm	calc'd.	found	calib.	calc'd.	found	calib.
<b>49a</b> ⊙( <i>n</i> -C <sub>5</sub> H <sub>11</sub> ) <sub>4</sub> NBr	4294.16	4291.77	-2.39	4591.85	4589.52	4592.08			
<b>49a</b> ⊙(2( <i>n</i> -C <sub>5</sub> H <sub>11</sub> ) <sub>4</sub> NBr)	4294.16	4286.37	-7.79	4591.85	4587.20	4595.54	4970.33	4966.47	4975.50
<b>49a</b> ⊙( <i>n</i> -C <sub>6</sub> H <sub>13</sub> ) <sub>4</sub> NBr	4294.16	4292.86	-1.30	4647.96	4645.04	4646.45			
<b>49a</b> ⊙( <i>n</i> -C <sub>7</sub> H <sub>15</sub> ) <sub>4</sub> NBr	4294.16	4291.63	-2.53	4704.07	4702.57	4705.34			

However, both 1:1 and 1:2 complexes are observed for the binding with  $(n\text{-C}_5\text{H}_{11})_4\text{NBr}$  (Figure 4.4 a). After addition of  $(n\text{-C}_5\text{H}_{11})_4\text{NBr}$  into the solution of **49a** in  $\text{THF-}d_8$ , two sets of upfield shifted guest signals are observed. The signal at  $\delta = 0.40$  ppm is assigned to the methyl proton of the encapsulated  $(n\text{-C}_5\text{H}_{11})_4\text{NBr}$  of the 1:1 complex. And the signal at  $\delta = -2.96$  ppm is assigned to the methyl proton of the encapsulated  $(n\text{-C}_5\text{H}_{11})_4\text{NBr}$  of the 1:2 complex. The integration ratio of the two methyl groups ( $I(\text{methyl of 1:2 complex}) / I(\text{methyl of 1:1 complex})$ ) increases with increasing guest concentration. Molecular ions for complexes with one and two guests are also observed in MALDI-TOF MS (Table 4.7). Complexation of one and two guests was further supported by a ROESY experiment, which shows exchange peaks between the methyl group of the free and encapsulated guests and between the methyl groups of the 1:1 complex and the methyl groups of the 1:2 complex. Attempts to obtain the binding constants  $K_1$  and  $K_2$  for the 1:1 and 1:2 complexes were not successful. The binding isotherm of a  $^1\text{H}$  NMR titration, which plots the binding site saturation  $S$  as a function of the total guest concentration, is shown in Figure 4.5. The curve strongly rises at lower guest concentration. However, it levels off at  $S = 70\%$ , which is lower than the expected total occupancy ( $S = 1$ ). Fitting of the entire dataset to a 1:2 binding model turned out to be impractical. One explanation might be the interaction of tetrapentylammonium cations with the outside of the capsule **49a**. Outside binding of tetraalkylammonium salts to capsules via cation- $\pi$  interactions has been reported before.<sup>[9]</sup> These weak cation- $\pi$  interactions could decrease the binding affinity of the nanocapsule for the encapsulated guests. Thus  $K_1$  and  $K_2$  become guest concentration dependent.

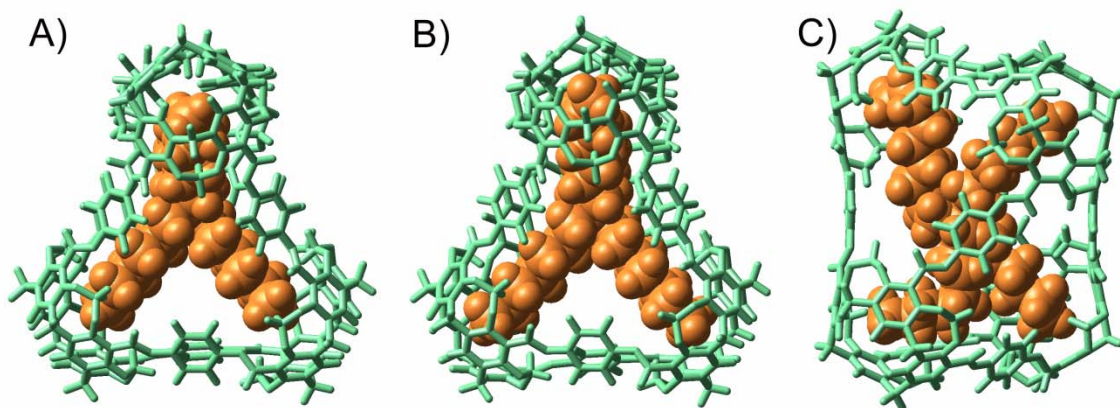


**Figure 4.5** Binding isotherm for the encapsulation of  $(n\text{-C}_5\text{H}_{11})_4\text{NBr}$  inside **49a** in THF- $d_8$  at  $-5\text{ }^\circ\text{C}$  showing saturation of binding sites  $S$  ( $0 \leq S \leq 1$ ; ▲), mole fraction of **49a**⊙( $n\text{-C}_5\text{H}_{11})_4\text{NBr}$  (□) and mole fraction of **49a**⊙( $2(n\text{-C}_5\text{H}_{11})_4\text{NBr}$ ) (○) as function of the guest concentration.

Formation of a 1:2 complex is rationalized by the packing coefficients ( $PC$ ) of the 1:1 and 1:2 complexes (Table 4.5). In solution the optimal  $PC$  in capsules is 0.55 for neutral guests, but may be higher for tetraalkylammonium compounds which are capable of forming  $\text{C-H}\cdots\pi$  interactions.<sup>[10]</sup> The  $PC$ s for **49a**⊙( $n\text{-C}_6\text{H}_{13})_4\text{NBr}$  and **49a**⊙( $n\text{-C}_7\text{H}_{15})_4\text{NBr}$  are 0.36 and 0.41, respectively. Upon encapsulation of two guests the cavity would be too crowded with  $PC = 0.72$  and  $0.82$ , respectively. For  $(n\text{-C}_5\text{H}_{11})_4\text{NBr}$ , the  $PC$  for the 1:1 and 1:2 complexes are 0.31 and 0.61, respectively. Therefore, encapsulation of two  $(n\text{-C}_5\text{H}_{11})_4\text{NBr}$  results in an almost ideal packing inside the capsule, which leads to higher complex stability.

The affinity difference for the 1:1 complexes of the tetraalkylammonium salts in THF- $d_8$

provides additional information about the guest conformation inside the capsule. Binding constants decrease in the order  $K_1((n\text{-C}_7\text{H}_{15})_4\text{NBr}) > K_1((n\text{-C}_6\text{H}_{13})_4\text{NBr}) \gg K_1((n\text{-C}_8\text{H}_{17})_4\text{NBr})$  (Table 4.6). In  $^1\text{H}$  NMR spectra, complexation induced shift (CIS) of the guest signals have indicated that alkyl chains fully extend towards the center of the cavitands of **49a** (Table 4.5). The methyl groups of encapsulated  $(n\text{-C}_7\text{H}_{15})_4\text{NBr}$  experience more shielding than those of encapsulated  $(n\text{-C}_6\text{H}_{13})_4\text{NBr}$  ( $\Delta\delta = 3.65$  vs. 2.94 ppm), which suggests that  $(n\text{-C}_7\text{H}_{15})_4\text{NBr}$  interacts stronger with the cavitand  $\pi$  system. This is simply because the  $n\text{-C}_7\text{H}_{15}$  group has one more methylene than the  $n\text{-C}_6\text{H}_{13}$  group. Therefore the alkyl chain can reach deeper into the cavity, which is consistent with the energy-minimized space-filling models of the two complexes (Figure 4.6 a and b).<sup>[5]</sup> Complexation with  $(n\text{-C}_8\text{H}_{17})_4\text{NBr}$  was not observed. A space-filling model of the hypothetical complex **49a**⊙ $(n\text{-C}_8\text{H}_{17})_4\text{NBr}$  indicates that several *gauche* conformations are required to accommodate the guest (Figure 4.6 c). Each *gauche* interaction is expected to result in an energy penalty of 0.5 - 0.6 kcal/mol.<sup>[8]</sup> Therefore the raised guest conformational energy might be the reason for the absence of the  $(n\text{-C}_8\text{H}_{17})_4\text{NBr}$  complex, even though it has a good cavity occupancy ( $PC = 0.47$ ).



**Figure 4.6** Energy-minimized space-filling model of **49a**⊙(*n*-C<sub>6</sub>H<sub>13</sub>)<sub>4</sub>N<sup>+</sup> (A); **49a**⊙(*n*-C<sub>7</sub>H<sub>15</sub>)<sub>4</sub>N<sup>+</sup> (B) and **49a**⊙(*n*-C<sub>8</sub>H<sub>17</sub>)<sub>4</sub>N<sup>+</sup> (C) (MM3,<sup>[5]</sup> gas-phase). Coloring: **49a** aquamarine; guest orange.

Solvent has a substantial effect on the binding process of (*n*-C<sub>7</sub>H<sub>15</sub>)<sub>4</sub>NBr (Table 4.6). No complexation was observed in CDCl<sub>3</sub>. However, the binding is ~35 times stronger in toluene-*d*<sub>8</sub> than in THF-*d*<sub>8</sub>. Furthermore, binding in toluene-*d*<sub>8</sub> is entropy driven, while binding in THF-*d*<sub>8</sub> is enthalpy controlled. Enthalpy-entropy compensation has been widely observed in host-guest complexation.<sup>[11]</sup> In THF-*d*<sub>8</sub>, host-solvent and guest-solvent interactions are weak. Encapsulation of (*n*-C<sub>7</sub>H<sub>15</sub>)<sub>4</sub>NBr leads to a negative enthalpy change resulting from favorable C-H⋯π interactions due to the induced positive charge of the alkyl chains ( $\Delta H_{298} = -6.6$  kcal/mol). On the other hand, these strong interactions decrease the degree of freedom of the complex, which is entropically unfavorable ( $T\Delta S_{298} = -4.3$  kcal/mol). In toluene-*d*<sub>8</sub>, stronger host-solvent and guest-solvent interactions are expected: primarily π-π stacking, cation-π and C-H⋯π interactions. Therefore, desolvation of the host cavity and of the guest releases these ordered solvent molecules into the bulk phase. Hence, the entropy of the system increases

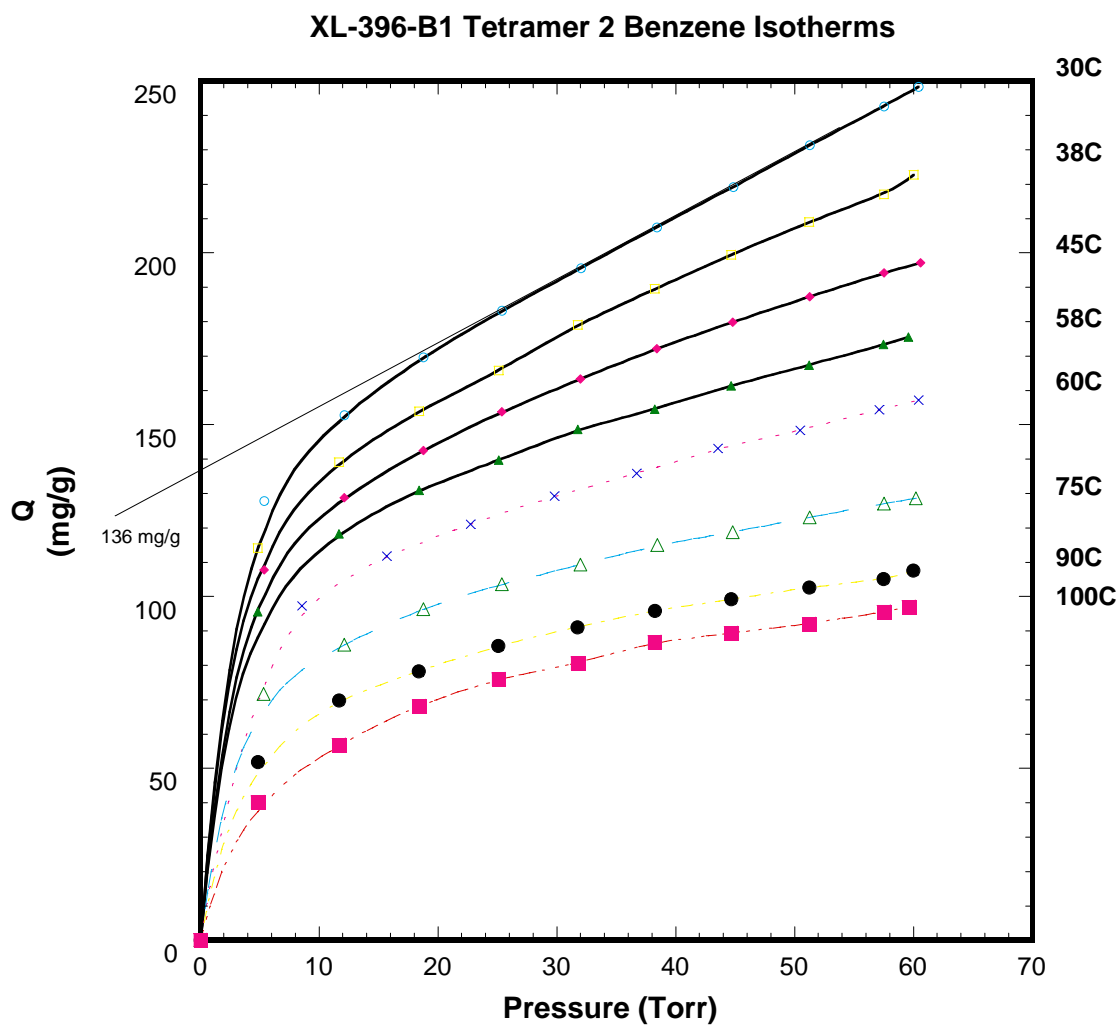
significantly ( $T\Delta S_{298} = 5.9$  kcal/mol). On the other hand the binding is enthalpically unfavorable ( $\Delta H_{298} = 1.3$  kcal/mol), simply, because the host-guest C-H $\cdots\pi$  interactions do not fully compensate for the loss of toluene-host and toluene-guest interactions.

#### 4.2.5 Hydrocarbon adsorption inside nanocapsules

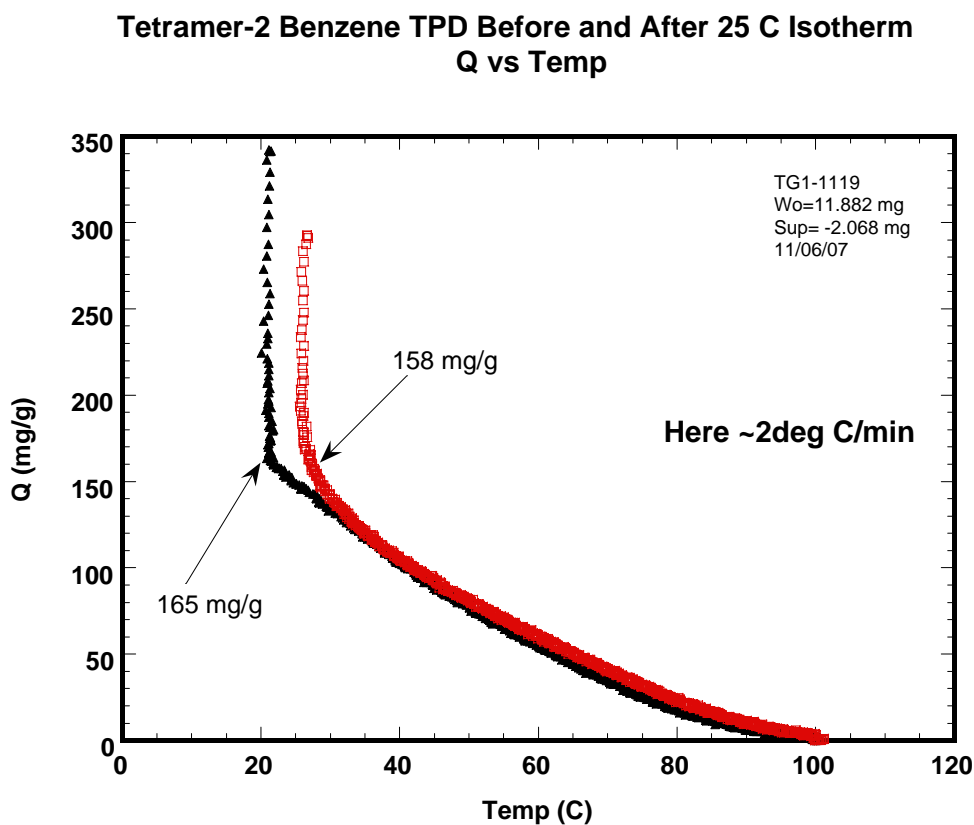
Gas-solid adsorption is crucial to many industrial applications, such as separation, hydrogen storage and heterogeneous catalysis. Supramolecular assemblies have been used to separate hydrocarbons in solution.<sup>[12]</sup> However, hydrocarbon adsorption in the solid phase is rarely reported, except for MOFs, COFs, and zeolites.<sup>[14]</sup>

Dr. David Olson and co-workers have shown that nanocapsules **49a-c** adsorb hexane, benzene and *p*-xylene in the solid state. For example, nine benzene molecules are adsorbed inside the nanocapsule **49a** (Figure 4.7 and 4.8). Temperature programmed desorption (TPD) experiment of **49a** loaded with benzene molecules shows that an initial rapid desorption from Q (benzene/**49a**) = ~300 mg/g to 165 mg/g takes place at 25 °C (Figure 4.8). Upon raising the temperature to 100 °C, Q slowly decreases to zero. The initial rapid desorption is caused by benzene molecules adsorbed to the outside of the capsule, which are very weakly interacting with the capsule. The following slow desorption is due to benzene molecules adsorbed inside the capsule. The presence of multiple C-H $\cdots\pi$  and  $\pi$ - $\pi$  stacking interactions significantly increase benzene-host interactions inside the capsule, which slowed the desorption process. We assume that each benzene molecule occupies the same amount of space as it does in the liquid state (148.4 Å<sup>3</sup>). From the break point at Q (benzene/**49a**) = 165 mg/g, it is estimated that there

are 9 benzene molecules adsorbed in the capsule **49a**, corresponding to a total volume of  $1330 \text{ \AA}^3$ . This is consistent with the calculated cavity volume of the tetramer **49a** ( $1250 \pm 100 \text{ \AA}^3$ ).



**Figure 4.7** Adsorption isotherms of **49a** with benzene.



**Figure 4.8** TPD profile of **49a** loaded with benzene at 25 °C.

### 4.3 Conclusions

Three new tetracavitand nanocapsules **49a-c** have been synthesized through the one-pot, multi-component assembly approach, whereby rigid linear diamines are used as the building blocks. These distorted tetrahedral polyimino capsules are formed with almost quantitative yields. It has been calculated that the nanocapsules have cavity volumes of 1200~1500 Å<sup>3</sup>. Binding experiments with medium-size tetraalkylammonium bromides indicate that only one guest is generally encapsulated inside the capsules. Co-encapsulation of two guests is also observed, if space occupancy is close to the optimal value  $PC = 0.55$ . Binding is entropy driven in toluene-*d*<sub>8</sub> and enthalpy driven in THF-*d*<sub>8</sub>.



The capsule is also capable of adsorbing hydrocarbons in the solid state. These adsorption studies allow the estimation of the cavity volume by assuming that the adsorbed hydrocarbon guest molecules are “liquid state like” in the inner cavities.<sup>[10a]</sup>

## 4.4 Experimental section

### 4.4.1 General procedure

All reactions were conducted under argon. Reagents and chromatography solvents were purchased from Aldrich and used without further purification except that chloroform was passed through  $K_3CO_3$  prior to use.  $^1H$  NMR spectra recorded in  $CDCl_3$ , toluene- $d_8$  or THF- $d_8$  were referenced to residual  $CHCl_3$ ,  $CHD_2C_6D_5$  and  $(CHDCD_2CD_2CD_2)O$  at 7.26 ppm, 2.09 ppm and 1.73 ppm, respectively.  $^{13}C$  NMR spectra recorded in  $CDCl_3$  or toluene- $d_8$  were referenced to  $^{13}CDCl_3$  at 77.0 ppm and  $^{13}CD_3C_6D_5$  at 20.8 ppm, respectively. Mass spectra were recorded on an Applied Biosystems Voyager DE-Pro mass spectrometer (MALDI-TOF). 2',4',6'-Trihydroxylacetophenone (THAP) was used as the matrix. Gel permeation chromatography (GPC) was performed on a Thermo SpectraSYSTEM HPLC system equipped with dual wavelength UV/Vis detector (280 nm), Eppendorf CH-30 column heater and two Jordi GPC columns (cross linked DVB;  $10^3$  Å pore size; MW cutoff ~ 25,000; 7.8mm × 30cm) with  $CH_2Cl_2/1\%$   $NEt_3$  as mobile phase at a flow of 1 mL/min. Approximate molecular weights of analytes were determined from a semi logarithmic calibration plot ( $\ln(MW)$  against retention time) using the following molecular weight standards: benzene (MW 78); cavitand **40** (MW 928); a NMP hemicarceplex (MW 2348),<sup>[13]</sup> and polyaminonanocapsules **47a-c** (MW 3941, 5912 and 7882).<sup>[1]</sup>

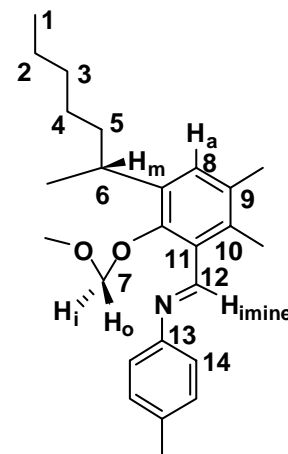
#### 4.4.2 DOSY experiments

DOSY NMR experiments were performed on a 500 MHz Varian spectrometer equipped with a gradient system capable of producing magnetic field pulse gradients in the  $z$ -direction of about 50 G<sup>-1</sup>/cm. A 5 mm broadband probe was used to carry out all the measurements. Samples were put into a 4 mm NMR tube that was inserted in a 5 mm NMR tube to reduce convection. Temperature was controlled at 298 K. Samples were equilibrated at least 10 min before the measurement started. The diffusion experiments were performed using the pulse sequence Dbppste (Bipolar Pulse Pair Stimulated Echo Experiment) that is implemented in the NMR software VnmrJ. The diffusion delay ( $\Delta$ ) was set to 0.15 sec. The gradient pulse strength ( $g_{zlv11}$ , G<sub>z</sub>) was varied from 400 to 25000 G/cm. For all the other parameters, the default values were used. The diffusion rate constant and its error reported are the mean average of the diffusion rate constants of each individual capsule proton signal in a  $D$  against  $\delta$  plot and the SE of mean, respectively.

#### 4.4.3 Synthesis of hexadecaiminonanocapsule **49a** (*Procedure A*)

A solution of cavitand **40** (105.6 mg, 0.114 mmol), *para*-phenylenediamine **48a** (25.0 mg, 0.231 mmol) and CF<sub>3</sub>CO<sub>2</sub>H (TFA) (0.79  $\mu$ L, 0.0107 mmol) in toluene (21.0 mL) was stirred for 0.5 h. Then 3 Å molecular sieves were added into the flask and stirring continued overnight. The mixture was filtered and solid anhydrous K<sub>2</sub>CO<sub>3</sub> was added to the filtrate. After stirring for 5 h, the K<sub>2</sub>CO<sub>3</sub> was filtered off and the filtrate was concentrated under reduced pressure. The yellow residue was dried at high vacuum

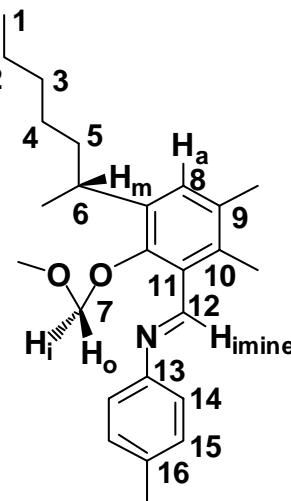
overnight (121 mg, 99% yield, >95% purity based on  $^1\text{H}$  NMR integration).  $^1\text{H}$  NMR (500 MHz, toluene- $d_8$ , 25  $^\circ\text{C}$ ),  $\delta_{\text{H}}$  (ppm): 8.71 (s, 8 H,  $\text{H}_{\text{imine}}$ ), 8.28 (s, 8 H,  $\text{H}_{\text{imine}}$ ), 7.65 (s, 8 H,  $\text{H}_{\text{aryl}}$ ), 7.60 (s, 8 H,  $\text{H}_{\text{aryl}}$ ), 7.01 (s, 16 H,  $\text{H}_{\text{aryl}}$ ), 6.73 (s, 16 H,  $\text{H}_{\text{aryl}}$ ), 6.28 (d,  $J = 8.20$  Hz, 4 H,  $\text{H}_{\text{outer}}$ ), 5.99 (d,  $J = 7.80$  Hz, 8 H,  $\text{H}_{\text{outer}}$ ), 5.53 (t,  $J = 7.79$  Hz, 4 H,  $\text{H}_{\text{methine}}$ ), 5.37 (t,  $J = 8.20$  Hz, 8 H,  $\text{H}_{\text{methine}}$ ), 5.17 (d,  $J = 8.20$  Hz, 4 H,  $\text{H}_{\text{inner}}$ ), 5.14 (t,  $J = 7.79$  Hz, 4 H,  $\text{H}_{\text{methine}}$ ), 4.83 (d,  $J = 7.79$  Hz, 8 H,  $\text{H}_{\text{inner}}$ ), 4.01 (d,  $J = 7.38$  Hz, 4 H,  $\text{H}_{\text{outer}}$ ), 3.97 (d,  $J = 7.79$  Hz, 4 H,  $\text{H}_{\text{inner}}$ ), 2.49-2.26 (m, 32 H), 1.54-1.25 (m, 96 H), 0.92-0.88 (m, 48 H).  $^{13}\text{C}$  NMR (125 MHz, toluene- $d_8$ , 25  $^\circ\text{C}$ ),  $\delta_{\text{C}}$  (ppm): 156.83 (C12), 156.77 (C12), 155.76 (C10), 155.57 (C10), 154.49 (C10), 154.31 (C12), 154.25 (C12), 153.72 (C10), 153.18 (C13), 151.76 (C13), 140.09 (C9), 140.08 (C9), 138.99 (C9), 138.86 (C9), 124.69 (C11), 124.66 (C11), 122.78 (C8), 122.56 (C8), 122.15 (C14), 121.74 (C14), 102.08 (C7), 101.35 (C7), 99.72 (C7), 37.33 (C6), 37.18 (C6), 37.03 (C6), 32.48 (C4), 32.34 (C4), 30.90 (C4), 30.44 (C5), 30.31 (C5), 30.04 (C5), 28.21 (C3), 28.16 (C3), 28.11 (C3), 23.24 (C2), 23.20 (C2), 23.18 (C2), 14.32 (C1), 14.31 (C1), 14.27 (C1). MALDI-TOF MS: calcd for  $\text{C}_{272}\text{H}_{288}\text{N}_{16}\text{O}_{32}$  4294.16 ( $\text{M} + \text{H}^+$ , 100%), found 4294.02. GPC:  $t_{\text{R}} = 12.91\text{min}$  (column temperature 25  $^\circ\text{C}$ ).



#### 4.4.4 Synthesis of hexadecaiminonanocapsule 49b

From **40** (99.6 mg, 0.107 mmol), benzidine **48b** (40.3 mg, 0.219 mmol) and  $\text{CF}_3\text{CO}_2\text{H}$  (TFA) (0.8  $\mu\text{L}$ , 0.0107 mmol) in chloroform (10.0 mL) according to *procedure A*. Deep yellow solid (121 mg, 92% yield, >95% purity based on  $^1\text{H}$  NMR integration).  $^1\text{H}$  NMR

(500 MHz, CDCl<sub>3</sub>, 25 °C),  $\delta_{\text{H}}$  (ppm): 8.66 (s, 8 H, H<sub>imine</sub>), 8.51 (s, 8 H, H<sub>imine</sub>), 7.61 (d,  $J = 8.30$  Hz, 16 H, H<sub>aryl</sub>), 7.54 (d,  $J = 8.30$  Hz, 16 H, H<sub>aryl</sub>), 7.29 (s, 8 H, H<sub>aryl</sub>), 7.28 (s, 8 H, H<sub>aryl</sub>), 7.19 (d,  $J = 8.30$  Hz, 16 H, H<sub>aryl</sub>), 7.06 (d,  $J = 8.30$  Hz, 16 H, H<sub>aryl</sub>), 5.91 (d,  $J = 7.64$  Hz, 4 H, H<sub>outer</sub>), 5.87 (d,  $J = 7.31$  Hz, 8 H, H<sub>outer</sub>), 5.46 (d,  $J = 6.97$  Hz, 4 H, H<sub>outer</sub>), 5.06-5.00 (m, 12 H, H<sub>methine</sub>), 4.93 (t,  $J = 7.97$  Hz, 4 H, H<sub>methine</sub>), 4.82 (d,  $J = 7.64$  Hz, 4 H, H<sub>inner</sub>), 4.75 (d,  $J = 7.31$  Hz, 8 H, H<sub>inner</sub>), 4.36 (d,  $J = 6.97$  Hz, 4 H, H<sub>inner</sub>),

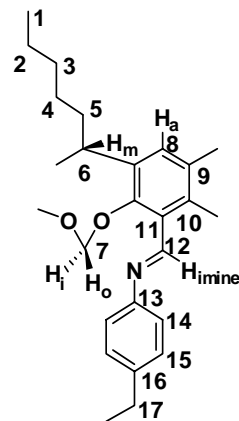


2.31 (br s, 32 H), 1.48-1.39 (m, 96 H), 0.98-0.94 (m, 48 H). <sup>13</sup>C NMR (125 MHz, CDCl<sub>3</sub>, 25 °C),  $\delta_{\text{C}}$  (ppm): 156.50 (C12), 155.36 (C12), 154.37 (C10), 154.22 (C10), 153.77 (C10), 152.89 (C10), 152.14 (C13), 151.80 (C13), 139.25 (C16), 138.96 (C16), 138.70 (C10), 138.50 (C9), 138.46 (C9), 138.26 (C9), 127.64 (C15), 127.52 (15), 124.10 (C11), 123.79 (C11), 122.27 (C8), 122.10 (C8), 121.48 (C14), 121.11 (C14), 100.67 (C7), 100.55 (C7), 99.67 (C7), 36.55 (C6), 36.44 (C6), 31.99 (C4), 31.96 (C4), 31.94 (C4), 29.93 (C5), 29.82 (C5), 29.51 (C5), 27.61 (C3), 27.59 (C3), 27.57 (C3), 22.73 (C2), 22.70 (C2), 14.11 (C1). MALDI-TOF MS: calcd for C<sub>320</sub>H<sub>320</sub>N<sub>16</sub>O<sub>32</sub> 4902.41(M + H<sup>+</sup>, 100%), found 4902.62. GPC:  $t_{\text{R}} = 12.54$  min (column temperature 25 °C).

#### 4.4.5 Synthesis of hexadecaiminonanocapsule 49c

From **40** (110.2 mg, 0.119 mmol), 4,4'-ethylenedianiline **48c** (51.1 mg, 0.241 mmol) and CF<sub>3</sub>CO<sub>2</sub>H (TFA) (0.05  $\mu$ L, 0.00067 mmol) in CHCl<sub>3</sub> (11.0 mL) according to *procedure A*. Reaction times: 2 h without and 1 h with 3 Å molecular sieves. Bright yellow solid (141 mg, 92% yield, >90% purity based on <sup>1</sup>H NMR integration). <sup>1</sup>H NMR (400 MHz, CDCl<sub>3</sub>,

25 °C),  $\delta_{\text{H}}$  (ppm): 8.60 (s, 8 H,  $\text{H}_{\text{imine}}$ ), 8.55 (s, 8 H,  $\text{H}_{\text{imine}}$ ), 7.29 (d,  $J$  = 8.49 Hz, 16 H,  $\text{H}_{\text{aryl}}$ ), 7.27 (br s, 16 H,  $\text{H}_{\text{aryl}}$ ), 7.22 (d,  $J$  = 8.29 Hz, 16 H,  $\text{H}_{\text{aryl}}$ ), 7.05 (d,  $J$  = 8.19 Hz, 16 H,  $\text{H}_{\text{aryl}}$ ), 6.99 (d,  $J$  = 8.10 Hz, 16 H,  $\text{H}_{\text{aryl}}$ ), 5.81 (d,  $J$  = 7.51 Hz, 12 H,  $\text{H}_{\text{outer}}$ ), 5.71 (d,  $J$  = 7.51 Hz, 4 H,  $\text{H}_{\text{outer}}$ ), 5.04-4.93 (m, 16 H,  $\text{H}_{\text{methine}}$ ), 4.78 (d,  $J$  = 7.71 Hz, 4 H,  $\text{H}_{\text{inner}}$ ), 4.71 (d,  $J$  = 7.73 Hz, 8 H,  $\text{H}_{\text{inner}}$ ), 4.53 (d,  $J$  = 7.06 Hz, 4 H,  $\text{H}_{\text{inner}}$ ), 2.90 (s, 32 H,  $\text{H}_{\text{Ar-CH}_2}$ ), 2.31 (br s, 32 H), 1.54-1.35 (m, 96



H), 0.98-0.94 (m, 48 H).  $^{13}\text{C}$  NMR (125 MHz,  $\text{CDCl}_3$ , 25 °C),  $\delta_{\text{C}}$  (ppm): 155.48 (C12), 155.14 (C12), 154.20 (C10), 154.05 (C10), 153.61 (C10), 153.14 (C10), 150.88 (C13), 150.57 (C13), 140.40 (C16), 140.06 (C16), 139.05 (C9), 138.91 (C9), 138.67 (C9), 138.53 (C9), 128.90 (C15), 128.81 (15), 124.13 (C11), 124.08 (C11), 122.06 (C8), 121.96 (C8), 120.98 (C14), 120.82 (C14), 100.65 (C7), 100.51 (C7), 100.06 (C7), 38.18 (C17), 37.39 (C17), 36.48 (C6), 36.44 (C6), 31.98 (C4), 31.96 (C4), 31.94 (C4), 29.89 (C5), 29.75 (C5), 29.63 (C5), 27.61 (C3), 27.57 (C3), 22.72 (C2), 22.71 (C2), 22.70 (C2), 14.10 (C1). IR (NaCl),  $\nu$  ( $\text{cm}^{-1}$ ): 2957, 2932, 2860, 1622, 1581, 1504, 1468, 1448, 1242, 1206, 1093, 958. MALDI-TOF MS: calcd for  $\text{C}_{336}\text{H}_{352}\text{N}_{16}\text{O}_{32}$  5126.66 ( $\text{M} + \text{H}^+$ , 100%), found 5126.15. GPC:  $t_{\text{R}}$  = 12.03 min (column temperature 60 °C).

#### 4.4.6 Reduction of 49c

$\text{NaBH}_3\text{CN}$  in THF solution (1M, 0.47ml, 0.47 mmol) was added dropwise over 10 min into a mixture of tetramer **49c** (30.0 mg, 0.00585 mmol) and  $\text{Ni}(\text{AcO})_2$  (25.7mg, 0.103 mmol) in THF (14.6 ml). The mixture was stirred overnight at room temperature. The solvent was removed. The residue was stirred with 10 ml  $\text{H}_2\text{O}$  and 1 ml  $\text{NH}_3/\text{H}_2\text{O}$  for 20

min. It was extracted with 30 ml CH<sub>2</sub>Cl<sub>2</sub>. The organic layer was washed with 10 ml saturated NaHCO<sub>3</sub> aq. Then, the organic layer was concentrated and the product was precipitated with methanol. The crude product was dried overnight at high vacuum at room temperature to yield an off-white solid. The solid was redissolved in 1 ml CH<sub>2</sub>Cl<sub>2</sub> and precipitated with methanol. The mixture was filtered and the residue was washed with 3 × 1 ml methanol. The residue was dissolved in CH<sub>2</sub>Cl<sub>2</sub> and the solution was concentrated. The residue was dried overnight at high vacuum at room temperature. The crude product was purified by HPLC (PricetonSPHER-300 Silica 300Å, 5 μ, 150 × 4.6 mm, 1 ml/min, 280 nm, *t<sub>R</sub>* = 4.55 min) to give **50** as a white solid (23 mg; 72% yield based on cavitand **40** used for the synthesis of **49c**). <sup>1</sup>H NMR (300 MHz, CDCl<sub>3</sub>, 25 °C): δ = 7.20 (d, *J* = 13.4 Hz, 16H, aryl-H), 7.13 (d, *J* = 8.49 Hz, 16H, aryl-H), 7.02 (d, *J* = 8.49 Hz, 16H, aryl-H), 6.69 (d, *J* = 8.38 Hz, 16H, aryl-H), 6.56 (d, *J* = 8.38 Hz, 16H, aryl-H), 5.97 (d, *J* = 6.95 Hz, 4 H, H<sub>o</sub>), 5.91 (d, *J* = 6.95 Hz, 8 H, H<sub>o</sub>), 5.80 (d, *J* = 6.95 Hz, 4 H; H<sub>o</sub>), 4.89-4.81 (m, 16 H, H<sub>m</sub>), 4.46 (d, *J* = 6.83 Hz, 12 H, H<sub>i</sub>), 4.38 (d, *J* = 6.37 Hz, 4 H, H<sub>i</sub>), 4.19-4.11 (m, 16 H, aryl-CH<sub>2</sub>-N), 4.06 (d, *J* = 10.76 Hz, 8 H, aryl-CH<sub>2</sub>-N), 3.98 (d, *J* = 10.23 Hz, 8 H, aryl-CH<sub>2</sub>-N), 2.84-2.71 (m, 32 H, H<sub>g</sub>), 2.32-2.20 (m, 32 H), 1.50-1.33 (m, 96 H), 0.98-0.92 (m, 48 H). <sup>13</sup>C NMR (100.6 MHz, CDCl<sub>3</sub>, 25 °C), δ<sub>C</sub> (ppm): 153.99 (C10), 153.82 (C10), 153.67 (C10), 146.56 (C13), 145.94 (C13), 138.60 (C9), 138.44 (C9), 138.20 (C9), 132.43 (C16), 132.17 (C16), 129.28 (C15), 129.00 (15), 125.42 (C11), 124.32 (C11), 120.07 (C8), 119.85 (C8), 114.05 (C14), 113.62 (C14), 100.39 (C7), 99.86 (C7), 99.67 (C7), 39.55 (C12), 38.71 (C12), 37.95 (C17), 37.67 (C17), 37.05 (C6), 32.03 (C4), 30.19 (C5), 27.62 (C3), 22.69 (C2), 14.10 (C1). MS (MALDI-TOF) *m/z*: 5159.07 (M+H<sup>+</sup>, 100%); Calcd for C<sub>336</sub>H<sub>384</sub>N<sub>16</sub>O<sub>32</sub>+H<sup>+</sup>: 5159.92.

## 4.5 References

1. a) X. Liu, Y. Liu, G. Li, R. Warmuth, *Angew. Chem. Int. Ed.* **2006**, *45*, 901; b) X. Liu, R. Warmuth, *J. Am. Chem. Soc.*, **2006**, *128*, 14120; c) X. Liu, Y. Liu, R. Warmuth, *Supramol. Chem.* **2008**, *20*, 41.
2. a) D. J. Cram, S. Karbach, H.-E. Kim, C. B. Knobler, E. F. Maverick, J. L. Ericson, R. C. Helgeson, *J. Am. Chem. Soc.*, **1988**, *110*, 2229; b) H. Jude, D. J. Sinclair, N. Das, M. S. Sherburn, P. J. Stang, *J. Org. Chem.* **2006**, *71*, 4155.
3. G. Ercolani, *J. Phys. Chem. B* **2003**, *107*, 5052.
4. D. Wu, A. Chen, C. Johnson Jr., *J. Magn. Reson. Ser. A* **1995**, *115*, 260.
5. N. L. Allinger, Y. H. Yuh, J.-H. Lii, *J. Am. Chem. Soc.*, **1989**, *111*, 8551.
6. M. Holz, X. Mao, D. Seiferling, *J. Chem. Phys.* **1996**, *104*, 669.
7. A. Shivanyuk, J. Rebek, Jr., *Chem. Commun.* **2002**, 2326.
8. M. Yamanaka, A. Shivanyuk, J. Rebek, Jr., *J. Am. Chem. Soc.* **2004**, *126*, 2939.
9. L. Avram, Y. Cohen, *Org. Lett.* **2003**, *5*, 1099.
10. a) S. Mecozzi, J. Rebek Jr., *Chem. Eur. J.* **1998**, *4*, 1016; b) A. Shivanyuk, J. Fries, S. Doering, J. Rebek, Jr., *J. Org. Chem.* **2003**, *68*, 6489.
11. E. V. Anslyn, D. A. Dougherty, *Modern Physical Organic Chemistry*, University Science Books, USA, **2006**, p. 207-222.
12. a) C. L. D. Gibb, B. C. Gibb, *J. Am. Chem. Soc.*, **2006**, *128*, 16498; b) V. Stastny, D. M. Rudkevich, *J. Am. Chem. Soc.* **2007**, *129*, 1018.
13. R. Warmuth, E. F. Maverick, C. B. Knobler, D. J. Cram, *J. Org. Chem.* **2003**, *68*, 2077.
14. S. T. Mough, J. C. Goeltz, K. T. Holman, *Angew. Chem. Int. Ed.* **2004**, *43*, 5631.

## Chapter 5 Dynamic combinatorial libraries of polyimino nanocapsules

### 5.1 Introduction

Combinatorial chemistry plays an important role in pharmaceutical industry. The marriage of dynamic covalent chemistry and combinatorial chemistry provides a new attractive approach towards diverse mixtures.<sup>[1]</sup> Dynamic combinatorial chemistry generates a library of compounds under thermodynamic control. Individual molecules in the library can be amplified through the introduction of a template and/or additional weak interactions.<sup>[2]</sup>

Dynamic combinatorial libraries (DCL) can be constructed through either noncovalent or reversible covalent bonding chemistry.<sup>[2a,3]</sup> Using reversible covalent bonding chemistry, macrocyclic receptors have been synthesized through imine, ester and disulfide formation/exchange. Otto and coworkers have also reported the synthesis of dynamic libraries of disulfide cages in water.<sup>[4]</sup>

Our previous studies have shown that the condensation reaction between tetraformyl cavitand **40** and rigid linear diamines, such as *para*-phenylenediamine **48a**, gives tetrameric nanocapsules quantitatively.<sup>[5]</sup> On the other hand, dimeric capsules are formed quantitatively, if kinked diamines, such as *meta*-phenylenediamine **41** or 1,3-diaminopropane **44a**, are used.<sup>[6]</sup> In this chapter, dynamic combinatorial libraries of polyimino nanocages, generated from a combination of different kinked diamines or a combination of kinked diamines and rigid linear diamines, will be discussed.



## 5.2 Results and discussion

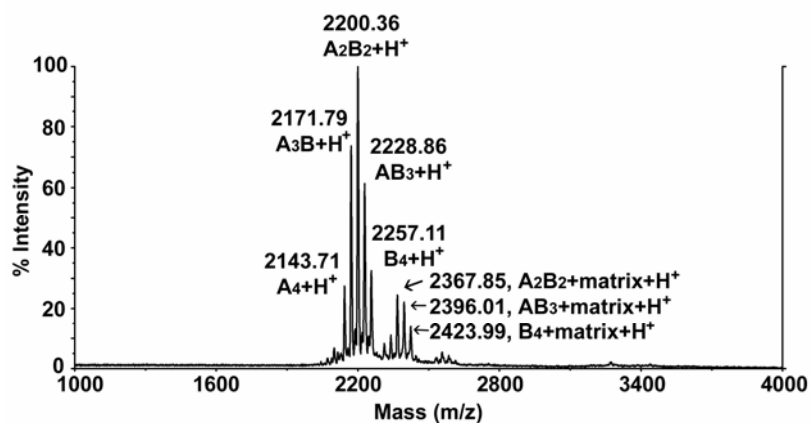
### 5.2.1 System selection

As has been reported before, the condensation between tetraformyl cavitand **40** and *meta*-phenylenediamine **41** or *meta*-xylylenediamine **44d** forms quantitatively dimeric capsules in either chloroform or toluene.<sup>[6]</sup> Both diamines have predefined 120° angles between the two amino groups and *meta*-xylylenediamine has two more methylene groups. On the other hand, the condensation between **40** and *para*-phenylenediamine **48a** or benzidine **48b** forms quantitatively tetrameric capsules - with *para*-phenylenediamine in toluene, with benzidine in chloroform.<sup>[5]</sup> Both are rigid linear linkers (Scheme 4.1 and Table 4.1). Therefore, eleven combinations, including six binary systems, four ternary systems and one quaternary system are possible with these four diamine linkers (**41**, **44d**, **48a**, and **48b**). However, only five of the eleven systems can be studied due to the solvent effect on the formation of the tetrameric capsules. Among them, DCLs of *meta*-phenylenediamine, *meta*-xylylenediamine and benzidine will be studied in chloroform-*d* and DCLs of *meta*-phenylenediamine and *para*-phenylenediamine in toluene-*d*<sub>8</sub>. In the remaining of this chapter, the linkers *meta*-phenylenediamine, *meta*-xylylenediamine, benzidine, and *para*-phenylenediamine are symbolized with the letters **A**, **B**, **C**, and **D**, respectively.

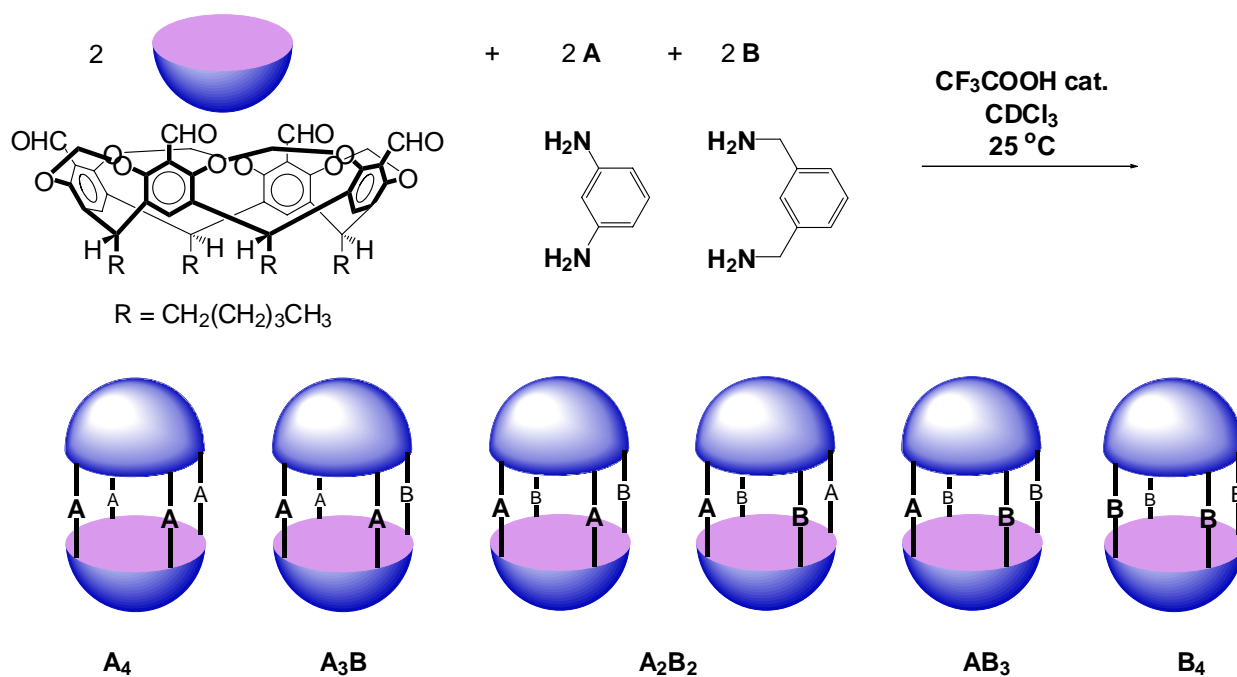
### 5.2.2 DCL from *meta*-phenylenediamine (**A**) and *meta*-xylylenediamine (**B**)

The binary system of *meta*-phenylenediamine and *meta*-xylylenediamine resulted in the formation of a library with only dimeric capsules present. After mixing tetraformyl cavitand (1 equiv.) with *meta*-phenylenediamine (1 equiv.) and *meta*-xylylenediamine (1

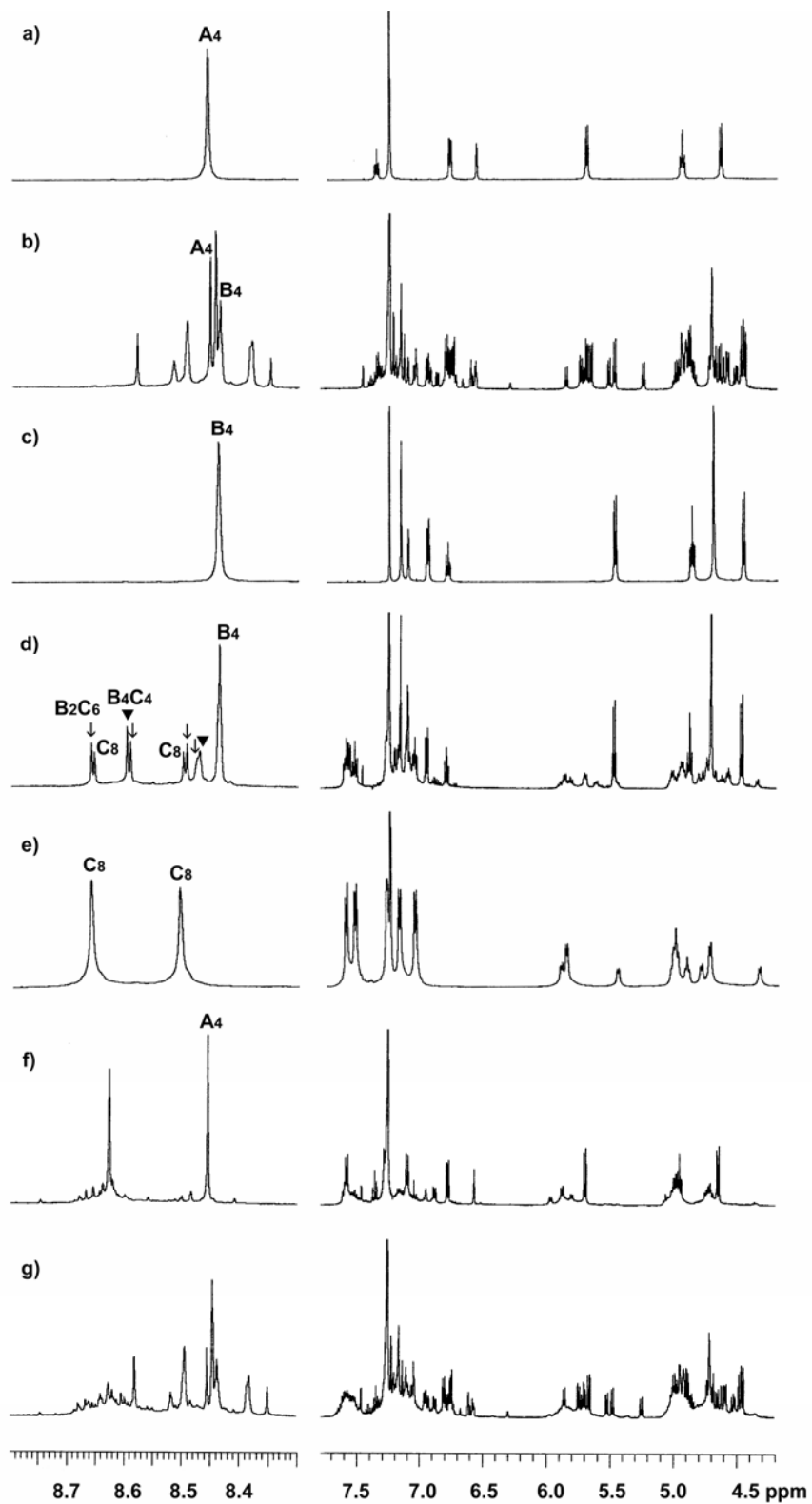
equiv.) in the presence of catalytic amounts of trifluoroacetic acid (TFA) in  $\text{CDCl}_3$ , the library reached equilibrium within one day. The MALDI-TOF mass spectrum of the reaction mixture showed peaks with  $m/z$  values of 2143.71, 2171.79, 2200.36, 2228.86, 2257.11 for the octaiminohemicarcerands **A**<sub>4</sub>, **A**<sub>3</sub>**B**, **A**<sub>2</sub>**B**<sub>2</sub> (two regioisomers presumably), **AB**<sub>3</sub> and **B**<sub>4</sub> with relative intensity 26:71:96:59:30 (ratio in %), respectively (Figure 5.1 and Scheme 5.1), which is close to the statistical distribution 1:4:6:4:1 (6.25%:25%:37.5%:25%:6.25%) except that too much **A**<sub>4</sub> and **B**<sub>4</sub> are present. The imine region in the <sup>1</sup>H NMR spectrum ( $\delta$  = 8.6-8.3 ppm) of the equilibrated reaction mixture shows eight sharp signals with integration ratio of ~1.9:1.9:4.9:4.7:5.4:4.5:4.0:1.0 (Figure 5.2 b). Signals at  $\delta$  = 8.455 and 8.438 ppm are assigned to the homodimers **A**<sub>4</sub> and **B**<sub>4</sub> (Figure 5.2 a and c). They have equal intensity and their sum accounts for ~26% of the total integration of the imine region, which is consistent with the MALDI-TOF MS distribution. The other signals are assigned to the heterodimers. A similar product distribution was observed by Cram, Stoddart and coworkers in the formation of octaiminohemicarcerands from unsubstituted and substituted *meta*-phenylenediamine.<sup>[6a]</sup> Neither higher molecular weight oligomers nor polymeric products were observed in the GPC chromatogram of the reaction mixture. Addition of reactants in a different order still generated the same mixture. However, no linker exchange was observed upon mixing preformed **A**<sub>4</sub> and **B**<sub>4</sub> in the presence of excess **A** and **B** (1~2%). The extremely slow exchange rate has been observed earlier in the formation of octaiminohemicarcerands from unsubstituted and substituted *meta*-phenylenediamine.<sup>[6a]</sup> This is probably due to the much higher effective molarity of freely dangling **A** in **A**<sub>4</sub> (or **B** in **B**<sub>4</sub>) compared to the free **B** (or **A**) in the solution.



**Figure 5.1** MALDI-TOF mass spectrum of DCL from **A** and **B**.



**Scheme 5.1** The product distribution of DCL from **A** and **B**.



**Figure 5.2** Partial  $^1\text{H}$  NMR spectra (500 MHz,  $\text{CDCl}_3$ , 25  $^\circ\text{C}$ ) of a)  $\text{A}_4$ , c)  $\text{B}_4$ , e)  $\text{C}_8$ , and DCLs from **40** and b)  $\text{A} + \text{B}$ ; d)  $\text{B} + \text{C}$ ; f)  $\text{A} + \text{C}$ ; g)  $\text{A} + \text{B} + \text{C}$ .

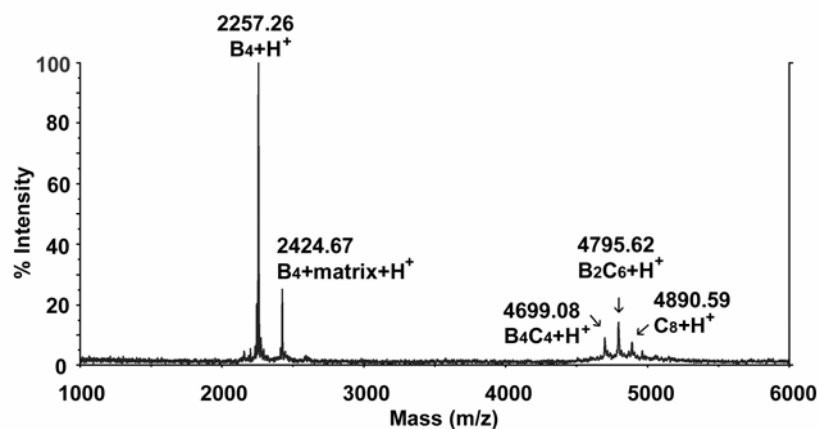
The product distribution in the DCL indicates the isoenergetic nature of the library members. On one hand, the angles between two C<sub>aryl</sub>-C<sub>carbonyl</sub> bonds of opposing aromatic units are 61° in the cavitand building blocks.<sup>[7]</sup> On the other hand, both of the diamines have predefined 120 ° angles between the two amino groups. Therefore the geometric arrangement of the formyl groups in the cavitand and of the amino groups in the diamines results in the exclusive formation of dimeric capsules. Bridging unit exchange doesn't change the stabilities of the heterodimers compared to those of the homodimers, even though *meta*-xylylenediamine has a slightly longer spacer. The increased flexibility might be able to release any strain that is generated due to different lengths of the bridging units.

Hemicarcerands bridged by three tetramethylenedioxy groups and a fourth unique bridge have been synthesized from a tetrahydroxyl cavitand in 20~35% yield.<sup>[8]</sup> The imine bonds of the library members can be reduced to give kinetically stable octaminohemicarcerands, which provides an alternative way to generate hemicarcerands with different bridging units.

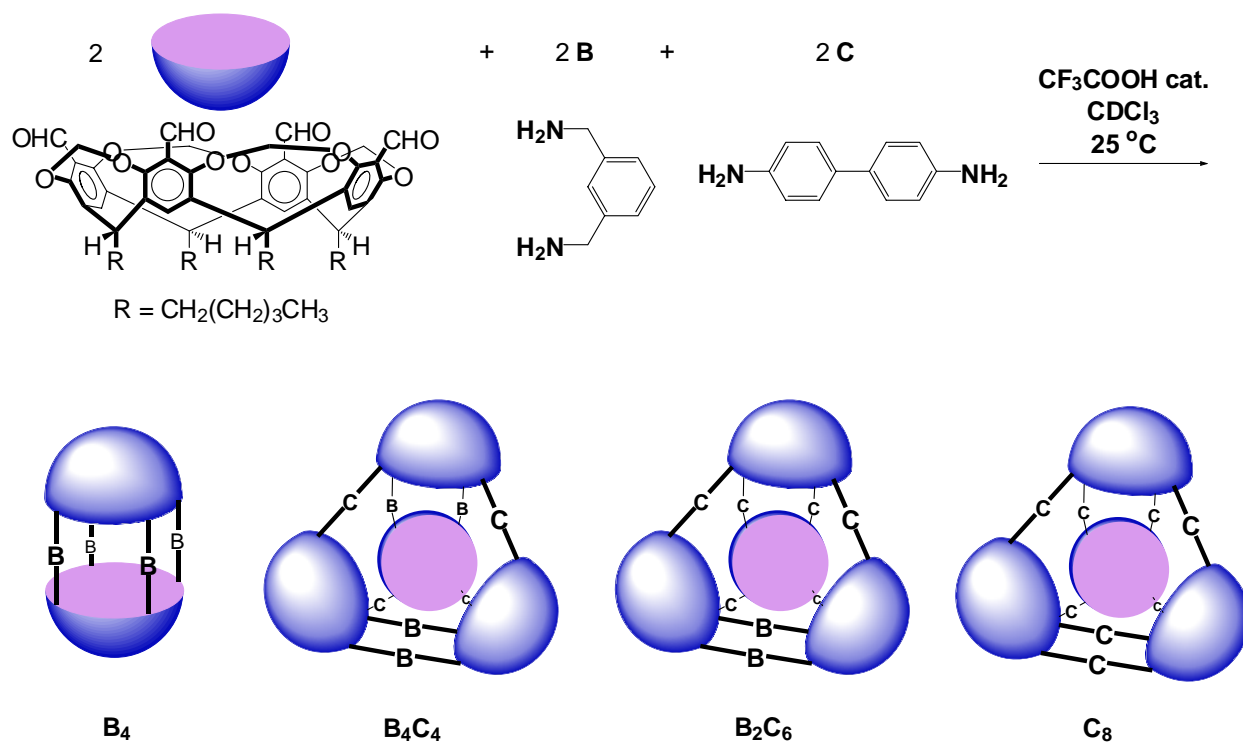
### 5.2.3 DCL from *meta*-xylylenediamine (B) and benzidine(C)

The combination of *meta*-xylylenediamine and benzidine resulted in the formation of a library composed of homodimer (**B**<sub>4</sub>), homotetramer (**C**<sub>8</sub>) and heteromeric capsules. Tetraformyl cavitand (1 equiv.) was mixed with *meta*-xylylenediamine (1 equiv.) and benzidine (1 equiv.) in the presence of cat. TFA in CDCl<sub>3</sub>. The library reached equilibrium over five days. The MALDI-TOF mass spectrum of the equilibrated reaction mixture showed peaks with *m/z* values of 2257.26 for the octaiminohemicarcerand **B**<sub>4</sub>

(Figure 5.3 and Scheme 5.2). Signals at  $m/z = 4699.08$ ,  $4795.62$ ,  $4890.59$  correspond to the tetrameric species **B<sub>4</sub>C<sub>4</sub>**, **B<sub>2</sub>C<sub>6</sub>** and **C<sub>8</sub>**. The relative ion abundance of the library in the MALDI-TOF MS does not necessarily reflect the solution concentration, since dimeric capsules usually have higher ionization efficiency than tetrameric ones, due to the lower molecular weight. The imine region of the  $^1\text{H}$  NMR spectrum ( $\delta = 8.7$ - $8.4$  ppm) of the equilibrated reaction mixture gives nine signals with the integration ratio of  $\sim 1.35:1.15:1.9:1.35:1.15:1.35:1.35:1.9:7$  (Figure 5.2 d). The signals at  $\delta = 8.438$  ppm and at  $\delta = 8.654$  and  $8.499$  ppm are assigned to the homodimer **B<sub>4</sub>** (Figure 5.2 c) and the homotetramer **C<sub>8</sub>** (Figure 5.2 e), respectively. Signals at  $\delta = 8.598$  and  $8.471$  ppm are assigned to the heterotetramer **B<sub>4</sub>C<sub>4</sub>**, and those at  $\delta = 8.660$ ,  $8.592$ ,  $8.494$  and  $8.476$  ppm to the heterotetramer **B<sub>2</sub>C<sub>6</sub>**. These assignments are based on the signal intensities in libraries that have different *meta*-xylylenediamine/benzidine ratios. No other oligomers were observed in the GPC chromatogram of the reaction mixture.



**Figure 5.3** MALDI-TOF mass spectrum of DCL from **B** and **C**.



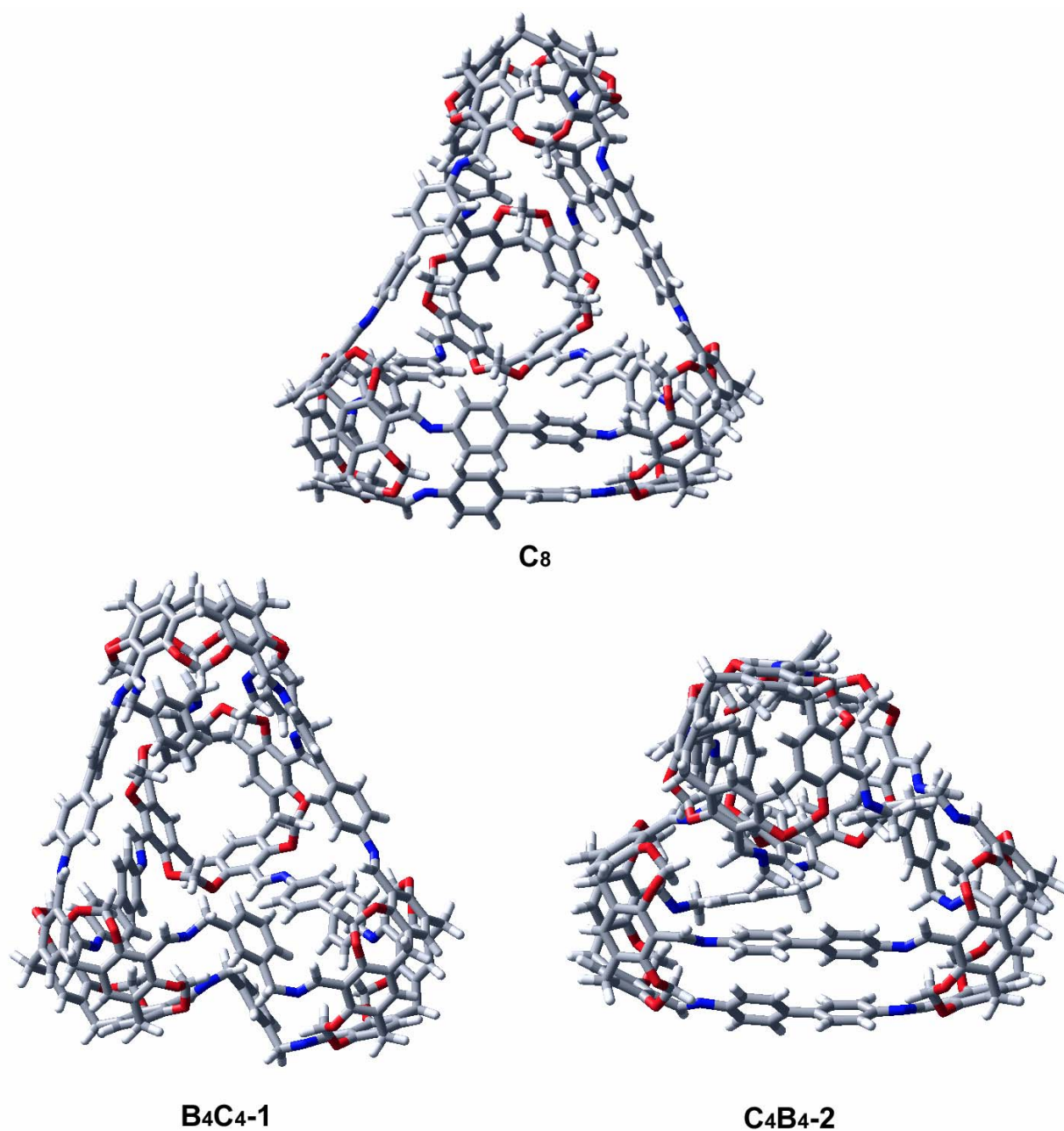
**Scheme 5.2** The product distribution of DCL from **B** and **C**.

The heterotetramers  $\text{B}_4\text{C}_4$  and  $\text{B}_2\text{C}_6$  are probably formed through exchange of two adjacent benzidine linkers, that doubly connected cavitands in the homotetramer  $\text{C}_8$ , against free *meta*-xylylenediamine. The benzidine linkers (**C**) in  $\text{C}_8$  that are part of a rectangular and triangular opening are likely under higher strain as compared to benzidine linkers that are part of two triangular openings. Exchange of these higher strained linkers against **B** releases energy. Therefore in the heterodimer  $\text{B}_4\text{C}_4$ , all of the four less stable benzidine bridging units are replaced with *meta*-xylylenediamine bridges (Scheme 5.2).  $\text{B}_4\text{C}_4$  should have two different imine signals in the  $^1\text{H}$  NMR spectrum (ratio 1:1). In  $\text{B}_2\text{C}_6$ , only two of the less stable benzidine bridging units are replaced by *meta*-xylylenediamine (Scheme 5.2). Therefore it should have four different imine signals

in the  $^1\text{H}$  NMR spectrum (ratio 1:1:1:1). Overall six additional imine signals should be observed in the  $^1\text{H}$  NMR spectrum in addition to signals for homodimer **B**<sub>4</sub> and homotetramer **C**<sub>8</sub>. Indeed this is what is observed in the imine region of the  $^1\text{H}$  NMR spectrum of the reaction mixture (Figure 5.2 d). Based on the integration ratio of the imine signals, the four species are present in a ratio **B**<sub>4</sub>: **B**<sub>4</sub>**C**<sub>4</sub>: **B**<sub>2</sub>**C**<sub>6</sub>: **C**<sub>8</sub> = 3:2.3:1.7:1, which is different from the statistical ratio of 2:1:2:1. This indicates that **B**<sub>4</sub>**C**<sub>4</sub> is the most stable capsule. The absence of heterotetramer **B**<sub>6</sub>**C**<sub>2</sub> indicates that the tetrameric species fall apart as soon as six of the eight linkers are exchanged.

Molecular mechanics calculations using the MM3 force field provided information about the relative stabilities of the homotetramer **C**<sub>8</sub> and the heterotetramers **B**<sub>4</sub>**C**<sub>4</sub>-1 and **C**<sub>4</sub>**B**<sub>4</sub>-2. Here, **B**<sub>4</sub>**C**<sub>4</sub>-1 is used to represent **B**<sub>4</sub>**C**<sub>4</sub> in Scheme 5.2, in which both of the two adjacent benzidine linkers, that doubly connected cavitands in **C**<sub>8</sub>, are exchanged against *meta*-xylylenediamine, whereas in **C**<sub>4</sub>**B**<sub>4</sub>-2 the other four benzidine linkers of **C**<sub>8</sub> are exchanged against *meta*-xylylenediamine. The lowest energy conformations of **C**<sub>8</sub>, **B**<sub>4</sub>**C**<sub>4</sub>-1 and **C**<sub>4</sub>**B**<sub>4</sub>-2 were obtained by molecular dynamics simulations. For each host, stochastic molecular dynamics (MM3\* force field; vacuum) were carried out for 2000 ps at T = 500 K. Every 40 ps a snapshot of the nanocapsule was saved (50 structures). Each snapshot was energy-minimized (MM3\* force field;<sup>[11b]</sup> chloroform solvation model<sup>[11c]</sup>) and the lowest energy structure was used as input for a second molecular dynamics run under the same conditions. This procedure was repeated until the lowest energy structure did not change any more. The lowest energy conformations of **C**<sub>8</sub>, **B**<sub>4</sub>**C**<sub>4</sub>-1 and **C**<sub>4</sub>**B**<sub>4</sub>-2 obtained by this procedure are shown in Figure 5.4.





**Figure 5.4** Energy-minimized structures of tetramer C<sub>8</sub>, B<sub>4</sub>C<sub>4</sub>-1 and C<sub>4</sub>B<sub>4</sub>-2.

In order to determine the total conformational energy in the flexible linker groups of each host,  $\Delta E_{\text{total}}$ , two calculations were performed. 1) The strain energy  $\Delta E_{\text{strain}}$  in linkers -CH=N-X-N=CH-, due to improper bond angles, torsions, and bond lengths, was

computed.  $\Delta E_{\text{strain}}$  also contains long- and short-distance interactions between the linkers of a host (van der Waals interactions, dipole-dipole interactions, induced dipole-dipole interactions and CH- $\pi$  interactions). 2) The acetal-linker interaction energy  $\Delta E_{\text{acetal-linker}}$ , which may stabilize the structure primarily due to C-H $\cdots\pi$  interactions, was computed. The total conformational energy  $\Delta E_{\text{total}}$ , that is used to compare the three hosts, is the sum of  $\Delta E_{\text{strain}}$  and  $\Delta E_{\text{acetal-linker}}$ :

$$\Delta E_{\text{total}} = \Delta E_{\text{strain}} + \Delta E_{\text{acetal-linker}}, \quad (5.1)$$

As an example, the calculation of  $\Delta E_{\text{total}}$  for tetramer **C<sub>8</sub>** is outlined as follows. First, the strain in the imine-cavitand part was calculated (Scheme 5.3). To do this, **C<sub>8</sub>** was energy-minimized (structure **a** in Scheme 5.3). Then, the X groups of the linkers were replaced with hydrogens and the current energy of the tetraimine cavitands CE(**b1**) was calculated (step 1). Second, the cavitands were moved apart (step 2) and energy-minimized to obtain energy ME(**d1**) (step 3). Finally, those hydrogen atoms in structure **d1**, which were added in step 1, were removed and added back. Subsequently, the current energy CE(**e1**) was calculated (step 4). CE(**e1**) was used to correct CE(**b1**) for improper N-H bond lengths in step 1. The strain energy in the imine-cavitand part of tetramer **C<sub>8</sub>** was obtained from equation 5.2 (Table 5.1):

$$\Delta E_1 = [\text{CE}(\mathbf{b1}) - [\text{CE}(\mathbf{e1}) - \text{ME}(\mathbf{d1})]] - \text{ME}(\mathbf{d1}) = \text{CE}(\mathbf{b1}) - \text{CE}(\mathbf{e1}), \quad (5.2)$$

The same procedure was applied to calculate the strain energy in the complete linkers -CH=N-X-N=CH- of tetramer **C**<sub>8</sub> ( $\Delta E_2$ ) by deleting the cavitands in step 1 (Scheme 5.4 and Table 5.1), and in the imines themselves ( $\Delta E_3$ ) by cutting cavitands and linker -X- groups (Scheme 5.5 and Table 5.1). The strain energy was calculated from these incremental energies as follows (Table 5.1):

$$\Delta E_{\text{strain}} = \Delta E_1 + \Delta E_2 - \Delta E_3, \quad (5.3)$$

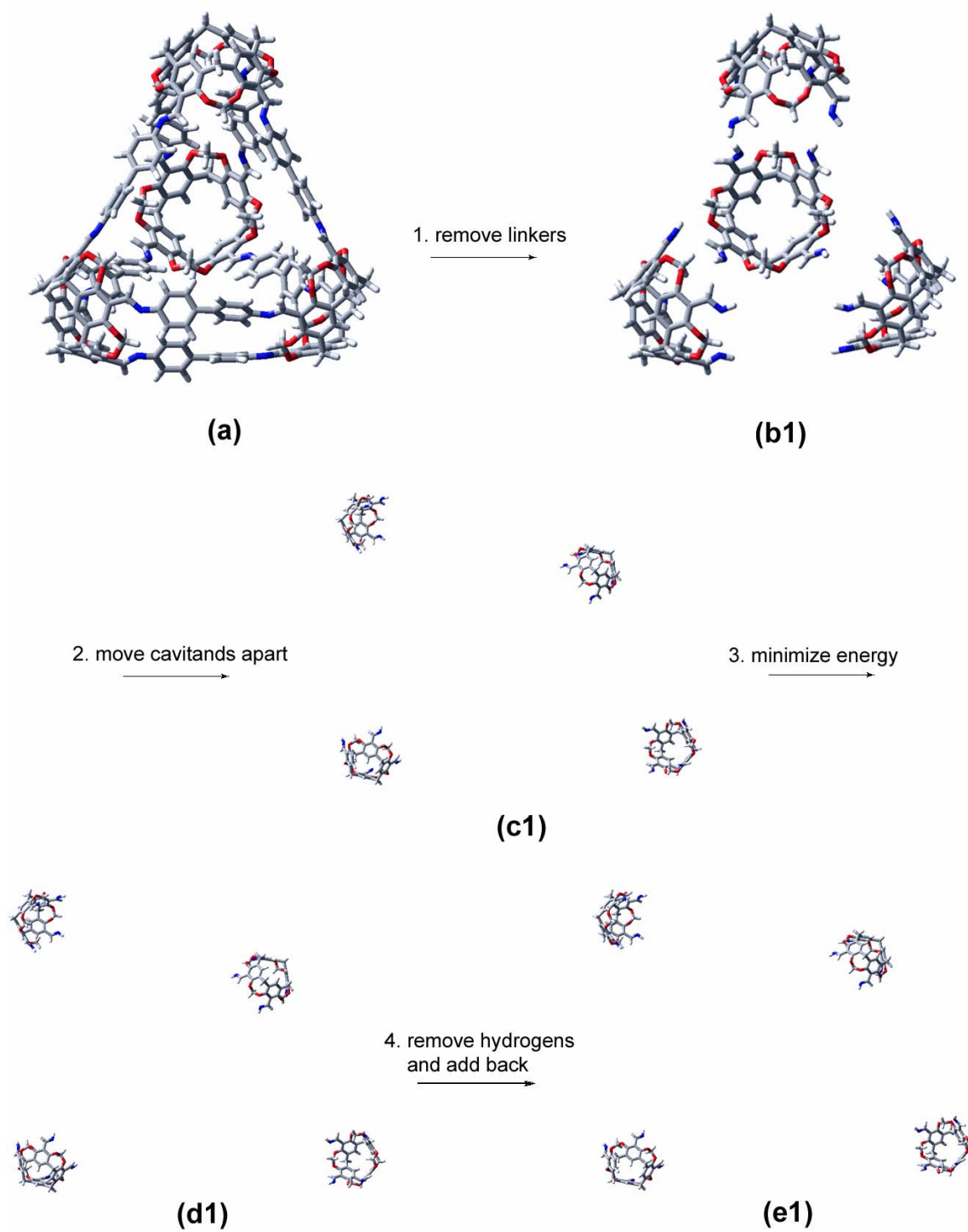
The acetal-linker interaction energy  $\Delta E_{\text{acetal-linker}}$  of tetramer **C**<sub>8</sub> is the difference between the current energy changes of step **a** → **b4** (CE(**a**) - CE(**b4**)) and step **b1** → **b5** (CE(**b1**) - CE(**b5**)), in which the acetal groups are removed (Scheme 5.6 and Table 5.1):

$$\Delta E_{\text{acetal-linker}} = [\text{CE}(\mathbf{a}) - \text{CE}(\mathbf{b4})] - [\text{CE}(\mathbf{b1}) - \text{CE}(\mathbf{b5})], \quad (5.4)$$

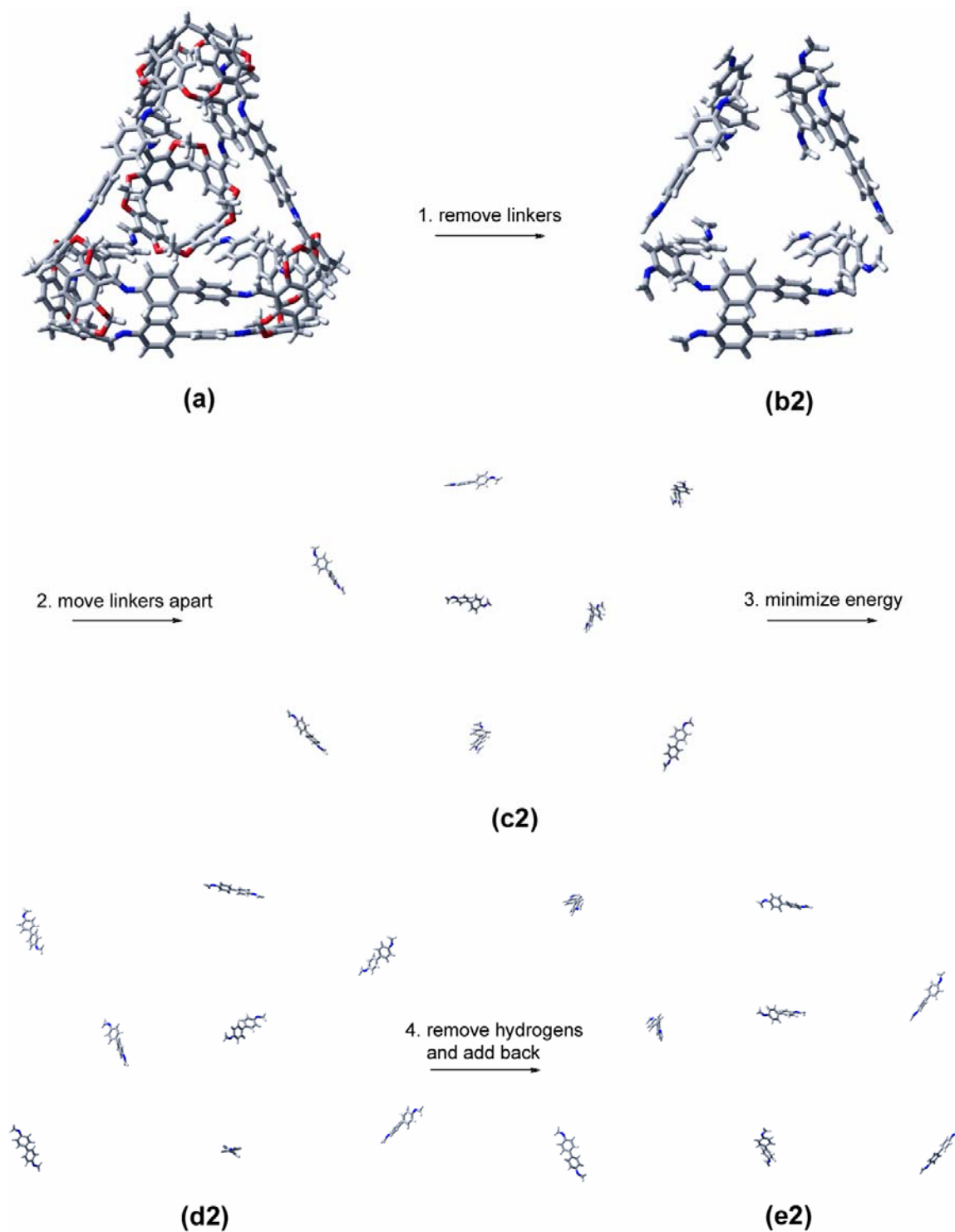
Finally, the total conformational energy of **C**<sub>8</sub> was obtained from equation 5.1 and is listed in Table 5.1. The energies  $\Delta E_{\text{total}}$  for **B**<sub>4**C**<sub>4-1</sub> and **C**<sub>4**B**<sub>4-2</sub> were calculated through the same procedure as described above for **C**<sub>8</sub> (Table 5.1). Tetramer **B**<sub>4**C**<sub>4-1</sub> is 5.3 kcal/mol more stable than the homotetramer **C**<sub>8</sub>. On the other hand, tetramer **C**<sub>4**B**<sub>4-2</sub> is 1.1 kcal/mol less stable than **C**<sub>8</sub>. This supports our previous assignment of the structure of the heterotetramer **B**<sub>4**C**<sub>4</sub> (Scheme 5.2). Additional strain energy calculations, in which  $\Delta E_2$  of  $\Delta E_{\text{strain}}$  in **C**<sub>8</sub> was dissected into its contributions from the two different linkers, show that the adjacent benzidine linkers, that doubly connected cavitands, have a 3.8 kcal/mol higher strain energy than the other four benzidine linkers.</sub></sub></sub></sub></sub>

**Table 5.1** Strain energy and acetal-linker stabilization energy in three tetramers **C<sub>8</sub>**, **B<sub>4</sub>C<sub>4</sub>-1**, and **C<sub>4</sub>B<sub>4</sub>-2** (kcal/mol).

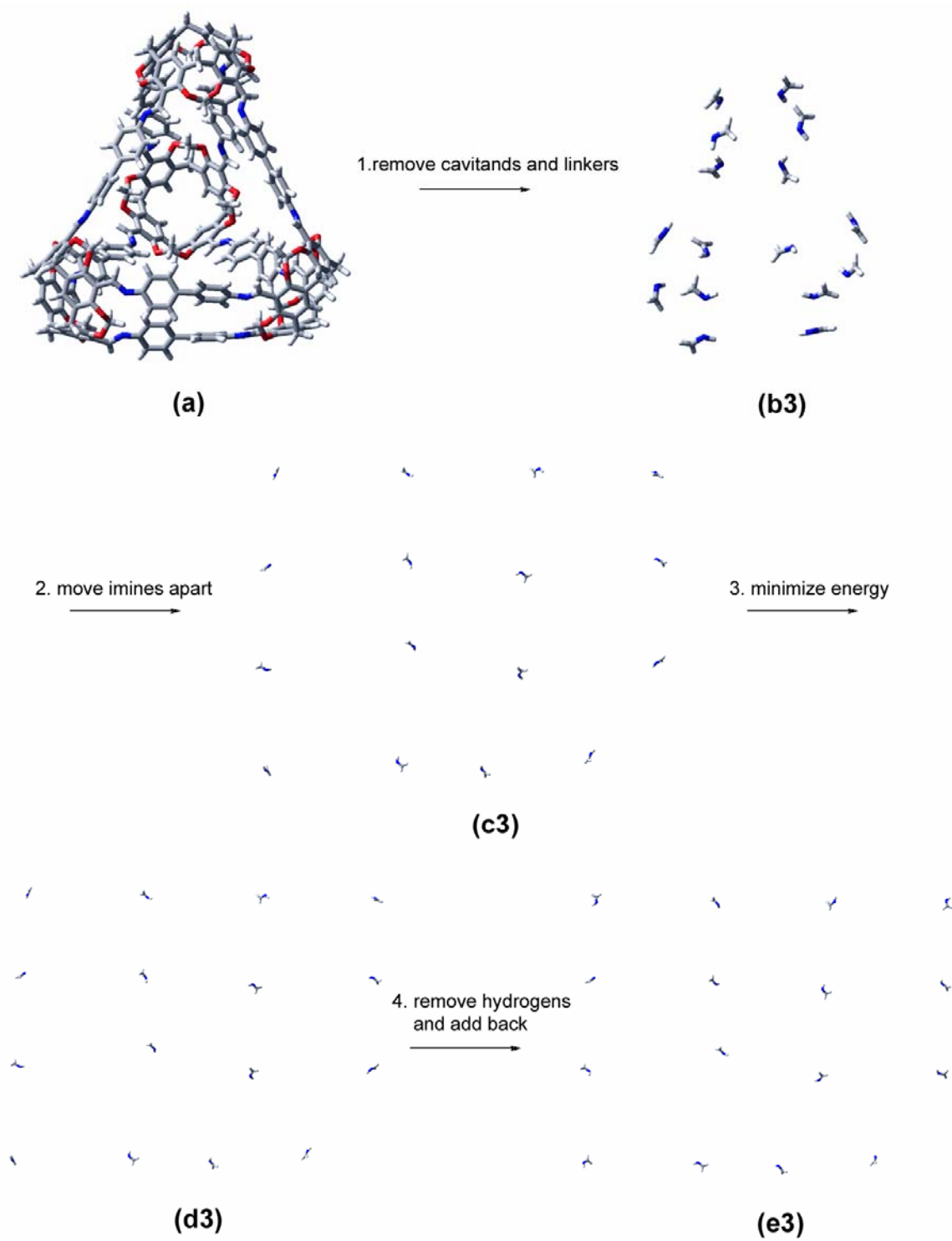
nanocapsule	$\Delta E_1$	$\Delta E_2$	$\Delta E_3$	$\Delta E_{\text{strain}}$	$\Delta E_{\text{acetal-linker}}$	$\Delta E_{\text{total}}$
<b>C<sub>8</sub></b>	11.2	6.9	8.0	10.1	-5.3	4.8
<b>B<sub>4</sub>C<sub>4</sub>-1</b>	10.3	3.6	3.7	10.2	-10.7	-0.5
<b>C<sub>4</sub>B<sub>4</sub>-2</b>	13.1	9.2	6.5	15.8	-9.9	5.9



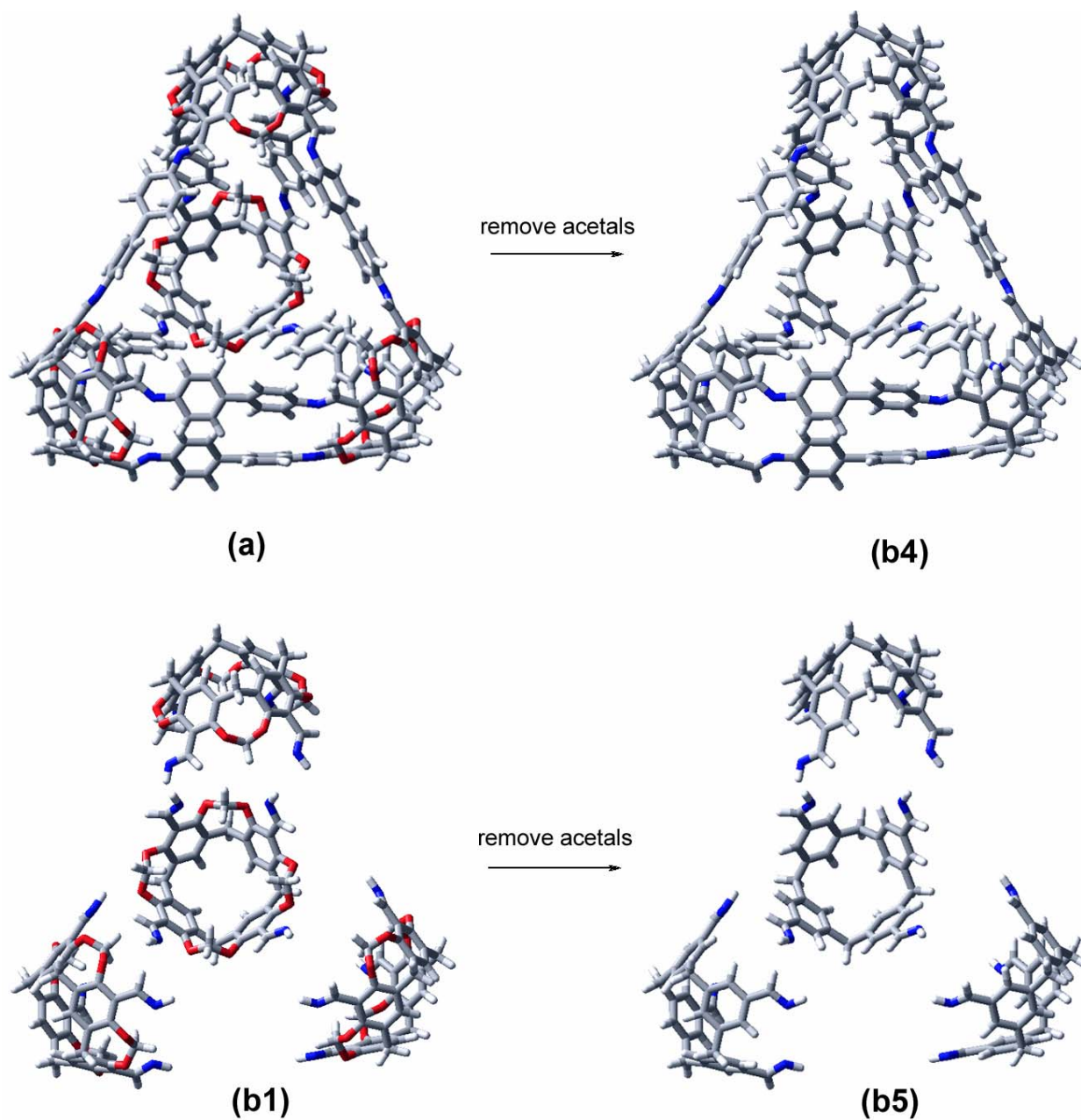
**Scheme 5.3** Calculation of the strain energy in the imine-cavitand part of tetramer  $C_8$ .



**Scheme 5.4** Calculation of the strain energy in the complete linkers of tetramer  $C_8$ .



**Scheme 5.5** Calculation of the strain energy in the imines of tetramer  $C_8$ .



**Scheme 5.6** Calculation of the acetal-linker interaction energy in tetramer  $C_8$ .

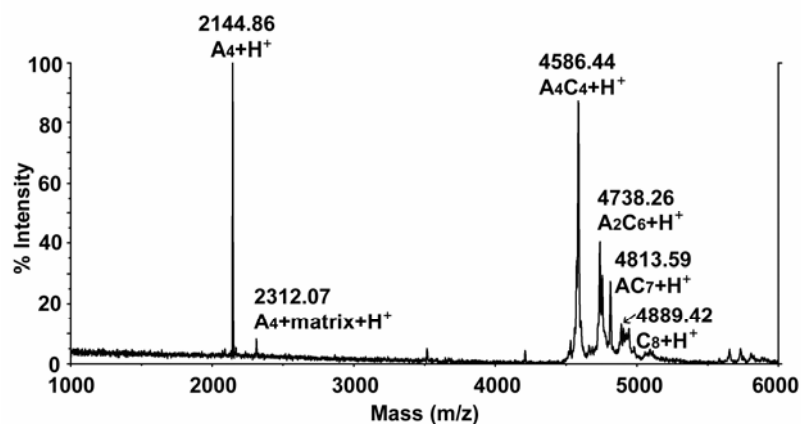
#### 5.2.4 DCL from *meta*-phenylenediamine (A) and benzidine (C)

The combination of *meta*-phenylenediamine and benzidine resulted in a complex mixture.

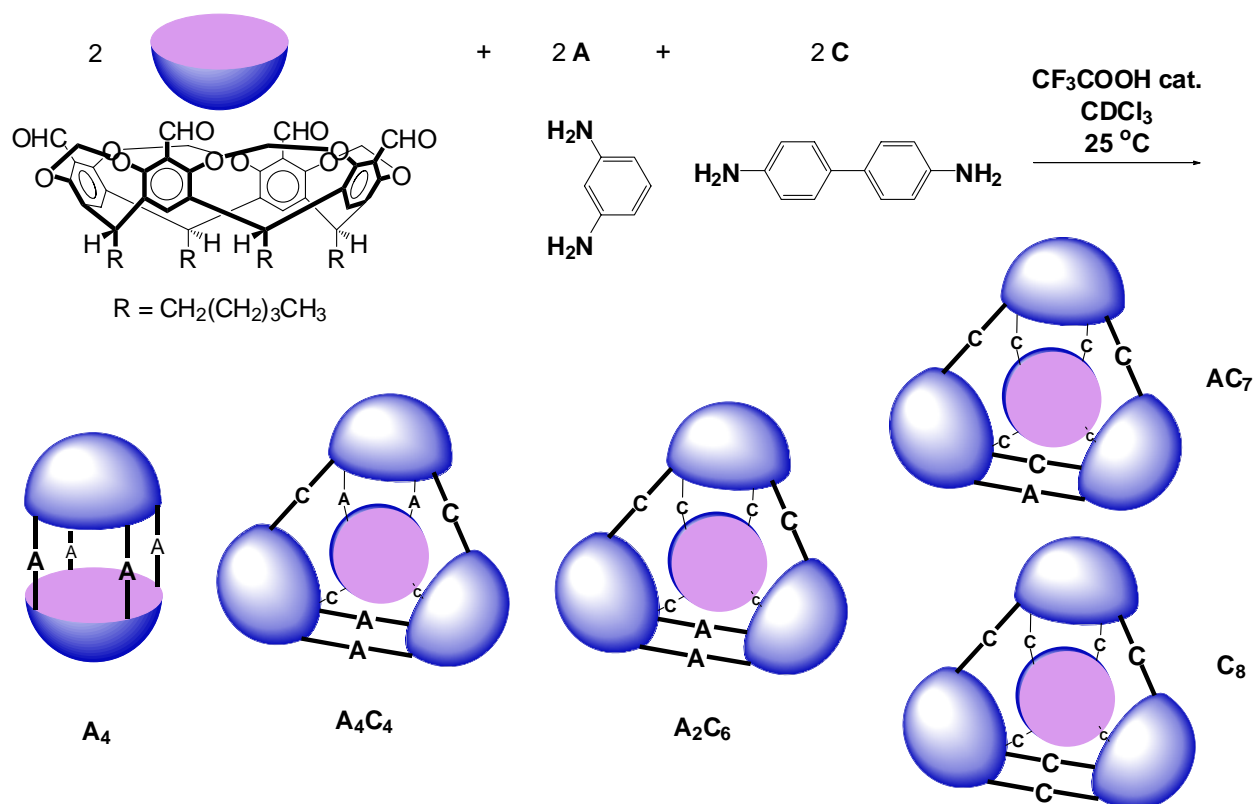
Tetraformyl cavitand (1 equiv.) was mixed with *meta*-phenylenediamine (1 equiv.) and



benzidine (1 equiv.) in the presence of cat. TFA in  $\text{CDCl}_3$ . The library reached equilibrium over five days. The MALDI-TOF mass spectrum of the equilibrated reaction mixture revealed a signal at  $m/z = 2144.86$  for octaiminohemicarcerand **A**<sub>4</sub> (Figure 5.5 and Scheme 5.7). The signals at  $m/z = 4586.44$ , 4738.26, 4813.59, and 4889.42 correspond to the tetrameric species **A**<sub>4</sub>**C**<sub>4</sub>, **A**<sub>2</sub>**C**<sub>6</sub>, **A****C**<sub>7</sub> and **C**<sub>8</sub>. However, the imine region in the  $^1\text{H}$  NMR spectrum ( $\delta = 8.8\text{--}8.4$  ppm) of the equilibrated reaction mixture gives only two major signals (Figure 5.2 f). One of the signals at  $\delta = 8.456$  ppm is assigned to the homodimer **A**<sub>4</sub> (Figure 5.2 a). The other signal at  $\delta = 8.627$  ppm is tentatively assigned to the 16 imine protons of **A**<sub>4</sub>**C**<sub>4</sub>, which must be a major component in the mixture based on the MALDI-TOF MS spectrum (Figure 5.5). Also, a very important observation is that only trace amounts of **C**<sub>8</sub>, if at all, formed. Most likely, the major library members are **A**<sub>4</sub> and **A**<sub>4</sub>**C**<sub>4</sub>. The other minor signals underneath the two major ones might arise from the other tetrameric species observed in the MALDI-TOF MS (Figure 5.5). GPC of the reaction mixture indicates the presence of small amounts of pentameric species, which were also observed in the MALDI-TOF MS spectrum.



**Figure 5.5** MALDI-TOF mass spectrum of DCL from **A** and **C**.



**Scheme 5.7** The product distribution of DCL from **A** and **C**.

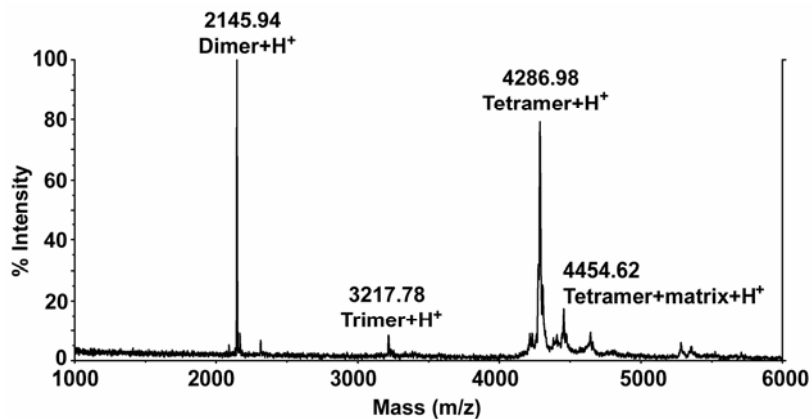
### 5.2.5 DCL from *meta*-phenylenediamine (**A**), *meta*-xylylenediamine (**B**) and benzidine (**C**)

The library containing all three building blocks gave even more complicated results. The condensation of tetraformyl cavitand (1 equiv.) with *meta*-phenylenediamine (**A**, 0.67 equiv.), *meta*-xylylenediamine (**B**, 0.67 equiv.) and benzidine (**C**, 0.67 equiv.) reached an equilibrium after five days. MALDI-TOF MS yielded weak signals for the tetrameric species due to the poorer ionization efficiency compared to the dimeric species present.

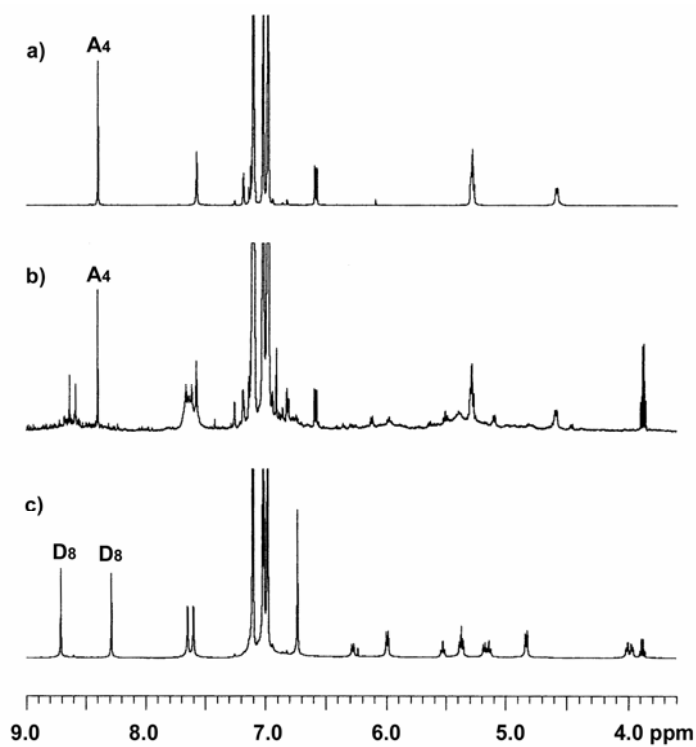
However, careful examination of the  $^1\text{H}$  NMR spectrum of the final reaction mixture shows that the dimeric capsules, observed in the binary library containing **A** and **B** (Figure 5.2 b), are major components (Figure 5.2 g). The intensities of the imine signals, assigned to these dimeric capsules, make up approximately 2/3 of the total integration in the imine region. Therefore, the other imine signals must be primarily from **C**<sub>8</sub> hosts with partial cleaved acetals, which would explain the complexity of these signals. Acetal cleavage has been observed during the formation of polyimino container molecules.<sup>[9]</sup>

### 5.2.6 DCL from *meta*-phenylenediamine (**A**) and *para*-phenylenediamine (**D**)

The library from *meta*-phenylenediamine (**A**) and *para*-phenylenediamine (**D**) was prepared in toluene-*d*<sub>8</sub> by mixing tetraformyl cavitand (1 equiv.) with *meta*-phenylenediamine (1 equiv.) and *para*-phenylenediamine (1 equiv.) in the presence of cat.TFA. The system quickly equilibrated within one day. In the MALDI-TOF mass spectrum of the reaction mixture, signals for dimeric, trimeric and tetrameric species are observed at  $m/z$  = 2145.94, 3217.78 and 4286.98 (Figure 5.6). However, they couldn't be deconvoluted into homologous or heterogeneous cages, since the two diamines are structural isomers. In the imine region of the  $^1\text{H}$  NMR spectrum of the final reaction mixture ( $\delta$  = 9.0-8.0 ppm), a clear singlet is observed for the homodimer **A**<sub>4</sub> at  $\delta$  = 8.398 ppm (Figure 5.7 a and b). The other two singlets at  $\delta$  = 8.632 and 8.583 ppm do not belong to the homotetramer **D**<sub>8</sub> (Figure 5.7 b and c). Further assignments are difficult due to the large number of signals. The large number of signals may again be a result of partial acetal cleavage in the heteromeric capsules.<sup>[9]</sup> GPC of the reaction mixture indicates the presence of dimeric, tetrameric and pentameric species.



**Figure 5.6** MALDI-TOF mass spectrum of DCL from **A** and **D**.



**Figure 5.7** Partial <sup>1</sup>H NMR spectra (500 MHz, toluene-*d*<sub>8</sub>, 25 °C) of a) **A**<sub>4</sub>, c) **D**<sub>8</sub>, and b) the DCL from tetraformyl cavitand **40** and linker **A** and **D**.

### 5.3 Conclusions

Dynamic combinatorial libraries of polyimino nanocapsules have been prepared through the condensation of tetraformyl cavitand **40** with relatively rigid diamino linkers under thermodynamical control. The libraries were analyzed by MALDI-TOF MS,  $^1\text{H}$  NMR and GPC. Species other than the homodimers/homotetramers were also observed and several proton signals were successfully assigned to heterotetramers of the form  $\text{B}_4\text{C}_4$  and  $\text{B}_2\text{C}_6$ . This opens a new way to generate non-symmetrical covalent bonded nanocages, which might be difficult to accomplish with traditional kinetic covalent synthesis. A main problem observed during equilibration is acetal cleavage in tetrameric cages. This made NMR assignment of structures difficult. A possible solution may be the reaction of the equilibrated mixtures with  $\text{BrCH}_2\text{Cl}/\text{Cs}_2\text{CO}_3$  to reintroduce the acetal groups.

### 5.4 Experimental section

#### 5.4.1 General procedure

All reactions were conducted under argon. Reagents and chromatography solvents were purchased from Aldrich and used without further purification except that  $\text{CDCl}_3$  was passed through  $\text{K}_2\text{CO}_3$  prior to use.  $^1\text{H}$  NMR spectra recorded in  $\text{CDCl}_3$  and toluene- $d_8$  were referenced to residual  $\text{CHCl}_3$  and  $\text{CHD}_2\text{C}_6\text{D}_5$  at 7.26 ppm and 2.09 ppm, respectively. Mass spectra were recorded on an Applied Biosystems Voyager DE-Pro mass spectrometer (MALDI-TOF). 2',4',6'-Trihydroxylacetophenone (THAP) was used as the matrix. Gel permeation chromatography (GPC) was performed on a Varian *prostar* 210 HPLC system equipped with dual wavelength UV/Vis detector (280 nm), Eppendorf CH-30 column heater and two Jordi GPC columns (cross linked DVB;  $10^3$  Å pore size;

MW cutoff  $\sim$  25,000; 7.8 mm  $\times$  30 cm) with  $\text{CH}_2\text{Cl}_2$ /1%  $\text{NEt}_3$  as mobile phase at a flow of 1 mL/min. Approximate molecular weights of analytes were determined from a semi logarithmic calibration plot ( $\text{Ln}(\text{MW})$  against retention time) using the following molecular weight standards: benzene (MW 78); cavitand **40** (MW 928); a NMP hemicarceplex (MW 2348),<sup>[10]</sup> and polyaminonanocapsules **47a-c** (MW 3941, 5912 and 7882).<sup>[6b,c]</sup>

#### 5.4.2 Preparation of DCLs

**DCL of A and B.** Solutions of *meta*-phenylenediamine ( $2.40 \times 10^{-5}$  mmol/ $\mu\text{l}$  in  $\text{CDCl}_3$ , 91.1  $\mu\text{l}$ ), *meta*-xylylenediamine ( $2.36 \times 10^{-5}$  mmol/ $\mu\text{l}$  in  $\text{CDCl}_3$ , 92.9  $\mu\text{l}$ ) and 1 v% TFA/ $\text{CDCl}_3$  (1  $\mu\text{l}$ ), were added into a solution of tetraformyl cavitand **40** (2.03 mg,  $2.19 \times 10^{-3}$  mmol) in  $\text{CDCl}_3$  (466  $\mu\text{l}$ ). Then, one bead of 4 Å molecular sieves was added. The solution was transferred into an NMR tube and left at room temperature without stirring.

**DCL of B and C.** Solutions of *meta*-xylylenediamine ( $2.36 \times 10^{-5}$  mmol/ $\mu\text{l}$  in  $\text{CDCl}_3$ , 87.4  $\mu\text{l}$ ), benzidine ( $2.11 \times 10^{-5}$  mmol/ $\mu\text{l}$  in  $\text{CDCl}_3$ , 97.5  $\mu\text{l}$ ) and 1 v% TFA/ $\text{CDCl}_3$  (1  $\mu\text{l}$ ), were added into a solution of tetraformyl cavitand **40** (1.91 mg,  $2.06 \times 10^{-3}$  mmol) in  $\text{CDCl}_3$  (465  $\mu\text{l}$ ). Then, one bead of 4 Å molecular sieves was added. The solution was transferred into an NMR tube and left at room temperature without stirring.

**DCL of A and C.** Solutions of *meta*-phenylenediamine ( $2.40 \times 10^{-5}$  mmol/ $\mu\text{l}$  in  $\text{CDCl}_3$ , 100.6  $\mu\text{l}$ ), benzidine ( $2.11 \times 10^{-5}$  mmol/ $\mu\text{l}$  in  $\text{CDCl}_3$ , 114.5  $\mu\text{l}$ ) and 1 v% TFA/ $\text{CDCl}_3$  (1  $\mu\text{l}$ ), were added into a solution of tetraformyl cavitand **40** (2.24 mg,  $2.41 \times 10^{-3}$  mmol) in

$\text{CDCl}_3$  (435  $\mu\text{l}$ ). Then, one bead of 4 Å molecular sieves was added. The solution was transferred into an NMR tube and left at room temperature without stirring.

**DCL of A, B and C.** Solutions of *meta*-phenylenediamine ( $2.40 \times 10^{-5}$  mmol/ $\mu\text{l}$  in  $\text{CDCl}_3$ , 91.7  $\mu\text{l}$ ), *meta*-xylylenediamine ( $2.36 \times 10^{-5}$  mmol/ $\mu\text{l}$  in  $\text{CDCl}_3$ , 93.4  $\mu\text{l}$ ), benzidine ( $2.11 \times 10^{-5}$  mmol/ $\mu\text{l}$  in  $\text{CDCl}_3$ , 104.3  $\mu\text{l}$ ) and 1 v% TFA/ $\text{CDCl}_3$  (1  $\mu\text{l}$ ), were added into a solution of tetraformyl cavitand **40** (3.06 mg,  $3.30 \times 10^{-3}$  mmol) in  $\text{CDCl}_3$  (361  $\mu\text{l}$ ). Then, one bead of 4 Å molecular sieves was added. The solution was transferred into an NMR tube and left at room temperature without stirring.

**DCL of A and D.** Solutions of *meta*-phenylenediamine ( $4.33 \times 10^{-5}$  mmol/ $\mu\text{l}$  in toluene- $d_8$ , 48.3  $\mu\text{l}$ ), *para*-phenylenediamine ( $4.65 \times 10^{-5}$  mmol/ $\mu\text{l}$  in toluene- $d_8$ , 45.0  $\mu\text{l}$ ) and 1 v% TFA/ toluene- $d_8$  (0.6  $\mu\text{l}$ ), were added into a solution of tetraformyl cavitand **40** (1.94 mg,  $2.09 \times 10^{-3}$  mmol) in toluene- $d_8$  (557  $\mu\text{l}$ ). Then, one bead of 4 Å molecular sieves was added. The solution was transferred into an NMR tube and left at room temperature without stirring.

### 5.4.3 Molecular mechanics calculations and molecular dynamics simulations

Molecular mechanics calculations were carried out using MAESTRO<sup>[11a]</sup>: MM3\* force field,<sup>[11b]</sup> GB/SA chloroform solvation model,<sup>[11c]</sup> 5000 maximal iterations. Molecular dynamics simulations were carried out using MAESTRO: MM3\* force field, gas phase, shake all bonds mode, simulation temperature 500 K, timestep 1.5 fs, equilibration time 50 ps, simulation time 2000 ps.<sup>[11d]</sup>

## 5.5 References

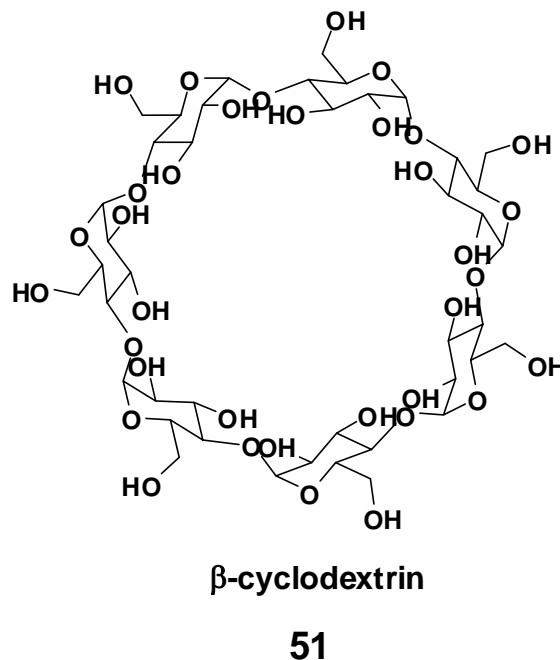
1. P. T. Corbett, J. Leclaire, L. Vial, K. R. West, J-L Wietor, J. K. M. Sanders, S. Otto, *Chem. Rev.* **2006**, *106*, 3652.
2. a) F. Hof, C. Nuckolls, J. Rebek, Jr., *J. Am. Chem. Soc.*, **2000**, *122*, 4251; b) S. Xu, N. Giuseppone, *J. Am. Chem. Soc.* **2008**, *130*, 1826.
3. a) D. Ajami, M. P. Schramm, A. Volonterio, J. Rebek, Jr., *Angew. Chem. Int. Ed.* **2007**, *46*, 2007, 46, 242; b) N. Giuseppone, J.-L. Schmitt, J.-M. Lehn, *Angew. Chem. Int. Ed.* **2004**, *43*, 4902.
4. K. R. West, K. D. Bake, S. Otto, *Org. Lett.* **2005**, *7*, 2615.
5. X. Liu, Y. Liu, R. Warmuth. *Supramol. Chem.* **2008**, *20*, 41.
6. a) S. Ro, S. J. Rowan, A. R. Pease, D. J. Cram, J. F. Stoddart, *Org. Lett.* **2000**, *2*, 2411; b) X. Liu, Y. Liu, G. Li, R. Warmuth, *Angew. Chem. Int. Ed.* **2006**, *45*, 901; c) X. Liu, R. Warmuth, *J. Am. Chem. Soc.* **2006**, *128*, 14120.
7. a) D. J. Cram, S. Karbach, H.-E. Kim, C. B. Knobler, E. F. Maverick, J. L. Ericson, R. C. Helgeson, *J. Am. Chem. Soc.*, **1988**, *110*, 2229; b) H. Jude, D. J. Sinclair, N. Das, M. S. Sherburn, P. J. Stang, *J. Org. Chem.* **2006**, *71*, 4155.
8. J. Yoon, C. Sheu, K. N. Houk, C. B. Knobler, D. J. Cram, *J. Org. Chem.* **1986**, *61*, 9323.
9. Y. Liu, X. Liu, R. Warmuth, *Chem. Eur. J.*, **2007**, *13*, 8953.
10. R. Warmuth, E. F. Maverick, C. B. Knobler, D. J. Cram, *J. Org. Chem.* **2003**, *68*, 2077.
11. a) MAESTRO, version 5.1.020, Schrodinger, LLC, copyright 1999-2002; Columbia University, copyright 1996-98; b) N. L. Allinger, Y. H. Yuh, J.-H. Lii, *J. Am. Chem. Soc.*, **1989**, *111*, 8551; c) W. C. Still, A. Tempczyk, R. C. Hawley, T. Hendrickson, *J. Am. Chem. Soc.*, **1990**, *112*, 6127; d) F. Guarnieri, W. C. Still, *J. Comput. Chem.* **1994**, *15*, 1302.



## Chapter 6 Synthesis of water-soluble nanocapsules

### 6.1 Introduction

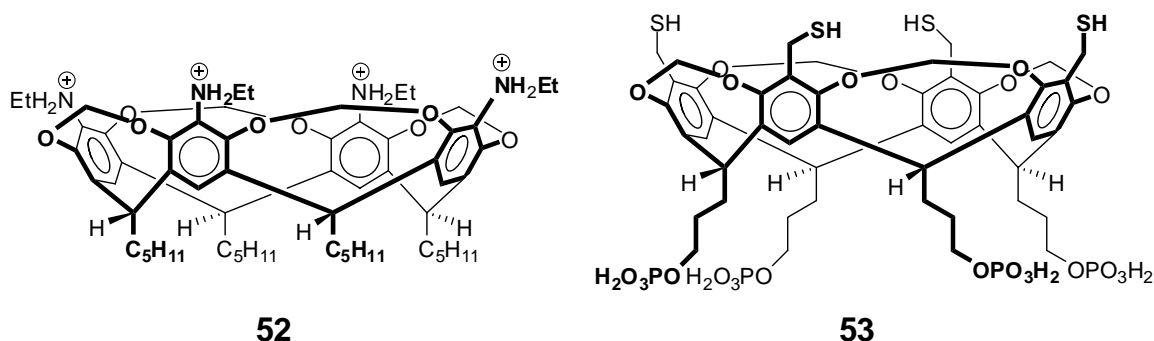
Many biological processes take place in aqueous solution. Water solubility is desirable, if the nanocapsules are to be used in biochemical and biomedical applications.<sup>[1]</sup> Perhaps, the simplest water soluble receptors are cyclodextrins (Figure 6.1).<sup>[2]</sup> Cyclodextrins, which are seminatural products from starch, are produced in thousands of tons every year and are broadly used in the food, cosmetic and pharmaceutical industry.<sup>[3]</sup>



**Figure 6.1** Water-soluble macrocyclic host:  $\beta$ -cyclodextrin.

Numerous studies have focused on the synthesis of water soluble cavitands and their binding properties.<sup>[4]</sup> The upper rim of cavitands can be functionalized with hydrophilic groups or charged moieties, such as hydroxyl, quaternary ammonium and carboxylic acid (Figure 6.2). The feet of cavitands can also be functionalized in the same way, even

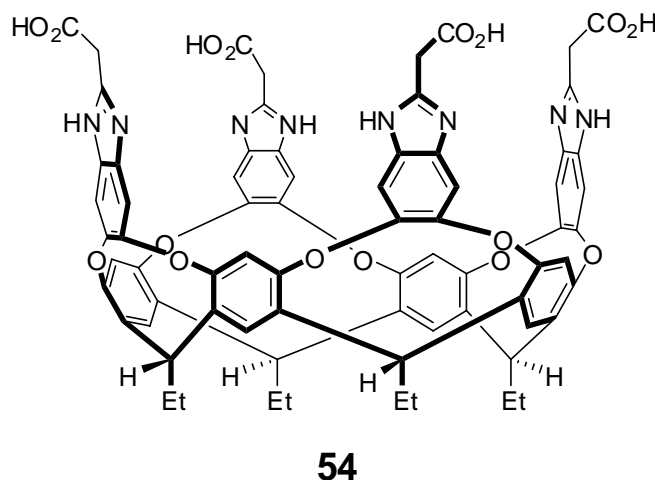
though it is synthetically more challenging.<sup>[4b]</sup> These cavitands usually demonstrate relatively weak binding abilities ( $K = 10\text{--}10^3\text{ M}^{-1}$ ) due to the shallow cavity.<sup>[5]</sup>



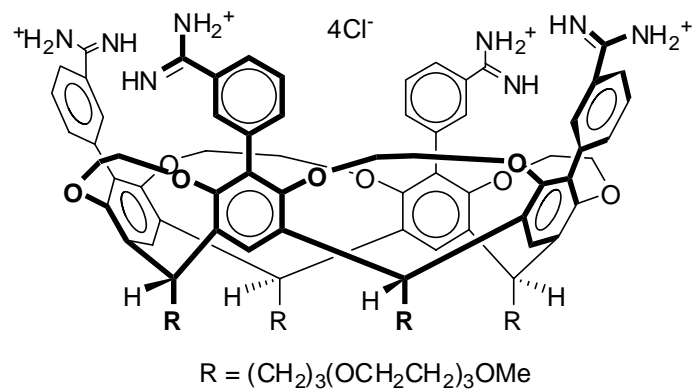
**Figure 6.2** Water-soluble cavitands bearing quaternary ammonium moieties at the upper rim or phosphoric acid in the feet.

Deep water-soluble cavitands have been designed by Rebek, Diederich and Gibb (Figure 6.3-5).<sup>[6]</sup> Aromatic belts are extended above the shallow cavitand through covalent synthesis. Additional water-solubilizing groups are then attached to the elongated hemisphere. The strongly enlarged preorganized aromatic pocket greatly increases the hydrophobicity of the cavity. Furthermore, in Diederich's deep cavitand **55** the aromatic rings can change their orientation and fold around guest molecules. Additional interactions including ion pairing and hydrogen bonding are possible when this host binds charged guests. In general, the binding ability of the deep water-soluble cavitands is much higher than that of the shallow cavitands, and guest exchange is usually slow on the NMR time scale. For example, Rebek's deep water-soluble cavitand **54** has binding affinity  $K > 10^3\text{ M}^{-1}$  with tetraalkylammonium salts in water (Figure 6.3).<sup>[6a]</sup> It also works as an effective phase-transfer catalyst.<sup>[6b]</sup> Diederich's bowl-shaped receptor **55** forms stable 1:1 complexes with nucleotides in tris/HCl-buffered water with association

constants ranging from  $10^3$  -  $10^6$   $M^{-1}$  (Figure 6.4).<sup>[6c]</sup> The binding affinity of this host increases with increasing guest charge, as has earlier been observed in the binding of nucleotides by polyammonium macrocycles.<sup>[7]</sup> Gibb's deep-cavity cavitand **56** forms a capsular 2:1 complex around steroids with stability constants higher than  $10^8$   $M^{-1}$  in water (Figure 6.5).<sup>[6d]</sup> In water, even hydrocarbon gases can act as templates to promote the dimeric capsule formation. The observed affinity difference allowed separation of these gases.<sup>[6e]</sup> Capsule formation in water based on non-covalent interactions has also been reported by Reinhoudt and coworkers (Figure 6.6).<sup>[8]</sup> Through ionic interactions, two calix[4]arene moieties **57** and **58** assemble into a molecular capsule **59**, which encapsulates small molecules in water.

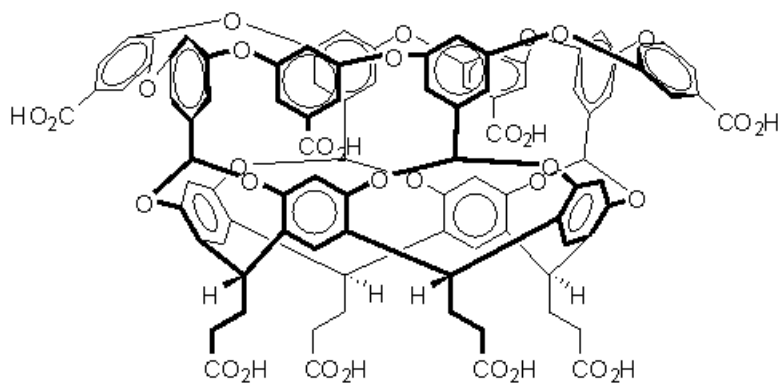


**Figure 6.3** Rebek's water-soluble tetracarboxyl deep cavitand **54**.

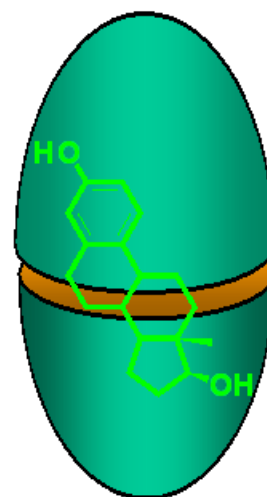


**55**

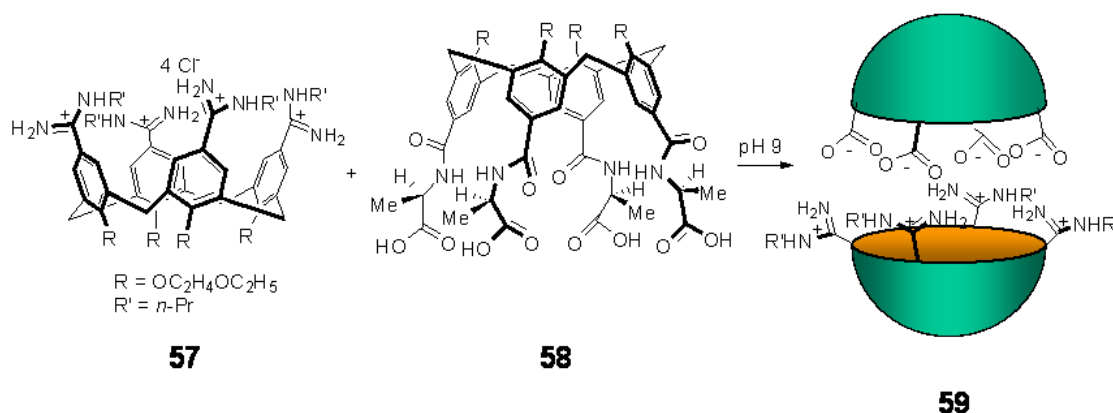
**Figure 6.4** Diederich's water-soluble PEG-footed deep cavitanth **55**.



**56**

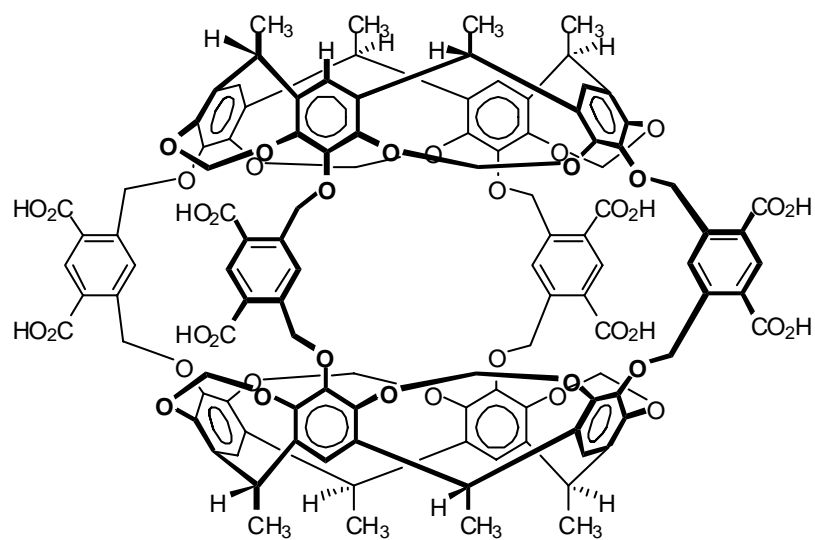
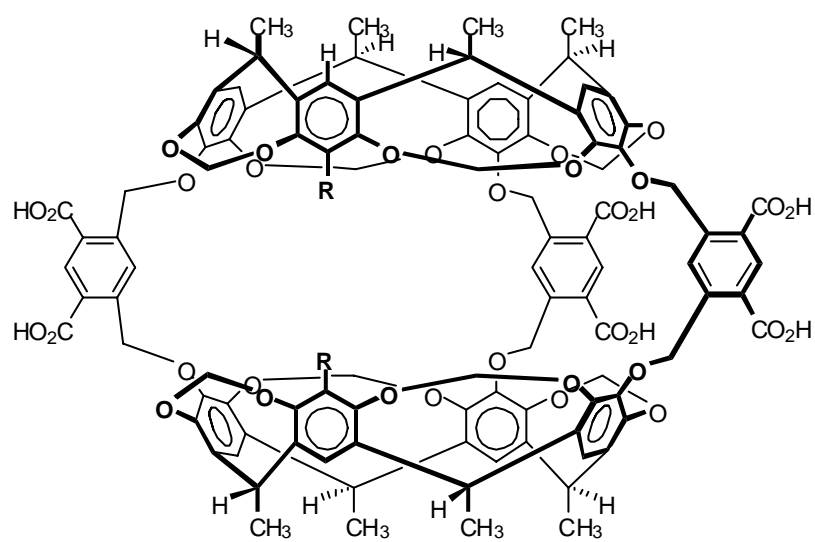


**Figure 6.5** Gibb's water-soluble deep cavitanth **56** bearing eight carboxylic acid groups and its 2:1 capsular complex.



**Figure 6.6** Molecular capsule **59** from two calix[4]arene moieties **57** and **58** through ionic interactions.

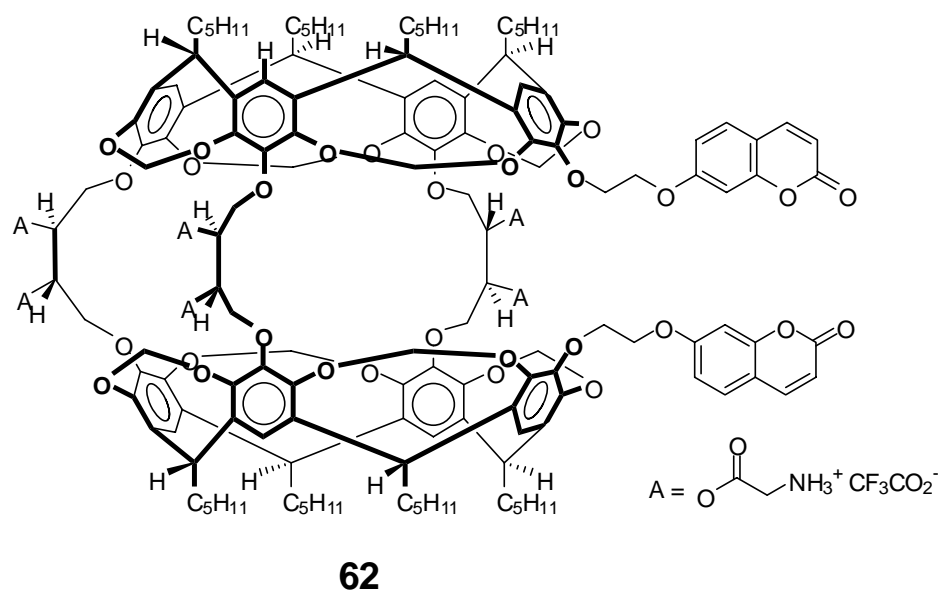
The first water-soluble hemicarcerand **60** was reported by Cram in 1997 (Figure 6.7).<sup>[9a]</sup> **60** has methyl groups as feet and two carboxylic acid groups in each linker. At pH = 9 in aqueous solution, **60** binds 14 different neutral molecules, ranging from non-polar naphthalene to moderately polar ethyl acetate, to form 1:1 complexes. Clearly the binding is due to the hydrophobic effect. That is, it is driven by desolvation of the guest and the inner phase of the host. However, the binding of quaternary ammonium salts is not observed, which suggests that the desolvation energy of the free guest is too high. Further studies by microcalorimetry with a tris-bridged analogue **61** of **60** revealed that the binding constants range between  $10^3$  and  $10^7 \text{ M}^{-1}$  for thirteen guests.<sup>[9b]</sup> Binding affinity depends on guest hydrophobicity and shape. Chirality has also been incorporated into a water-soluble hemicarcerand-like host **62** developed by Warmuth and Singh (Figure 6.8).<sup>[9c]</sup> Diastereomeric excess in complexation with racemic guests was observed in water.

**60**

R = OH or H

**61**

**Figure 6.7** The first water-soluble hemicarcerand **60** and its tris-bridged analogue **61**.



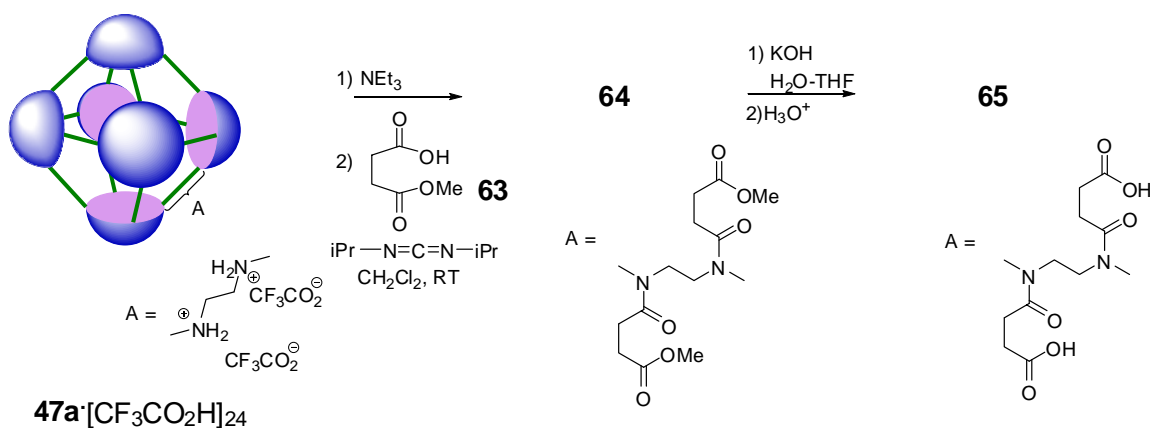
**Figure 6.8** Water-soluble hemicarcerand-like chiral host **62**.

We have reported that polyimino nanocapsules can be synthesized in a one-port procedure with high efficiency.<sup>[10]</sup> The imine bonds can be reduced and the subsequent polyamino nanocapsules can be purified and characterized. Here, we will show that the amino groups of the octahedral nanocapsule can be functionalized with carboxylic acid groups to increase its water solubility. Also, octahedral nanocapsules with polar hydroxyl feet will be described and binding of anionic organic compounds in aqueous solution demonstrated. Finally, the synthesis of a rhombicuboctahedral nanocapsule with polar hydroxyl feet will be detailed.

## 6.2 Results and discussion

### 6.2.1 Attachment of carboxylic acid groups to the linkers of the octahedral nanocapsule with pentyl feet

The amino groups in the linkers of **47a** were functionalized by attaching carboxylic acid groups via a tether (Scheme 6.1). Firstly, the hexamer trifluoroacetate salt **47a**·24TFA was deprotonated with triethylamine and then acylated with monomethyl succinate **63** in the presence of N,N'-diisopropylcarbodiimide (DIC).<sup>[11]</sup> Twenty-four methyl succinic ester groups were successfully attached to **47a**, which was supported by MALDI-TOF MS of the final reaction mixture. Saponification of the methyl esters of **64** with KOH produced **65**, which has free acids. However, solubility tests showed that **65** was not soluble in basic aqueous solution. Therefore, tethers with two carboxylic acids were attached to **47a**.

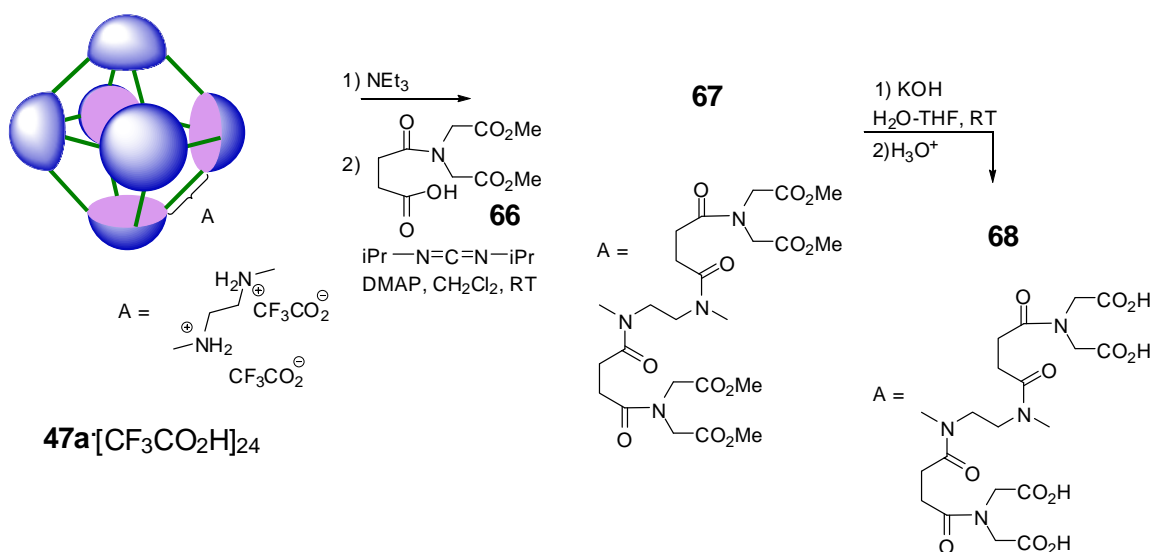


**Scheme 6.1** Attachment of twenty-four carboxylic acid groups to the linkers of the octahedral nanocapsule with pentyl feet.

Derivatization of **47a** with succinic acid derivative **66** gave **67**, in which the number of



methyl ester groups is doubled (Scheme 6.2).<sup>[12]</sup> This means that saponification may provide a capsule with forty-eight carboxylic acid groups. After hydrolysis with base, **68** showed a water solubility of 4~5 mg/ml at pH 9. The complexation of organic compounds, such as  $\text{Me}_4\text{N}^+\text{Br}^-$ , toluene, and naphthalene was studied in water. Unfortunately, no binding was observed with these molecules. Hexamer **68** probably forms aggregates in water. This was supported by strong line broadening in the  $^1\text{H}$  NMR spectrum of basic aqueous solutions of **68**. An infinite network may have formed, in which the nonpolar pentyl feet are intercalated and the polar carboxylic acid groups interact with each other. Reinhoudt et al. have reported that the aggregation behavior of water-soluble cavitands depends on the alkyl chain length of the feet.<sup>[13]</sup> They observed that a water-soluble methyl-footed cavitand did not aggregate in water, whereas the pentyl- and undecyl-footed analogues did.



**Scheme 6.2** Attachment of forty-eight carboxylic acid groups to the linkers of the pentyl-footed octahedral nanocapsule **47a**.

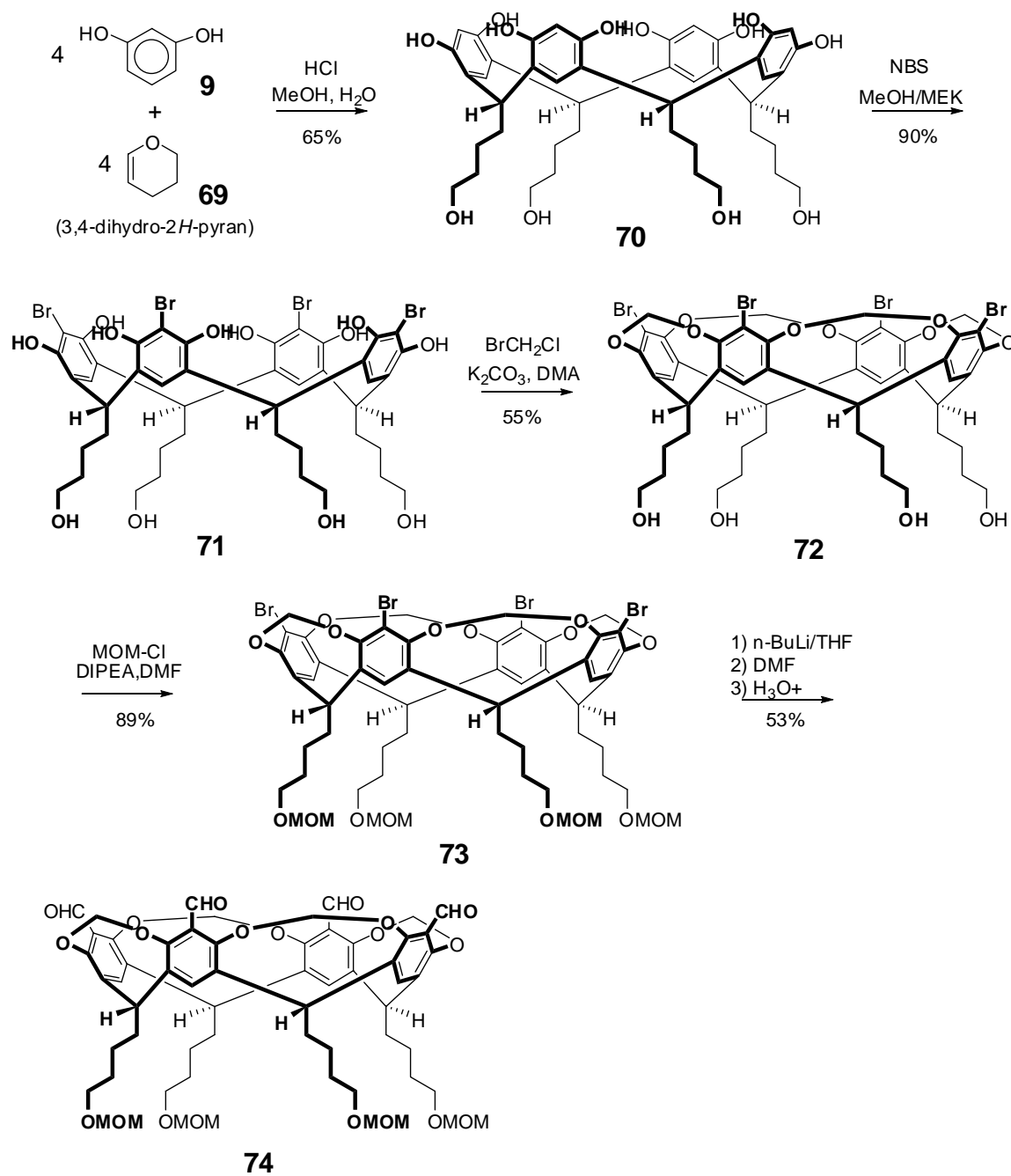
### 6.2.2 Synthesis of a water soluble octahedral nanocapsule with butanol feet groups

The pentyl group in the feet of cavitand **13** is non-polar and very hydrophobic. Introducing hydroxyl groups into the feet significantly increases the polarity of cavitand **72**. The butanol-footed tetrabromocavitand **72** was synthesized in three steps according to a reported procedure (Scheme 6.3).<sup>[4a]</sup> The hydroxyl groups were protected as methoxy methyl (MOM) ether to give **73** in 89% yield.<sup>[14]</sup> Formylation, based on the procedure used for pentyl-footed cavitand **40**, gave the desired tetraformylcavitand **74** in 53% yield after column chromatography.<sup>[15]</sup> A small amount of Et<sub>3</sub>N was added into the mobile phase during flash column chromatography to prevent MOM group cleavage. Tetraformyl cavitands with different protecting groups, such as *tert*-butyldimethylsilyl (TBS) and *tert*-butyldiphenylsilyl (TBDPS) were also synthesized.<sup>[14]</sup> However, the condensation reactions between the latter cavitand and ethylenediamine **43** yielded only ~38% polyimino hexamer, which is considerably less than the result reported before with pentyl feet (~80%) (Table 6.1).<sup>[10a]</sup> This is probably due to steric effects by the bulky protecting groups (TBDPS) during the nanocapsule growth.

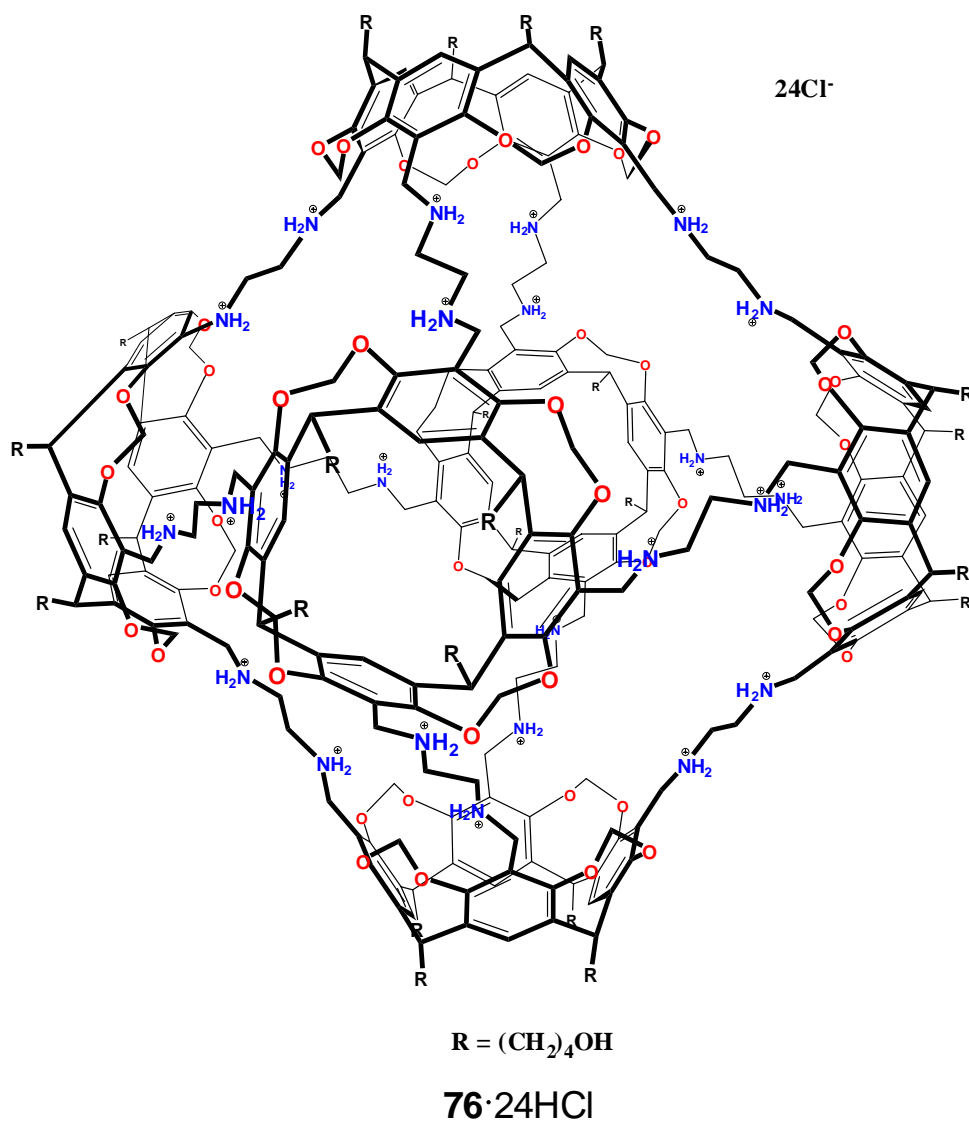
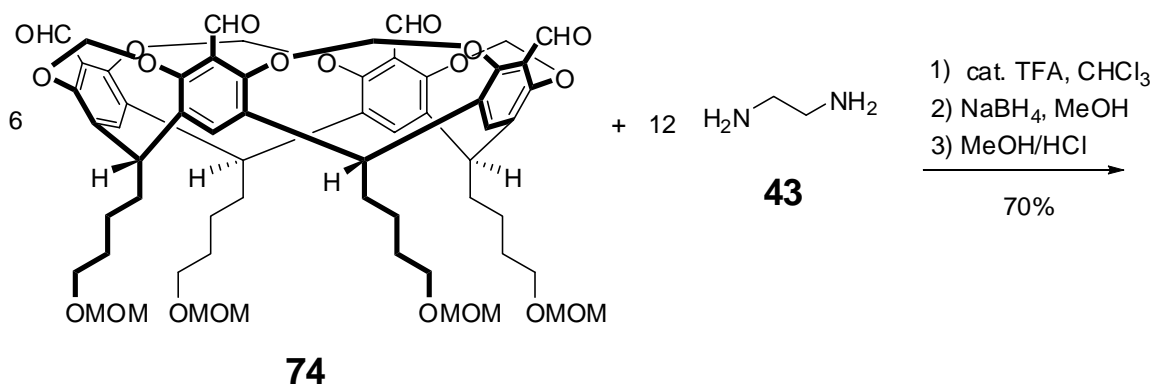
**Table 6.1** Yields of polyimino hexamer in the TFA-catalyzed condensation of ethylenediamine **43** and cavitands with different feet.

cavitand (feet)	<b>40</b> (-C <sub>5</sub> H <sub>11</sub> )	<b>74</b> (-C <sub>4</sub> H <sub>9</sub> OMOM)	<b>75</b> (-C <sub>4</sub> H <sub>9</sub> OTBDPS)
% yield	80	75	38

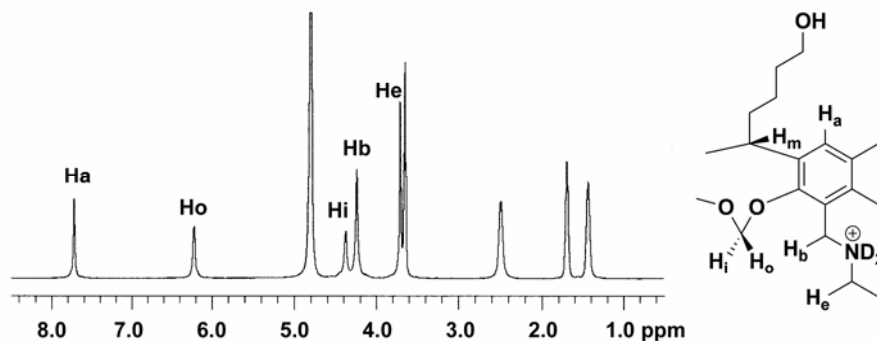
However, good hexamer yields were obtained in the condensation between MOM-protected tetraformyl cavitand **74** and ethylenediamine **43** in chloroform in the presence of catalytic amounts of TFA (Table 6.1 and Scheme 6.4). After the equilibrium was reached, the mixture was reduced with NaBH<sub>4</sub>. Boramines were hydrolyzed with concentrated HCl in methanol (10 v%). MOM groups were also removed in this step.<sup>[14]</sup> The product gradually crystallized out as its HCl salt. Simple filtration separated the product from side-products and gave 70% yield of **76**·24HCl based on the starting tetraformyl cavitand **74**. This **76**·24HCl salt has a solubility of 10-15 mg/ml in water at pH ~4.5. The <sup>1</sup>H NMR spectrum of **76**·24HCl in D<sub>2</sub>O shows higher than 95% purity (Figure 6.9).



**Scheme 6.3** Synthesis of MOM-protected butanol-footed tetraformyl cavitand **74**.



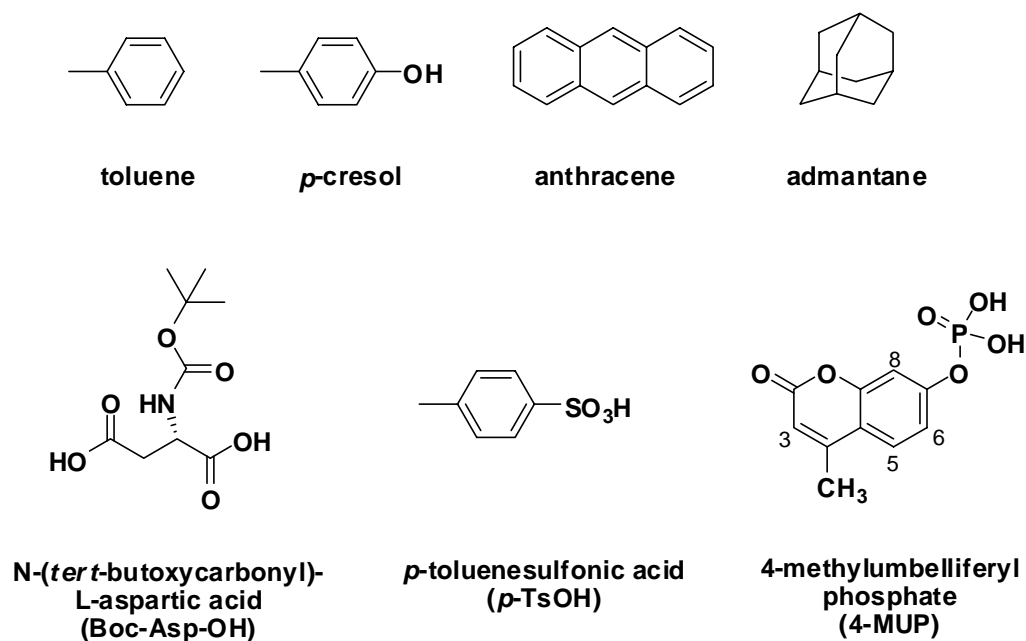
**Scheme 6.4** Condensation of tetraformyl cavitand **74** and ethylenediamine **43** followed by reduction leading to water-soluble octahedral nanocapsule **76·24HCl**.



**Figure 6.9**  $^1\text{H}$  NMR spectrum (0.2 wt% DCl/D<sub>2</sub>O, 25 °C, 500 MHz) of **76**·24HCl.

### 6.2.3 Complexation studies

$^1\text{H}$  NMR spectroscopy was used to study the host-guest binding interactions between **76**·24HCl and organic molecules in water. No complexation was observed with neutral organic guest molecules (Figure 6.10), such as toluene, *p*-cresol, anthracene or adamantane, even after sonication and heating at 60 °C.



**Figure 6.10** Neutral and negatively charged organic guest molecules.

Complexation was observed with negatively charged organic molecules (Figure 6.10). The binding of *N*-(*tert*-butoxycarbonyl)-L-aspartic acid (Boc-Asp-OH) was studied in the presence of acetic acid buffer at pD 4.7. In the  $^1\text{H}$  NMR spectrum of the complex, only one set of signals for Boc-Asp-OH was observed. Compared to free Boc-Asp-OH, the methylene protons and the methyl protons are both upfield shifted (Table 6.2 and 6.3). These upfield shifts indicate that the guest is inside the cavity, where it experiences the shielding effect of the aromatic subunits of **76**. The presence of only one set of guest signals suggests that the guest in/out exchange is fast on the NMR time scale at ambient temperature, leading to averaged signals.

Determination of complexation constants requires knowledge about the amount of free and complexed guest/host. This can be calculated from the average guest chemical shift  $\delta_{\text{guest}}$ , the shift of the free guest  $\delta_{\text{free}}$ , and that of the bound guest  $\delta_{\text{complexed}}$  by assuming that each bound guest experiences the same upfield shift. In the above complexation studies with **76**·24HCl, 1:6 host/guest complex stoichiometry is assumed: (1) In CPK models up to six guests fit into the cavity of **76**; (2) Single cavitand hosts accommodate one guest molecule in organic or aqueous solution. For example, cavitands modified with quaternary ammonium groups at the upper rim form 1:1 complexes with anionic aromatic guests with binding constants  $K = 10^2 - 10^4 \text{ M}^{-1}$ .<sup>[18]</sup> The formation of 1:1 complexes with *p*-cresol or *p*-toluene sulfonate has also been observed for cavitands with pyridinium moieties ( $K = 10^2 \text{ M}^{-1}$ ).<sup>[13]</sup>

From the above NMR titrations, the chemical shifts of bound Boc-Asp-OH  $\delta_{\text{complexed}}$ ,

which is needed to determine the amount of complexed guest, could not be obtained.

**Table 6.2** Chemical shifts and diffusion rates ( $D$ ,  $\times 10^{-6}$  cm<sup>2</sup>/s) for the free guests and free **76**·24HCl in D<sub>2</sub>O at 25 °C.

compd.	Boc-Asp-OH <sup>i</sup>	<i>p</i> -TsOH <sup>ii</sup>	4-MUP	<b>76</b>
$\delta(\text{CH}_3, \text{ppm})$	1.448	2.39	2.53 <sup>iii</sup>	
$D$ ( $10^{-6}$ cm <sup>2</sup> /s)	5.15	7.42	5.10 <sup>ii</sup>	1.36

<sup>i</sup> pD 4.7; <sup>ii</sup> pD 1.0; <sup>iii</sup> pD 4.5, sodium salt.

**Table 6.3** Upfield shifts of the *tert*-butyl protons and the guest diffusion rates ( $D$ ,  $\times 10^{-6}$  cm<sup>2</sup>/s) for the encapsulation of Boc-Asp-OH in **76**·24HCl in D<sub>2</sub>O at 25 °C (pD 4.7, [**76**] = 0.21 mM)

[G]/equiv.	0.60	1.81	3.62	5.42	7.23	12.1	18.1	24.1	42.2	60.3
$\Delta\delta/\text{ppm}$	0.228	0.189	0.155	0.134	0.120	0.082	0.069	0.058	0.040	0.029
$D$		3.37	3.78	3.87	3.91	4.09	4.15			
$\delta_{\text{complexed}}$		1.046	1.019	1.051	1.080	1.154	1.187			

Diffusion NMR studies (DOSY) provide an alternative method to determine the amount of complexed and free guest, if guest exchange is fast on the NMR time scale.<sup>[24]</sup> In a host-guest binding equilibrium, the measured diffusion constant of the guest  $D_{\text{guest}}$  is a weighted average of the diffusivity of the free ( $D_{\text{free guest}}$ ) and complexed guest ( $D_{\text{complexed guest}}$ ).

$$D_{\text{guest}} = X_{\text{complexed}} \times D_{\text{complexed guest}} + (1 - X_{\text{complexed}}) \times D_{\text{free guest}}, \quad (6.1)$$



In equation 6.1,  $X_{\text{complexed}}$  is the mol fraction of the complexed guest.  $D_{\text{free guest}}$  and  $D_{\text{free host}}$  can be determined independently. If the guest is much smaller than the host, it is valid to assume that  $D_{\text{complexed guest}}$  is equal to  $D_{\text{host}}$  and that  $D_{\text{host}}$  remains constant during the titration.<sup>[24]</sup>

$$D_{\text{guest}} = X_{\text{complexed}} \times D_{\text{free host}} + (1 - X_{\text{complexed}}) \times D_{\text{free guest}}, \quad (6.2)$$

From  $X_{\text{complexed}}$ ,  $\delta_{\text{free}}$  (Table 6.2) and  $\delta_{\text{guest}}$  ( $\delta_{\text{guest}} = \delta_{\text{free}} + \Delta\delta$ , Table 6.3),  $\delta_{\text{complexed}}$  can be calculated:

$$\delta_{\text{guest}} = X_{\text{complexed}} \times \delta_{\text{complexed}} + (1 - X_{\text{complexed}}) \times \delta_{\text{free}}, \quad (6.3)$$

For Boc-Asp-OH, the averaged  $\delta_{\text{complexed}}$  is  $1.090 \pm 0.066$  ppm (Table 6.3).

From  $\delta_{\text{complexed}}$  and equation 6.3,  $X_{\text{complexed}}$  for the NMR titration points at different guest concentrations in Table 6.3 can be calculated. From  $X_{\text{complexed}}$  and the guest concentration  $[\text{guest}]_{\text{total}}$ , the complexed host concentration can be calculated for a 1:6 host/guest complex stoichiometry (Equation 6.4). Plotting binding site saturation  $S$  (Equation 6.5) against guest concentration  $[\text{guest}]_{\text{total}}$  and subsequent curve fitting (Figure 6.11 and Table 6.4) yields the single site microscopic constant  $Q$  and stepwise stoichiometric formation constants  $K_n$  (Equation 6.6 and 6.7).<sup>[25]</sup>

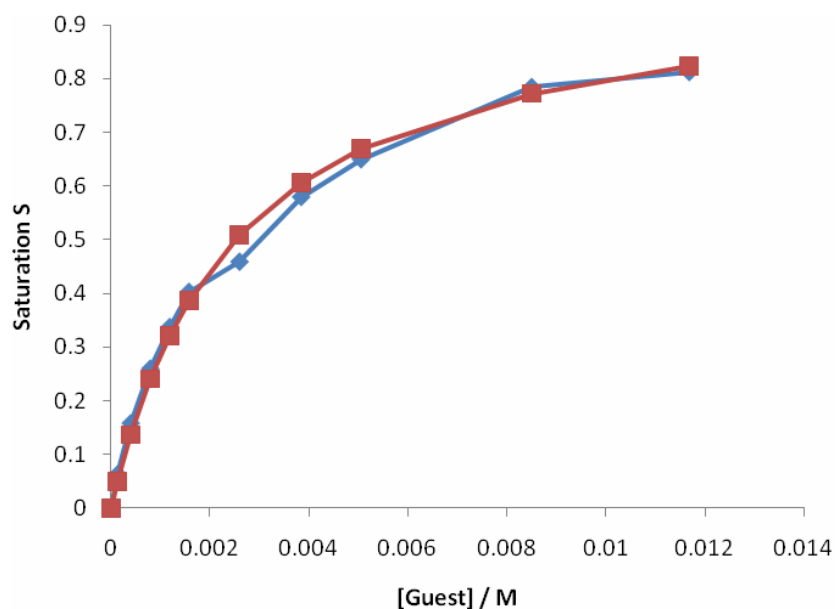
$$[\text{host}]_{\text{complexed}} = [\text{guest}]_{\text{total}} \times X_{\text{complexed}} / 6, \quad (6.4)$$

$$S = [\text{host}]_{\text{complexed}} / [\text{host}]_{\text{total}}, \quad (6.5)$$

$$S = (0 + 1/6 \times K_1 \times [G] + 2/6 \times K_1 \times K_2 \times [G]^2 + 3/6 \times K_1 \times K_2 \times K_3 \times [G]^3 + 4/6 \times K_1 \times K_2 \times K_3 \times K_4 \times [G]^4 + 5/6 \times K_1 \times K_2 \times K_3 \times K_4 \times K_5 \times [G]^5 + 6/6 \times K_1 \times K_2 \times K_3 \times K_4 \times K_5 \times K_6 \times [G]^6) / (1 + K_1 \times [G] + K_1 \times K_2 \times [G]^2 + K_1 \times K_2 \times K_3 \times [G]^3 + K_1 \times K_2 \times K_3 \times K_4 \times [G]^4 + K_1 \times K_2 \times K_3 \times K_4 \times K_5 \times [G]^5 + K_1 \times K_2 \times K_3 \times K_4 \times K_5 \times K_6 \times [G]^6), \quad (6.6)$$

$$K_n = Q \times (6 - n + 1) / n, \quad (6.7)$$

In equation 6.6 and 6.7, it is assumed that there is no cooperativity in the binding, which means that the six binding sites are identical and independent.<sup>[25]</sup>



**Figure 6.11** Binding isotherm for the encapsulation of Boc-Asp-OH in **76**·24HCl in D<sub>2</sub>O at 25 °C (pD 4.7, [**76**] = 0.21 mM) showing binding site saturation  $S$  ( $0 \leq S \leq 1$ ) as a function of the guest concentration [Guest]: experimental data (◆) and best fit (■).

**Table 6.4**  $Q$  and  $K_n$  ( $M^{-1}$ ) for the binding of **76**·24HCl with Boc-Asp-OH (pD 4.7) and *p*-TsOH (pD 1.0) in D<sub>2</sub>O at 25 °C.

guest	$Q$	$K_1$	$K_2$	$K_3$	$K_4$	$K_5$	$K_6$
Boc-Asp-OH	$400 \pm 35$	2400	1000	533	300	160	67
<i>p</i> -TsOH	$150 \pm 25$	900	375	200	113	60	25

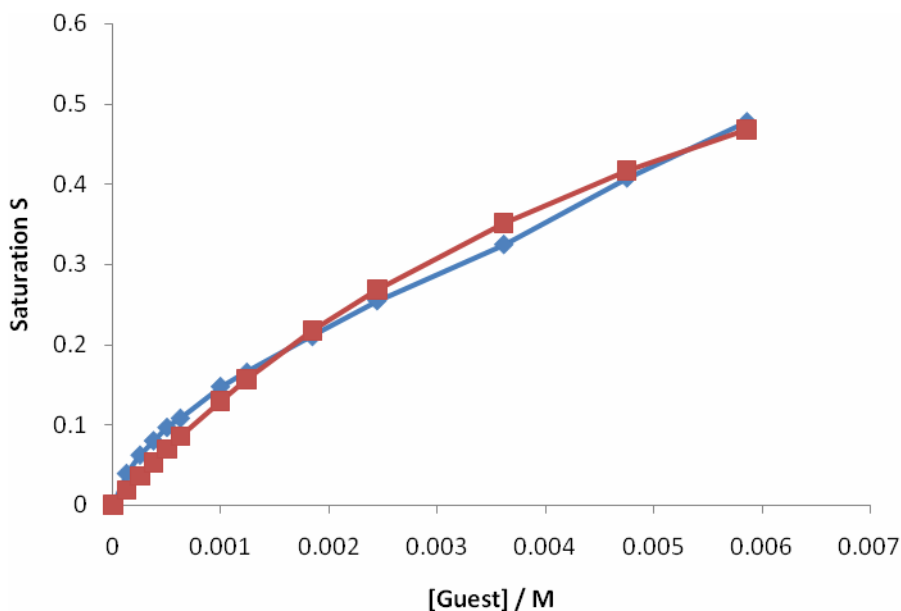
Binding was also observed for *para*-toluenesulfonic acid (*p*-TsOH, Table 6.2 and 6.5). The binding was strongly affected by the buffer in the solution (Table 6.6). The upfield shift of the methyl protons for the encapsulation of *p*-TsOH in **76** increases in the order  $\Delta\delta$  (acetate) <  $\Delta\delta$  (DCl) <  $\Delta\delta$  (no buffer). This is probably due to competitive electrostatic interactions of the buffer anions with the ammonium groups of the host **76**. Additional evidence for inside binding comes from the observation that the signal for the inward pointing protons ( $H_{\text{inner}}$ ) of **76** is upfield-shifted by up to 0.3 ppm, which is due to the shielding effect from the phenyl ring of the encapsulated *p*-TsOH. Again only one set of signals was observed for the guest. From the <sup>1</sup>H NMR titrations and DOSY experiments in D<sub>2</sub>O at pD 1 (Table 6.5), an averaged  $\delta_{\text{complexed}} = 0.906 \pm 0.103$  ppm for the methyl protons of bound *p*-TsOH was determined and was used to calculate  $Q$  and  $K_n$  (Figure 6.12 and Table 6.4).

**Table 6.5** Upfield shifts of the methyl protons and guest diffusion rates ( $D$ ,  $\times 10^{-6}$  cm<sup>2</sup>/s) for the encapsulation of  $p$ -TsOH in **76**·24HCl in D<sub>2</sub>O at 25 °C (pD 1.0, [**76**] = 0.22 mM)

[G]/equiv.	0.57	1.13	1.70	2.27	2.83	4.53	5.67	8.50	11.3	17.0	22.7	28.3
$\Delta\delta/\text{ppm}$	0.62	0.49	0.42	0.38	0.34	0.29	0.26	0.22	0.20	0.17	0.16	0.15
$D$		5.44	5.84				6.35			6.66		
$\delta_{\text{complexed}}$		0.890	0.782				0.920			1.033		

**Table 6.6** Buffer effect on the upfield shifts of the methyl protons for the encapsulation of  $p$ -TsOH in **76**·24HCl in D<sub>2</sub>O at 25 °C ( $[p\text{-TsOH}] = 0.13$  mM, [**76**] = 0.22 mM).

buffer	CD <sub>3</sub> CO <sub>2</sub> D/CD <sub>3</sub> CO <sub>2</sub> <sup>-</sup> Na <sup>+</sup>	DCl	N/A
pD	4.7	1.0	4.2
$\Delta\delta/\text{ppm}$	0.10	0.62	2.23

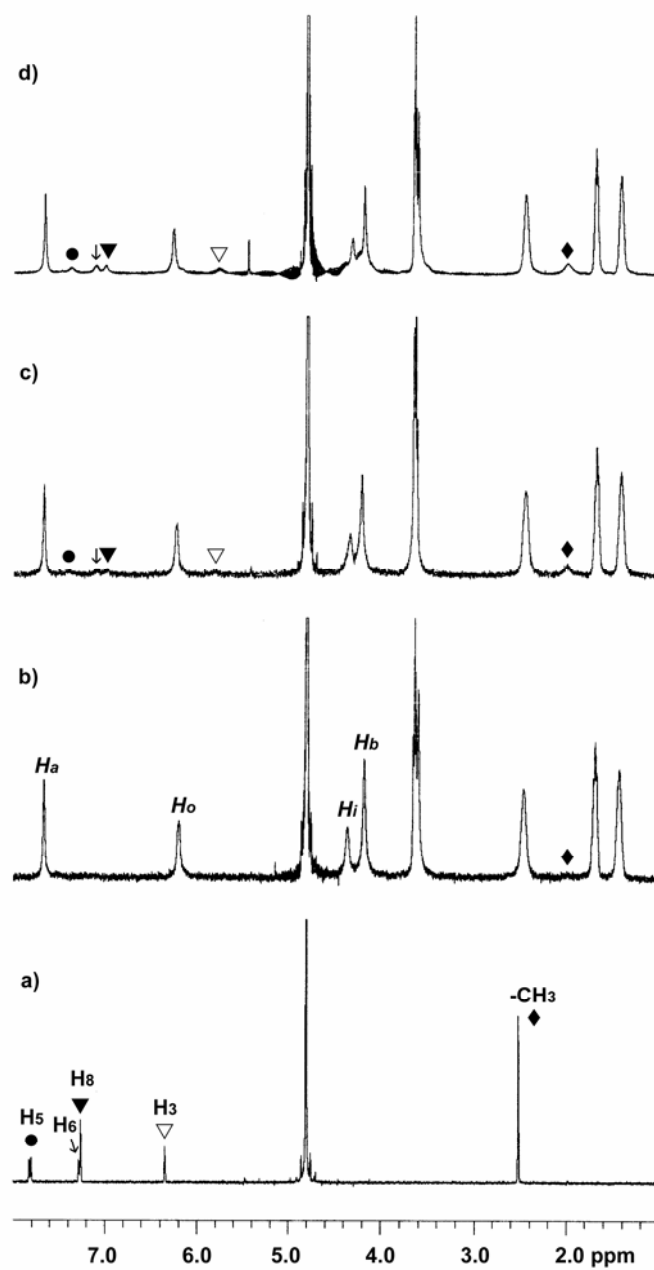


**Figure 6.12** Binding isotherm for the encapsulation of *p*-TsOH inside the octahedral hexamer **76**·24HCl in D<sub>2</sub>O at 25 °C (pD 1.0, [**76**] = 0.22 mM) showing binding site saturation  $S$  ( $0 \leq S \leq 1$ ) as a function of the guest concentration: experimental data (◆) and best fit (■).

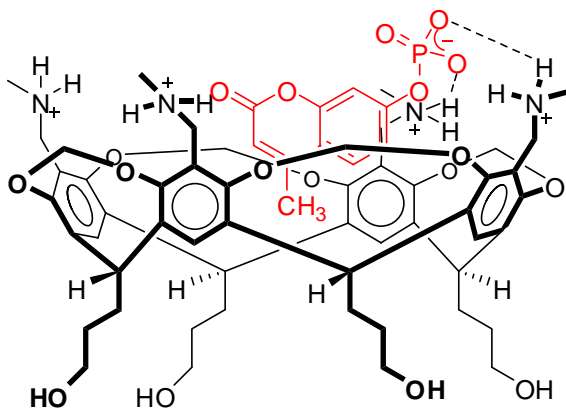
Encapsulation with the more hydrophobic guest 4-methylumbelliferyl phosphate (4-MUP) was also studied by <sup>1</sup>H NMR (Table 6.2 and 6.7). The complexation induced upfield shifts of the guest signals provided information about the guest orientation inside **76**. For example, the methyl protons as well as the protons at the 3- and 5- position (see Figure 6.10) are upfield-shifted by  $\Delta\delta = 0.51$ , 0.57 and 0.45 ppm, respectively in a sample containing 4.6 equivalents of guest per host at pD 4.3 (Figure 6.13). Smaller upfield shifts are observed for the protons at the 6- and 8- position ( $\Delta\delta = 0.17$  and 0.26 ppm, respectively), which indicates that they experience less shielding. This is consistent with the proposed orientation of the phosphate guest inside the cavity shown in Figure 6.14.

**Table 6.7** Upfield shifts of the methyl protons for the encapsulation of 4-MUP (monosodium salt) in **76**·24HCl in D<sub>2</sub>O at 25 °C (pD 4.2, [**76**] = 0.24 mM)

[G]/equiv.	0.92	1.38	1.84	2.30	3.67	4.59
$\Delta\delta/\text{ppm}$	0.65	0.63	0.61	0.60	0.57	0.53



**Figure 6.13**  $^1\text{H}$  NMR spectra (500 MHz,  $\text{D}_2\text{O}$ , 25 °C) of a) 4-MUP and **76**·24HCl in the presence of 4-MUP b) 0.9 equiv., c) 2.8 equiv., and d) 4.6 equiv., pD 4.3, [**76**] = 0.21 mM.



**Figure 6.14** Proposed partial structure of the complex formed between 4-MUP and **76**·24HCl.

NMR titrations and DOSY experiments to determine the binding constants with 4-MUP were not successful. At the experimental concentration, host **76** started precipitating after addition of 5-7 equivalents of the guest. This indicates strong interactions between encapsulated 4-MUP and host **76**. It is further supported by the much smaller guest proton  $\Delta\delta$  change at the initial stage of the titration compared to those observed in the binding experiments with *p*-TsOH (Table 6.5 and 6.7) and the substantially stronger guest signal broadening (Figure 6.13 and Table 6.8).



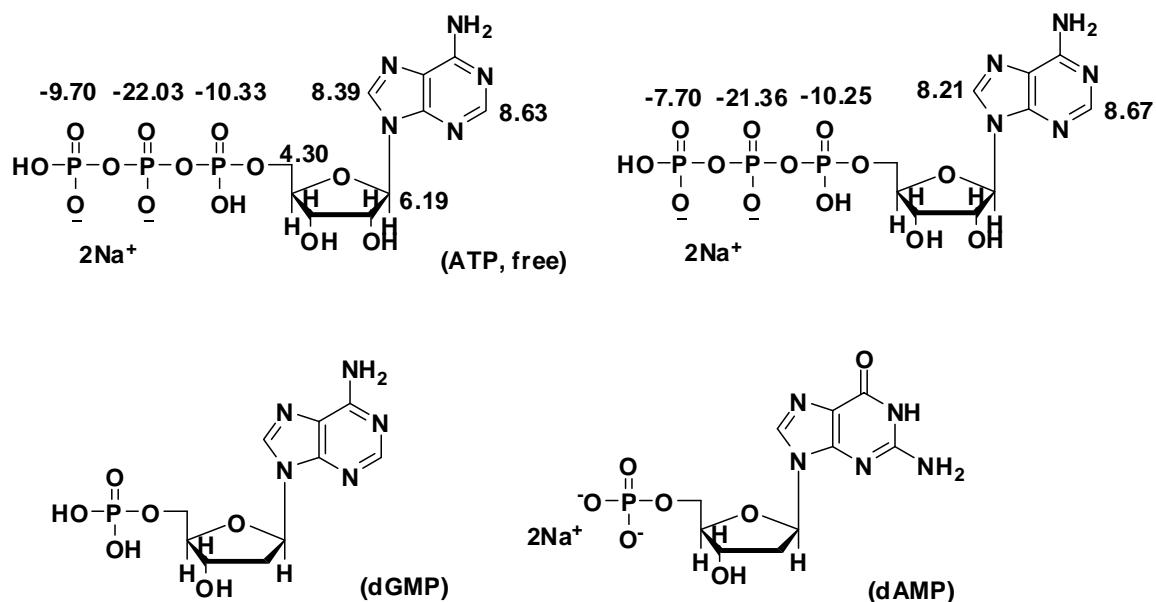
**Table 6.8** Line width (LW) of the guest methyl protons of encapsulated Boc-Asp-OH (pD 4.7), *p*-TsOH (pD 1.0) and 4-MUP (pD 4.2, sodium salt) inside **76**·24HCl in D<sub>2</sub>O at 25 °C ([**76**] = 0.22 mM).

compd.		Boc-Asp-OH	<i>p</i> -TsOH	4-MUP	<b>76</b> (feet -CH <sub>2</sub> -)
equiv.(guest: <b>76</b> )		3.62	4.53	3.67	
LW	free	1.80	2.28	2.30	21.9
(Hz)	complexed	25.0	5.04	63.2	22.8

These results suggest that binding is the result of cooperative action of electrostatic interactions, hydrogen bonding and the hydrophobic effect, which is consistent with earlier observations by other groups. For example, in 1986, Schneider et al. reported strong affinity of a methyl-footed resorcin[4]arene for tetramethylammonium salts in basic aqueous solution ( $K = 10^5 \text{ M}^{-1}$ ), which was attributed to favorable electrostatic interactions, since neutral molecules have no affinity.<sup>[16]</sup> Calix[4]arenes, having sulfonate groups at the upper rim, complex L- $\alpha$ -amino acids while calix[4]arenes, lacking the sulfonate groups, do not.<sup>[17]</sup> Favorable CH- $\pi$  or  $\pi$ - $\pi$  interactions between the guests' aliphatic or aromatic apolar residues and the aromatic cavitand subunits of **76** also contribute to the complexation.

The binding interaction with nucleotides (ATP, dGMP and dAMP) was also studied (Figure 6.15). In all cases, guest signals broadened significantly upon mixing with the host solution. However, no obvious upfield shifted signals were observed for the guest

protons. This is probably due to the electrostatic interaction of the guest molecules with the outer surface of the nanocage host, which is further supported by downfield shifts of the phosphorus signals in the  $^{31}\text{P}$  NMR of solution of **76** containing nucleotides.<sup>[7]</sup>

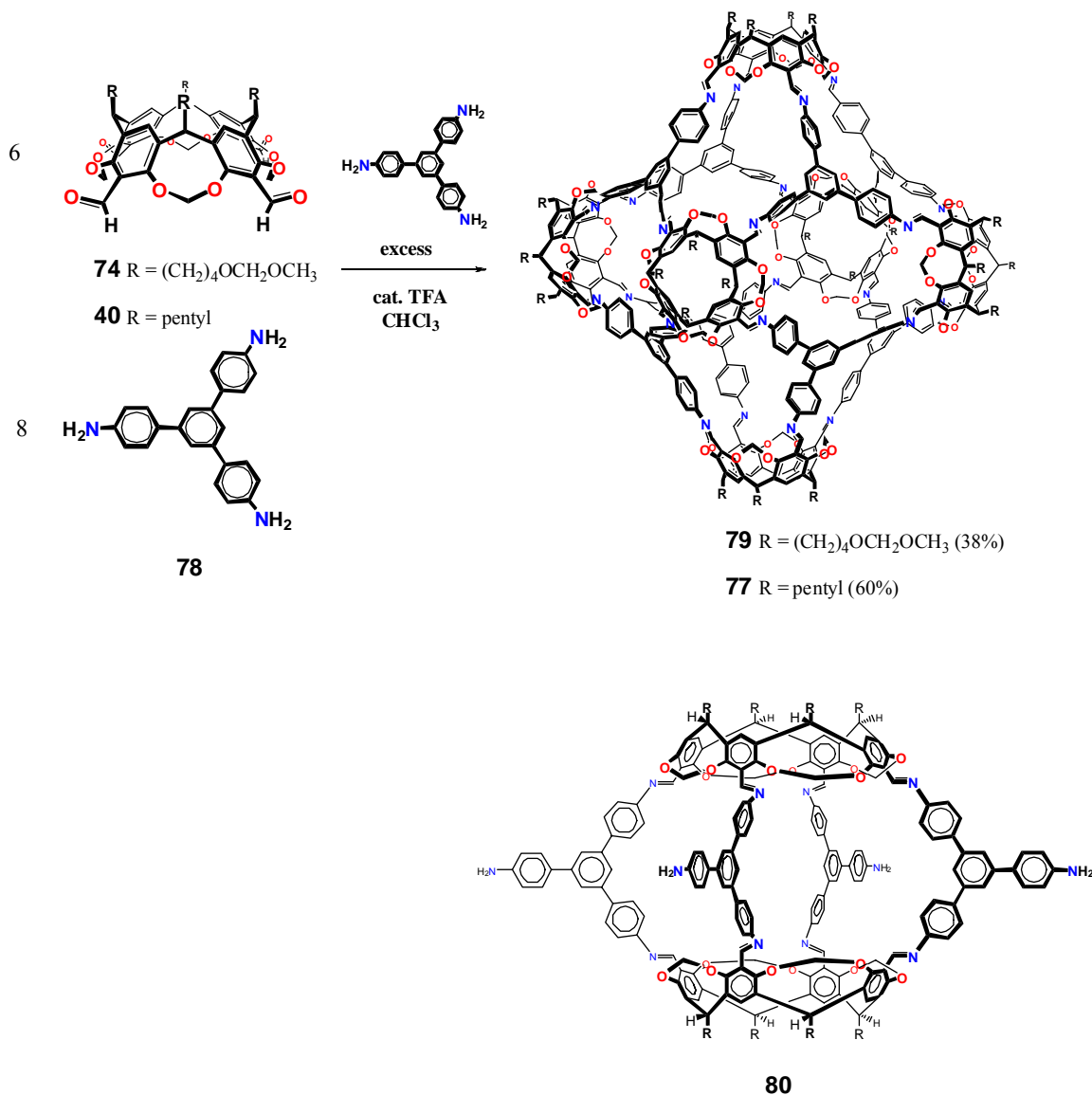


**Figure 6.15** Nucleotides and the chemical shifts with or without the presence of the host **76** (pD = 4.3, [**76**] = 0.2 mM).

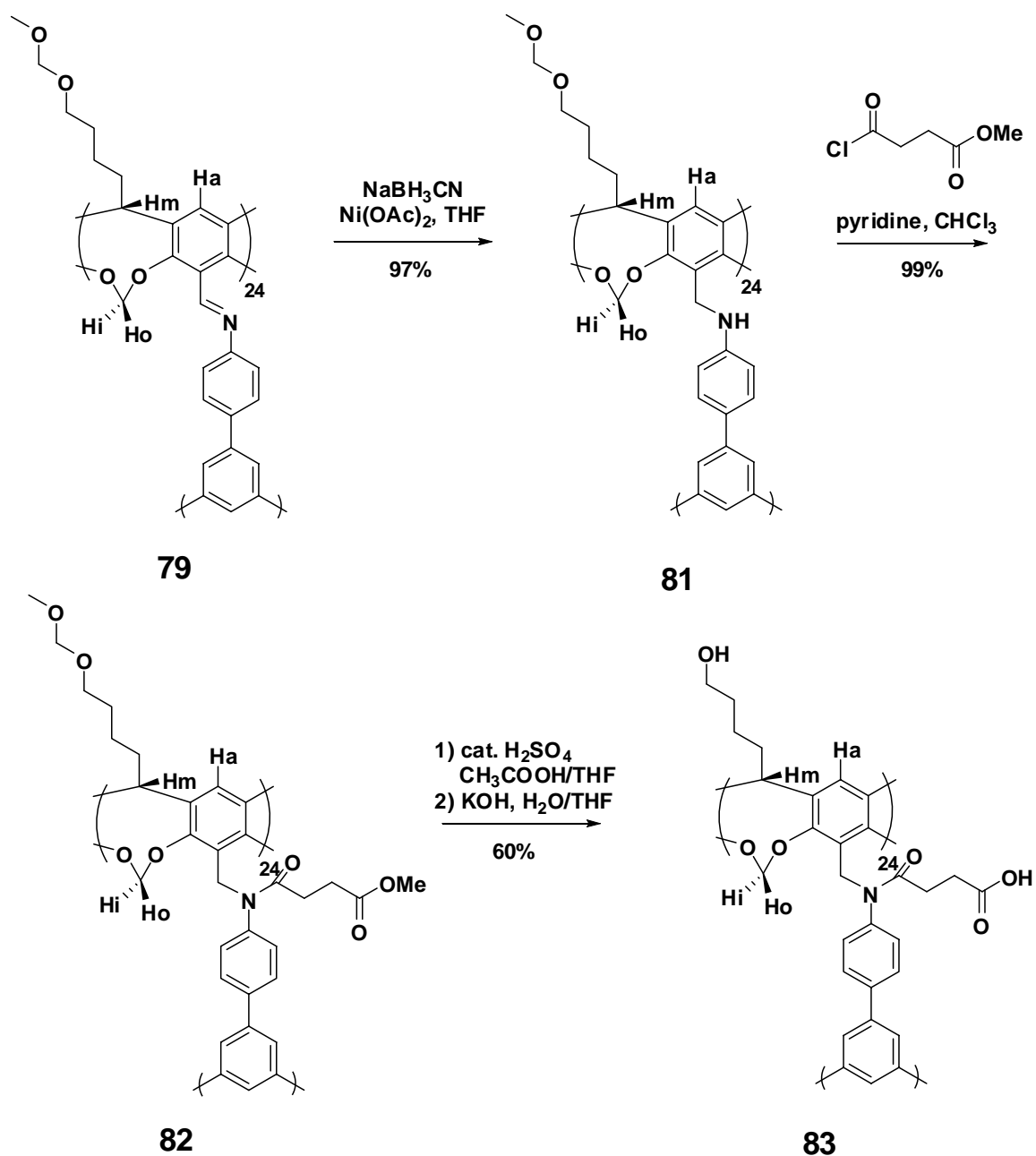
#### 6.2.4 Synthesis of a water-soluble rhombicuboctahedral nanocapsule

The affinity of water-soluble nanocapsules for organic compounds in aqueous solution may be increased by increasing the hydrophobicity of the cavity. This can be achieved by introducing aromatic rings into the host shell. Such a host is the rhombicuboctahedral nanocapsule **77**, which has been synthesized recently by our group using the condensation reaction between six tetraformyl cavitands **40** and eight 1,3,5-tris(*p*-aminophenyl)benzenes **78**.<sup>[10c]</sup> In the rhombicuboctahedral nanocapsule, the host shell contains 32 additional aromatic rings as compared to the octahedral nanocapsule reported

before.<sup>[10a]</sup> In my study, MOM-protected tetraformyl cavitand **74** was used to construct the rhombicuboctahedral nanocapsule **79** using a modified synthesis (Scheme 6.5). As compared to the earlier method,<sup>[10c]</sup> no slow addition was needed. Furthermore, the total reaction time was reduced to less than two days, which minimized acetal cleavage reactions.<sup>[10c]</sup>



**Scheme 6.5** Condensation of tetraformyl cavitand **74** and 1,3,5-tris(*p*-aminophenyl)benzene **78** leading to rhombicuboctahedral nanocapsule **79**.



**Scheme 6.6** Reduction of the polyimino rhombicuboctahedral nanocapsule **79** and post functionalization.

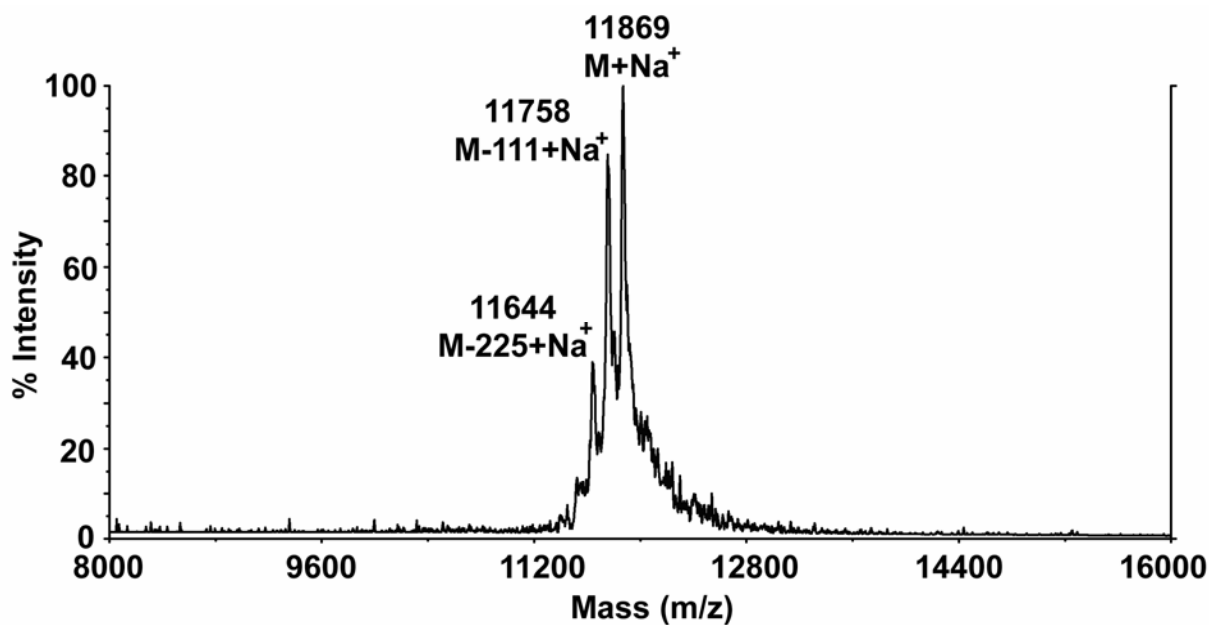
The construction of rhombicuboctahedral nanocapsule **79** was achieved by direct mixing stoichiometric amounts of the building blocks: MOM-protected tetraformyl cavitand **74** with 1,3,5-tris(*p*-aminophenyl)benzene **78** at a concentration of  $[\mathbf{74}] = 6.43 \text{ mM}$ . The

reaction mixture equilibrated overnight yielding predominantly pentameric species. In order to accelerate transimination, excess 1,3,5-tris(*p*-aminophenyl)benzene **78** was added and the mixture was slowly concentrated to half of its volume within one day, after which the reaction was stopped by addition of triethylamine. The mixture was passed through a pad of silica gel to separate **79** from dimer **80** and excess triamine **78**, which gave rhombicuboctahedral nanocapsule **79** in ~40% yield.

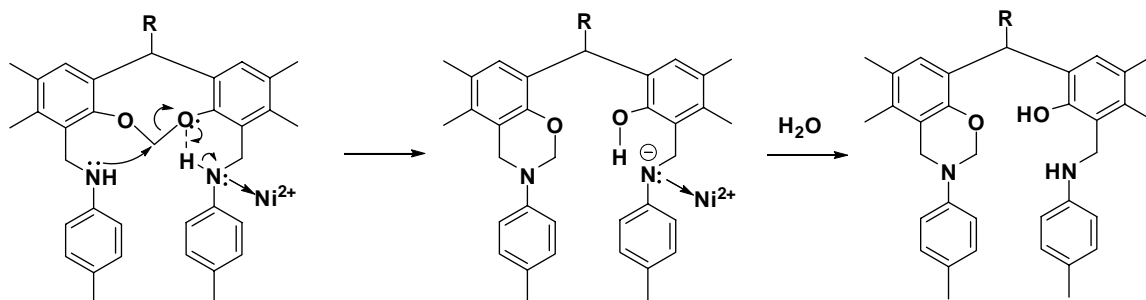
Polyimino nanocapsule **79** was subsequently reduced to polyamino nanocapsule **81** by reaction with NaBH<sub>3</sub>CN in THF catalyzed by Ni(OAc)<sub>2</sub> (Scheme 6.6).<sup>[19]</sup> This step was done overnight and was quantitative. It worked even in the presence of dimer **80** and/or excess triamine **78**. The structure of reduced hexamer **81** was supported by <sup>1</sup>H and <sup>13</sup>C NMR spectroscopy and MALDI-TOF MS.

The following acylation of the twenty-four amino groups of **81** with methyl succinyl chloride had to be carried out in the presence of a weak base, such as pyridine or NaHCO<sub>3</sub> (Scheme 6.6). If a stronger base, such as K<sub>2</sub>CO<sub>3</sub>, was used, Claisen-type side reactions occurred. While monitoring the reaction by MALDI-TOF MS, it was found that, in addition to the fully reacted capsule **82** ( $m/z = 11869$ , M+Na<sup>+</sup>, 100%), capsules lacking up to two methyl succinyl groups were also present ( $m/z = 11758$ , M-111+Na<sup>+</sup>, 85%;  $m/z = 11644$ , M-225+Na<sup>+</sup>, 40%) (Figure 6.16). Adding additional reagents, heating (60 °C) or longer reaction time didn't change the product ratio. This suggested that the polyamino nanocapsule sample was not homogeneous and contained nanocapsules that lack one or two reactive amino groups. Such capsules could be generated by Ni<sup>2+</sup> catalyzed

intramolecular formation of small amounts of benzoxazines during the reduction step (Scheme 6.7). Benzoxazines have been prepared through condensation of phenols, amines, and formaldehyde and are stable compounds.<sup>[20]</sup> Benzoxazine formation in such small amounts (< 2-3% of all acetals) is not detectable by MS, and difficult to observe in the  $^1\text{H}$  NMR spectrum of the polyamino hexamer **81**. The phenol groups generated in this reaction may be too hindered to undergo acylation.

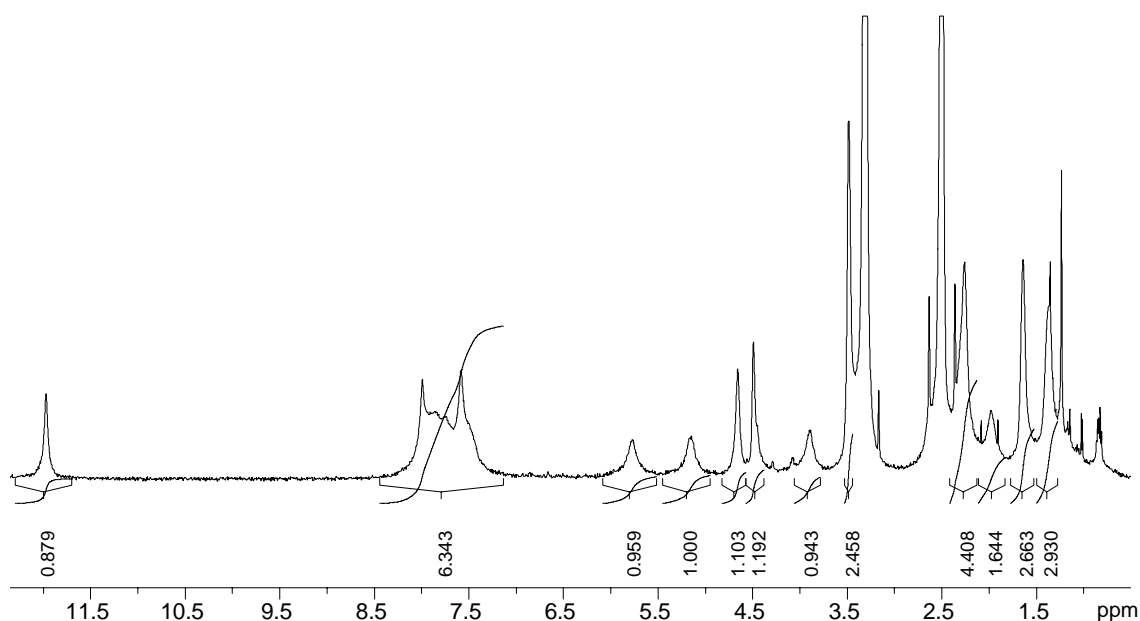


**Figure 6.16** MALDI-TOF mass spectrum of the acylation product **82**.



**Scheme 6.7** Proposed mechanism of intramolecular benzoxazine formation.

Purification of **82** by normal phase HPLC was not possible, due to the acid lability of the MOM-protecting groups. Thus, the MOM-protecting groups of **82** were first changed into acetate groups which, together the succinyl methyl esters, were subsequently cleaved by basic hydrolysis to give the butanol-footed polycarboxyl nanocapsule **83** (Scheme 6.6). Major byproducts present in the crude product are species that lack one or two succinyl linkers. In the MALDI-TOF mass spectrum of the product, other than the major clusters for  $M+H^+$  and  $M+Na^+$ , two clusters with  $m/z = 10381$  and  $10282$  are also observed, which are assigned to these byproducts. Nanocapsule **83** is soluble in DMSO, or methanol/chloroform. It is also well soluble in basic aqueous solution ( $\sim 15$  mg/ml). The  $^1H$  NMR spectrum of **83**, recorded in  $DMSO-d_6$ , is consistent with its composition (Figure 6.17). However, in basic  $D_2O$ , the signals are very broad, even more than in  $DMSO-d_6$ . Recording the spectrum at high temperature ( $80^\circ C$ ) or addition of 15 v%  $CD_3OD$  into the NMR sample didn't sharpen the signals significantly. The reason for the strong line broadening is not clear. DOSY experiments of **83** in  $D_2O$  revealed a diffusion rate  $D \sim 1.0 \times 10^{-6} \text{ cm}^2/\text{s}$ , which indicates the presence of single molecules instead of larger aggregates in solution. Thus, line broadening may be a consequence of slow conformational changes of the host involving rotations around the amide bonds.



**Figure 6.17**  $^1\text{H}$  NMR spectrum (500 MHz,  $\text{DMSO}-d_6$ , 25  $^\circ\text{C}$ ) of nanocapsule **83**.

### 6.3 Future application of the water-soluble nanocapsules in drug-delivery system

A large number of active pharmaceutical ingredients (API) exhibit low bioavailability and need to be protected from enzymatic or acid-catalyzed breakdown in the body.<sup>[21]</sup> Therefore, it is necessary to develop efficient carrier-based drug delivery systems. There are commonly three types of carriers in drug delivery system: liposomes, polymeric micelles, and micro- and nano-particles and capsules. Hemicarcerands have been used to encapsulate small drug molecules, such as amantadine.<sup>[22]</sup> This anti-influenza drug was also encapsulated by Rebek's water soluble cavitand-based host.<sup>[6a]</sup> In addition, Gibb and coworker encapsulated different steroids in a self-assembled deep cavitand dimer.<sup>[6d]</sup> Delivery devices for larger drug molecules need to be developed. Our water soluble



nanocapsules possess large portals and a roomy inner cavity and potentially may serve as devices for drug delivery and controlled release applications.

## 6.4 Conclusions

Different water-soluble nanocapsules constructed from six cavitands have been prepared. Pentyl-footed octahedral nanocapsule **68** formed aggregates in water after the amino groups were functionalized with carboxylic acids. However, polyammonium octahedral nanocapsule **76** with polar hydroxyl feet groups is readily soluble in water and has demonstrated binding of negatively charged organic compounds in aqueous solution. Binding is the result of the cooperative action of electrostatic interactions, hydrogen bonding interactions and the hydrophobic effect. A butanol-footed polycarboxyl rhombicuboctahedral nanocapsule **83** has been synthesized and binding studies are in progress.

## 6.5 Experimental section

### 6.5.1 General procedure

All reactions were conducted under argon. Reagents and chromatography solvents were purchased from Aldrich and used without further purification except that chloroform was passed through  $K_2CO_3$  prior to use.  $^1H$  NMR spectra recorded in  $CDCl_3$ ,  $D_2O$  or  $DMSO-d_6$  were referenced to residual  $CHCl_3$ , HDO and  $CD_3S(O)CD_2H$  at 7.26 ppm, 4.80 ppm and 2.50 ppm, respectively.  $^{13}C$  NMR spectra recorded in  $CDCl_3$  were referenced to  $^{13}CDCl_3$  at 77.0 ppm. Mass spectra were recorded on an Applied Biosystems Voyager DE-Pro mass spectrometer (MALDI-TOF). 2',4',6'-Trihydroxyacetophenone (THAP)

was used as matrix. Gel permeation chromatography (GPC) was performed on a Varian *prostar* 210 HPLC system equipped with dual wavelength UV/Vis detector (280 nm), Eppendorf CH-30 column heater and two Jordi GPC columns (cross linked DVB;  $10^3$  Å pore size; MW cutoff  $\sim$  25,000; 7.8mm  $\times$  30cm) with CH<sub>2</sub>Cl<sub>2</sub>/1% NEt<sub>3</sub> as mobile phase at a flow of 1 mL/min. Approximate molecular weights of analytes were determined from a semi logarithmic calibration plot (Ln(MW) against retention time) using the following molecular weight standards: benzene (MW 78); cavitand **40** (MW 928); a NMP hemicarceplex (MW 2348),<sup>[23]</sup> and polyaminonanocapsules **47a-c** (MW 3941, 5912 and 7882).<sup>[10]</sup>

### 6.5.2 NMR complexation studies

Acetate buffer (pD 4.7, 103 mM) was prepared from acetic acid-*d*<sub>4</sub> and 40 wt% NaOD/D<sub>2</sub>O. A Boc-Asp-OH solution (87.8 mM) was prepared by dissolving Boc-Asp-OH in acetate buffer. **76**·24HCl (1.06 mg) was dissolved in 0.7 ml acetate buffer (0.22 mM) and placed into an NMR tube. This solution was titrated with the Boc-Asp-OH solution. Before and after each addition, <sup>1</sup>H NMR spectra were recorded on a 400 MHz Varian FT-NMR instrument. DCl buffer (pD 1.0, 100 mM) was prepared by diluting conc. DCl/D<sub>2</sub>O solution. A *p*-TsOH solution (87.9 mM) was prepared by dissolving *p*-TsOH in the DCl buffer. A solution of **76**·24HCl in DCl buffer (1.06 mg in 0.7 ml solution, 0.22 mM) was placed in an NMR tube and titrated with *p*-TsOH solution as described for Boc-Asp-OH. A solution of 4-MUP was adjusted to pD 4.5 with NaOD/D<sub>2</sub>O (final concentration 78.6 mM). This solution was used to titrate **76**·24HCl (1.17 mg in 0.7 ml D<sub>2</sub>O, 0.24 mM, pD 4.2) as described for Boc-Asp-OH.

### 6.5.3 DOSY experiments

DOSY NMR experiments were performed on a 400 MHz Varian spectrometer equipped with a gradient system capable of producing magnetic field pulse gradients in the  $z$ -direction of about 50 G<sup>-1</sup>/cm. A 5 mm broadband probe was used to carry out all the measurements. Samples were prepared as described in the previous section and were loaded into a 5 mm NMR tube. Temperature was controlled at 298 K. Samples were equilibrated at least 10 min before the measurement started. The diffusion experiments were performed using the pulse sequence Dbppste (Bipolar Pulse Pair Stimulated Echo Experiment), which is implemented in the NMR software VnmrJ. The diffusion delay ( $\Delta$ ) was set at 0.05 sec. The gradient pulse strength ( $G_z$ ) was varied from 400 to 25000 G/cm. For all the other parameters, the default values were used. The field gradients were calibrated with the <sup>1</sup>H signal in a D<sub>2</sub>O sample containing 1% H<sub>2</sub>O. The literature value of  $D(\text{HDO}) = (1.902 \pm 0.002) \times 10^{-5} \text{ cm}^2\text{s}^{-1}$  was used for the self-diffusion rate of HDO at 25 °C.<sup>[26]</sup>

### 6.5.4 Synthesis of **65**

Triethylamine (43  $\mu\text{l}$ , 0.309 mmol) was added to a suspension of **47a**·24TFA (100 mg, 0.0116 mmol) in 30 ml dichloromethane. The solution was stirred at room temperature for 20 min. Then, monomethyl succinate **63** (74 mg, 0.560 mmol) and N,N'-diisopropylcarbodiimide (DIC, 95  $\mu\text{l}$ , 0.614 mmol) was added and stirring continued for 7.5 days. The clear, slightly yellow solution was washed with 1 M HCl aq. (30 ml), sat. NaHCO<sub>3</sub> aq. (30 ml), H<sub>2</sub>O (30 ml) and brine (30 ml). The solution was concentrated and the crude product was dried under high vacuum to give **64** as a slightly yellow oil (144.5

mg). MALDI-TOF MS for  $C_{480}H_{624}N_{24}O_{120}$  calc'd 8651.19 ( $M+H^+$ ), found 8651.59. Crude **64** was subjected to saponification without purification. **64** (81.2 mg) was dissolved in 10 ml THF and 1 M KOH aq. (1.4 ml, 1.4 mmol) was added. The mixture was stirred at room temperature for 2 days, after which it was concentrated. The residue was partitioned between 10 ml EtOAc and 5 ml 1 M HCl aq.. The organic layer was separated, dried over  $MgSO_4$  and concentrated. **65** was obtained as a slightly yellow solid (27.6 mg, 51% yield based on **47a**).

### 6.5.5 Synthesis of **66**

Triethylamine (370  $\mu$ l, 2.65 mmol) was added to a suspension of dimethyl iminodiacetate hydrochloride (500 mg, 2.53 mmol) in 20 ml acetonitrile. The solution was stirred at room temperature for 30 min. Succinic anhydride (278 mg, 2.78 mmol) was added and stirring continued for 1 day. The mixture was concentrated and the residue was partitioned between 10 ml EtOAc and 5 ml 1 M HCl aq.. The organic layer was washed with brine 10 ml, dried over  $MgSO_4$  and concentrated. **66** was obtained as a slightly yellow oil (280 mg, 42% yield), which slowly solidified over time at room temperature.  $^1H$  NMR ( $CDCl_3$ , 25 °C, 300 MHz),  $\delta_H$ : 4.21(s, 2 H, -CONCH<sub>2</sub>-), 4.19(s, 2 H, -CONCH<sub>2</sub>-), 3.79 (s, 3 H, -COCH<sub>3</sub>), 3.73 (s, 3 H, -COCH<sub>3</sub>), 2.77-2.64 (m, 4 H, HO<sub>2</sub>CCH<sub>2</sub>CH<sub>2</sub>CON-).  $^{13}C$  NMR ( $CDCl_3$ , 25 °C, 75 MHz),  $\delta_C$ : 177, 172, 170, 169, 53, 52, 50, 48, 30, 29, 28. MS (ESI): for  $C_{10}H_{15}NO_7$ , calc'd: 260.1 ( $M-H$ )<sup>-</sup>; found: 259.9.

### 6.5.6 Synthesis of **68**

Triethylamine (22  $\mu$ l, 0.0158 mmol) was added to a suspension of **47a**·24TFA (50 mg, 0.00578 mmol) in 10 ml dichloromethane. The solution was stirred at room temperature for 20 min. **66** (73 mg, 0.279 mmol) and N,N'-diisopropylcarbodiimide (DIC, 47  $\mu$ l, 0.304 mmol) were added and stirring continued for 3.5 days. The clear, slightly yellow solution was washed with 1 M HCl aq. (10 ml), sat. NaHCO<sub>3</sub> aq. (10 ml), and brine (10 ml). It was dried over MgSO<sub>4</sub>, concentrated and dried under high vacuum. Crude **67** was obtained as an oil (102.3 mg). Crude **67** was subjected to saponification without purification. It was dissolved in 8.5 ml THF and 1 M KOH aq. (3.0 ml, 3.0 mmol) was added. The mixture was stirred at room temperature for 2.5 days. It was concentrated and partitioned between 20 ml EtOAc and 5 ml 1 M HCl aq.. The organic layer was dried over MgSO<sub>4</sub> and concentrated. NaOH aq. (10 ml, 1 M) was added to the residue. The suspension was sonicated and filtered. The white precipitate containing the sodium carboxylate of **68** was washed with CH<sub>2</sub>Cl<sub>2</sub> to remove diisopropyl urea and then dried under high vacuum (42.2 mg, 65% yield based on **47a**). <sup>1</sup>H NMR (400 MHz, D<sub>2</sub>O, pD 9, 25 °C),  $\delta_{\text{H}}$  (ppm): 7.47 (br s, 24 H, H<sub>aryl</sub>), 6.00 (br s, 24 H, H<sub>outer</sub>), 5.32 (br s, 24 H, H<sub>methine</sub>), 4.71 (br s, 24 H, H<sub>inner</sub>), 3.94 (br s, 96 H, -NCOCH<sub>2</sub>CH<sub>2</sub>CON-), 2.81 (br s, 96 H, -NCOCH<sub>2</sub>CO<sup>-</sup>Na<sup>+</sup>), 2.37 (br s, 48 H), 1.39 (br s, 144 H), 0.91 (br s, 72 H).

### 6.5.7 Synthesis of MOM-protected tetrabromocavitand **73**

Tetrabromocavitand with butanol feet **72** (1.0 g, 0.876 mmol) was dried overnight at high vacuum at 110 °C. It was dissolved in 20 ml DMF under argon. Diisopropylethyl amine (2.32 ml, 14.0 mmol) was added into the solution. After 10 min, chloromethyl methyl

ether (0.8 ml, 10.5 mmol) was added and stirring continued at room temperature for 5.5 h. Then, DMF was removed under reduced pressure. The residue was dissolved in 50 ml EtOAc and washed twice with 50 ml 0.2 M HCl aq.. The aqueous layer was further extracted with 30 ml EtOAc. The organic layers were combined, washed with 20 ml saturated NaHCO<sub>3</sub> aq., 30 ml brine, dried with MgSO<sub>4</sub> and concentrated. The slightly yellow foam was dried under high vacuum at room temperature overnight (1.03 g, 89%). <sup>1</sup>H NMR (CDCl<sub>3</sub>, 25 °C, 300 MHz),  $\delta_{\text{H}}$ : 7.03(s, 4H), 5.95(d,  $J$  = 7.4 Hz, 4H), 4.89(t,  $J$  = 8.0 Hz, 4H), 4.61(s, 8H), 4.39(d,  $J$  = 7.4 Hz, 4H), 3.54(t,  $J$  = 6.5 Hz, 8H), 3.35(s, 12H), 2.26(m, 8H), 1.73(m, 8H), 1.46(m, 8H). <sup>13</sup>C NMR (CDCl<sub>3</sub>, 25 °C, 75 MHz),  $\delta_{\text{C}}$ : 152.1, 139.1, 118.9, 113.7, 98.4, 96.5, 67.6, 55.2, 37.5, 29.6, 24.4. MS (MALDI-TOF):  $m/z$  (M+Ag<sup>+</sup>, 100%), calc'd: 1425.02; found: 1425.25. Elemental analysis: calc'd for C<sub>56</sub>H<sub>68</sub>O<sub>16</sub>Br<sub>4</sub>: C, 51.08; H, 5.21; found: C, 51.47; H, 5.42.

#### 6.5.8 Synthesis of MOM protected tetraformyl cavitand **74**

Tetrabromocavitand **73** (0.5 g, 0.38 mmol) was dried under high vacuum at 110 °C overnight. Then, it was dissolved in 20 ml dry THF and cooled down to –78 °C while protected under argon. n-BuLi (2.5 M hexane solution, 1.22 ml, 3.04 mmol) was syringed into the flask. The solution was stirred at –78 °C. After 20 min, it was warmed up to 0 °C for 30 min and re-cooled to –78 °C. Dry DMF (1.18 ml, 15.2 mmol, dried over 3 Å molecular sieves for 24 h) was added by syringe. After stirring at –78 °C for 10 min, the solution was warmed up to room temperature and stirred for one additional hour. 10 ml 5 wt% NH<sub>4</sub>Cl aq. was added and stirring continued for 10 min. The mixture was extracted

with EtOAc (1 × 40 ml and 2 × 20 ml). The organic layers were combined, washed with 30 ml saturated NaHCO<sub>3</sub> aq., 30 ml brine, dried over MgSO<sub>4</sub> and concentrated. The yellow residue was dried under high vacuum. The crude product was purified by silica gel column chromatography (Et<sub>2</sub>O/CH<sub>2</sub>Cl<sub>2</sub>/Et<sub>3</sub>N 8:1:0.036 gradient to Et<sub>2</sub>O/CH<sub>2</sub>Cl<sub>2</sub>/Et<sub>3</sub>N 3:2:0.036) to give **74** as a white powder (0.225 g, 53%). <sup>1</sup>H NMR (CDCl<sub>3</sub>, 25 °C, 300 MHz), δ<sub>H</sub>: 10.25(s, 4H), 7.29(s, 4H), 5.90(d, *J* = 7.6 Hz, 4H), 4.94(t, *J* = 8.1 Hz, 4H), 4.62(s, 8H), 4.47(d, *J* = 7.6 Hz, 4H), 3.56(t, *J* = 6.4 Hz, 8H), 3.36(s, 12H), 2.29(m, 8H), 1.75(m, 8H), 1.48(m, 8H). <sup>13</sup>C NMR (CDCl<sub>3</sub>, 25 °C, 125.7 MHz), δ<sub>C</sub>: 189.8, 154.7, 139.0, 124.6, 124.5, 100.1, 96.5, 67.5, 55.2, 35.8, 29.6, 29.3, 24.4. MS (MALDI-TOF): *m/z* (M+Na<sup>+</sup>, 100%), calc'd: 1135.45; found: 1135.53. Elemental analysis: calc'd. for C<sub>60</sub>H<sub>72</sub>O<sub>20</sub>: C, 64.74; H, 6.52; found: C, 64.94; H, 6.12.

### 6.5.9 Synthesis of butanol-footed hexameric nanocapsule **76**

Hexamer **76** was prepared according to a procedure developed for hexamer **47a**.<sup>[10a]</sup> Tetraformylcavitand **74** (569 mg, 0.511 mmol), ethylenediamine (63.4 mg, 1.05 mmol) and trifluoroacetic acid (TFA, 6.1 μl, 0.0821 mmol) were dissolved in 47 ml chloroform (passed through a pad of K<sub>2</sub>CO<sub>3</sub>). The slightly yellow solution was stirred at room temperature under argon for 41 hrs. To the stirred solution, NaBH<sub>4</sub> (4.04 g, 107 mmol) was added. After 3 min, 0.4 ml dry methanol (dried over 3 Å molecular sieves for 24 hrs) was added. After 5 min, additional 4.3 ml dry methanol was added and the mixture was stirred at room temperature overnight. The solvents were removed under reduced pressure. The white residue was sonicated with 30 ml water for 10 min and the mixture was filtered. The white residue was transferred into a 250 ml RB flask and stirred with

170 ml methanol. Then, 17 ml concentrated HCl was added dropwise into the flask. Stirring was continued at room temperature under argon for 3 days (white precipitates gradually formed after 1 day). The mixture was filtered and the white residue was washed three times with 1 ml cold methanol. The residue was dried under high vacuum overnight to give **76**·24HCl as a slightly yellowish powder (409 mg, 70% yield based on **74**). <sup>1</sup>H NMR (0.2 wt% DCl/D<sub>2</sub>O, 25 °C, 500 MHz),  $\delta_{\text{H}}$ : 7.72(s, 24H), 6.22(s, 24H), 4.37(s, 24H), 4.24(s, 48H), 3.70(s, 48H), 3.64(t,  $J = 6.0$  Hz, 48H), 2.49(s, 48H), 1.70(m, 48H), 1.44(s, 48H). <sup>13</sup>C NMR (0.2 wt% DCl/D<sub>2</sub>O, 25 °C, 125 MHz),  $\delta_{\text{C}}$ : 153.4, 138.8, 123.9, 117.9, 100.4, 61.9, 42.8, 41.5, 37.0, 31.2, 28.8, 23.6. MS (MALDI-TOF) for C<sub>336</sub>H<sub>432</sub>N<sub>24</sub>O<sub>72</sub>:  $m/z$  (M+Na<sup>+</sup>, exact mass), calc'd: 5978.08; found: 5978.32.

#### 6.5.10 Synthesis of MOM protected rhombicuboctahedral nanocapsule **79**

1,3,5-Tris-(*p*-aminophenyl) benzene **78** (105.36 mg, 0.300 mmol) was dissolved in CHCl<sub>3</sub> (35.0 ml). MOM-protected tetraformyl cavitand **74** (250.52 mg, 0.225 mmol) was added into the solution. Then, 1% TFA in CHCl<sub>3</sub> (73  $\mu$ l, 0.0098 mmol TFA) was added. The solution was stirred at room temperature under argon for 14 hrs. Additional **78** (215 mg, 0.613 mmol) was added and the mixture was sonicated for 15 min. The mixture was stirred for additional 23 hrs, whereby the solvent was slowly evaporated to ~20 ml. Et<sub>3</sub>N (0.4 ml) was added to stop the reaction. The mixture was combined with a second batch, which was prepared under exactly the same conditions. The combined solutions were concentrated to ~ 20 ml and passed through a silica gel plug saturated with 1%Et<sub>3</sub>N/CHCl<sub>3</sub> (35 mm x 27mm). The product was eluted with 1%Et<sub>3</sub>N/CHCl<sub>3</sub> and 5 ml fractions were collected. Since the dimeric capsule **80** is soluble in CHCl<sub>3</sub> and did not



precipitate during the synthesis, as observed earlier,<sup>[10c]</sup> it was necessary to check the fractions during the separation by GPC in order to obtain pure hexamer **79**. The first seven fractions contained pure product and were combined and concentrated down to give **79** as reddish crystals (260 mg, 38% yield). <sup>1</sup>H NMR (500 MHz, CDCl<sub>3</sub>, 25 °C),  $\delta_{\text{H}}$  (ppm): 8.78 (s, 24 H, H<sub>imine</sub>), 7.66 (s, 24 H, H<sub>aryl</sub>), 7.63 (d,  $J = 8.72$  Hz, 48 H, H<sub>aryl</sub>), 7.31 (s, 24 H, H<sub>aryl</sub>), 7.27 (d, 48 H, H<sub>aryl</sub>), 5.94 (d,  $J = 6.66$  Hz, 24 H, H<sub>outer</sub>), 5.08 (t,  $J = 7.85$  Hz, 24 H, H<sub>methine</sub>), 4.70 (d,  $J = 7.02$  Hz, 24 H, H<sub>inner</sub>), 4.64 (s, 48 H, -OCH<sub>2</sub>OCH<sub>3</sub>), 3.59 (t,  $J = 6.53$  Hz, 48 H, -CH<sub>2</sub>OCH<sub>2</sub>OCH<sub>3</sub>), 3.38 (s, 72 H, -OCH<sub>2</sub>OCH<sub>3</sub>), 2.38(m, 48 H), 1.81(m, 48 H), 1.54(m, 48 H). <sup>13</sup>C NMR (125 MHz, CDCl<sub>3</sub>, 25 °C),  $\delta_{\text{C}}$  (ppm): 155.0, 154.0, 151.4, 142.0, 139.5, 138.8, 128.3, 123.7, 122.1, 121.5, 96.5, 67.7, 55.2, 36.4, 29.7, 24.5. MALDI-TOF MS: calc'd. for C<sub>552</sub>H<sub>552</sub>N<sub>24</sub>O<sub>96</sub> 9059.4 (M + H<sup>+</sup>), found 9058.38.

#### 6.5.11 Reduction of MOM-protected rhombicuboctahedral nanocapsule **79** to form **81**

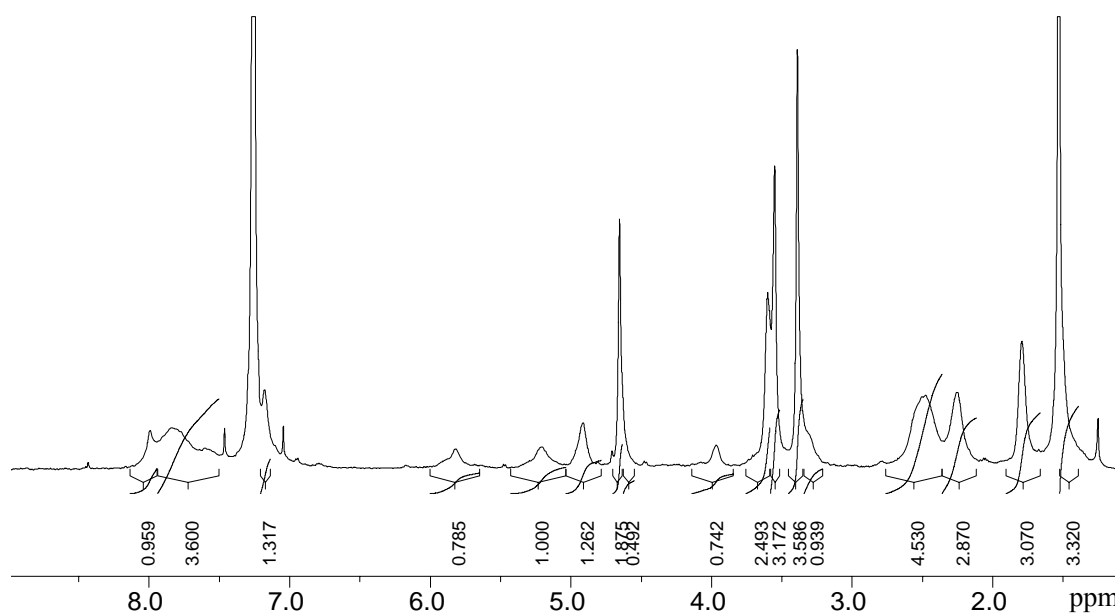
Hexamer **79** (240 mg, 0.0265 mmol) was dissolved in THF (98 ml). Ni(AcO)<sub>2</sub>·4H<sub>2</sub>O (235 mg, 0.952 mmol) was added. Then, NaBH<sub>3</sub>CN in THF (1.0 M, 9.54 ml) was syringed into the reaction solution over 10 min. The yellow mixture was stirred at room temperature under argon for 18.5 hrs. The solvent was removed under reduced pressure. The slightly yellow residue was stirred with conc. NH<sub>3</sub> aq./H<sub>2</sub>O (20 ml / 100 ml) for 10 min. A white precipitate formed. The mixture was extracted with CH<sub>2</sub>Cl<sub>2</sub> (200 ml). The organic layer was washed with saturated NaHCO<sub>3</sub> aq. (100 ml) and brine (100 ml). It was dried over Na<sub>2</sub>SO<sub>4</sub>, concentrated down and dried under high vacuum to give **81** as a slightly yellow solid (235 mg, 97% yield). <sup>1</sup>H NMR (500 MHz, CDCl<sub>3</sub>, 25 °C),  $\delta_{\text{H}}$  (ppm):

7.47 (s, 24 H,  $H_{\text{aryl}}$ ), 7.44 (d,  $J = 8.5$  Hz, 48 H,  $H_{\text{aryl}}$ ), 7.22 (s, 24 H,  $H_{\text{aryl}}$ ), 6.83 (d,  $J = 9.0$  Hz, 48 H,  $H_{\text{aryl}}$ ), 6.02 (d,  $J = 6.0$  Hz, 24 H,  $H_{\text{outer}}$ ), 4.91 (t,  $J = 8.0$  Hz, 24 H,  $H_{\text{methine}}$ ), 4.65 (s, 48 H,  $-\text{OCH}_2\text{OCH}_3$ ), 4.43 (d,  $J = 6.0$  Hz, 24 H,  $H_{\text{inner}}$ ), 4.10 (bs, 48 H,  $-\text{ArCH}_2\text{NH}-$ ), 4.02 (s, 24 H,  $-\text{NH}-$ ), 3.59 (t,  $J = 6.5$  Hz, 48 H,  $-\text{CH}_2\text{OCH}_2\text{OCH}_3$ ), 3.39 (s, 72 H,  $-\text{OCH}_2\text{OCH}_3$ ), 2.34 (m, 48 H), 1.79 (m, 48 H), 1.52 (m, 48 H).  $^{13}\text{C}$  NMR (125 MHz,  $\text{CDCl}_3$ , 25 °C),  $\delta_{\text{C}}$  (ppm): 153.8, 148.2, 142.5, 138.5, 132.8, 128.5, 124.2, 124.1, 120.0, 114.7, 99.4, 96.5, 67.7, 55.2, 40.1, 36.9, 29.9, 29.7, 24.5. MALDI-TOF MS: calc'd. for  $\text{C}_{552}\text{H}_{660}\text{N}_{24}\text{O}_{96}$  9107.78 ( $\text{M} + \text{H}^+$ ), found 9107.10.

#### 6.5.12 Acylation of MOM-protected rhombicuboctahedral nanocapsule **81** to form **82**

Hexamer amine **81** (60 mg, 0.00658 mmol) was dissolved in 30 ml dry  $\text{CHCl}_3$ . Molecular sieves (4 Å) and pyridine (38 ul, 0.470 mmol) were added into the stirred solution. After 10 min, methyl succinyl chloride (19 ul, 0.155 mmol) was added and stirring continued at room temperature. After one day, additional methyl succinyl chloride (19 ul, 0.155 mmol) was added. After another day, additional pyridine (19 ul, 0.234 mmol) and methyl succinyl chloride (19 ul, 0.155 mmol) were added and stirring continued for one more day. The reaction solution was filtered to remove molecular sieves. Then, it was washed with 0.1 M HCl (20 ml) and sat.  $\text{NaHCO}_3$  (2 x 40 ml). It was stirred with sat.  $\text{NaHCO}_3$  for 30 min. The layers were separated and the organic layer washed with brine (20 ml), dried over  $\text{MgSO}_4$ , and concentrated down. **82** was obtained as an off-white solid (78 mg, yield 99%).  $^1\text{H}$  NMR (500 MHz,  $\text{CDCl}_3$ , 25 °C),  $\delta_{\text{H}}$  (ppm): 8.00 (s, 24 H,  $H_{\text{aryl}}$ ), 7.96-7.41 (br m, 96 H,  $H_{\text{aryl}}$ ), 7.19 (s, 24 H,  $H_{\text{aryl}}$ ), 5.83 (br s, 24 H,  $H_{\text{outer}}$ ), 5.21 (br s, 24 H,

ArCH<sub>2</sub>N), 4.92 (br s, 24 H, H<sub>methine</sub>), 4.66 (s, 48 H, -OCH<sub>2</sub>OCH<sub>3</sub>), 3.97 (br s, 24 H, H<sub>inner</sub>), 3.61 (br s, 48 H, -CH<sub>2</sub>OCH<sub>2</sub>OCH<sub>3</sub>), 3.56 (s, 72 H, -CO<sub>2</sub>CH<sub>3</sub>) 3.39 (s, 72 H, -OCH<sub>2</sub>OCH<sub>3</sub>), 3.32 (br s, 24H, ArCH<sub>2</sub>N), 2.49 (br m, 96 H, -COCH<sub>2</sub>CH<sub>2</sub>CO-), 2.26 (m, 48 H), 1.80 (m, 48 H), 1.50 (m, 48 H). MALDI-TOF MS: calc'd. for C<sub>672</sub>H<sub>744</sub>N<sub>24</sub>O<sub>168</sub> 11868 (M + Na<sup>+</sup>), found: 11869.



### 6.5.13 MOM-deprotection and saponification of rhombicuboctahedral nanocapsule to form **83**

Hexamer **82** (22.5 mg, 0.0019 mmol) was dissolved in a solution of acetic acid/THF 1:1 (4.0 ml) containing catalytic amounts of conc. H<sub>2</sub>SO<sub>4</sub> (2 ul). The solution was stirred at

room temperature for 3 days. Then, it was transferred into a beaker and stirred with 20 ml  $\text{CH}_2\text{Cl}_2$  and 20 ml sat.  $\text{NaHCO}_3$  aq. for 10 min. The layers were separated. The organic layer was washed with 20 ml sat.  $\text{NaHCO}_3$  aq., 20 ml brine, dried over  $\text{MgSO}_4$  and concentrated. A slightly yellow solid was obtained (17.5 mg). The solid was subjected to saponification. It was dissolved in 5 ml THF. 1 M KOH aq. (1 ml, 1 mmol) was added and the solution stirred at room temperature for 2 days. Then, the solvents were removed under reduced pressure and the residue was acidified with 2 M HCl aq.. The white precipitate was filtered off, washed with water until neutral and dried under high vacuum. **83** was obtained as a slightly yellowish solid (12 mg, 60%).  $^1\text{H}$  NMR (500 MHz,  $\text{DMSO}-d_6$ , 25 °C),  $\delta_{\text{H}}$  (ppm): 11.98 (s, 24H,  $-\text{CO}_2\text{H}$ ), 8.24-7.14 (br m, 144 H,  $\text{H}_{\text{aryl}}$ ), 5.79 (br s, 24 H,  $\text{H}_{\text{outer}}$ ), 5.15 (br s, 24 H,  $\text{H}_{\text{methine}}$ ), 4.66 (s, 24H,  $\text{ArCH}_2\text{N}$ ), 4.50 (s, 24H,  $\text{ArCH}_2\text{N}$ ), 3.90 (br s, 24 H,  $\text{H}_{\text{inner}}$ ), 3.49 (br s, 48 H,  $-\text{CH}_2\text{OH}$ ), 2.31 (br m, 48 H,  $-\text{COCH}_2\text{CH}_2\text{CO}-$ ), 2.26 (m, 48 H), 1.98 (br m, 48 H,  $-\text{COCH}_2\text{CH}_2\text{CO}-$ ), 1.64 (m, 48 H), 1.37(m, 48 H). MALDI-TOF MS: calc'd. for  $\text{C}_{600}\text{H}_{600}\text{N}_{24}\text{O}_{144}$  10451 ( $\text{M} + \text{H}^+$ ), found: 10460.

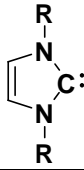
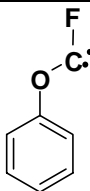
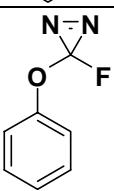
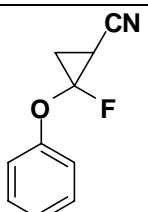
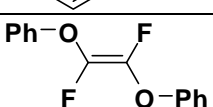
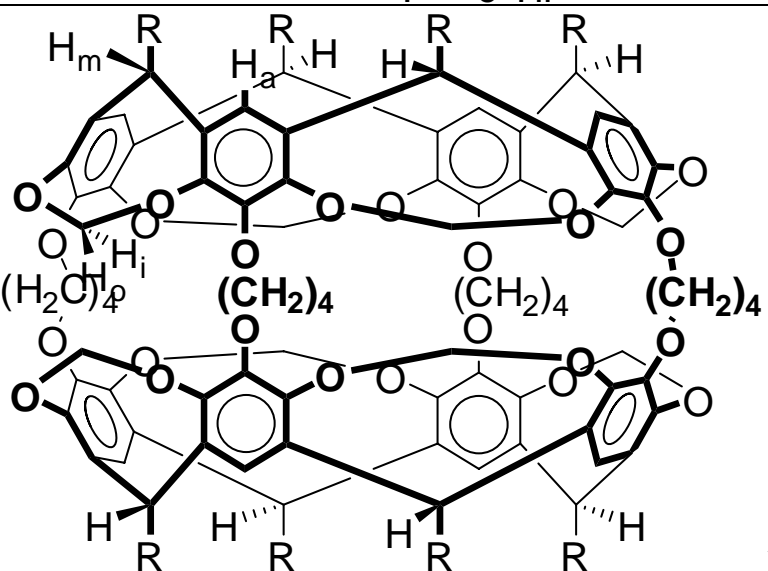
## 6.6 References

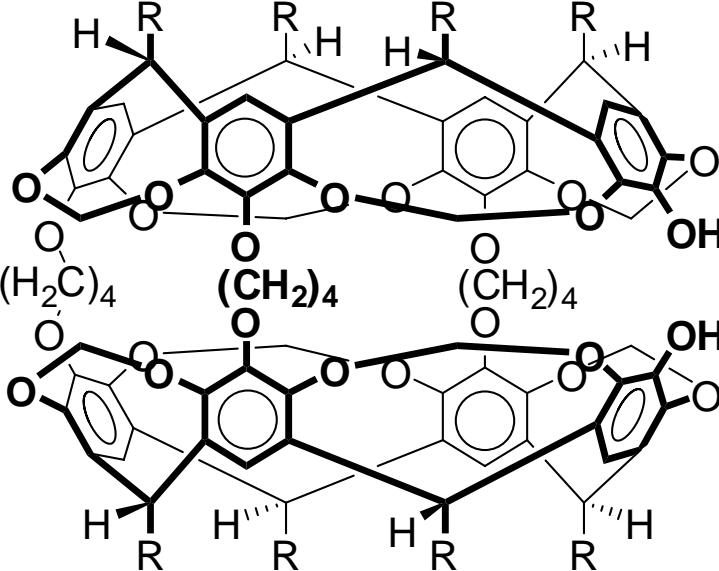
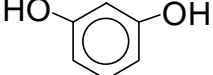
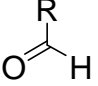
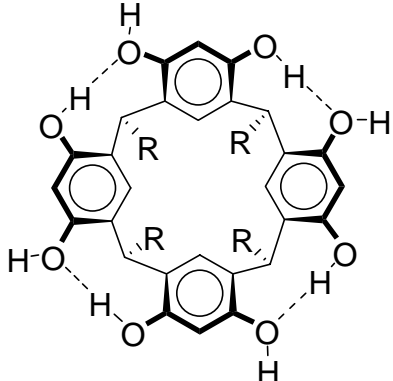
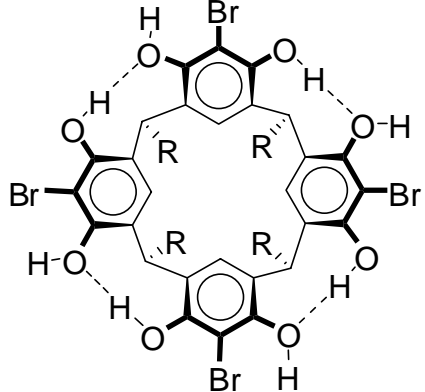
1. R. Warmuth, J. Yoon, *Acc. Chem. Res.* **2001**, 34, 95.
2. F. Diederich, *Angew. Chem. Int. Ed.* **2007**, 46, 68.
3. J. Szejtli, *Chem. Rev.* **1998**, 98, 1743.
4. a) B. C. Gibb, R. G. Chapman, J. C. Sherman, *J. Org. Chem.* **1996**, 61, 1505; b) A. R. Mezo, J. C. Sherman, *J. Org. Chem.* **1998**, 63, 6824; c) O. Middel, W. Verboom, D. N. Reinhoudt, **2002**, 15, 2587;
5. S. X. Gui, J. C. Sherman, *Chem. Commun.* **2001**, 24, 2680.
6. a) S. M. Biros, E. C. Ullrich, F. Hof, L. Trembleau, J., Jr. Rebek, *J. Am. Chem. Soc.* **2004**, 126, 2870; b) R. J. Hooley, S. M. Biros, J. Rebek Jr., *Angew. Chem. Int. Ed.* **2006**, 45, 3517; c) L. Sebo, F. Diederich, *Helvetica Chimica Acta*, **2000**, 83, 93; d) C.

- L. D. Gibb, B. C. Gibb, *J. Am. Chem. Soc.*, **2004**, *126*, 11408; e) C. L. D. Gibb, B. C. Gibb, *J. Am. Chem. Soc.*, **2006**, *128*, 16498.
7. M. W. Hosseini, J.-M. Lehn, *Helvetica Chimica Acta*, **1987**, *70*, 1312.
  8. F. Corbellini, L. D. Costanzo, M. Crego-Calama, S. Geremia, D. N. Reinhoudt, *J. Am. Chem. Soc.*, **2003**, *125*, 9946.
  9. a) J. Yoon, D. J. Cram, *Chem. Commun.* **1997**, 497-498; b) E. L. Piatnitski, R. A. Flowers II, K. Deshayes, *Chem. Eur. J.* **2000**, *6*, 999; c) H. Singh, R. Warmuth, *Tetrahedron*, **2002**, *58*, 1257.
  10. a) X. Liu, Y. Liu, G. Li, R. Warmuth, *Angew. Chem. Int. Ed.* **2006**, *45*, 901; b) X. Liu, R. Warmuth, *J. Am. Chem. Soc.* **2006**, *128*, 14120; c) Y. Liu, X. Liu, R. Warmuth, *Chem. Eur. J.*, **2007**, *13*, 8953-8959; d) X. Liu, Y. Liu, R. Warmuth, *Supramol. Chem.* **2008**, *20*, 41.
  11. a) F. A. Carey, R. J. Sundberg, *Advanced Organic Chemistry*, 4<sup>th</sup> edition, Part B: Reaction and Synthesis, Kluwer Academic/Plenum Publishers, **2000**, 166-179; b) D. J. Abraham, M. Mokotoff, *J. Med. Chem.* **1983**, *26*, 549.
  12. C. R. Woods, T. Ishii, D. L. Boger, *J. Am. Chem. Soc.* **2002**, *124*, 10676.
  13. M. H. B. G. Gansey, F. K. G. Bakker, M. C. Feiters, H. P. M. Geurts, W. Verboom, D. N. Reinhoudt, *Tetrahedron Lett.* **1998**, *39*, 5447.
  14. T. W. Greene, P. G. M. Wuts, *Protective Groups in Organic Synthesis*, John Wiley and Sons, Inc., New York, **1999**, 17-246.
  15. A) M. L. C. Quan, D. J. Cram, *J. Am. Chem. Soc.* **1991**, *113*, 2754; b) S. Mendoza, P. D. Davidov, A. E. Kaifer, *Chem. Eur. J.* **1998**, *4*, 864; c) E. S. Barrett, J. L. Irwin, P. Turner, M. S. Sherburn, *J. Org. Chem.* **2001**, *66*, 8227.
  16. H.-J. Schneider, D. Güttes, U. Schneider, *Angew. Chem. Int. Ed. Engl.* **1986**, *25*, 647.
  17. G. Arena, A. Contino, F. G. Gulino, A. Magrì, F. Sansone, D. Sciotto, R. Ungaro, *Tetrahedron Lett.* **1999**, *40*, 1597.
  18. D.-R. Ahn, T. W. Kim, J.-I. Hong, *Tetrahedron Lett.* **1999**, *40*, 6045.
  19. M. C. L. Quan, PhD thesis, University of California at Los Angeles, **1990**, Chapter III, 93-171.
  20. a) W. J. Burke, J. L. Bishop, E. L. Mortensen Glennie, W. N. Bauer, Jr., *J. Org. Chem.* **1965**, *30*, 3423; b) K. Neuvonen, K. Pihlaja, *J. Chem. Soc. Perkin Trans. II* **1988**, 461.
  21. S. Svenson, *Carrier-Based Drug Delivery*, American Chemical Society, Washington, DC, **2004**.
  22. D. J. Cram, *Nature*, **1992**, *356*, 29.

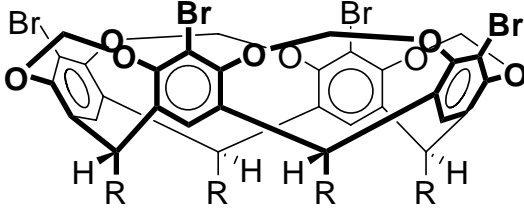
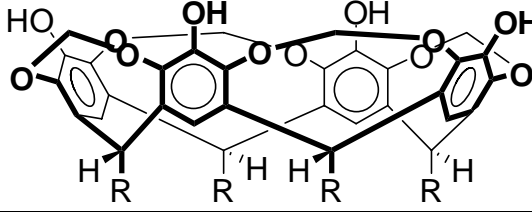
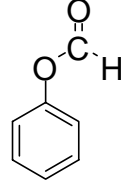
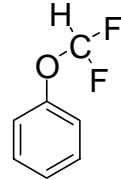
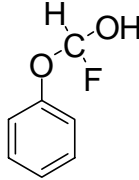
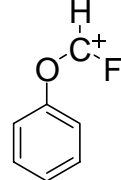
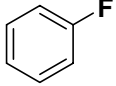
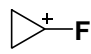
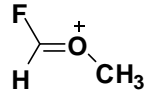
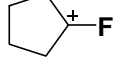
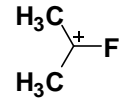
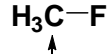
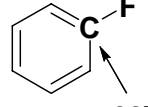
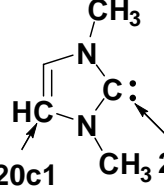
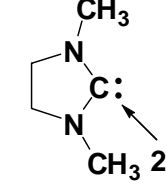
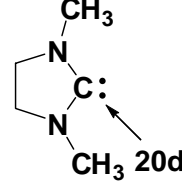
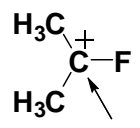
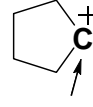
23. R. Warmuth, E. F. Maverick, C. B. Knobler, D. J. Cram, *J. Org. Chem.* **2003**, 68, 2077.
24. Y. Cohen, L. Avram, L. Frish, *Angew. Chem. Int. Ed.* **2005**, 44, 520.
25. H.-J. Schneider, A. Yatsimirsky, *Principles and methods in Supramolecular Chemistry*, John Wiley & Sons, Ltd. Chichester, England, **2000**, 137-226 .
26. M. Holz, H. Weingartner, *J. Magn. Reson.* **1991**, 92, 115.

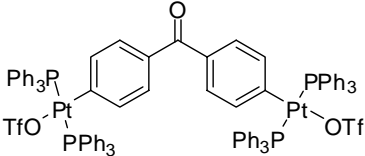
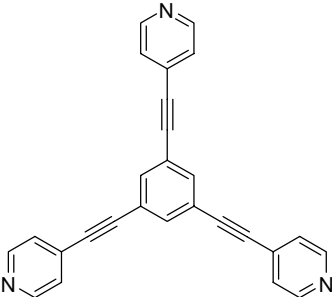

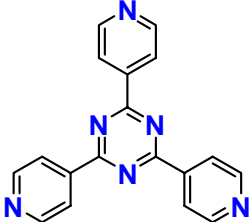
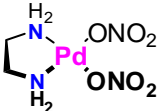
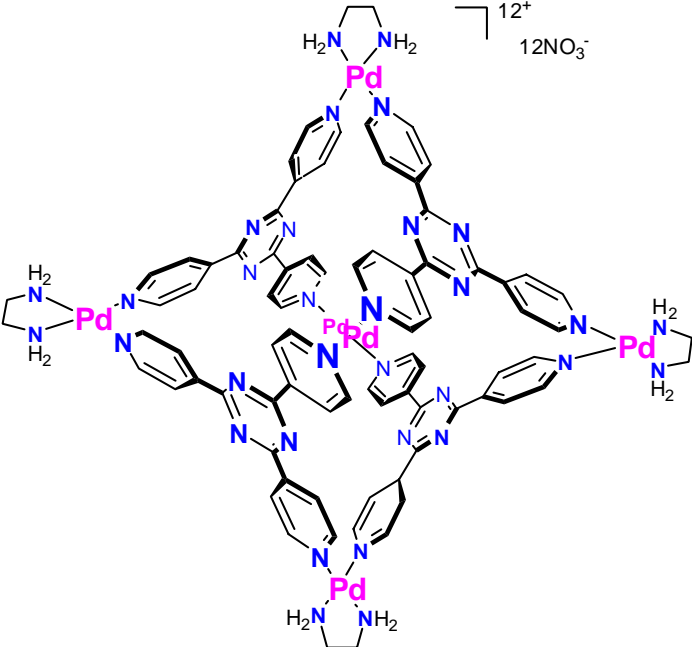
## Appendix. Compound number and structure

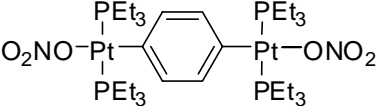
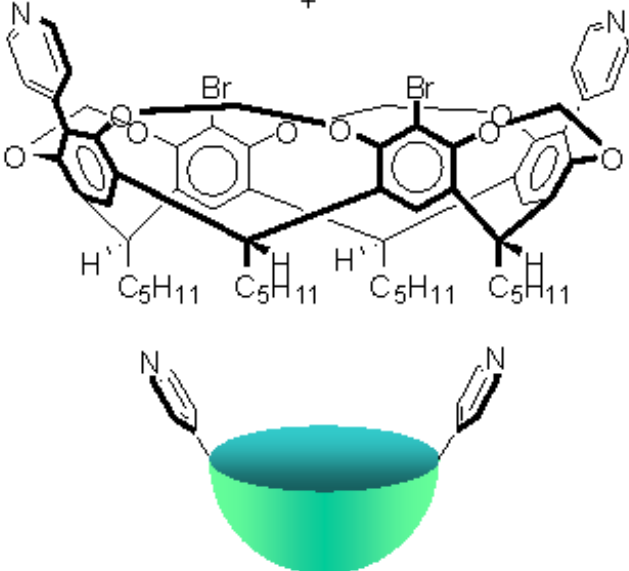
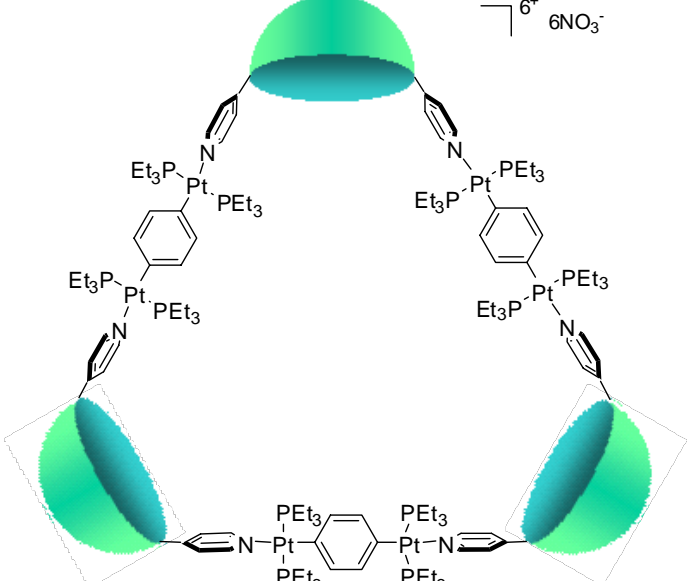
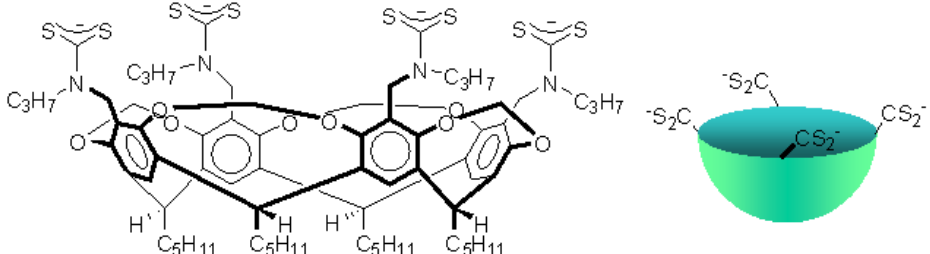
compd #	structure
1	$\text{:CH}_2$
2	 <p>R = admantyl</p>
3	
4	
5	
6	
7	 <p>R = pentyl</p>

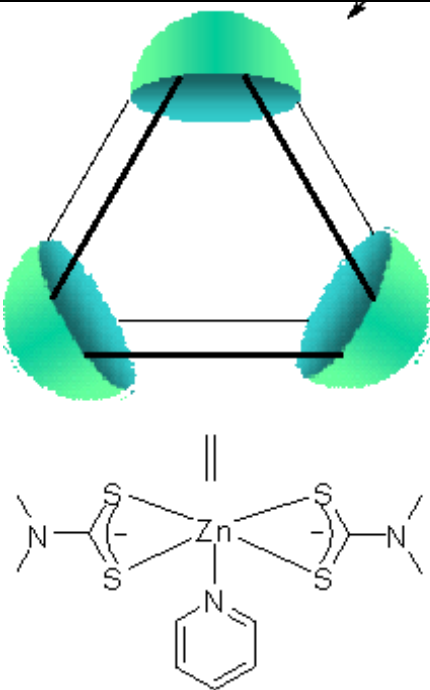
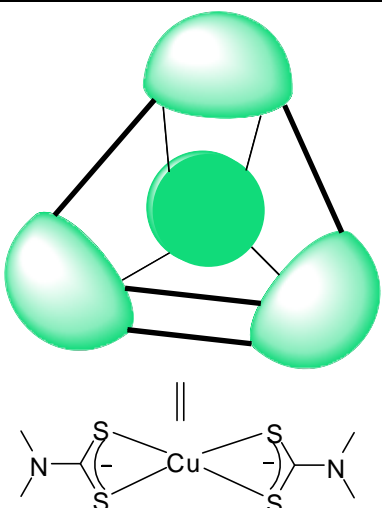
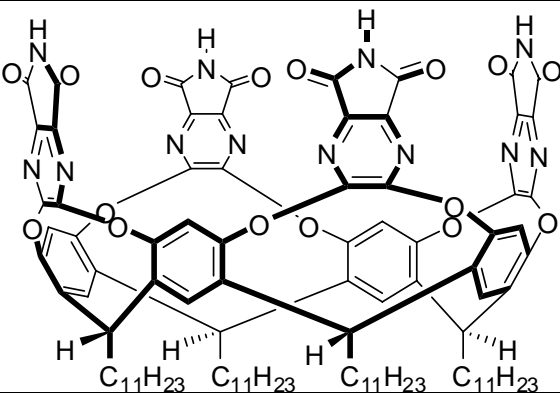
8	 <p style="text-align: right;">R = pentyl</p>
9	
10	 <p style="text-align: center;">R = CH<sub>2</sub>(CH<sub>2</sub>)<sub>3</sub>CH<sub>3</sub></p>
11	 <p style="text-align: right;">R = pentyl</p>
12	 <p style="text-align: right;">R = pentyl</p>

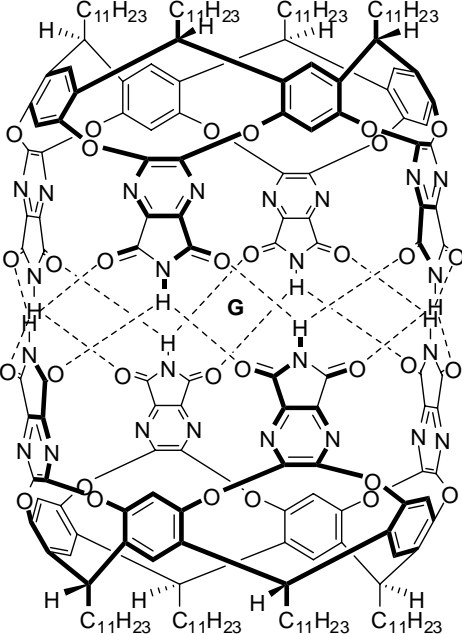
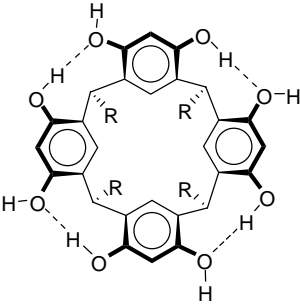
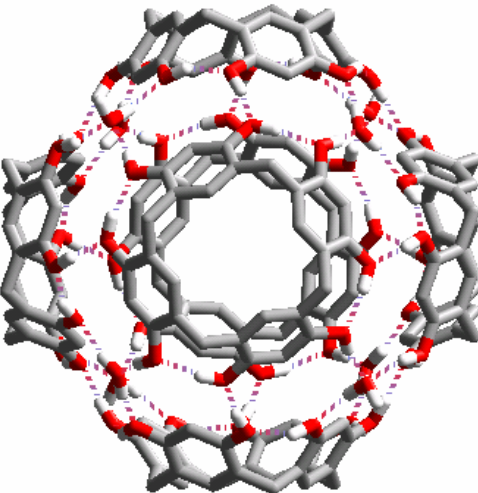


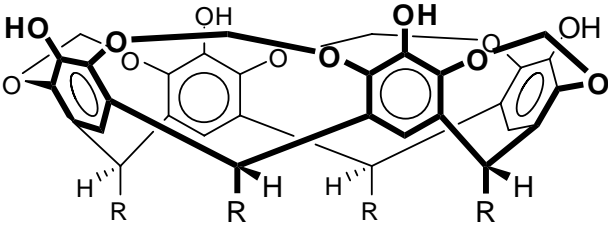
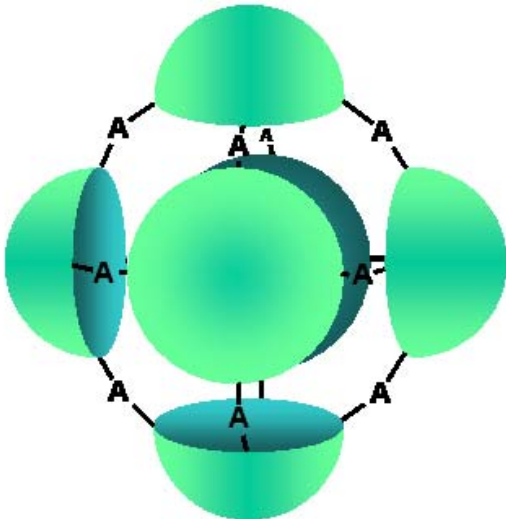
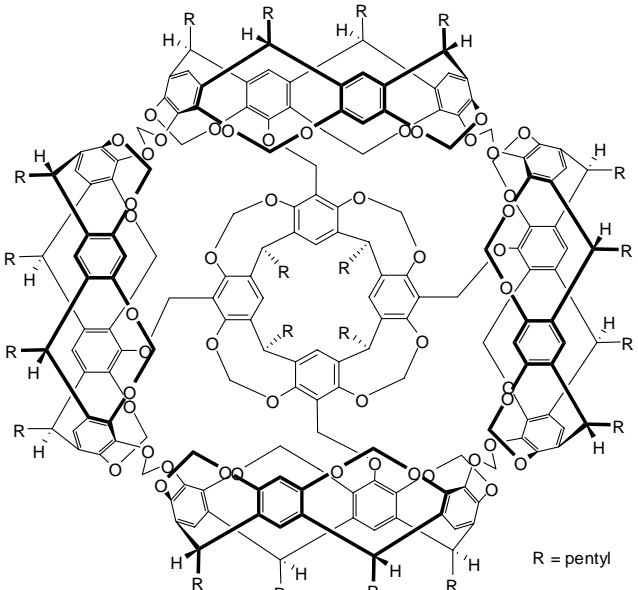
13	 <p>R = pentyl</p>						
14	 <p>R = pentyl</p>						
15							
16							
17							
18							
19a-f	$\text{CH}_3\text{F}$ <b>19a</b>	 <b>19b</b>	 <b>19c</b>	 <b>19d</b>	 <b>19e</b>	 <b>19f</b>	
20a-f	 <b>20a</b>	 <b>20b</b>	 <b>20c1</b>	 <b>20c2</b>	 <b>20d</b>	 <b>20e</b>	 <b>20f</b>

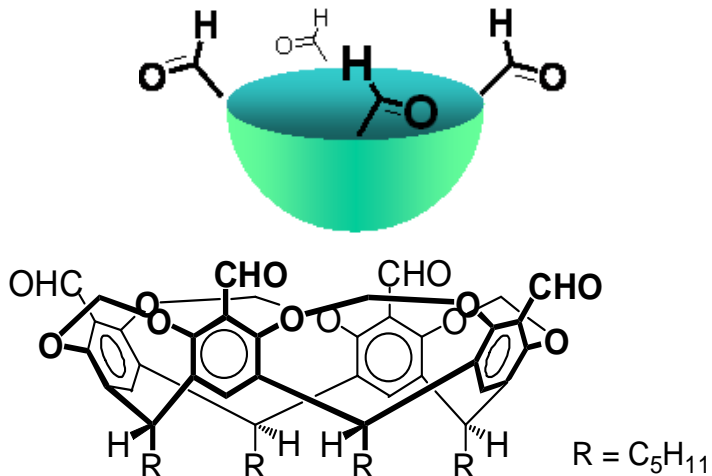
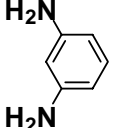
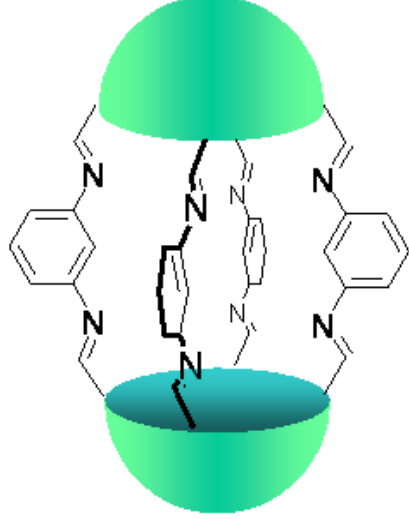
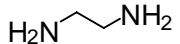
21	
22	
23	
24	
25	
26	

27	
28	
29	
30	

31	 <p>The 3D model shows three green lobes representing orbitals arranged in a triangle, connected by lines. A double arrow points to the top lobe. Below it is the chemical structure of a zinc complex: a central Zn atom is coordinated by two bidentate ligands (each with two sulfur atoms and a nitrogen atom) and a pyridine ring. The ligands are shown in a simplified representation with lines and sulfur (S) and nitrogen (N) labels.</p>
32	 <p>The 3D model shows four green lobes representing orbitals arranged in a tetrahedral-like pattern, connected by lines. Below it is the chemical structure of a copper complex: a central Cu atom is coordinated by two bidentate ligands (each with two sulfur atoms and a nitrogen atom). The ligands are shown in a simplified representation with lines and sulfur (S) and nitrogen (N) labels.</p>
33	 <p>The structure shows a large macrocyclic molecule with a central cavity. It features four benzene rings connected by ether linkages. Each benzene ring is substituted with a long alkyl chain (C<sub>11</sub>H<sub>23</sub>) and a complex heterocyclic group containing nitrogen and oxygen atoms. The structure is highly symmetrical and complex.</p>

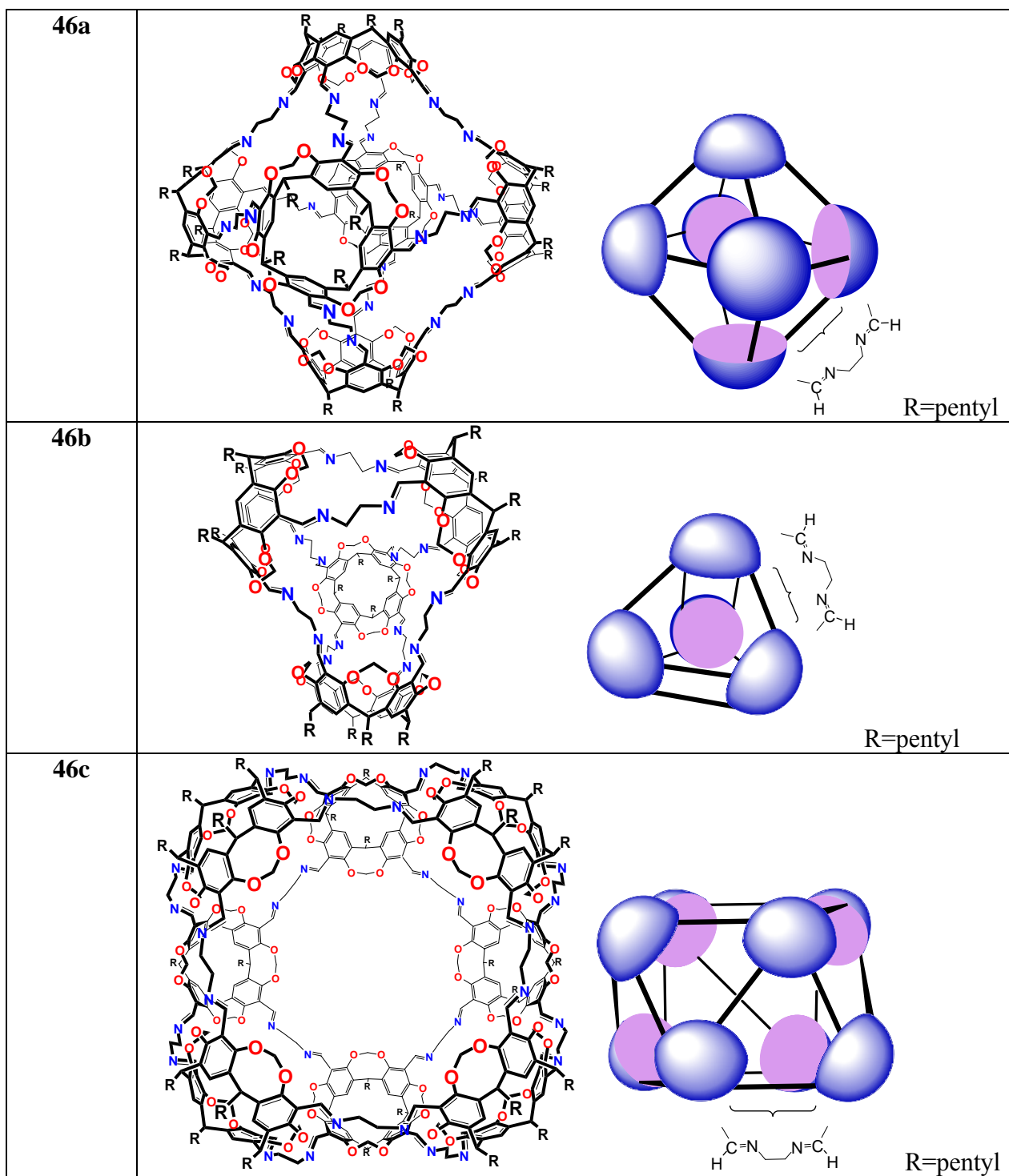
34	
35	 <p><math>R = \text{CH}_3 \text{ or } \text{C}_{11}\text{H}_{23}</math></p>
36	

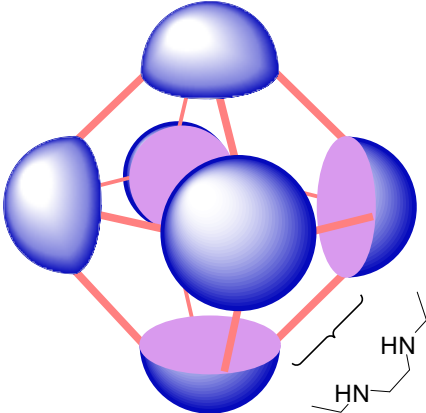
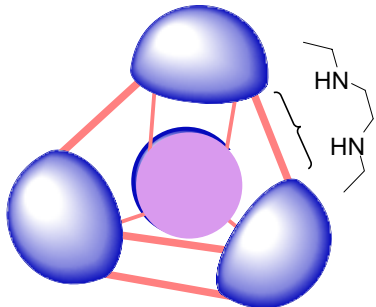
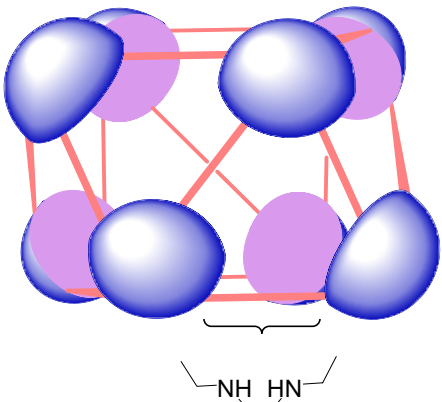
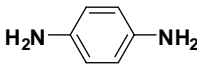
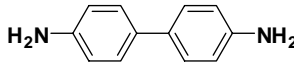
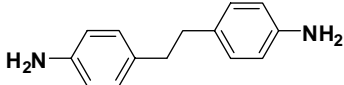
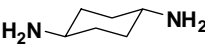
37	 <p style="text-align: center;"><math>R = \text{CH}_2\text{CH}_2\text{C}_6\text{H}_5</math></p>
38	 <p style="text-align: center;"><b>A = O-CH<sub>2</sub>-O</b></p>
39	 <p style="text-align: right;"><math>R = \text{pentyl}</math></p>

40	
41	
42	
43	

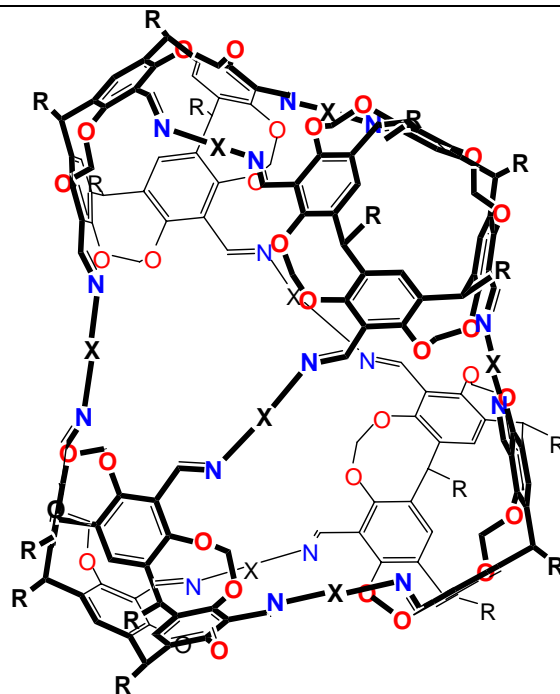
<b>44a-j</b>	<div data-bbox="865 195 943 268"><math>\begin{array}{c} \text{H}_2\text{N} \\ \diagdown \\ \text{H}_2\text{N}-\text{X} \end{array}</math></div> <div data-bbox="550 327 737 369"><chem>NCCCN</chem></div> <div data-bbox="618 401 678 436"><b>44a</b></div> <div data-bbox="786 327 997 369"><chem>NCCCCN</chem></div> <div data-bbox="867 401 927 436"><b>44b</b></div> <div data-bbox="1013 327 1260 369"><chem>NCCCCCN</chem></div> <div data-bbox="1105 401 1166 436"><b>44c</b></div> <div data-bbox="553 516 716 636"><chem>NCC1=CC=CC=C1CN</chem></div> <div data-bbox="597 657 657 693"><b>44d</b></div> <div data-bbox="753 516 992 604"><chem>NCC1=CC=C(C=C1)CN</chem></div> <div data-bbox="846 657 906 693"><b>44e</b></div> <div data-bbox="1029 516 1328 604"><chem>Nc1ccc(cc1)Cc2ccc(N)cc2</chem></div> <div data-bbox="1149 657 1209 693"><b>44f</b></div> <div data-bbox="565 772 753 919"><chem>Nc1ccc(cc1)C(=O)O</chem></div> <div data-bbox="602 936 662 972"><b>44g</b></div> <div data-bbox="781 810 980 873"><chem>Nc1ccc(N)cc1</chem></div> <div data-bbox="850 936 911 972"><b>44h</b></div> <div data-bbox="1013 779 1166 884"><chem>N[C@H]1CC[C@@H](N)C1</chem></div> <div data-bbox="1052 936 1112 972"><b>44i</b></div> <div data-bbox="1192 779 1328 863"><chem>N[C@H]1CC[C@@H](N)C1</chem></div> <div data-bbox="1224 936 1284 972"><b>44j</b></div>
<b>45a-g</b>	<div data-bbox="656 982 1008 1539"></div> <div data-bbox="1019 1524 1243 1558">for -X-, see <b>44a-j</b></div>





47a	
47b	
47c	
48a-d	<p style="text-align: center;"><math>\text{H}_2\text{N}-\text{X}-\text{NH}_2</math></p> <div style="display: flex; justify-content: space-around; align-items: flex-start;"> <div style="text-align: center;">  <p><b>48a</b></p> </div> <div style="text-align: center;">  <p><b>48b</b></p> </div> </div> <div style="display: flex; justify-content: space-around; align-items: flex-start; margin-top: 20px;"> <div style="text-align: center;">  <p><b>48c</b></p> </div> <div style="text-align: center;">  <p><b>48d</b></p> </div> </div>

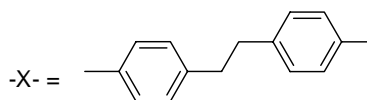
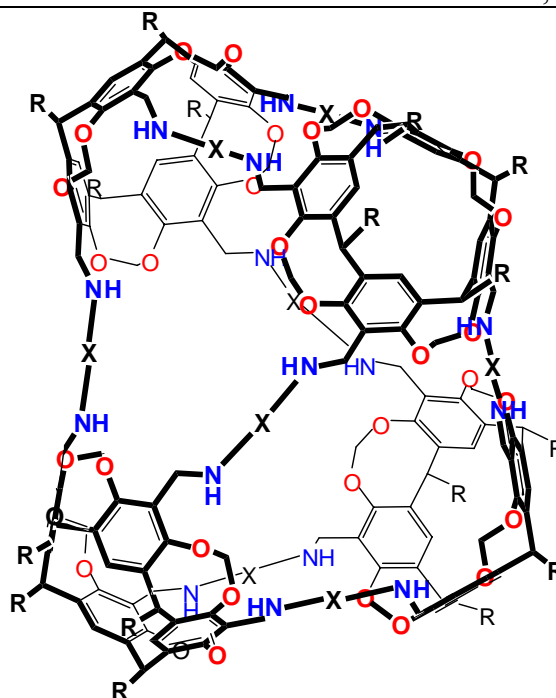
49a-d

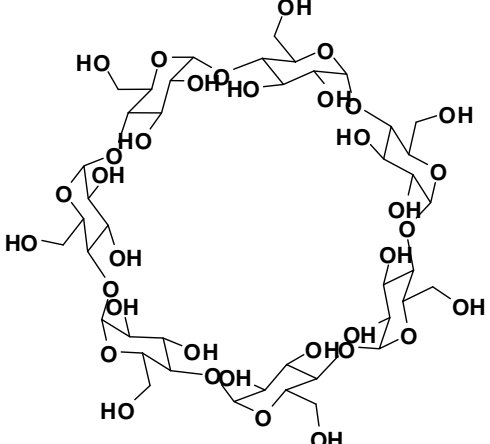
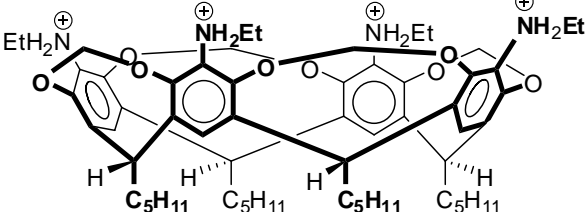
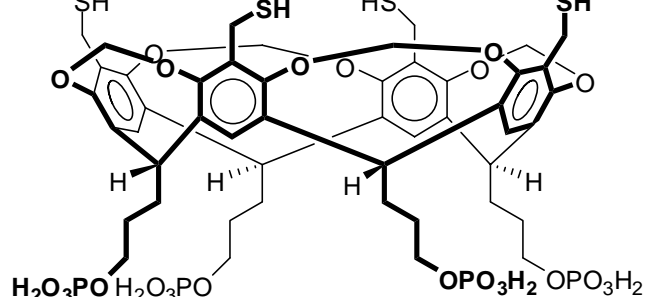
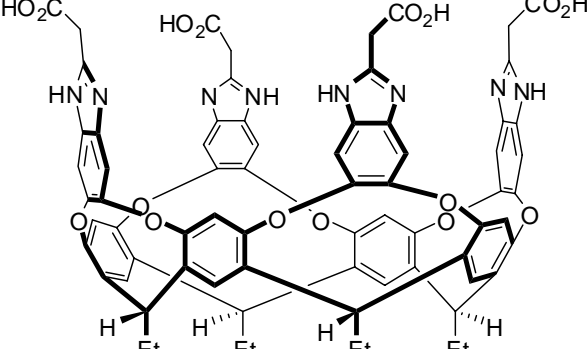


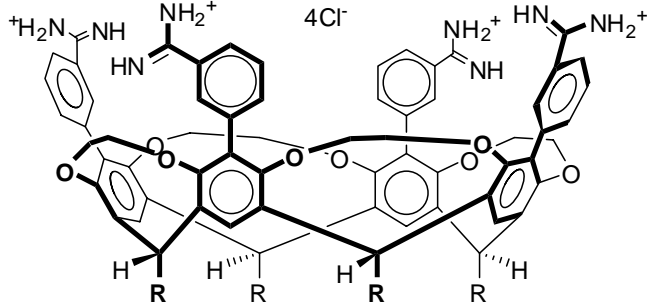
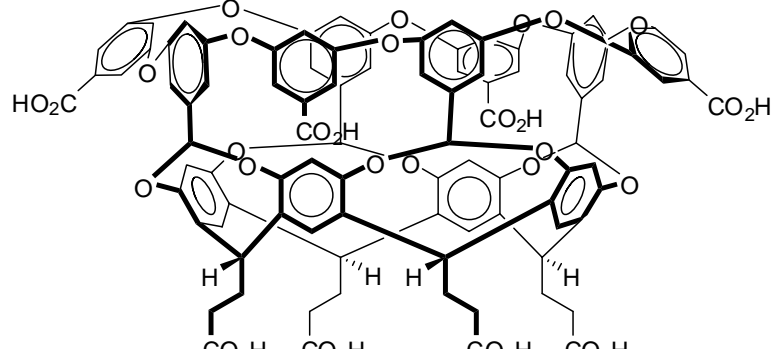
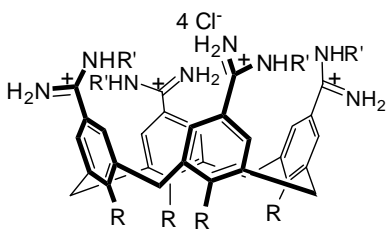
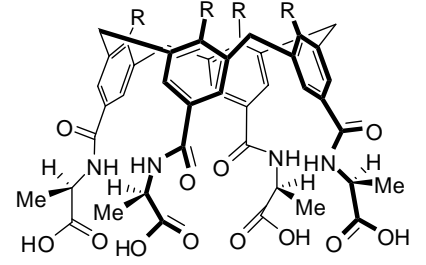
R = pentyl

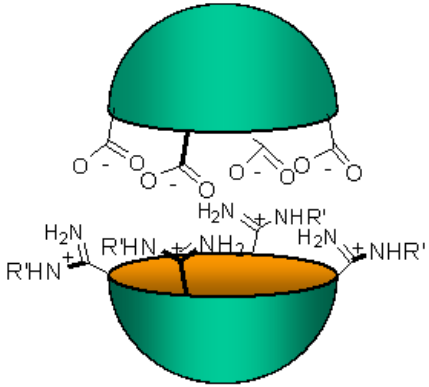
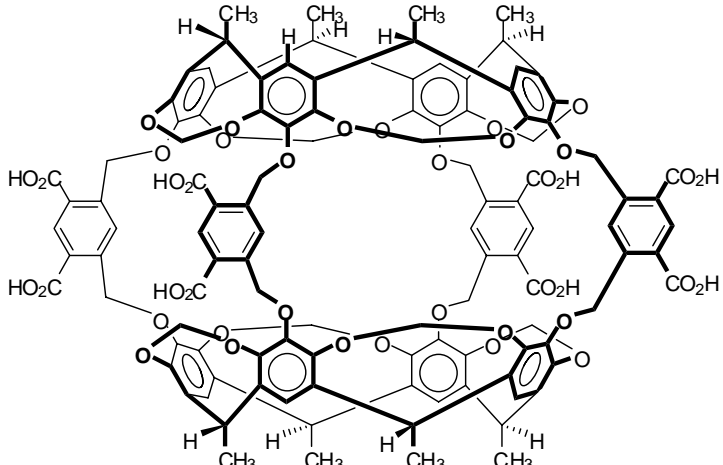
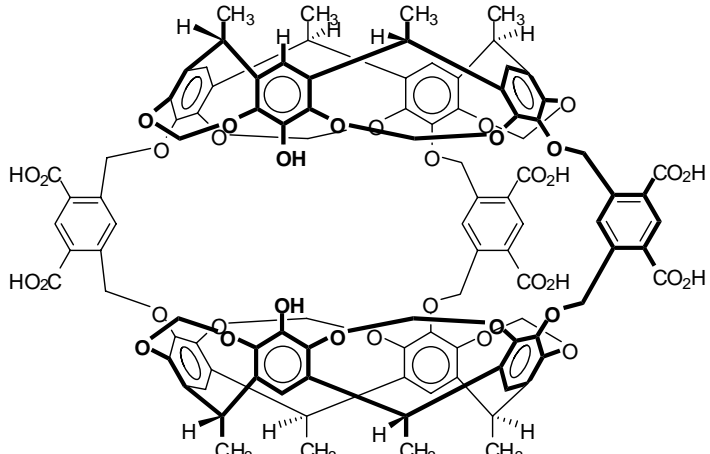
for -X-, see 48a-d

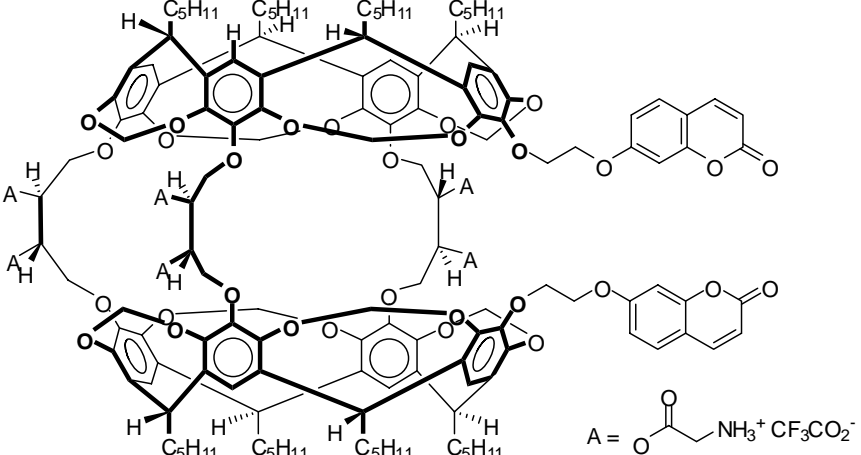
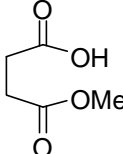
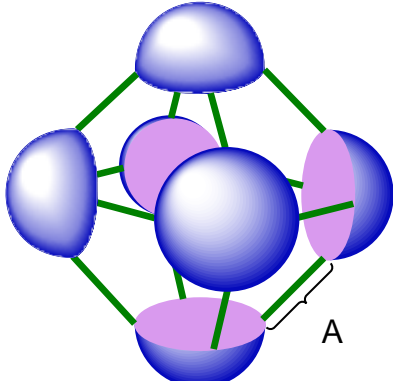
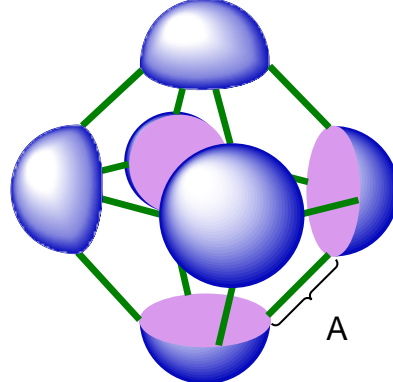
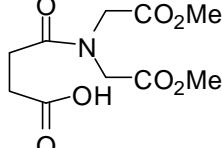
50

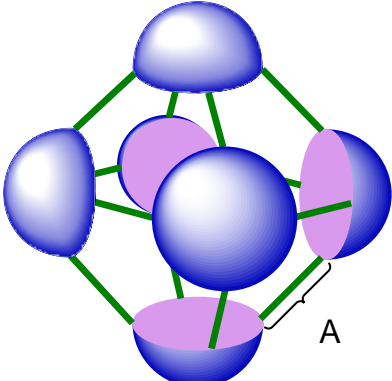
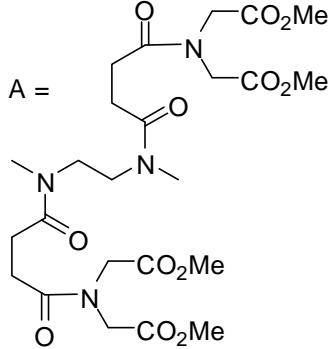
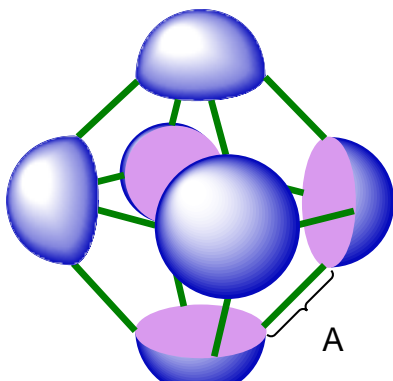
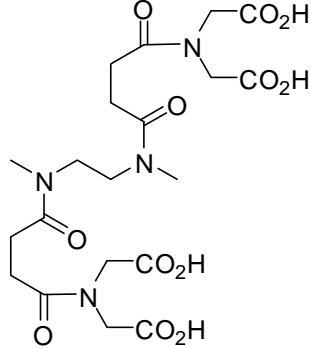
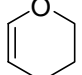
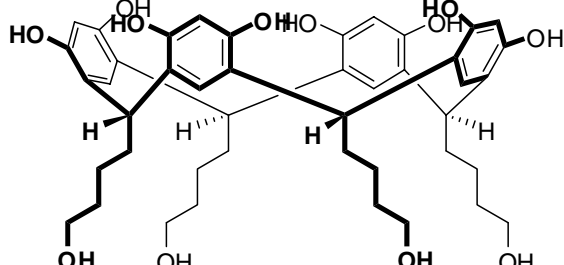
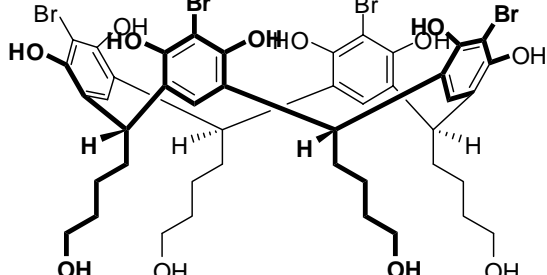
R = C<sub>5</sub>H<sub>11</sub>

51	
52	
53	
54	

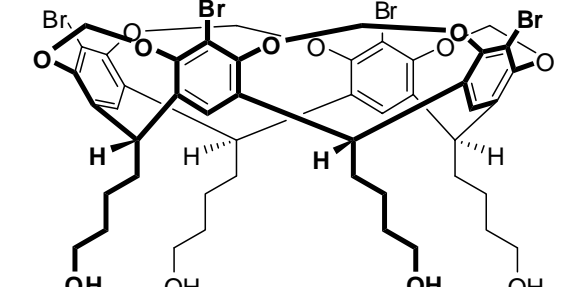
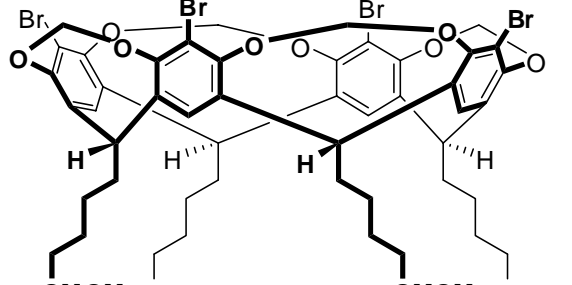
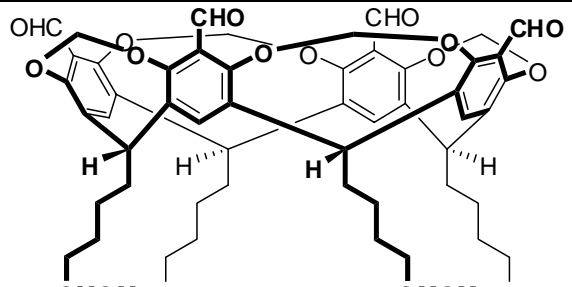
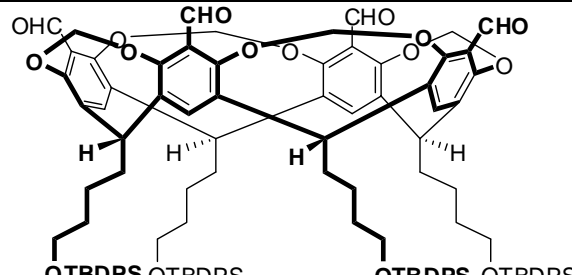
55	 <p><math>R = (CH_2)_3(OCH_2CH_2)_3OMe</math></p>
56	
57	 <p><math>R = OC_2H_4OC_2H_5</math>  <math>R' = n\text{-Pr}</math></p>
58	 <p><math>R = OC_2H_4OC_2H_5</math></p>

59	 <p>Diagram illustrating a molecular cage structure. The cage is composed of two hemispherical parts, one green (top) and one orange (bottom). The cage is functionalized with various groups, including carboxylate groups (<math>\text{COO}^-</math>) and amine groups (<math>\text{H}_2\text{N}</math>, <math>\text{R}'\text{HN}^+</math>, <math>\text{NHR}'</math>).</p>
60	 <p>Chemical structure of a macrocyclic molecule. The structure features a central ring system composed of four repeating units, each containing a benzene ring and a methyl group (<math>\text{CH}_3</math>). The macrocycle is functionalized with multiple carboxylic acid groups (<math>\text{CO}_2\text{H}</math>) and methyl groups (<math>\text{CH}_3</math>).</p>
61	 <p>Chemical structure of a macrocyclic molecule, similar to 60, but with an additional hydroxyl group (<math>\text{OH}</math>) on the central ring system.</p>

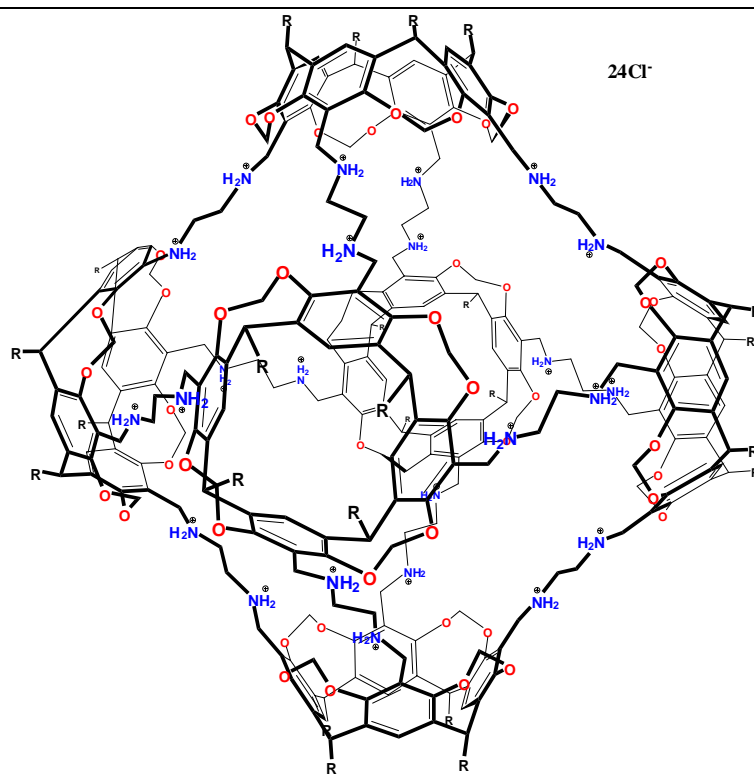
62	 <p><math>A = \text{O} \text{---} \text{CH}_2 \text{---} \text{NH}_3^+ \text{CF}_3\text{CO}_2^-</math></p>
63	 <p><math>A = \text{O} \text{---} \text{CH}_2 \text{---} \text{COOH}</math></p>
64	 <p><math>A = \text{O} \text{---} \text{CH}_2 \text{---} \text{COOMe}</math></p> <p>R = pentyl</p>
65	 <p><math>A = \text{O} \text{---} \text{CH}_2 \text{---} \text{COOH}</math></p> <p>R = pentyl</p>
66	 <p><math>A = \text{O} \text{---} \text{CH}_2 \text{---} \text{CO}_2\text{Me}</math></p>

67	 <p>A = </p> <p>R = pentyl</p>
68	 <p>A = </p> <p>R = pentyl</p>
69	
70	
71	

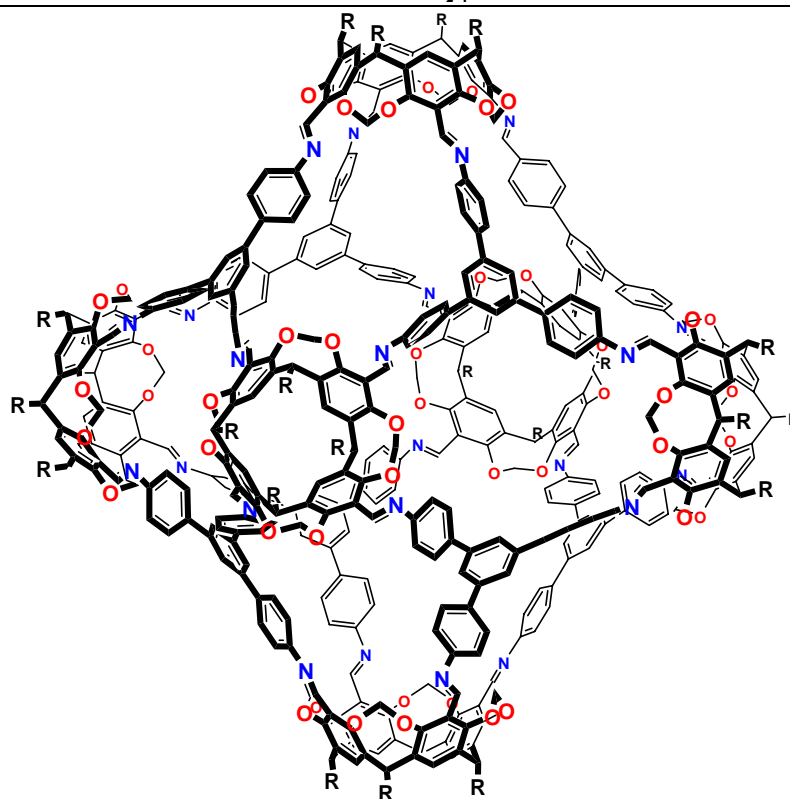


72	
73	
74	
75	

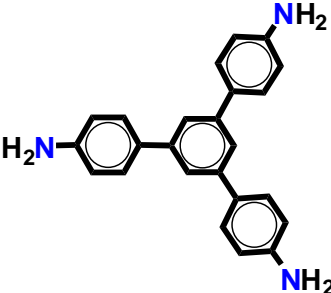
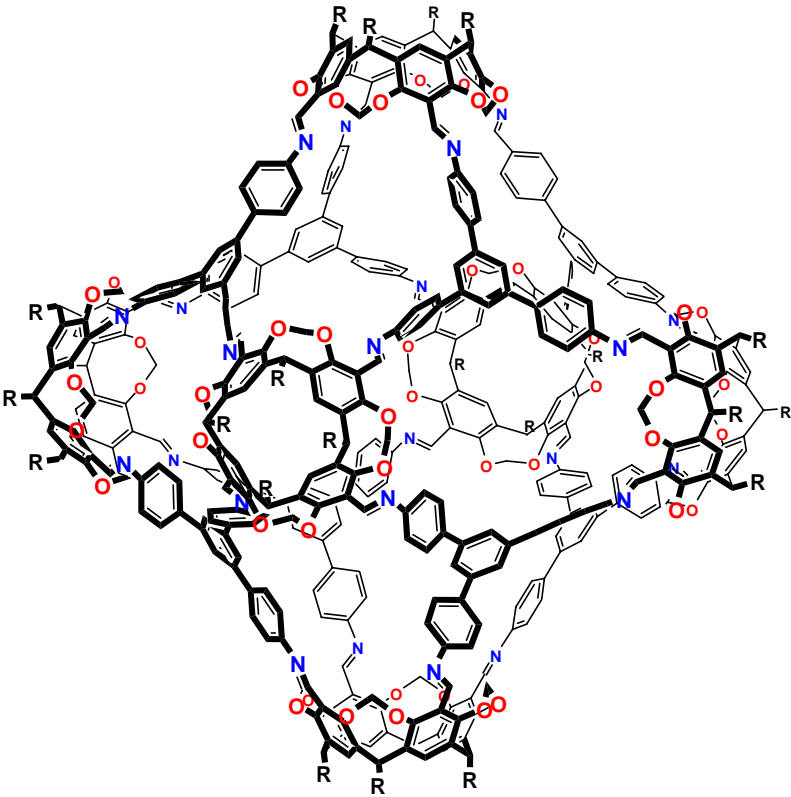
76·24HCl

R = (CH<sub>2</sub>)<sub>4</sub>OH

77

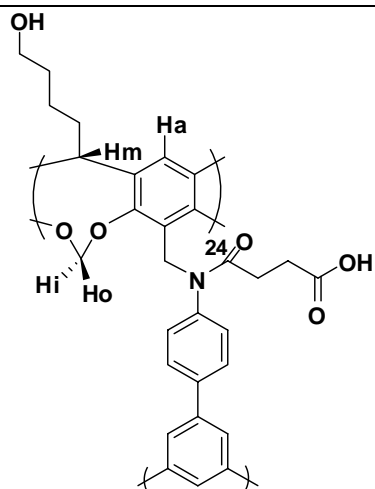


R = pentyl

78	
79	 <p data-bbox="836 1339 1156 1381"><math>R = (CH_2)_4OCH_2OCH_3</math></p>



83



## Curriculum Vita

Xuejun Liu

## EDUCATION

- September 2003-October 2008, Rutgers University, New Brunswick, New Jersey, Organic Chemistry, PhD
- September 2000-July 2003, Nanjing University, Nanjing, China, Physical Chemistry, MS
- September 1996-July 2000, Nanjing University, Nanjing, China, Polymer Science, BS

## PUBLICATIONS

- **Liu, X.**; Liu, Y.; Warmuth R. "Multi-component synthesis of tetracavitand nanocapsules." *Supramol. Chem.*, 2008, 20, 41-50.
- Liu, Y.; **Liu, X.**; Warmuth R. "Multicomponent dynamic covalent assembly of a rhombicuboctahedral nanocapsule." *Chem. Eur. J.*, 2007, 13, 8953-8959.
- **Liu, X.**; Warmuth R. "A simple one-pot multicomponent synthesis of an octahedral nanocontainer molecule." *Nature Protocols*, 2007, 2, 1288-1296.
- **Liu, X.**; Warmuth R. "Solvent effects in thermodynamically controlled multicomponent nanocage syntheses." *J. Am. Chem. Soc.*, 2006, 128, 14120-14127.
- **Liu, X.**; Liu, Y.; Li G.; Warmuth R. "One-pot, 18-component synthesis of an octahedral nanocontainer molecule." *Angew. Chem. Int. Ed.*, 2006, 45, 901-904. This work was highlighted in *Chem. & Eng. News*, 2006, 84(2), 9.
- **Liu, X.**; Chu G.; Moss R. A.; Sauers R. R.; Warmuth R. "Fluorophenoxycarbene inside a hemicarcerand: a bottled singlet carbene." *Angew. Chem. Int. Ed.*, 2005, 44, 1994-1997. This work was highlighted in *Chem. & Eng. News*, 2005, 83(9), 12.
- **Liu, X.**; Gu X.; Shen J. "Structure, surface acidity/basicity and redox properties of V<sub>2</sub>O<sub>5</sub>/TiO<sub>2</sub> catalysts." *Chinese J. Catalysis*, 2003, 24(9), 674-680.

## PATENT

- Shen J.; Fu Y.; Hong T.; **Liu X.** "Preparation and application of selective oxidation catalysts for manufacturing methylal from methanol by one-step reaction." *China Patent*, 2005, 12 pp, CN 1634655 A 20050706.